Electron-responsive molecular materials and organized assemblies based on Pi-radicals as building blocks.

Wathiq Sattar Abdul-Hassan

Communauté
UNIVERSITÉ Grenoble Alpes

THÈSE

Pour obtenir le grade de

DOCTEUR DE LA COMMUNAUTÉ UNIVERSITÉ GRENOBLE ALPES

Spécialité : **Chimie physique moléculaire et structurale**

Arrêté ministériel : 25 mai 2016

Présentée par

Wathiq Sattar ABDUL-HASSAN

Thèse dirigée par **Eric SAINT AMAN** et **Guy ROYAL**

Préparée au sein du **Département de Chimie Moléculaire**
dans **l'École Doctorale de Chimie et Sciences du Vivant**

Matériaux moléculaire électro-stimulables et assemblages organisés reposant sur des briques élémentaires de type pi-dimères

Electron-responsive molecular materials and organized assemblies based on elementary pi-dimer bricks

Thèse soutenue publiquement le **14 février 2018,**
devant le jury composé de :

Madame Eleonora-Mihaela UNGUREANU
Professeur, Université Polytechnique de Bucarest (Rapporteur)
Monsieur Charles DEVILLERS
Maître de Conférences, Université de Bourgogne (Rapporteur)
Madame Isabelle MALFANT
Professeur, Université Toulouse III(Examinateur)
Monsieur Michael HOLZINGER
Directeur de Recherche, Université Grenoble Alpes (Président)
Monsieur Guy ROYAL
Professeur, Université Grenoble Alpes (Directeur de thèse)
Monsieur Eric SAINT AMAN
Professeur, Université Grenoble Alpes (Directeur de thèse)
Monsieur Denis Roux
Maître de Conférences, Université Grenoble Alpes (Invité)

Symbols and Abbreviations

TTF: tetrathiafulvalene
V^{2+}: dimethyl viologen
$V^{+\bullet}$: dimethyl viologen radical
K_{Dim}: dimerization constant
SOMO: singly occupied molecular orbital
ESR: electron spin resonance spectroscopy
ΔH_{Dim}: dimerization enthalpy
ΔS_{Dim}: dimerization entropy
CV: cyclic voltammetry
VRDE: voltammetry with rotating disc electrode
ΔE_p: potential separation (= E_{pa} - E_{pc})
E_{pc}: cathodic peak potential
E_{pa}: anodic peak potential
$E_{1/2}$: half-wave potential (= (E_{pa} + E_{pc})/2)
E_{app}: fixed applied potential at electrolysis
DMF: dimethylformamide
ACN: acetonitrile
DMSO: dimethyl sulfoxide
CB[8]: cucurbit[8]uril
DOSY: diffusion ordered spectroscopy
COSY: correlation spectroscopy
ROESY: rotating frame overhause effect spectroscopy
DEPTQ: distorsionless enhancement by polarization transfer including the detection of quaternary nuclei
HRMS-ESI: high resolution mass spectrometry-electrospray ionization
MALDI-Tof: Matrix-assisted laser desorption/ionization-Time of Flight Mass Spectrometry
$CBPQT^{4+}$: cyclobis(paraquate-p-phenylene)
DNP: 1,5-dioxynaphthalene
K_{Disp}: disproportionation constant
TBAP: tetrabutylammonium perchlorate
NIR: near infrared region
M: metal ion
DP: degree of polymerization
DMA: dimethylacetamide
TCE: 1,1,2,2-tetrachloroethane
LS: low-spin state
LB: Langmuir-Blodgett technique
DEAD: diethyl azodicarboxylate
NTf$^-$: (trifluoromethylsulfonyl)imide ion
OTf$^-$: triflate ion

TEOA: triethanolamine
CHTT: (1,8-di (p-2,2': 6', 2''- terpyridin-4-yl) tolyl)-1,4,8,11-tetraazacyclotetradecane
MLCT: metal to ligand charge transfer band

Table of Contents

Chapter III: Redox Responsive coordination polymers based on the viologen units

Chapter IV: Experimental part

General Introduction

The development of civilization has always been strictly related to the design and construction of devices - from wheel to jet engine - capable of facilitating the movement and travel of human. Nowadays, the miniaturization race leads scientists to investigate the possibility of designing and constructing machines and motors at the nanometer scale, that is, at the molecular level. Research on supramolecular chemistry has shown that molecules are convenient nanometer-scale building blocks that can be used to construct ultraminiaturized devices and machines. Chemists are in an ideal position to develop such a molecular approach to functional nanostructures because they are able to design, synthesize, investigate and operate with molecules. Much attention has been devoted in the last few years to the design, construction and evaluation of a wide range of wonderful molecules that can be regarded as "Molecular Devices and Machines". This domain was fully recognized in 2016, when the Nobel Prize in Chemistry was awarded to Jean-Pierre Sauvage, Sir J. Fraser Stoddart and Bernard L. Feringa for their work on molecular machines. Currently, a very active field of research concerns the study of switchable molecules used to control the properties of a material. The integration of these structures in a device where they behave as an active component or the preparation of an active material by molecular assembly is the first motivation of these studies. The nature of the molecular switches and their incorporation into the material or devices are defined by the possible fields of application. However, if a wide variety of multifunctional molecules is now available; many conceptual and technical obstacles remain and hamper the implementation of the corresponding functional molecular materials. Indeed, beyond their synthesis, the real challenge now is to connect these molecules to the macroscopic world and to "communicate" with them. This implies to integrate them into devices and materials while retaining their specific properties. It is also possible to create macroscopic effects using the properties of small molecules.

In this thesis work, we are interested in development of new redox molecular switches based on non-covalent association or π-dimerization among radicals of viologen bricks (viologen = bis-alkylated 4,4'-bipyridine). In a first bibliographic chapter, we describe main characteristics of viologen moieties and their multiple uses as active components in redox-switchable molecular systems and we will present some significant examples from the literature.

Chapter II presents two complementary parts. First, our goal was to investigate the redox properties of new cyclophanes containing two viologen units in their structures and to

evaluate their ability to generate intramolecular π-dimers in organic solvents following their electrochemical reduction. Then, these compounds have been investigated by electrochemistry and spectroelectrochemistry to demonstrate the possible formation of redox-activated inclusion complexes. These latters result from the encapsulation of dimethyl viologen radicals within the cavities of cyclic bis-viologen radicals.

Chapter III is devoted to the preparation and study of novel redox responsive coordination polymers. These dynamic polymers were prepared by spontaneous association of polytopic organic ligands containing viologen units with transitions metal cations. The strategy was to control the morphology of the metallopolymers using the redox properties of the viologen groups that are incorporated in their main chains. The synthesis of the ligands and their switching properties will be presented first. Then, the preparation of the metallopolymers by self-assembly and their properties will be exposed. The interesting switching properties and movement of the polymers in solution have been investigated by electrochemical study, absorption and ESR spectroscopy and viscosity measurements.

Chapter IV concerns the experimental part. The synthesis and characterization of the molecular systems and materials are presented and the different techniques and methods used for their characterization are detailed. Annexes have also been added. In particular, the synthesis of several viologen derivatives that were prepared during this work (but not used in the work reported in this manuscript) is described.

CHAPTER I

Redox controlled viologen-based assemblies:
A LITERATURE SURVEY

1. Preamble

To achieve essential comprehension of chemical architectures, it is necessary to know the nature of bonding holding atoms together. Both in solution and in the solid states, inter- or intramolecularly stacking is a typical wonder of planar conjugated molecules. In particular, stacking may be driven by electrostatic attractions between electron-rich aromatic donor(s) and electron-deficient aromatic acceptor(s)[1-4] such as tetrathiafulvalene (TTF) - viologen (V) donor–acceptor system.[5-16] Solvophobicity is another important driving force for the stacking of identical or different conjugated molecules.[18-20]

Another less conventional stacking pattern includes the π-homodimerization among conjugated radical anions or cations. The driving force for this stacking has been shown to be mainly the inherent multicenter covalent π-π bonding of radical cation species. This driving force dominates the repulsive electrostatic interactions among the ions, despite the fact that solvophobicity and/or attractive electrostatic interactions of the counter ions might also contribute to overcome on these repulsive electrostatic interactions.[21, 22] Because of all the reported examples, the stacking is constantly reversible with no time dependence, the stacking ought to be an ordinary non-covalent interaction.

The π-dimerization of planar radical species was first observed in the middle of the last century[23-28] in both the solid state and in concentrated solutions at low temperatures. An entire scope of various types of planar radical species, varying in both the size of the planar systems and in the charge of the dimer components, has been observed to form such types of dimeric associations. Probably the most well-known radical π-dimeric species delineated in Figure 1, are the dimers of radical cations of tetrathiafulvalene, viologens, zinc porphyrines[29], oligothiophene [30], oligopyrroles[31], and pleiadienes.[32]

In this chapter, we will focus on redox-responsive switchable architectures based on non-covalent and reversible π-association between viologen radical cation units. Some representative examples from the literatures will be described.

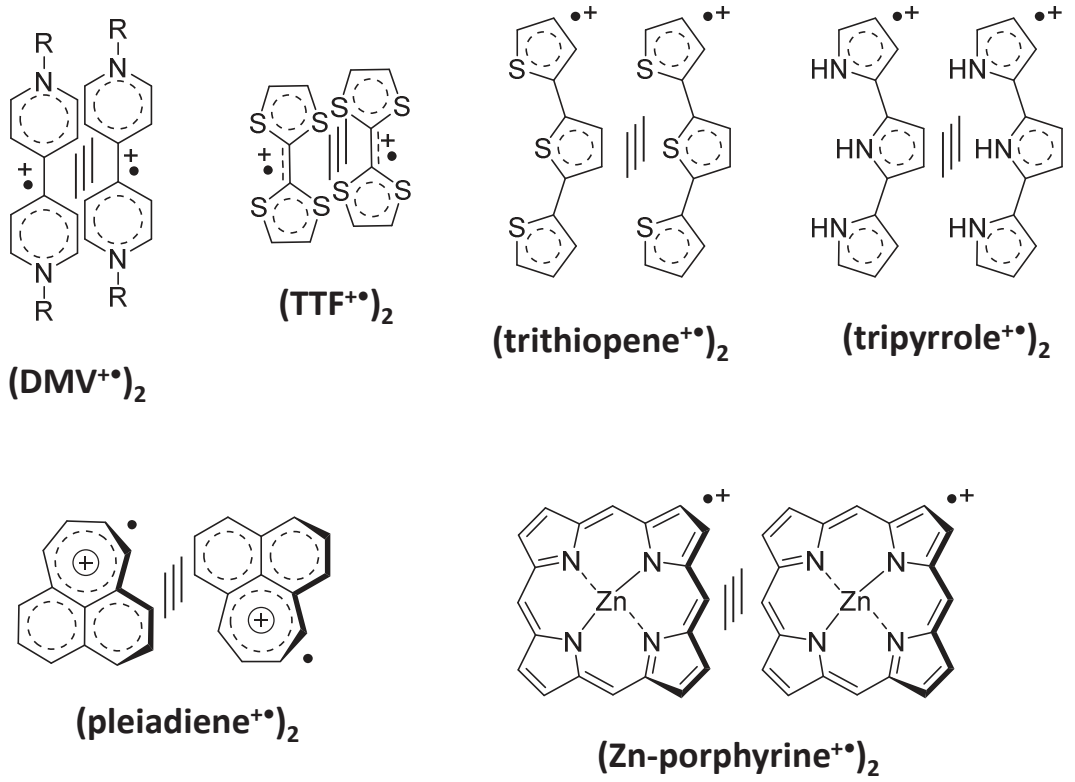

Figure 1: Common dimeric conjugated radical cations of dimethyl viologen $(DMV^{+\bullet})_2$, tetrathiafulvalene $(TTF^{+\bullet})_2$, trithiophene $(trithiophene^{+\bullet})_2$, tripyrrole $(tripyrrole^{+\bullet})_2$, pleiadiene $(pleiadiene^{+\bullet})_2$ and zinc porphyrine (Zn- porphyrine $^{+\bullet})_2$.[29-32]

2.1 Dimeric systems based on viologens

Viologens, formed by the diquaternization of 4,4'-bipyridine, are formally named as the 1,1'-disubstituted-4,4'-bipyridinium salts if the two substituents at nitrogen are the same, and as 1-substituent-1'-substituent'-4,4'-bipyridinium should they differ. If the substituent is the methyl group, the resultant dication is commonly called "methyl viologen". This compound was found to be an efficient herbicide and was originally investigated as a redox indicator in biological studies. The common name "viologen" was found by Michaelis (1933) who first noted the violet color resulting when 1,1'-dimethyl-4,4'-bipyridinium salt (DMV^{2+}) underwent a one-electron reduction to form a radical cation (as a dimer).[33, 34]

2.2 The three common redox states of viologen

The viologen derivatives exist generally in three main oxidation states as represented below:

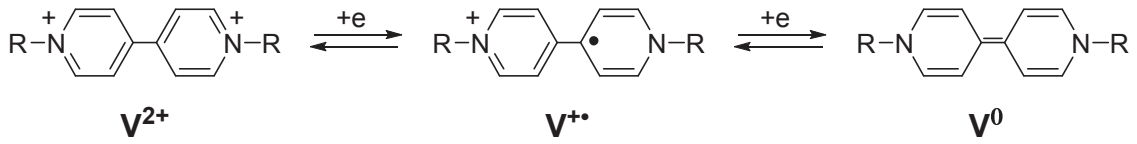

Figure 2: Three common viologen redox states.[33]

Among the three common viologen redox states, the dication form is the most stable. It absorbs strongly in the UV region and is colorless unless optical charge transfer with the counter anions exists. The extent of such charge transfer is impotent for anions such as chloride and is somewhat stronger for iodide. For example, the methyl viologen as its iodide salt has a glossy red color.[35]

The one-electron reduction of viologen dication forms radical cations ($V^{+\bullet}$), see Figure 2. Its stability is attributable to the delocalization of the unpaired electron throughout the π-framework of the two pyridyl groups arranged in coplanar conformation, together with the N and N' substituents bearing some of the charge.[36] Evans *et al*[37] have shown that the unpaired electron density is delocalized through all the 14 atoms and if electronic constraints permit, conjugation may extend over the substituents.

In contrast to the viologen radical cation ($V^{+\bullet}$), the di-reduced viologen (V^{0}) has been less investigated and is formed by one- or two-electron reduction of the viologen radical cation ($V^{+\bullet}$) or the dication viologen (V^{2+}) respectively. Magnetic susceptibility measurements have shown that the di-reduced viologen is diamagnetic in the solid state indicating that the spins are paired. Like the viologen radical cation ($V^{+\bullet}$), the di-reduced viologen (V^{0}) is colored, red-brown for simple alkyl viologens and scarlet-red for aryl viologens.[33]

2.3 Dimerization of viologen radical cations

Interestingly, the radical cations of viologen are intensively colored, with high molar absorption coefficients, owing to optical charge transfer between the (formally) +1 and 0 valent nitrogens.[38] In water, the blue color of methyl viologen radical cation can mutate to purple when increasing the concentration. Upon warming these purple solutions, the color becomes blue again and this color change is fully reversible. These changes are attributed to the monomer-dimer equilibrium (Figure 3):

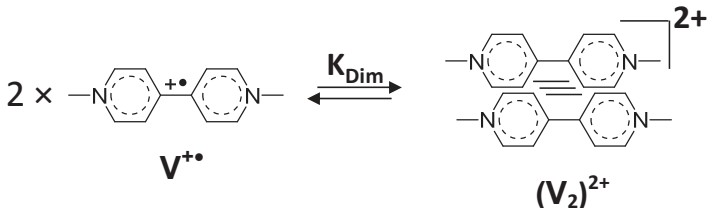

Figure 3: The monomer-dimer equilibrium controlled by dimerization constant K_{Dim}.

Such equilibrium was first proposed by Schwarz in 1962,[39, 26] who estimated the equilibrium constant of dimerization for ethyl viologen (1 M) in aqueous solution to be 3.8×10^2 ($mol.dm^{-3}$) at 298 K. Such constant is increasing at low temperature. Figure 4 shows the UV-visible spectra of both the monomer and dimer forms for methyl viologen radical cation in water. The absorption bands of the dimerized structure are shifted to lower wavelengths (the Davydov shift).[40] This blue shift is due to the interactions between the transition dipole moments on adjacent molecules in the dimer. Since the transition dipoles are face-to-face, then for an intramolecular transition of the planar molecules of the dimer, the dipole interaction is repulsive. Thus, an extra energy is required to excite this transition in the dimer, and consequently, the energies of dimer transitions are blue-shifted with respect to those of the monomer.[40]

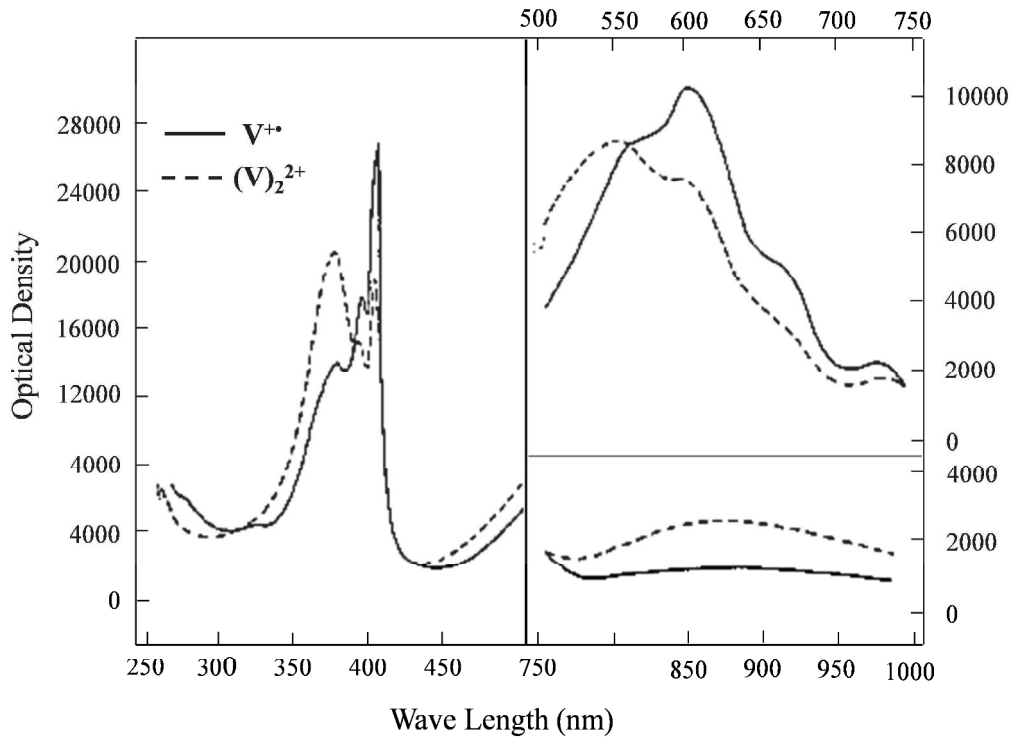

Figure 4: UV-visible spectra of the monomer $V^{+\bullet}$ (solid lines) and the dimer $(V)_2^{2+}$ (dotted lines) for methyl viologen in water.[26]

The shape of the absorption bands in the region 400-600 nm for both the monomer and the dimer does not dramatically change, meaning that they have the same transitions responsible for these bands with only minimal structural differences between the spectra of the two species.[26]

In addition to the absorption bands in the region 400-600 nm, an important diagnostic band is observed in near IR region for the viologen dimer form, not present in that of the monomer. This absorption band corresponds to an allowed electronic transition from the filled bonding molecular orbital (which is resulting from the interaction between two SOMO orbitals (Singly Occupied Molecular Orbital) energy level owing originally to the interacted monomers) to anti-bonding orbital within the formed diamagnetic viologen dimer structure[40, 41] according to the energy scheme shown in figure 5.

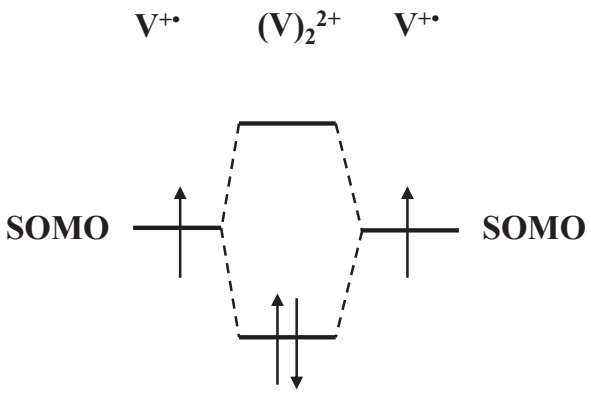

Figure 5: Schematic representation of the interaction between two SOMO orbitals centered on the two identical viologen radical cations in the dimer $(V)_2^{2+}$.[40, 41]

In an aqueous solution containing 1 M KCl, the 1,1'-dimethyl-4,4'-bipyridinium mono-radical cation ($DMV^{+\bullet}.I^-$) has been produced by reducing its dicationic form DMV^{2+} with sodium dithionate.[26] The viologen radical cation is characterized by an absorption band centered at 600 nm, while the viologen dimer $(DMV^{+\bullet})_2$ (Figure 3) has an absorption band around 870 nm. By measuring the absorption spectra at different concentrations, a value of 385 M^{-1} for the dimerization constant (K_{Dim}) was obtained (temperature was not indicated). However, reducing the temperature promotes the π-dimerization process and hence the viologen dimer stability.[37] By changing the temperature, both the paramagnetic non-associated viologen radical and diamagnetic π-dimerized viologen radical cations can be cycled reversibly.[42]

As expected from the singlet state electronic configuration of the dimerized viologen structures, their ESR spectra are silent only if the dimerization of the free radical cations is a quantitative process. Experimentally, traces of the paramagnetic non-dimerized viologen radicals could be always detected at room temperatures.[42] For example the dimerization constant for 1, 1'-ethyl-4, 4'-bipyridinium mono-radical cation ($EV^{+\bullet}.I^-$) was determined to be 1203 M^{-1} from ESR experiments.[37]

In general, the monomer-dimer equilibrium (Figure 3), is not monitored at room temperature in non-aqueous organic polar solvents such as methanol, acetonitrile, propylene carbonate, or dimethylformamide, due to the existence of the radical cation as an ion pair rather than as a fully dissociated species, thus preventing the formation of dimer in non-aqueous solvents.[26] The observed stability of the viologen dimers in water comes partly from the relatively large dispersion forces arising when large molecules are laid in close proximity. However, if dispersion forces were the major reason for the dimer stability in water (and they are not), then dimerization would readily occur in other non-aqueous solvents than only water. Since

the dimerization is not noted in non-aqueous solvents, then it is suggested that the energetic contributions arising from increased water-water interactions (inevitable since two radical ions now occupy a single solvent-bound cavity) are sufficient to overwhelm the repulsive coulombic forces apparent when two cations are close together, thus facilitating the dimerization in aqueous media.[43] For example, the complete dimerization for radical cations was observed at low temperatures, with high concentrations of radicals or highly polar solvent media (77 K at a concentration of 10^{-5} M in ethanol or 225 K at a concentration of 10^{-3} M in ethanol).[44]

2.4 Thermodynamics of dimerization

Since the monomer and dimer have distinctive absorption properties, the equilibrium constant, K_{Dim}, characterizing for the monomer-dimer equilibrium illustrated in eq. 1 can be obtained from UV-Visible spectroscopy, electrochemistry or ESR. In particular, the absence of ESR response is another important indication, suggesting the quantitative formation of π-dimers. The observation of an ESR signal may instead be the result of a low constant of dimerization leading to a significant concentration of free radicals.

The equilibrium between the monomer and the dimer of viologen radical cations can be determined by UV-Visible spectroscopy using the following equations[45-48]:

$$2V^{+\bullet} \rightleftharpoons (V)_2^{2+} \qquad \text{(eq. 1)}$$

$$A_{monomer} = [\text{monomer}] \times \varepsilon_{monomer} \times l \qquad \text{(eq. 2)}$$

$$A_{dimer} = [\text{dimer}] \times \varepsilon_{dimer} \times l \qquad \text{(eq. 3)}$$

Where: monomer = $V^{+\bullet}$, dimer = $(V)_2^{2+}$, A and ε: absorbance and molar absorption coefficient respectively.

Then, the equilibrium constant of dimerization can express in terms of absorption values as:

$$K_{Dim} = \frac{[\text{dimer}]}{[\text{monomer}]^2} = \frac{A_{dimer} \times (\varepsilon_{monomer})^2 \times l}{(A_{monomer})^2 \times \varepsilon_{dimer}} \qquad \text{(eq. 4)}$$

From the temperature dependence of K_{Dim}, the dimerization enthalpy (ΔH_{Dim}) could be determined (through Van't Hoff isochore) and then the dimerization entropies (ΔS_{Dim}) may be calculated from eq. 5:

$$\ln K_{Dim} = \frac{-\Delta H_{Dim}}{RT} + \frac{\Delta S_{Dim}}{R} \qquad \text{(eq. 5)}$$

Where K_{Dim} = dimerization constant, ΔH_{Dim} = enthalpy change, ΔS_{Dim} = change in entropy, R = universal gas constant (8.314472 J · mol^{-1} · K^{-1}), T = temperature (K).

The thermodynamic properties for the dimerization equilibrium of a variety of alkyl- and aryl-viologens in methanolic and aqueous solutions were calculated using either variable-temperature ESR measurements or UV-Visible spectroscopy.[37, 49-52] Although the entropy changes for aryl-viologens are negative as would be expected[51], the ΔS^o values for the dimerization of a series of alkyl-viologen are positive. To explain this increase in entropy upon dimerization, an assumption of removal the bound solvent molecules from the solvation shells of the viologen radical cation on dimerization was adopted. In other words, the entropy changes which dominate the dimerization reaction are resulting from solvent molecules gaining freedom when they are released during the dimerization. Consequently, the magnitude of entropy change indicates that many solvent molecules are liberated, so the two radical cations which form the dimer structure will occupy a small volume of space. This magnitude of the positive ΔS^o gives an indication as to how the viologen radical cations are placed with respect to each other in the dimer structure. If ΔS^o_{Dim} is large, then the two monomers must be held within a small solvent-bound cavity since many solvent molecules are to be released, i.e. they must be plane to plane to a significant extent of π-orbital.[49]

The thermodynamic data indicated that the dimerization reaction becomes more exothermic accompanied with an expected decrease of the entropy change when the viologen radical cation increases in size. Indeed, the big size of the viologen radical cation weakens the force holding the solvent molecules to the cation, thus reducing the increase in entropy which will occur when these solvent molecules are released on dimerization. At room temperature, the entropy term wins over the enthalpy term so that an increase in the radical cation size causes a shifting for the position of this equilibrium from dimer towards monomer.

2.5 Spectro-electrochemistry and electron-transfer reactions of viologens

As mentioned before, bis-pyridinium salts exist in three main oxidation states: bis-cationic species denoted by V^{2+}, and two reduced forms: $V^{+\bullet}$ and V^{0}. The cyclic voltammetry curves (CV) usually show two single-electron reversible waves. For example, the first reduction wave of 1, 1'-dimethyl-4, 4'-bipyridinium salt (DMV^{2+}) is fully reversible and can be cycled many times without significant side reaction. This wave, observed at $E^{1}_{1/2}$ = -0.86 V *vs*. Ag^{+}/ Ag (10^{-2} M), leads to the formation of radical cation ($DMV^{+\bullet}$). The second reduction ($E^{2}_{1/2}$ = -1.24 V) results in the fully reduced state (DMV^{0}), neutral quinone species.[53-55]

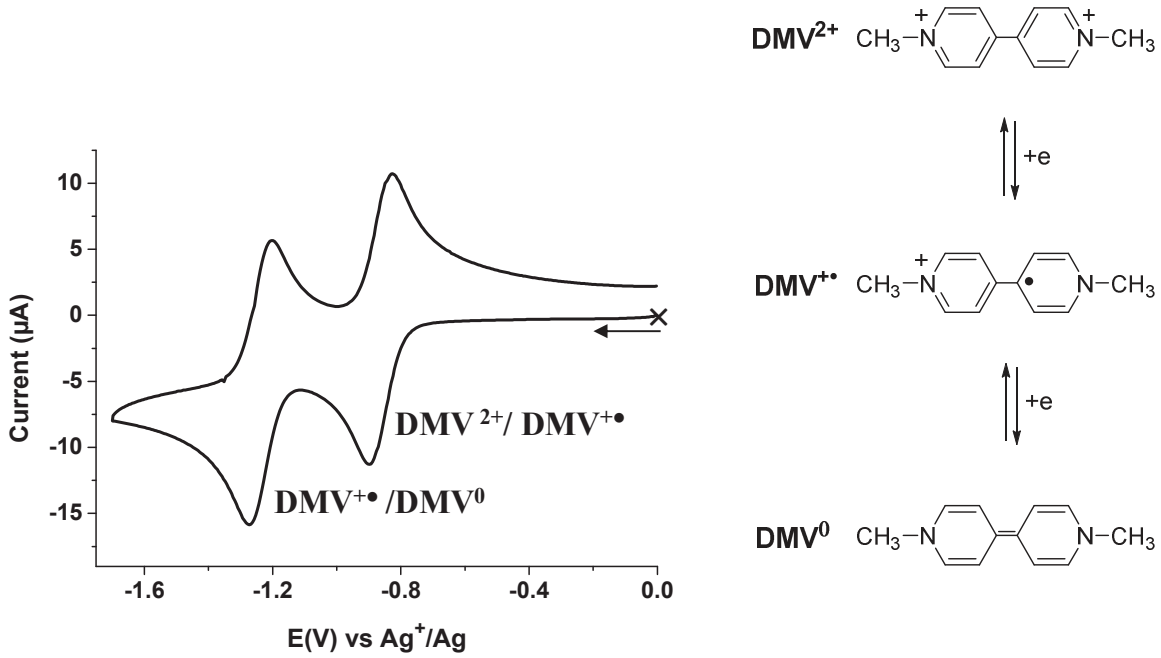

Figure 6: Cyclic voltammogram of 1,1'-dimethyl-4,4'-bipyridinium bis hexafluorophosphate ($DMV^{2+}.2PF_6^-$), 1 mM in DMF + 0.1 M TBAP, working electrode: 3 mm vitreous C, scan rate: 100 $mV.s^{-1}$, E vs Ag^{+}/Ag 10^{-2} M, 298 K.

The solubility of the three redox states of viologen and hence the reversibility of the two reduction processes depend on the solvent, counterion, and on the substituents. For example, the viologen radical cations are generally soluble in organic solvents if the counter anion is NO_3^-, ClO_4^-, BF_4^-, or PF_6^- , but are not soluble if the counter anion is F^-, Cl^-, Br^-, I^-, PO_4^{3-}, or SO_4^{2-}.[55, 56] The situation is slightly more complicated in aqueous solution because some anions cause a high solubility to both viologen radical cation and dication, whereas others

induce a high solubility to the dication but cause precipitation of the radical due to ion-pairing effects.

The nitrate anion is the only common anion which donates the solubility to a viologen radical-cation salt in both aqueous and non-aqueous solutions.[56] However, in aqueous solutions, a time-dependent nature of the ESR signal was noted for both heptyl and p-cyanophenyl viologen radical cations[57] (the signal height decreased with time, i.e. decreasing the radicals concentration). This effect is attributable to chemical oxidation of the radicals by the nitrate counter anion.[58, 59]

When the electrochemical reduction of viologen derivative salt is carried out in water, the color of the solution can vary from blue to purple depending on the monomer/dimer ratio. Several phenomena taking place both in solution or at the surface of the working electrode may be coupled to the reduction of V^{2+} to $V^{+\bullet}$ or/and $V^{+\bullet}$ reduction to V^0 (Figure 7). Among these processes, only π-dimerization (eq. 7) serves to explain the change in color of the solution depending on the substrate concentration.

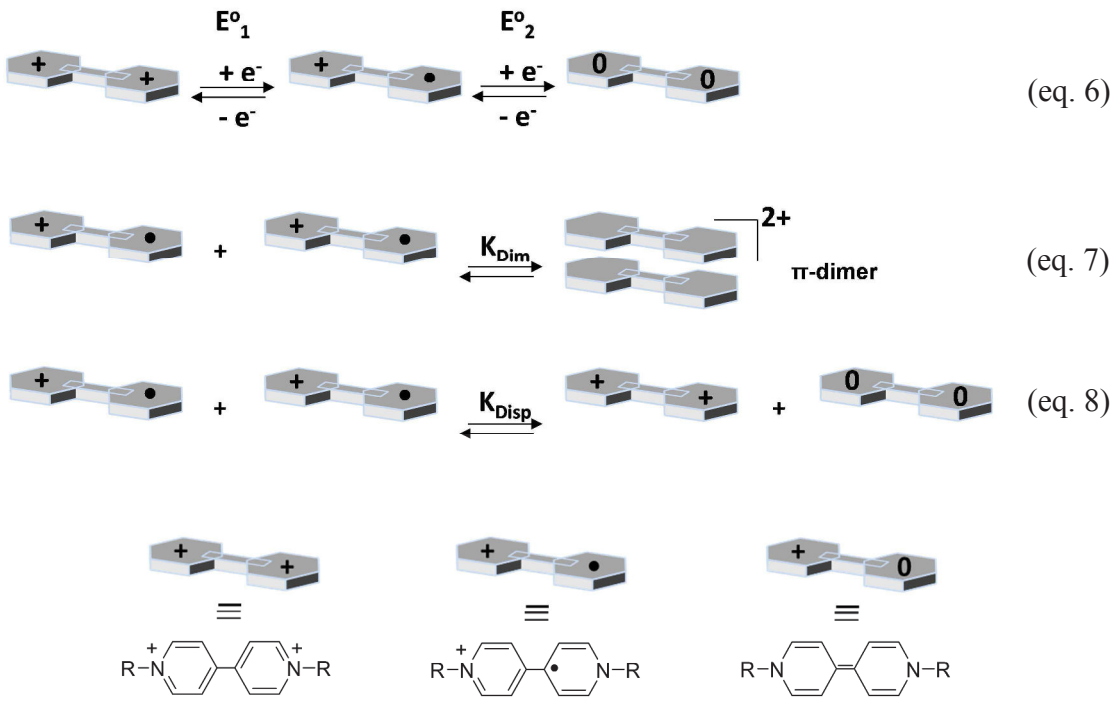

Figure 7: Schematic representation of the processes involved in the reduction of viologen. K_{Dim}: constant of π-dimerization and K_{Disp}: constant of disproportionation.[56]

In spite of earlier reduction studies of viologen derivatives in 1933 by Michaelis[34, 60], viologen radical cations were isolated much later due to their sensitivity to oxygen. Kochi *et al.* were the first to isolate and characterize the 1,1'-dimethyl-4,4'-bipyridinium mono-radical cation ($DMV^{+\bullet}PF_6^-$) in the solid state.[61]

In 2007[62], the π-dimerized 1, 1'-ethyl-4, 4'-bipyridinium radical cations ($EV^{+\bullet}.I^-$) in the solid state at room temperature has been isolated with $[Fe_4Pt(CO)_{16}]^{2-}$ as a counter ion. Within each dimer, the $[EV^{+\bullet}]$ moieties are perfectly eclipsed and display a mean distance of 3.275 Å between the planes defined by the two viologen units.

It was also shown[63] that the electronic absorption spectrum for viologen radical cations aggregations highly depends on the nature of the viologens. For example, the spectral changes of one-electron reduced species of unsymmetrical viologens, 1-methyl-1'-alkyl-4,4'-bipyridinium ($C_1V^{2+}Cm$: m = 1, 8, 9, 12, 14, 16, 18), have been investigated spectroelectrochemically in the 350-1500 nm region. The spectra of aggregations of viologen radical cations were obtained after subtracting the contribution of the monomeric viologen radical cation from the spectra of reduced viologens. The usual dimer spectrum of aggregates of viologen radical cations ($C_1V^{+\bullet}Cm$) when m is less than 8 showed structureless absorption bands around 880 (band I), 530 (band II) and 360 nm (band III). These bands are characteristic of ($C_1V^{+\bullet}Cm$) dimer with a face-to-face configuration. In contrast for cationic viologen radicals ($C_1V^{+\bullet}Cm$) with longer alkyl substituents (C_m with $m \geq 9$) bands I and II shift to a longer wavelength region (to 1120 and 540 nm respectively) and the extent of the shift is greater as the length of the alkyl substituent increases. Such effect is due to the formation of bigger aggregates of viologen radicals ($C_1V^{+\bullet}Cm$).

In general, owing to their low stability, these mentioned dimeric prototypical radicals have been detected in the solid state or in concentrated solutions at low temperatures only. The equilibrium between the paramagnetic free radical species and the resulted diamagnetic dimers still favored the dissociated monomeric forms even under these conditions.[64]

In addition, the effect of viologen radical structures on π-dimerization process has been very recently re-investigated by Winter and co-workers[65] in aqueous media at room temperature. Substitution either viologen core rings or the two nitrogen atoms by donating or withdrawing groups, as well as, increasing the conjugation with additional aryl rings were shown to have negligible effects on the π-dimerization among viologen cation radicals. The same trend was also found for N,N'-disubstituted viologens with more or less bulky groups.

Therefore, several efficient strategies have been developed to promote and enhance the stability of these dimers such as the encapsulation of the dimer by a rigid macrocycle[66-68], holding two radical cations in place with a pre-organized framework[69-81], or stabilizing the dimer using interlocked systems[82-84] or alkyl spacered viologens[37, 44, 51, 85-90]. Some representative systems are presented in the following paragraphs.

3. Alkyl spacered viologens

The electrochemical and spectroscopic behaviors of bis-viologen $\mathbf{2}^{4+}$, $\mathbf{3}^{4+}$ and $\mathbf{4}^{4+}$ and of the tris-viologen $\mathbf{5}^{6+}$, $\mathbf{6}^{6+}$ and $\mathbf{7}^{6+}$ compounds were studied in DMF and water and their properties were compared with those of the reference compound, diethyl viologen ($\mathbf{1}^{2+}$).[85] The structures of these viologen compounds are depicted in figure 8.

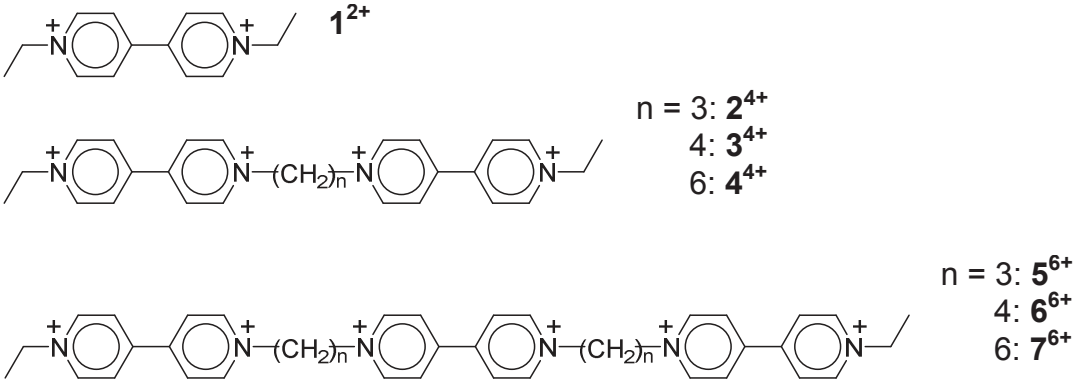

Figure 8: Bis- and tris-viologen species with flexible alkyl linkages and the corresponding reference viologen species $\mathbf{1}^{2+}$.[85]

The absorption spectra of both the bis- and tris-viologens and $\mathbf{1}^{2+}$ as their perchlorate salts in water are characterized by similar maximum wavelength (258 nm – 262 nm) and width at half maximum. This indicates the absence of interaction between the viologen units in their oxidized states.

The absorption spectra for the radicals of the bis-viologen $\mathbf{4}^{4+}$ and tris-viologen $\mathbf{7}^{6+}$ in DMF are essentially similar to that of the reference species $\mathbf{1}^{2+}$ (399 nm and 603 nm) which agrees very well with non-dimerized viologen radicals.[86] In contrast, the viologen radicals of $\mathbf{3}^{4+}$, $\mathbf{5}^{6+}$ and $\mathbf{6}^{6+}$ showed superimposed absorption spectra (~ 600 nm, 533 nm and 603 nm) of dimerized and non-dimerized species. Finally, the propylene spacered bis-viologen bis-radical

$\mathbf{2}^{2+\bullet}$ was the most associated (350 nm, 535 nm and 840). This indicates that the propylene spacer is the most favorable for the formation of face-to-face dimerization between viologen radicals.(37) In all cases, when the association between viologen radicals exists, the dimerization is intramolecular because the shapes of absorption spectra were independent of the viologen concentration. In addition, the bulk one-electron reduction per viologen unit of $\mathbf{2}^{4+}$ in water results in quantitative intramolecular dimerization, while both the dimerized and non-dimerized viologen radicals participate in the absorption spectrum of the $\mathbf{2}^{2+\bullet}$ in DMF.(85)

Figure 9 illustrates the schematic representation of dimerized viologen radical cations, with two possible dimerized structures in the tris-viologen compounds where only two viologen radical cation units are dimerized while the third viologen radical cation is not involved in the dimerization process.(85)

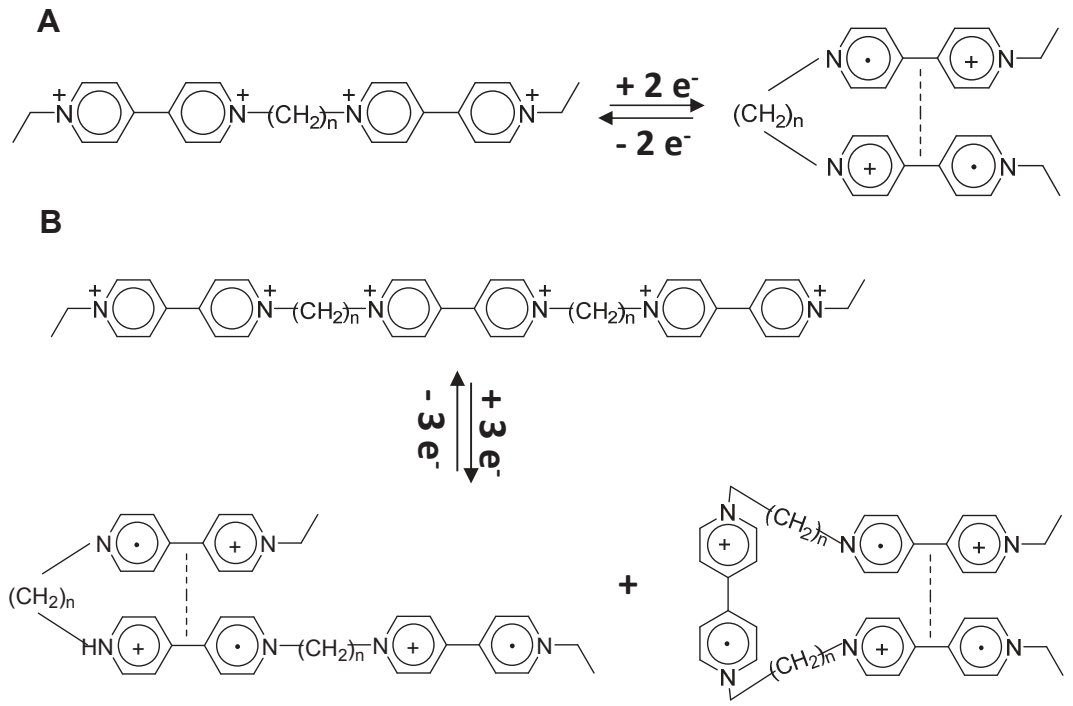

Figure 9: schematic representation for dimerized (A) bis-viologen bis-radical cations and (B) tris-viologen tris-radical cations.(85)

The electrochemical measurements showed that all the bis-viologens undergo two successive one-electron reductions. These measurements proved that the viologen radicals do not interact with each other in both hexylene spacered viologen radicals $\mathbf{4}^{2+\bullet}$ and $\mathbf{7}^{3+\bullet}$, *i.e.* each viologen radical act independently. In $\mathbf{3}^{2+\bullet}$ and $\mathbf{6}^{3+\bullet}$, with butylene spacers, the dimerization between the viologen radical cations is unfavorable conformationally.(87) Therefore, this dimerization is a

very slow process.[88] Indeed, it was previously demonstrated that the dimerization in the butylene spacered bis-viologen $\mathbf{3}^{2+\bullet}$ is entropically unfavorable (-88.7 J. mol^{-1}. K^{-1}) compared with those of the bis-viologen radicals $\mathbf{2}^{2+\bullet}$, $\mathbf{4}^{2+\bullet}$ and pentamethylene spacered bis-viologen radicals (-26.7 to -49.9 J. mol^{-1}. K^{-1}).[85] Finally, the two or three reductions of the propylene-spacered $\mathbf{2}^{4+}$ and $\mathbf{5}^{6+}$ respectively are strongly influenced by the dimerization between the viologen radicals. In $\mathbf{2}^{4+}$, the reduction of (V^{2+}-$V^{+\bullet}$) to ($V^{+\bullet}$-$V^{+\bullet}$) is easier than that of the reference compound $\mathbf{1}^{2+}$ while the next process (reduction of $V^{+\bullet}$-$V^{+\bullet}$ to $V^{+\bullet}$-V^{0}) is less favorable. This potential shifts can be attributed to the dimerization process which facilitates the introduction of the second electron to $\mathbf{2}^{4+}$ (V^{2+}-$V^{+\bullet}$ to $V^{+\bullet}$-$V^{+\bullet}$). In contrast, the introduction of the third electron dissociates the dimer which is an endothermic process. Thus, the second reduction of $\mathbf{2}^{4+}$ happens at a more negative potential compared with that of the reference compound. [85] This effect thus stabilizes the bis-reduced state (1 e^{-}/viologen unit).

The photoinduced two-electron reduction via UV irradiation (at $\lambda > 300$ nm) of 1, 1'-(1, 3-propanediyl)-bis (methyl)-4, 4'-bipyridinium) perchlorate ($\mathbf{8}^{4+}$, see figure 10) in the presence of 2-propanol in water led quantitively to the formation of the intramolecular π-dimerized form $(V\text{-}V)^{2+}$ of viologen radical cations ($V^{+\bullet}$-$V^{+\bullet}$)[89].

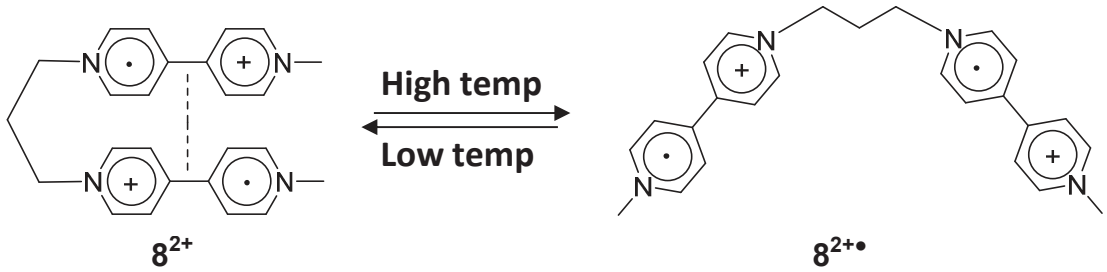

Figure 10: schematic representation for the reversible thermomagnetic switching from the diamagnetic π-dimer form $\mathbf{8}^{2+}$ to the paramagnetic bis-radical cations form $\mathbf{8}^{2+\bullet}$ in water at pH = 9.6 (0.045 M $NaHCO_3$/0.009 M NaOH buffer).[42]

This dimerized form which is generated by photoinduced or also by chemical reduction is well supported by the monotonous increase of the absorption maxima at ~ 850, 533 and 360 nm during the course of the photolysis or chemical reduction without any indication of the formation of the singly reduced bis-viologen (V^{2+}-$V^{+\bullet}$), even at the beginning of the reduction. Therefore, the disproportionation of the singly reduced bis-viologen (V^{2+}-$V^{+\bullet}$) to give the diamagnetic dimerized species $(V\text{-}V)^{2+}$ and the initial bis-viologen species (V^{2+}-V^{2+}) is essentially ruled out during the photoinduced reduction process. In contrast, the unimolecular

thermolysis of benzopinacol and the bis-viologen tetracations at 60°C in methanol results in the formation of the singly reduced bis-viologen (V^{2+}-$V^{+\bullet}$) through electron transfer from the generated benzhydrol radicals.[89] Regardless of the exothermicity of the intramolecular π-dimerization, this thermal reduction does not involve any intermolecular electron transfer process among the singly reduced bis-viologen (V^{2+}-$V^{+\bullet}$) leading to the formation of the bis-radical cations ($V^{+\bullet}$-$V^{+\bullet}$).[37, 51]

Thus, the diamagnetic π-dimer form of propyl-tethered bis(methyl viologen), $\mathbf{8}^{2+}$ is favored at room temperature with the existence of a small thermal population of the paramagnetic bis-radical cations form $\mathbf{8}^{2+\bullet}$. The equilibrium between the π-dimeric form toward the paramagnetic form has been controlled and followed by both UV-vis and ESR spectroscopies at various temperatures in water and DMSO media at low concentrations, Figure 10.[42]

The diamagnetic dimer/paramagnetic bis-radical equilibrium was achieved and cycled at alternating between high and low temperatures in water and DMSO media, promoting changes in magnetic and optical properties of the propyl-linked bis-viologen $\mathbf{8}^{4+}$.[42]

The polymethylene spacered bis-methyl viologen salts ($C_1V^{2+}C_nV^{2+}C_1$: n = 3-8, compounds $\mathbf{8}^{4+}$-$\mathbf{13}^{4+}$) were utilized as effective flexible molecular tweezers for the electron donor, 2-naphthol forming sandwich-type complexes, especially when n = 7 (Figure 11).[90]

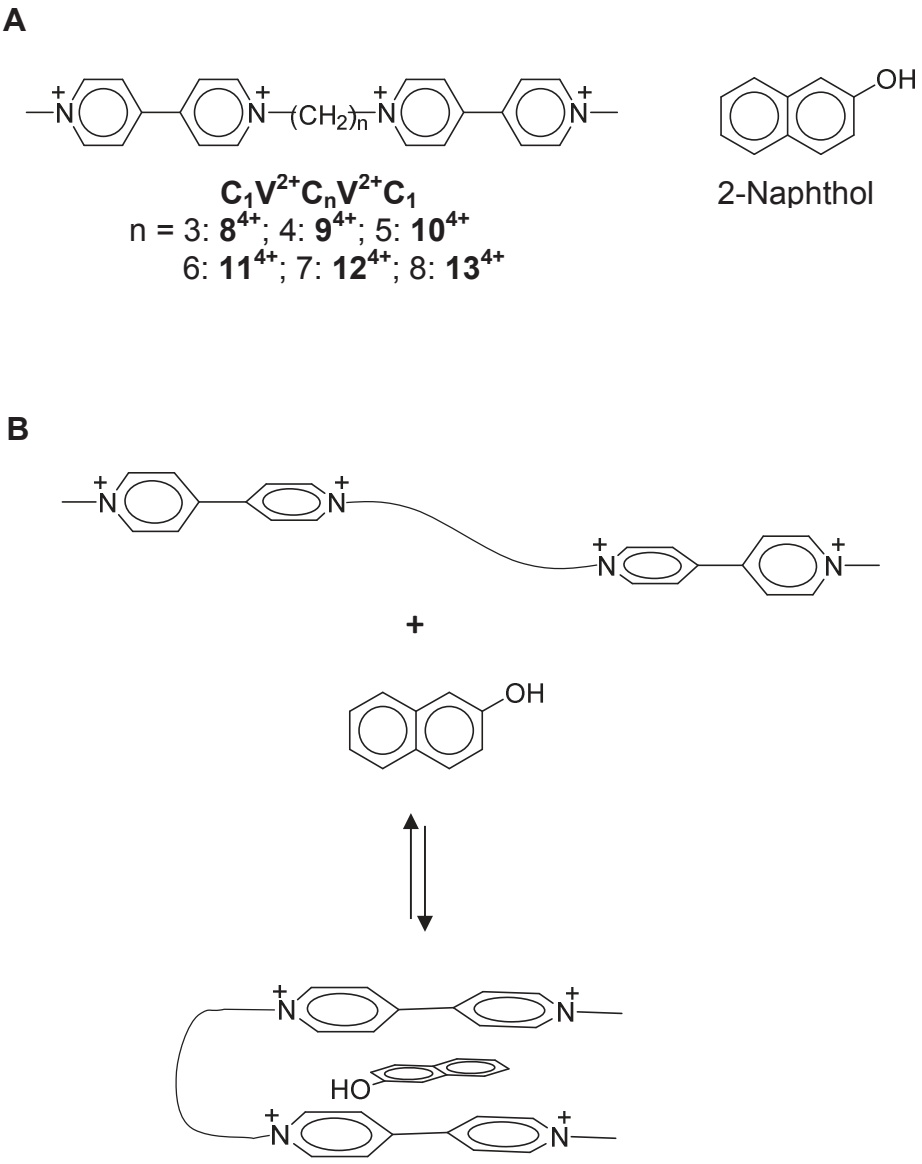

Figure 11: (A) schematic representation of both the polymethylene spacered bis (methyl viologen) derivatives and 2-naphthol and (B) schematic representation for the complexation equilibrium between the polymethylene spacered bis-methyl viologen derivative and 2-naphthol with their formed sandwich-type complex.[90]

The bis-viologens spacered with odd numbers of methylene groups form more stable charge transfer complexes with 2-naphthol than those spacered with even numbers of carbon atoms.

The bis-viologens with five or seven methylene groups as spacers showed more complexation with 2-naphthol than those with four, six and eight groups.[90] This even-odd trend was clarified by the backbone strain of folding that happens in the formation of sandwich-type complexes. Such a spacer length dependence of complexation is explained by an enthalpy change because of backbone strain in the sandwich-type complex. [90]

4. Inclusion complexes of viologens with cucurbit[8]uril

Kim and co-workers,[91] observed that upon a 2-electron reduction of the guest (DMV^{2+}) in the presence of cucurbit[8]uril (CB[8]), 1:1 inclusion complex DMV^{2+}-CB[8] can be converted completely and reversibly to the 2:1 inclusion complex of $(DMV^{+\bullet})_2$-CB[8], as illustrated in Figure 12. From spectroelectrochemical studies, the apparent dimerization constant of $DMV^{+\bullet}$ in the presence of equimolar CB[8] host was determined to be 2×10^7 M^{-1} which is about 10^5 times larger than that of $DMV^{+\bullet}$ alone in aqueous solution.

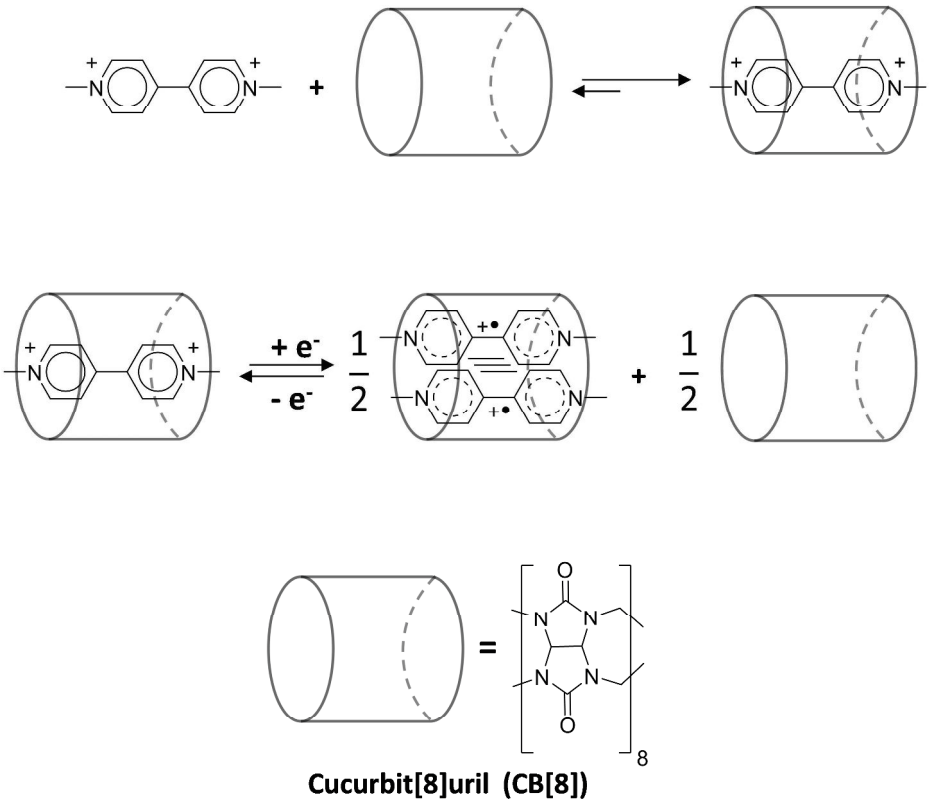

Figure 12: Schematic illustration for the inclusion of DMV^{2+} and $DMV^{+\bullet}$ in cucurbit[8]uril CB[8] to form the inclusion complexes: DMV^{2+}-CB[8] and $(DMV^{+\bullet})_2$-CB[8] respectively.[91]

The molecule cucurbit[8]uril (CB[8]), a highly symmetrical macropolycyclic cavitand comprising eight glycoluril units, has a large hydrophobic cavity bordered on the top and bottom with carbonyl functions.(92) Therefore, this molecule is considered as perfect hosts for hydrophobic planar guests in aqueous solution. In addition, due to its huge cavity, CB[8] accommodates serenely two equivalents of the hydrophobic guest. This significant enhancement in stability of the dicationic dimer $(DMV^{+\bullet})_2$ within the hydrophobic cavity of CB[8] can be attributed to the apparent high local concentration of $DMV^{+\bullet}$ dications within the cavity of CB[8]. (91)

Unprecedented three-states supramolecular switch has been achieved (93) using the cucurbit[8]uril capacity to encapsulate/release two guest molecules in controlled manner (Figure 13). The inclusion complexes of cucurbit[8]uril with hetero-guest-pair (Donor-Acceptor) or homo-guest-pair (two associated donors or two π-dimerized acceptors) have been exchanged and controlled reversibly by chemical or electrochemical stimuli. Addition of 1 equivalent of cucurbit[8]uril (CB[8]) into an aqueous solution containing a 1:1 mixture of tetrathiafulvalene derivative and dimethyl viologen DMV^{2+} under an inert atmosphere produced the 1:1:1 ternary inclusion complex $(DMV^{2+}.TTF)$-CB[8] (Figure 13). The latter inclusion complex is the predominant species under zero electrochemical bias whereas the reduction of the DMV^{2+} unites produced the encapsulated dimerized viologen radical cations $(DMV^{+\bullet})_2$-CB[8]. Finally, the oxidation of TTF units resulted in the formation of stable tetrathiafulvalene radicals dimer inside CB[8] cavity, $(TTF^{+\bullet})_2$-CB[8] with the subsequent ejection of the other species in each case. This dramatic interconversion has been also performed chemically.(94)

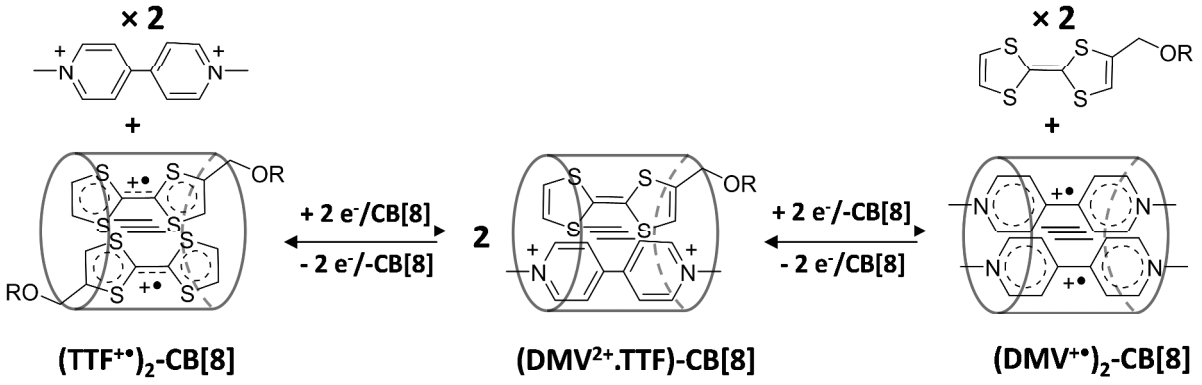

Figure 13: Schematic presentation of the significant function of CB[8] encapsulation for the stabilization of dimerized radicals. CB[8] improves essentially the formation and driving of three-state supramolecular switches: $(DMV^{2+}.TTF)$-CB[8], $(TTF^{+\bullet})_2$-CB[8], and $(DMV^{+\bullet})_2$-CB[8].(93)

The structure of the 1:1:1 ternary inclusion complex (DMV^{2+}.TTF)-CB[8] has been confirmed by ^{1}H-NMR, 2D NMR (ROESY and DOSY), UV-Visible and mass spectrometry. The formation of the donor-acceptor complex between DMV^{2+} and TTF guest units inside the cavity of CB[8] has been supported by un upfield shifting of ^{1}H-NMR signals for both DMV^{2+} and TTF protons relative to those in the free molecules. The diffusion-ordered NMR spectroscopy (DOSY) demonstrated the stability of the 1:1:1 ternary inclusion complex (DMV^{2+}.TTF)-CB[8] as the signals of DMV^{2+} and TTF are all lined up. Also from the diffusion coefficient of (DMV^{2+}.TTF)-CB[8] (2.37×10^{-10} m^2 s^{-1}), the hydrodynamic volume was assessed to be 2480 $Å^3$ which is almost 1.7 times larger than that of CB[8] alone (1500 $Å^3$).[93]

The UV-Visible spectrum of (DMV^{2+}.TTF)-CB[8] is characterized by a charge transfer absorption band at 925 nm while upon reduction (electrochemical or chemically with $Na_2S_2O_4$) of (DMV^{2+}.TTF)-CB[8], new bands at 366, 539, and 894 nm were observed. These absorption bands agree well with the drastic formation of the π-dimerized viologen radicals inside the CB[8] cavity[91], i.e. $(DMV^{+\bullet})_2$-CB[8].

5. Viologen-containing catenanes

Another interesting class of switchable systems containing viologens is catenanes. These systems are formed by reaction of a cyclic viologen or its precursor with cyclic electron donor which results in mechanically interlocked rings. If two rings are linked, the resulting double-ring structure is called a [2] catenane and the names [3]-, [4]- or [5]catenane mean that the catenanes are incorporating 3, 4 and 5 rings respectively.[95]

In the cyclobis(paraquat-4,4'-biphenylene) $\mathbf{14}^{4+}$ (Figure 14), the π-electron deficient ring system has the ability to allow co-occupancy of two π-electron-rich guests. Thus, interactions occurred between two heterocycles (TTF-TTF) housed within the host cyclophane $\mathbf{14}^{4+}$ as in $\mathbf{15}^{4+}$ (2:1 complex ($\mathbf{TTF_2\text{-}8}^{4+}$)) and using such system, [3]catenanes $\mathbf{16}^{4+}$ and $\mathbf{17}^{4+}$ have been prepared and investigated (Figure 14).[82]

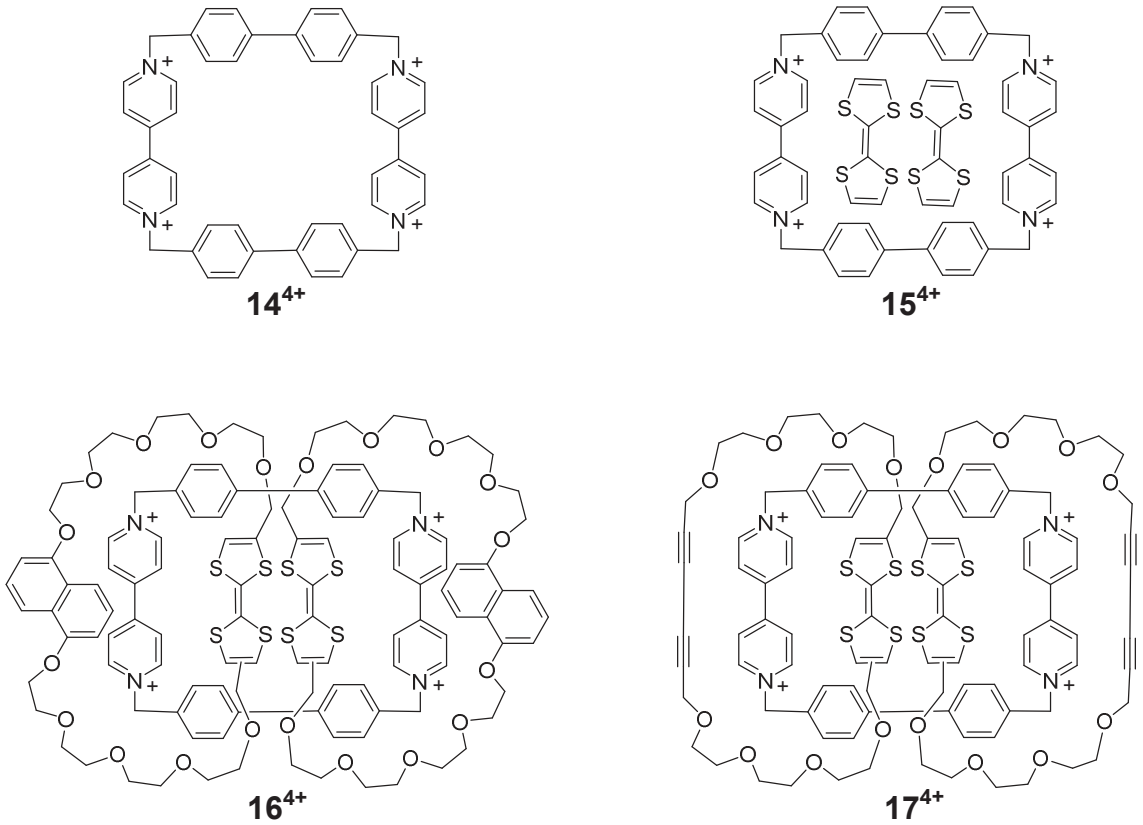

Figure 14: Structural formulas of the cyclobis(paraquat-4,4'-biphenylene) $\mathbf{14}^{4+}$, the [3]pseudorotaxane $\mathbf{15}^{4+}$, and the [3]catenanes $\mathbf{16}^{4+}$ and $\mathbf{17}^{4+}$.[82]

The X-ray crystallographic analyses performed on the [3]pseudorotaxane $\mathbf{15}^{4+}$ and the [3]catenanes $\mathbf{16}^{4+}$ and $\mathbf{17}^{4+}$ showed that the two TTF units are located comfortably inside the cyclophane $\mathbf{14}^{4+}$ cavity. In the [3]pseudorotaxane $\mathbf{15}^{4+}$, the TTF...TTF average interplanar distance was 3.77 Å. The stabilization of the TTF units within the cyclophane $\mathbf{14}^{4+}$ in the [3]pseudorotaxane $\mathbf{15}^{4+}$ cavity is due to the π-π stacking interactions between the bipyridinium faces and the involved TTF units. In addition to the latter interactions, the [C-H...O] hydrogen bondings occurred between some oxygen atoms of the crown ether and the α-bipyridinium hydrogens contribute in stabilizing the oxidized forms of the [3]catenanes $\mathbf{16}^{4+}$ and $\mathbf{17}^{4+}$.[96 - 98] Therefore, the planes of TTF units are being separated by 3.68 Å in $\mathbf{16}^{4+}$ and $\mathbf{17}^{4+}$.

The redox-induced switching process for the [3]catenanes $\mathbf{16}^{4+}$ are depicted in Figure 15. The same redox-induced switching trends are noted for the [3]catenanes $\mathbf{17}^{4+}$.

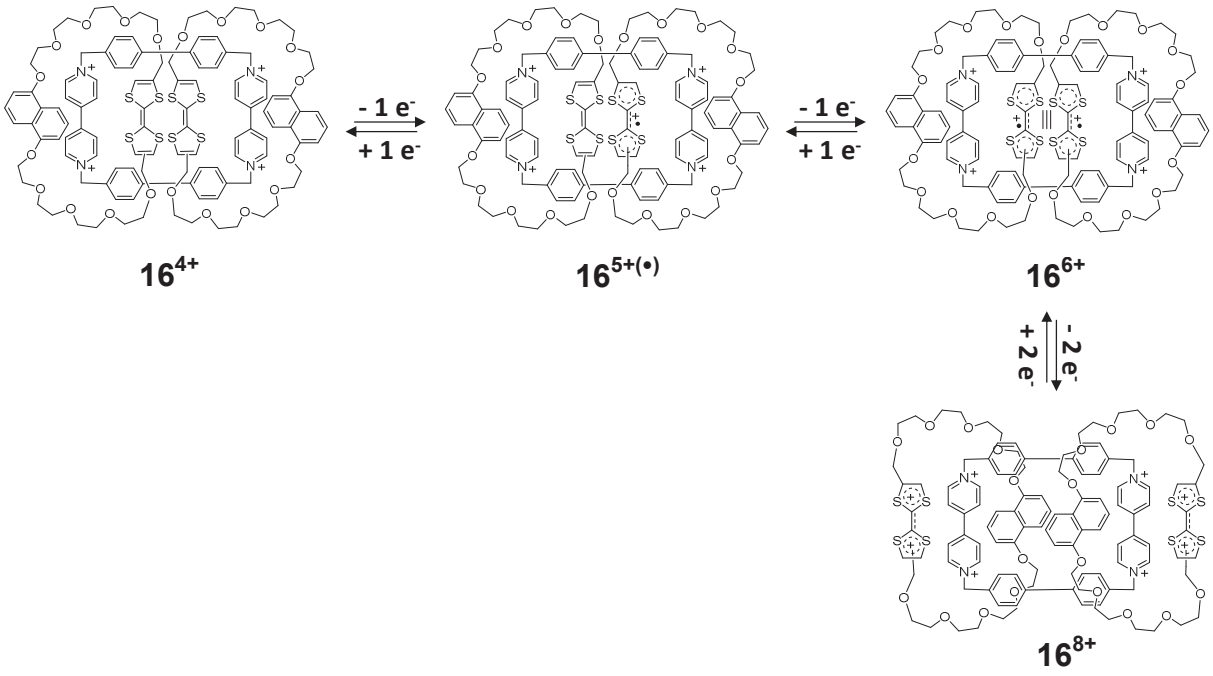

Figure 15: The redox-induced switching process for the [3]catenane $\mathbf{16}^{4+}$.[82]

The first two 1-electron oxidation processes led to the formation of the stabilized mixed-valence dimer: the paramagnetic $(TTF)_2^{+\bullet}$ species $\mathbf{16}^{5+(\bullet)}$ and the diamagnetic radical-cation dimer: $(TTF^{+\bullet})_2$ $\mathbf{16}^{6+}$ respectively. The further two-electron oxidation process led to the ejection of the TTF^{2+} units from inside the cyclophane cavity as result of the coulombic repulsion forces growing between the $\mathbf{14}^{4+}$ cavity and TTF^{2+} units and then the

dioxynaphthalene (DNP) stations occupy the cavity (**16**$^{8+}$). The reversibility of these processes was evidenced by the re-reduction processes of **16**$^{8+}$ and **17**$^{8+}$ which reformed the stabilized dimers $(TTF^{+\bullet})_2$ in **16**$^{6+}$ and **17**$^{6+}$ as well as the ground states **16**$^{4+}$ and **17**$^{4+}$.

6. Pre-organized multi-viologen derivatives

Related to cyclopyridinophanes, bridged bis-viologens have been prepared (**18**$^{4+}$, Figure 16) in which the two bipyridinium units are connected by flexible xylyl linkages.[99]

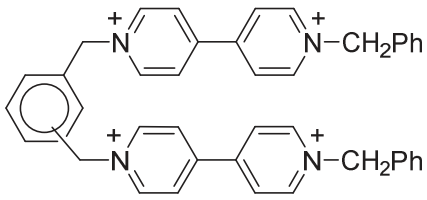

o-18^{4+}, m-18^{4+}, p-18^{4+}

Figure 16: Schematic presentation for bis-viologen species with flexible xylyl linkage.[99]

The electrochemical and spectral measurements have shown that the nature of the linkage separating the two bipyridinium units dictates the type and the efficiency of the bipyridinium radicals dimerization. The bis-viologen **p-18**$^{4+}$ persists as monomeric radical cation (95-98%) in 10^{-4} M solution of methanol or acetonitrile. As expected, intramolecular dimerization was observed with **o-18**$^{2+\bullet}$ and **m-18**$^{2+\bullet}$ and increases in the order **p-18**$^{2+\bullet}$ < **m-18**$^{2+\bullet}$ < **o-18**$^{2+\bullet}$. Harriman and co-workers[100] showed that after the two electron-reduction process for the analogous species (with methyl instead of benzyl groups) of **o-18**$^{4+}$ and **m-18**$^{4+}$, a species was formed with intramolecular radical association (overlap of bipyridinium π orbitals) where coulombic repulsions are minimised.

In each intramolecular dimerization, the two radical cations prefer close contacts and this can be achieved by skew stacking. It was shown that near IR absorption band attributed to the intramolecular dimerization are shifted to longer wavelengths when increasing the distance provided by the spacer between the radical cations. For example, the dimerized **o-18**$^{2+\bullet}$ shows a band at 830 nm which becomes very broad and locates at 980 nm in the dimerized **m-18**$^{2+\bullet}$. In these systems, energy levels of the dimerized viologen radicals are splitted into lower

ground state and higher excited state levels, and the difference between them and hence the near IR band energy decreases with the weakening of the dimerization. Similarly, increasing the temperature from 240 to 320 K weakens the interaction and thus causes a red shift (15-30 nm) of the intramolecular dimerization bands.[99]

Rosseinsky and Monk[101] have performed electrochemical and spectrochemical studies on a species having four bipyridyl units around a central durene core (**19**$^{8+}$, Figure 17 A).

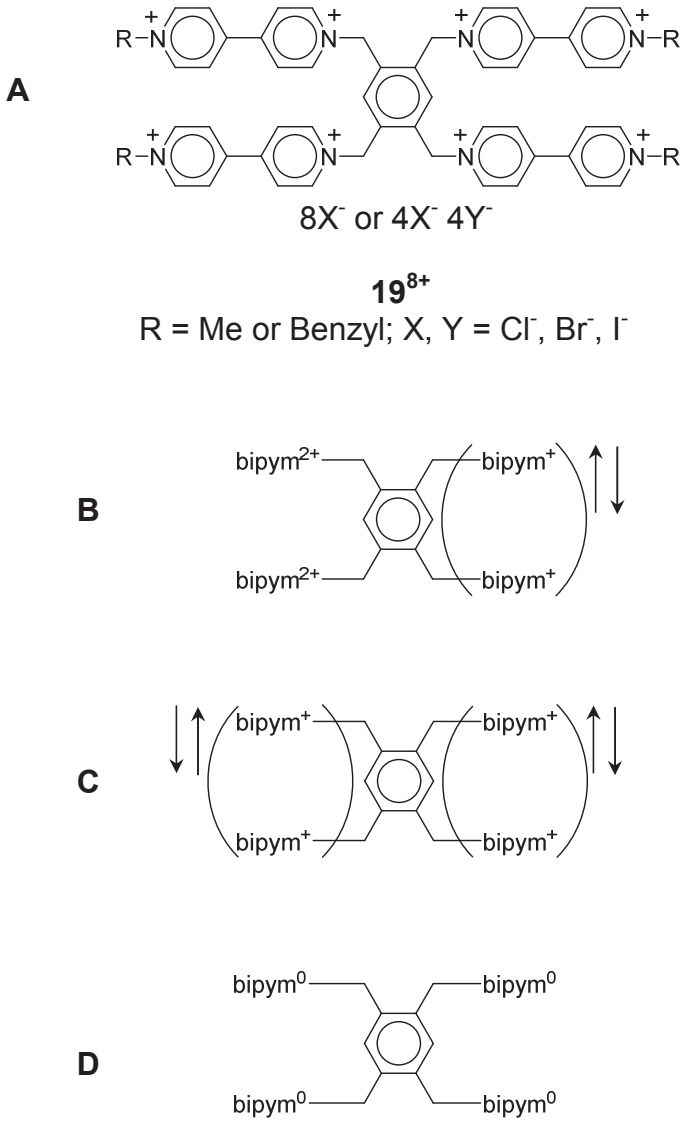

Figure 17: (A) Schematic presentation of four diquaternised bipyridine moieties spacered with a central durene core. Proposed structures of redox states of **19**$^{8+}$: (B) pink two-electron reduced species; (C) purple four-electron reduced species (D) beige fully reduced species. Opposed arrows represent possibly paired electron spins of the radical odd electrons of the half-reduced bipyridinium (bipym) moieties.[101]

Three separate reduction products were identified as illustrated in Figure 17 B-D. The first was a pink di-reduced species (Figure 17 B), with two of the viologen units forming the dicationic dimer. The double dimer (purple) was formed by a further two-electron reduction (Figure 17 C) and the third (beige) fully-reduced and the neutral product was formed after reduction with further four electrons.

A novel type of electrical and chemical switch molecules, $\mathbf{20}^{4+}$ and $\mathbf{21}^{4+}$ (Figure 18), were prepared and characterized by Su and co-workers.[102] The redox properties were investigated in DMF solutions by cyclic voltammetry. The cyclic voltammograms of both compounds: $\mathbf{20}^{4+}$ and $\mathbf{21}^{4+}$ are depicted in Figure 19.

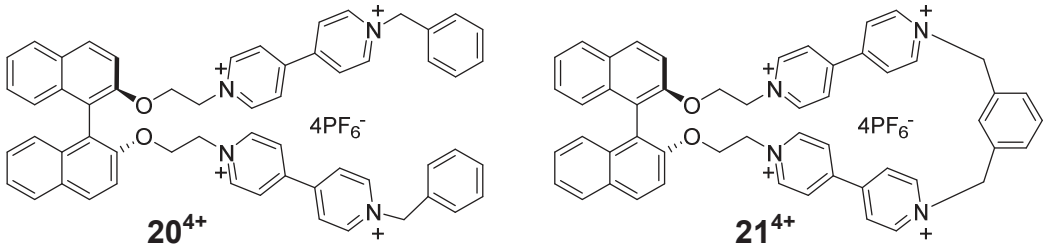

Figure 18: Schematic presentation for the open-ring and cyclic bis-viologens $\mathbf{20}^{4+}$ and $\mathbf{21}^{4+}$ respectively.[102]

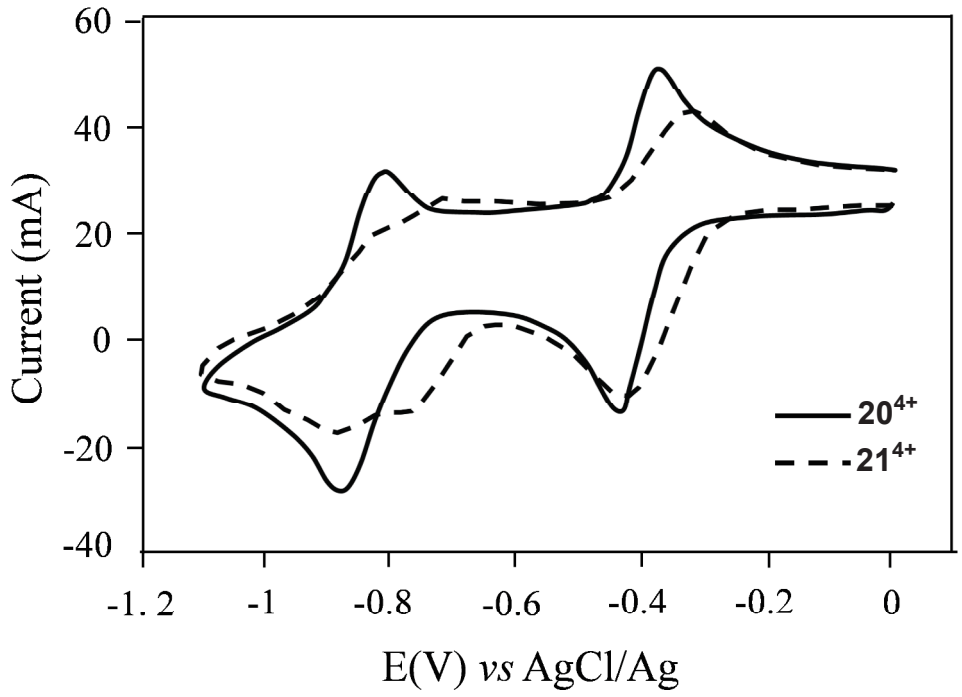

Figure 19: Cyclic voltammograms for the open-ring tetracation $\mathbf{20}^{4+}$ and the cyclic tetracation $\mathbf{21}^{4+}$ in DMF + 0.1 M Bu_4NClO_4, working electrode: glassy carbon disk (2mm in diameter), counter electrode: platinum stick (1 mm thick), E *vs* AgCl/Ag, 298 K.[102]

The open-ring tetracation $\mathbf{20}^{4+}$ displays two redox processes at $E_{1/2}$ = -0.40 and -0.85 V (*vs* AgCl/Ag, DMF + 0.1 M Bu_4NClO_4) which are comparable to the redox pattern of 1,1'-dipropyl-4,4'-bipyridinium tetra-hexafluorophosphate (BPP). This indicates that the two bipyridinium units in $\mathbf{20}^{4+}$ behave individually with no interaction between them.

Conversely, three redox processes at $E_{1/2}$ = -0.37, -0.74, and -0.86 V were found for the cyclic tetracation $\mathbf{21}^{4+}$. These reduction waves correspond to the formation of $\mathbf{21}^{(2+\bullet)}$, $\mathbf{21}^{+\bullet}$ and $\mathbf{21}^{0}$ respectively. Considering the similar chemical constitutions of $\mathbf{20}^{4+}$ and $\mathbf{21}^{4+}$, the intramolecular interaction between the two viologen radical cations in $\mathbf{21}^{(2+\bullet)}$ can explain this different redox behavior. Such interaction stabilizes both the bis-radical cation $\mathbf{21}^{(2+\bullet)}$ and the radical cation-neutral $\mathbf{21}^{+\bullet}$ forms.[102, 99, 103]

The bulk electrochemical or chemical reductions of $\mathbf{20}^{4+}$ and $\mathbf{21}^{4+}$ (1 - 3 × 10^{-4} M) results in the absorption spectra of non- and dimerized viologen radical cations respectively[104]. In addition, the intermolecular association was also demonstrated upon the electrochemical reduction for the open-ring tetracation $\mathbf{20}^{4+}$ at higher concentration (2.8 mM).

A three-dimensional redox-switchable system has been described in which twelve viologen subunits are grafted by means of flexible linkers onto a suitable hexa-substituted rigid scaffold (C60 fullerene core, Figure 20). The reversible molecular reorganization of discrete peripheral viologen groups around the sphere of C60 can be electrochemically controlled leading to π-dimerization and afford six viologen radical cation pairs, each pair being situated in a restricted space.[105] Figure 20 shows the schematic representation of the reversible switching between the charge-repelled form of $\mathbf{22}^{24+}$ (12 directions for viologen arms) and the dimerized viologen form $\mathbf{22}^{12+}$ (6 directions for dimerized viologen arms). This conversion is achieved by the reversible 12 electrons-reduction process and compared with the reversible dimerization of the reference compound $\mathbf{23}^{4+}$.

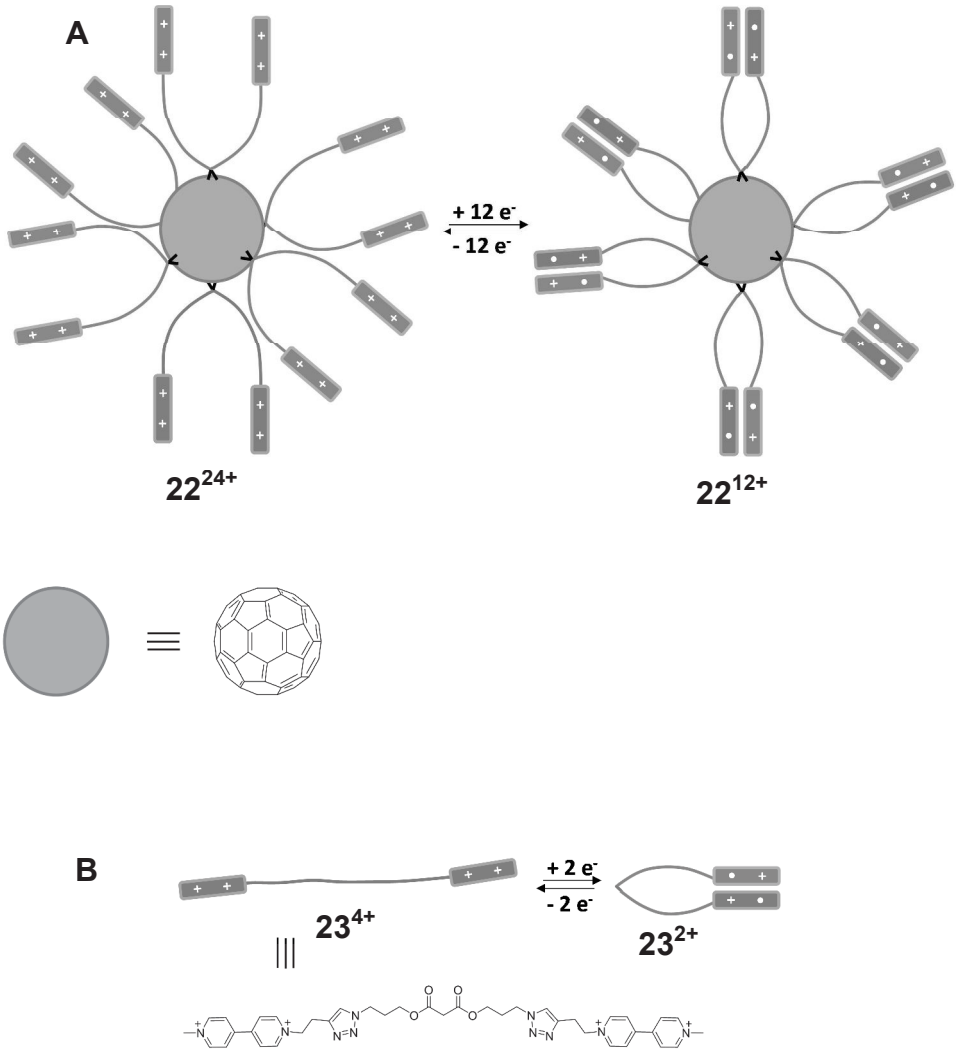

Figure 20: schematic representation of chemical or electrochemical (A) reversible switching between the charge-repelled form of $\mathbf{22}^{24+}$ and the dimerized viologen form $\mathbf{22}^{12+}$ and (B) reversible dimerization of the reference compound $\mathbf{23}^{4+}$.[105]

The electrochemical properties of $\mathbf{22}^{24+}$ and $\mathbf{23}^{4+}$ have been studied in dimethylformamide, acetonitrile and aqueous solutions by cyclic voltammetry and differential pulse voltammetry. The first reduction wave for $\mathbf{22}^{24+}$ and $\mathbf{23}^{4+}$ led to the formation of the viologen radical cation forms $\mathbf{22}^{(12+\bullet)}$ and $\mathbf{23}^{(2+\bullet)}$ respectively. These reduction processes are shifted significantly to less negative potentials compared to that of the dimethyl viologen as a result of the intramolecular dimerization between the viologen radicals. In the case of the $\mathbf{22}^{24+}$, a stronger dimerization occurred between its viologen radicals compared to the bis-viologen $\mathbf{23}^{4+}$ as evidenced by the larger positive shift of the first reduction. In addition, the first reduction of $\mathbf{22}^{24+}$ happened at more positive potential in aqueous solution than in DMF due to the more stabilized coupling between the viologen radical cations in aqueous solutions. Similar electronic absorption spectra for both of $\mathbf{22}^{(12+\bullet)}$ and $\mathbf{23}^{(2+\bullet)}$ have been featured which agree well with the interacted viologen radical forms. However, the form $\mathbf{22}^{(12+\bullet)}$ exhibited higher intensity diagnostic signature for the formation of π-dimers which supports again the stronger dimerization of the viologen radicals in $\mathbf{22}^{(12+\bullet)}$.(85 , 100, 106-110)

7. Conclusion, Perspectives and Objectives

This bibliographical chapter provides detailed characteristics of viologen moieties and their analogous involved in redox-switchable molecular systems and supramolecular architectures. Intra-molecular association or dimerization between these moieties as their radical forms is considered as the main driving forces within the switchable systems for the generation of the reversible electrochemical, photochemical or chemical-triggered movements. Several efficient strategies to enhance the stability of these dimers and consequently to promote the switching properties or movements have been selected and presented in this chapter.

In this context, our objective was to develop new types of molecular switches and materials containing the viologen unit. In chapter II, we will investigate the formation of two electrochemically induced molecular switches. The first is based on a viologen dimerization occurred within the reduced forms of two bis-viologen cyclophane derivatives. The formation of inclusion complexes was then investigated by the ability of these two reduced cyclophanes to encapsulate dimethyl viologen radical. In chapter III, we will develop novel electron-responsive coordination polymers employing again the π-dimerization between the viologen radicals as driving forces for their switchable movements. These coordination polymers change their morphology and viscosity properties in response to electrical and photochemical stimuli which promote the folding of the polymer chains.

References

1. C. A. Hunter and J. K. M. Sanders, *J. Am. Chem. Soc.*, **1990**, 112, 5525.
2. F. Cozzi, F. Ponzini, R. Annunziata, M. Cinquini and J. S. Siegel, *Angew. Chem. Int. Ed. Engl.*, **1995**, 34, 1019; *Angew. Chem.*, **1995**, 107, 1092.
3. C. A. Hunter, J. K. M. Sanders, G. S. Beddard and S. Evans, *J. Chem. Soc. Chem. Commun.*, **1989**, 1765.
4. D. B. Amabilino and J. Fraser Stoddart, *Pure Appl. Chem.*, **1993**, 65, 2351.
5. Z.-T. Li, P. C. Stein, N. Svenstrup, K. H. Lund and J. Becher, *Angew. Chem. Int. Ed. Engl.*, **1995**, 34, 2524; *Angew. Chem.*, **1995**, 107, 2719.
6. A. C. Fahrenbach, C. J. Bruns, D. Cao and J. F. Stoddart, *Acc. Chem. Res.*, **2012**, 45, 1581.
7. D. Canevet, M. Sall_, G. Zhang, D. Zhang and D. Zhu, *Chem. Commun.*, **2009**, 2245.
8. C. Wang, D. Zhang and D. Zhu, *J. Am. Chem. Soc.*, **2005**, 127, 16372.
9. Y. Liu, A. H. Flood, P. A. Bonvallet, S. A. Vignon, B. H. Northrop, H.-R. Tseng, J. O. Jeppesen, T. J. Huang, B. Brough, M. Baller, S. Magonov, S. D. Solares, W. A. Goddard, C.-M. Ho and J. F. Stoddart, *J. Am. Chem. Soc.*, **2005**, 127, 9745.
10. S. S. Andersen, A. I. Share, B. L. C. Poulsen, M. Kørner, T. Duedal, C. R. Benson, S. W. Hansen, J. O. Jeppesen and A. H. Flood, J. Am. Chem. Soc., **2014**, 136, 6373.
11. E. H. Witlicki, S. S. Andersen, S. W. Hansen, J. O. Jeppesen, E. W. Wong, L. Jensen and A. H. Flood, *J. Am. Chem. Soc.*, **2010**, 132, 6099.
12. F. Sun, F. Hu, G. Zhang and D. Zhang, *Chem. Asian J.*, **2012**, 7, 183.
13. M. Wielopolski, C. Atienza, T. Clark, D. M. Guldi and N. Martin, *Chem. Eur. J.*, **2008**, 14, 6379.
14. J. Santos, B. M. Illescas, Nazario Mart_n, J. Adrio, J. C. Carretero, R. Viruela, E. Orti, F. Spanig and D. M. Guldi, *Chem. Eur. J.*, **2011**, 17, 2957 –2964.
15. H.-P. Jia, J. Ding, Y.-F. Ran, S.-X. Liu, C. Blum, I. Petkova, A. Hauser and S. Decurtins, *Chem. Asian J.*, **2011**, 6, 3312.
16. H. Kobayashi, A. Kobayashi and H. Tajima, *Chem. Asian J.*, **2011**, 6, 1688.
17. M. L. Waters, *Curr. Opin. Chem. Biol.*, **2002**, 6, 736.
18. C. R. Martinez and B. L. Iverson, *Chem. Sci.*, **2012**, 3, 2191.
19. M. T. Stone, J. M. Heemstra and J. S. Moore, *Acc. Chem. Res.*, **2006**, 39, 11.
20. M. L. Waters, *Acc. Chem. Res.*, **2013**, 46, 873.

21. B.-Q. Wang, F.-F. Wang, F. Ma, Z.-R. Li, D. Wu, H.-L. Xu and F. L. Gu, *J. Comput. Methods Sci. Eng.*, **2010**, 10, 357.
22. M. Capdevila-Cortada and J. J. Novoa, *Chem. Eur. J.*, **2012**, 18, 5335.
23. K. H. Hausser and J. N. Murrell, *J. Chem. Phys.*, **1957**, 27, 500.
24. B. Badger, B. Brocklehurst and R. D. Russell, *Chem. Phys. Lett.*, **1967**, 1, 122.
25. B. Badger and B. Brocklehurst, *Nature*, **1968**, 219, 263.
26. E. M. Kosower, and J. L. Cotter, *J. Am. Chem. Soc.*, **1964**, 86, 5524.
27. R. H. Boyd and W. D. Phillips, *J. Chem. Phys.*, **1965**, 43, 2927.
28. I. C. Lewis and L. S. Singer, *J. Chem. Phys.*, **1965**, 43, 2712.
29. J. H. Fuhrhop, P. Wasser, D. Riesner and D. Mauzerall, *J. Am. Chem. Soc.*, **1972**, 94, 7996.
30. M. G. Hill, K. R. Mann, L. L. Miller and J. F. Penneau, *J. Am. Chem. Soc.*, **1992**, 114, 2728.
31. J. A. E. H. van Haare, L. Groenendaal, E. E. Havinga, R. A. J. Janssen and E. W. Meijer, *Angew. Chem. Int. Ed. Engl.*, **1996**, 35, 638; *Angew. Chem.*, **1996**, 108, 696.
32. L. van het Goor, P. T. van Duijnen, C. Koper, L. W. Jenneskens, R. W. A. Havenith and F. Hartl, *J. Solid State Electrochem.*, **2011**, 15, 2107.
33. P. M. S. Monk. The Viologens: Physicochemical Properties, Synthesis and Applications of the Salts of 4, 4'-Bipyridine. Chichester: John Wiley & Sons Ltd. **1998**.
34. L. Michaelis and E.S. Hill, *J. Gen. Physiol.*, **1933**, 16, 859.
35. D. R. Rosseinsky and P. M. S. Monk, *J. Chem. Soc., Faraday Trans.*, **1993**, 89, 219.
36. F. Ito and T. Nagamura*, J. Photochem. Photobiol.* C, **2007**, 8, 174.
37. A. G. Evans, J. C. Evans and M. W. Baker, *J. Am. Chem. Soc.*, **1977**, 99, 5882.
38. T. Sakano, F. Ito, T. Ono, O. Hirata, M. Ozawa and T. Nagamura, Thin Solid Films, **2010**, 519, 1458.
39. W. M. Schwarz, PHD. Thesis, University of Wisconsin, **1961**.
40. J. B. Torrance, B. A. Scott, B. Welber, F. B. Kaufman and P. E. Seiden, *Phys. Rev.* B **1979**, 19,730.
41. J.-M. Lü , S. V. Rosokha and J. K. Kochi, *J. Am. Chem. Soc.* **2003**, *125*, 12161.
42. M. R. Geraskina, A. T. Buck and A. H. Winter, *J. Org. Chem.*, **2014**, 79, 7723.
43. M. J. Blandamer, J. A. Brivati, M. F. Fox, M. C. R. Symons and G. S. P. Verma, *Trans. Faraday Soc.*, 1**967**, **63**, 1850.

44. V. Khodorkovsky, L. Shapiro, P. Krief, A. Shames, G. Mabon, A. Gorgues and M. Giffard, *Chem. Commun.*, **2001**, 2736.
45. J. F. Stargardt and F. M. Hawkridge, *Anal. Chim. Acta*, **1983**, 146, 1.
46. K. M. Shin, G. D. Watt, B. Zhang, J. N. Harb, R. G. Harrison, S. I. Kim and S. J. Kim, *J. Electroanal. Chem.*, **2006**, 598, 22.
47. K. Maruszewski, A. Hreniak, J. Czyżewski, and W. Stręk, *Opt. Mater.*, **2003**, 22, 221.
48. R. Dabestani, K. J. Reszka and M. E. Sigman, *J. Photochem. Photobiol.* A: Chem., **1998**, 117, 223.
49. A. G. Evans, J. C. Evans and M. W. Baker, *J. Chem. Soc., Perkin Trans. 2*, **1977**, 1787.
50. J. C. Evans, A. G. Evans, N. H. N.-Sorkhabi, A. Y. Obaid and C. C. Rowlands, *J. Chem. Soc., Perkin Trans. 2*, **1985**, 315.
51. J.C. Evans, M. H. N. Sorkhabi and C. C. Rowlands, *Tetrahedron*, **1982**, 2581.
52. A. G. Evans, J. C. Evans and M. W. Baker, *J. Chem. Soc., Perkin Trans. 2*, **1975**, 1310.
53. C. L. Bird and A. T. Kuhn, *Chem. Soc. Rev.*, **1981**, 10, 49.
54. A. Iordache, R. Kannappan, E. Métay, M.-C. Duclos, S. Pellet-Rostaing, M. Lemaire, A. Milet, E. Saint-Aman and C. Bucher, Org. Biomol. Chem., **2013**, 11, 4383.
55. A. Iordache, M. Oltean, A. Milet, F. Thomas, B. Baptiste, E. Saint-Aman and C. Bucher, J. Am. Chem. Soc., **2012**, 134, 2653.
56. R. G. Pearson. Survey of Progress in Chemistry, **1965**, 5, 1.
57. R. G. Compton, A. M. Waller, P. M. S. Monk and D. R. Rosseinsky, *J. Chem. Soc., Faraday Trans.*, **1990**, 86, 2583.
58. R. J. Jasinski, *J. Electrochem. Soc.*, **1977**, 124, 637.
59. H. T. van Dam and J. J. Ponjeé, *J. Electrochem. Soc.*, **1974**, 121, 1555.
60. L. Michaelis, *Chem. Rev.*, **1935**, 16, 243.
61. T. M. Bockman and J. K. Kochi, *J. Org. Chem.* **1990**, *55*, 4127.
62. C. Femoni, M. C. Iapalucci, G. Longoni, C. Tiozzo, J. Wolowska, S. Zacchini and E. Zazzaroni, *Chem. Eur. J.* **2007**, *13*, 6544.
63. C. Lee, Y. M. Lee, M. S. Moon, S. H. Park, J. W. Park, K. G. Kim and S.-J. Jeon , *J. Electroanal. Chem.*, **1996**, 416, 139.
64. J. M. Spruell, *Pure Appl. Chem.*, **2010**, 82, 2281.
65. M. R. Geraskina, A. S. Dutton, M. J. Juetten, S. A. Wood and A. H. Winter, *Angew. Chem. Int. Ed.*, **2017**, 56, 9435.
66. A. Y. Ziganshina, Y. H. Ko, W. S. Jeon and K. Kim, *Chem. Commun.*, **2004**, 806.

67. Y. H. Ko, E. Kim, I. Hwang and K. Kim, *Chem. Commun.*, **2007**, 1305.
68. M. Yoshizawa, K. Kumazawa and M. Fujita, *J. Am. Chem. Soc.*, **2005**, 127, 13456.
69. C. A. Christensen, L. M. Goldenberg, M. R. Bryce and J. Becher, *Chem. Commun.*, **1998**, 509.
70. H. Spanggaard, J. Prehn, M. B. Nielsen, E. Levillain, M. Allain and J. Becher, *J. Am. Chem. Soc.*, **2000**, 122, 9486.
71. J. Lyskawa, M. Sall_, J. Y. Balandier, F. Le Derf, E. Levillain, M. Allain, P. Viel and S. Palacin, *Chem. Commun.*, **2006**, 2233.
72. I. Aprahamian, J.-C. Olsen, A. Trabolsi and J. F. Stoddart, *Chem. Eur. J.*, **2008**, 14, 3889.
73. P.-T. Chiang, N.-C. Chen, C.-C. Lai and S.-H. Chiu, *Chem. Eur. J.*, **2008**, 14, 6546.
74. M. Hasegawa, K. Daigoku, K. Hashimoto, H. Nishikawa and M. Iyoda, *Bull. Chem. Soc. Jpn.*, **2012**, 85, 51.
75. C. Bejger, C. M. Davis, J. S. Park, V. M. Lynch, J. B. Love and J. L. Sessler, *Org. Lett.*, **2011**, 13, 4902.
76. E. Gomar-Nadal, L. Mugica, J. Vidal-Gancedo, J. Casado, J. T. L. Navarrete, J. Veciana, C. Rovira and D. B. Amabilino, *Macromolecules*, **2007**, 40, 7521.
77. C. Zhou, J. Tian, J.-L. Wang, D.-W. Zhang, X. Zhao, Y. Liu and Z.-T. Li, *Polym. Chem.*, **2014**, 5, 341.
78. W.-K. Wang, Y.-Y. Chen, H. Wang, D.-W. Zhang, Y. Liu and Z.-T. Li, *Chem. Asian J.*, **2014**, 9, 1039.
79. J. Tian, Y.-D. Ding, T.-Y. Zhou, K.-D. Zhang, X. Zhao, H. Wang, D.-W. Zhang, Y. Liu and Z.-T. Li, *Chem. Eur. J.*, **2014**, 20, 575.
80. L. Chen, S.-C. Zhang, H. Wang, Y.-M. Zhou, Z.-T. Li and D.-W. Zhang, *Tetrahedron*, **2014**, 70, 4778.
81. L. Zhang, T.-Y. Zhou, J. Tian, H. Wang, D.-W. Zhang, X. Zhao, Y. Liu and Z.-T. Li, *Polym. Chem.*, **2014**, 5, 4715.
82. J. M. Spruell, A. Coskun, D. C. Friedman, R. S. Forgan, A. A. Sarjeant, A. Trabolsi, A. C. Fahrenbach, G. Barin, W. F. Paxton, S. K. Dey, M. A. Olson, D. Ben_tez, E. Tkatchouk, M. T. Colvin, R. Carmielli, S. T. Caldwell, G. M. Rosair, S. G. Hewage, F. Duclairoir, J.-L. Seymour1, A. M. Z. Slawin, W. A. Goddard III, M. R. Wasielewski, G. Cooke and J. F. Stoddart, *Nat. Chem.*, **2010**, 2, 870.
83. G. Barin, A. Coskun, D. C. Friedman, M. A. Olson, M. T. Covin, R. Carmielli, S. K. Dey, O. A. Bozdemir, M. R. Wasielewski and J. F. Stoddart, *Chem. Eur. J.*, **2011**, 17, 213.

84. C. Wang, S. M. Dyar, D. Cao, A. C. Fahrenbach, N. Horwitz, M. T. Colvin, R. Carmieli, C. L. Stern, S. K. Dey, M. R. Wasielewski and J. F. Stoddart, *J. Am. Chem. Soc.*, **2012**, 134, 19136.
85. S.-I. Imabayashi, N. Kitamura and S. Tazuke, *J. Electroanal. Chem.*, **1988**, 243, 143.
86. T. Watanabe and K. Honda, *J. Phys. Chem.*, **1982**, 86, 2617.
87. M. Shimomura, K. Utsigi and K. Okuyama, *J. Chem. Soc., Chem. Commun.*, **1986**, 1805.
88. A. Deronzier, B. Galland and M. Vieira, *Nouv. J. Chim.*, **1982**, 6, 97.
89. M. Future and S. Nazakura, *Chem. Lett.*, **1980**, 821.
90. S. K. Lee, S. Y. Shin, S. Lee, C. Lee and J. W. Park, *J. Chem. Soc., Perkin Trans. 2*, **2001**, 1983.
91. W. S. Jeon, H.-J. Kim, C. Lee and K. Kim. *Chem. Commun.*, **2002**, 1828.
92. K. Kim, N. Selvapalam, Y. H. Ko, K. M. Park, D. Kim and J. Kim., *Chem. Soc. Rev.*, **2007**, 36, 267.
93. I. Hwang, A. Y. Ziganshina, Y. H. Ko, G. Yun and K. Kim, *Chem. Commun.*, **2009**, 416.
94. J. M. Spruell, *Pure Appl. Chem.*, **2010**, 82, 2281.
95. J. W. Steed, D. R. Turner and K. J. Wallace. Core Concepts in Supramolecular Chemistry and Nanochemistry: From Supramolecules to Nanotechnology. John Wiley & Sons Ltd. 2007.
96. F. M. Raymo, M. D. Bartberger, K. N. Houk and J. F. Stoddart, *J. Am. Chem. Soc.*, **2001**, 123, 9264.
97. O. Š. Miljanić , W. R. Dichtel , S. I. Khan , S. Mortezaei , J. R. Heath and J. F. Stoddart, *J. Am. Chem. Soc.*, **2007**, 129, 8236.
98. J. M. Spruell, W. F. Paxton, J.-C. Olsen, D. Benítez, E. Tkatchouk, C. L. Stern, A. Trabolsi, D. C. Friedman, W. A. Goddard and J. F. Stoddart, *J. Am. Chem. Soc.*, **2009**, 131, 11571.
99. W. Geuder, S. Hünig and A. Suchy, *Tetrahedron*, **1986**, 42, 1665.
100. P. Neta, M.-C. Richoux and A. Harriman, *J. Chem. Soc., Faraday Trans. 2*, **1985**, 81, 1427.
101. D. R. Rosseinsky and P. M. S. Monk, *J. Appl. Electrochem.*, **1994**, 24, 1213.
102. J. Deng, N. Song, Q. Zhou and Z. Su, *Org. Lett.*, **2007**, 9, 5393.
103. P. L. Anelli, P. R. Ashton, R. Ballardini, V. Balzani, M. Delgado, M. T. Gandolfi, T. T. Goodnow, A. E. Kaifer and D. Philp, *J. Am. Chem. Soc.*, **1992**, 114, 193.
104. T. Watanabe and K. Honda, *J. Phys. Chem.*, **1982**, 86, 2617.

105. J. Iehl, M. Frasconi, H.-P. J. de Rouville, N. Renaud, S. M. Dyar, N. L. Strutt, R. Carmieli, M. R. Wasielewski, M. A. Ratner, J.-F. Nierengartenc and J. Fraser Stoddart, *Chem. Sci.*, **2013**, 4, 1462.

106. S. Hünig, W. Geuder and A. Suchy, *Angew. Chem. Int. Ed. Eng.*, **1983**, 22, 489.

107. M. Itoh and E. M. Kosower, *J. Am. Chem. Soc.*, **1968**, 90, 1843.

108. J. W. Van Leeuwen, C. Van Dijk and C. Veeger, *Eur. J. Biochem.*, **1983**, 135, 601.

109. R. Kannappan, C. Bucher, E. Saint-Aman, J.-C. Moutet, A. Milet, M. Oltean, E. M´etay, S. Pellet-Rostaing, M. Lemaire and C. Chaix, *New J. Chem.*, **2010**, 34, 1373.

110. A. Iordache, M. Retegan, F. Thomas, G. Royal, E. Saint-Aman and C. Bucher, *Chem. Eur. J.*, **2012**, 18, 7648.

CHAPTER II

Electrochemical and spectroelectrochemical investigation of flexible bis-viologen cyclophanes and their inclusion complexes

Preamble

In this chapter, our objective was to investigate the ability of two cyclic bis-viologen molecules to generate π-dimers. Then, formation of redox activated molecular switches based on inclusion complexes has been investigated. These inclusion complexes involve encapsulation of dimethyl viologen radicals within the cavities of cyclic bis-viologen radicals' molecules.

1. Introduction

1.1 Viologen-Cyclopyridinophane

Cyclopyridinophanes or cyclophanes are molecules in which the viologen forms part of a cyclic structure.[1] These systems have been widely investigated because of their ability to form inclusion complexes with electron-rich species, the most famous example being the tetracationic "blue-box" (cyclo(bis(paraquat-*p*-phenylene)) developed by Stoddart.[2] In addition, and connected to our work, the close proximity of the two viologen units in cyclophanes may also facilitates their π-dimerization. In order to study the possibility and effect of dimerization between viologen radical cations in cyclophanes, several attempts have been made by preparing species with spacers of varying length and flexibility to bind the two viologen units.[3-9] Below are some representative examples and applications of such systems.

1.2 The cyclo(bis(paraquat-p-phenylene) system ($CBPQT^{4+}$)

In a pioneer study,[8, 9] Hünig *et al.* prepared three isomeric structures of cyclopyridinophane species ($CBPQT^{4+}$) in which two viologen units are inflexibly separated by ortho-ortho, ortho-meta, and meta-meta xylene bridges (Figure 2.1). It was shown that the π-dimerization which occurs between the two connected viologen radical cations upon the $1e^-$-reduction of the viologen subunits is exclusively intramolecular in the case of the ortho-ortho and ortho-meta isomers, *i.e.* without detected formation of intermolecular dimers. Probably because of its less-favorable geometry, the formation of interamolecular dimer with the meta-meta isomer is difficult and intermolecular association can be observed.[9]

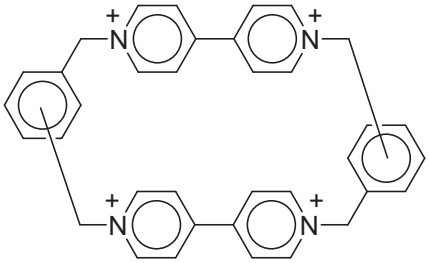

($CBPQT^{4+}$)

Figure 2.1: Schematic presentation for cyclopyridinophane species ($CBPQT^{4+}$) prepared by Hünig *et al*.[8, 9]

The cyclophane, cyclobis(paraquat-p-phenylene) ($CBPQT^{4+}$, para-para isomer), exhibits very interesting properties and has been much exploited. This π-electron deficient cycle, also named "blue box" by Stoddart,[2] is considered as one of the most common recognition components used to encircle single π-electron rich unit. For example, the association of $CBPQT^{4+}$ with redox-active π-electron-rich units, such as tetrathiafulvalene (TTF) has been employed in the electrochemical induced molecular switches, these latter was used in many studies, for information storage, micro-scale mechanical actuation, or molecular storage and release.[10]

The cyclobis(paraquat-p-phenylene) $CBPQT^{4+}$ can be also employed for a redox-controlled encapsulation of species. In particular, as represented in Figure 2.2, Stoddart *and coll.* found[11] that upon reduction of the $CBPQT^{4+}$ cycle into its corresponding diradical dication ($CBPQT^{2(+\bullet)}$), a strong inclusion complex may be formed with the dimethylviologen viologen radical cation ($V^{+\bullet}$) or close derivatives (Figure 2.2). This inclusion complex ($CBPQT^{2(+\bullet)}\subset V^{+\bullet}$) relies on the radical-radical interactions between the bipyridinium radical cation units ($BIPY^{+\bullet}$).[12] Reoxidation of this triradical cationic complex then releases the V^{2+} guest. The formation of the trisradical tricationic complex has been confirmed by X-ray crystallography.[11] It was observed that this inclusion complex is associated with three PF_6^- counter ions in the solid state. This is supporting the speculation that each of the $BIPY^{2+}$ units has been undoubtedly reduced to their radical cationic structure, $BIPY^{+\bullet}$. Also, the $V^{+\bullet}$ radical cation is located inside the cavity of the $CBPQT^{2(+\bullet)}$ ring adopting a centrosymmetric manner with a centroid-to-centroid separation was 3.22 Å between the $V^{+\bullet}$ radical cation and each of the $BIPY^{+\bullet}$ radical cation subunits of the cyclophane ring $CBPQT^{2(+\bullet)}$.

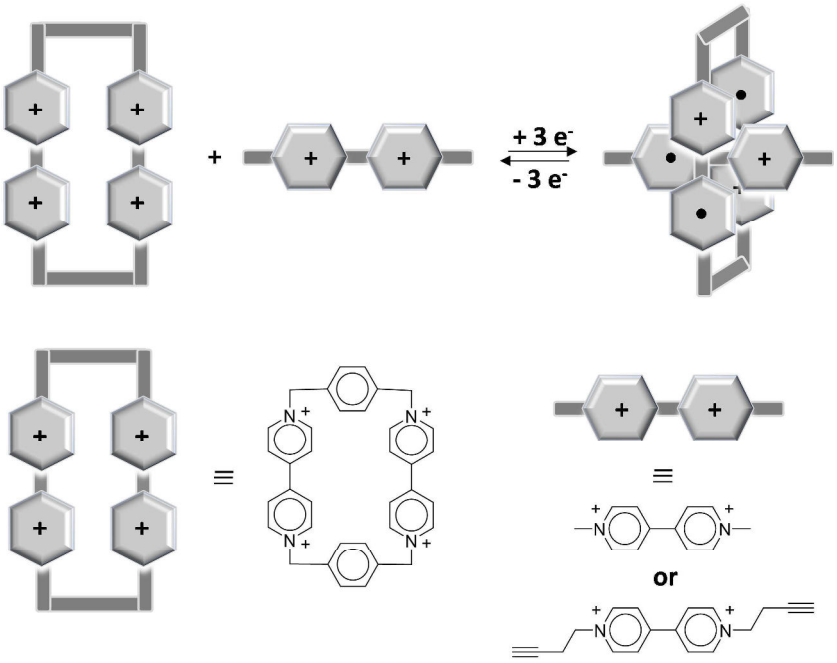

Figure 2.2: Schematic presentation of the formation of a 3-radical inclusion complex based on ($CBPQT^{4+}$) and BIPY units.[11]

The electronic spectrum of the 1:1 inclusion complex, $CBPQT^{2(+\bullet)}\subset V^{+\bullet}$, is characterized by absorption features of $BIPY^{+\bullet}$ radical-radical interactions, namely a broad near-IR band, as well as absorption bands in the 500-600 nm region.[12] Theoretical DFT calculation for the SOMO orbitals of the trisradical complex $CBPQT^{2(+\bullet)}\subset DMV^{+\bullet}$ revealed that the orbital

overlap happens essentially between the guest $V^{+\bullet}$ with only one of the $BIPY^{+\bullet}$ units in the $CBPQT^{2(+\bullet)}$ ring, while the other $BIPY^{+\bullet}$ remains almost free.[11, 12]

This result can be corroborated using cyclic voltammetry.[11, 12] As shown in Figure 2.3, the first reduction peak of an equimolar mixture of $CBPQT^{4+}$ and V^{2+} (-0.32 V *vs* Ag/AgCl) is a three-electron process: two electrons attributed to the diradical dication $CBPQT^{2(+\bullet)}$ and the third electron corresponding to the reduction of the V^{2+} to $V^{+\bullet}$. Consequently, the $V^{+\bullet}$ is included spontaneously inside the $CBPQT^{2(+\bullet)}$ cavity to form the trisradical triscationic complex $CBPQT^{2(+\bullet)}\subset V^{+\bullet}$. As written previously, in this inclusion complex, only one $BIPY^{+\bullet}$ unit of the cyclophane interacts with the $V^{+\bullet}$ group, the second $BIPY^{+\bullet}$ unit remaining free. For this reason, the second reduction wave observed at -0.76 V corresponds to the reduction of the free $BIPY^{+\bullet}$ unit of the ring to its neutral form while the remaining viologen radicals, stabilized as dimer, are both reduced via a two electron signal at more negative potential (-0.87 V). This interesting redox driven switch concept between the $CBPQT^{4+}$ host and V^{2+} guest has been employed to construct chemical and electrochemical switching within mechanically interlocked rotaxanes.[13]

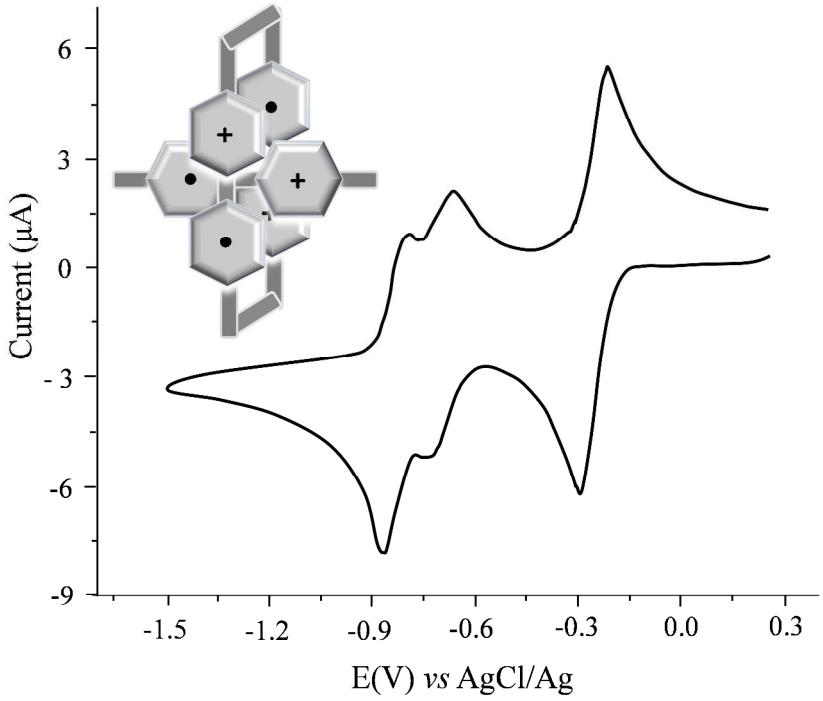

Figure 2.3: Cyclic voltamograms for a 1:1 mixture of $CBPQT^{4+}$ and V^{2+}. 1mM in CH_3CN + 0.1 M $TBAPF_6$, working electrode: 0.071 cm^2 glassy C, scan rate: 200 $mV.s^{-1}$, E *vs* AgCl/Ag, Temp.: 298 K.[11]

1.3 Rotaxane and pseudorotaxane

The $CBPQT^{4+}$ moiety has also been used for the preparation of ordered molecular assemblies such as rotaxanes and catenanes.[10, 13] A rotaxane is a mechanically interlocked molecular system consisting of a dumbbell-shaped molecule 'spindle' which is threaded through a macrocycle ring. The ends 'stoppers' of the dumbbell molecule are bulky components, larger than the internal diameter of the ring which prevents dissociation (unthreading) of the components. Rotaxane may comprise one or more ring-shaped species. Pseudorotaxanes are similar to rotaxanes except they do not have the bulky end groups. Therefore, the passage of the ring over the end groups is possible, allowing the dissociation of the pseudorotaxane components.[1]

For example, following the work presented previously[11], Stoddart and coll. have prepared and investigated the properties of the rotaxane $\mathbf{1}^{6+}$, composed of a $CBPQT^{4+}$ ring which is mechanically interlocked around a dumbbell containing a $BIPY^{2+}$ unit. $\mathbf{1}^{6+}$ and its cyclic voltammogramm are represented in Figure 2.4.

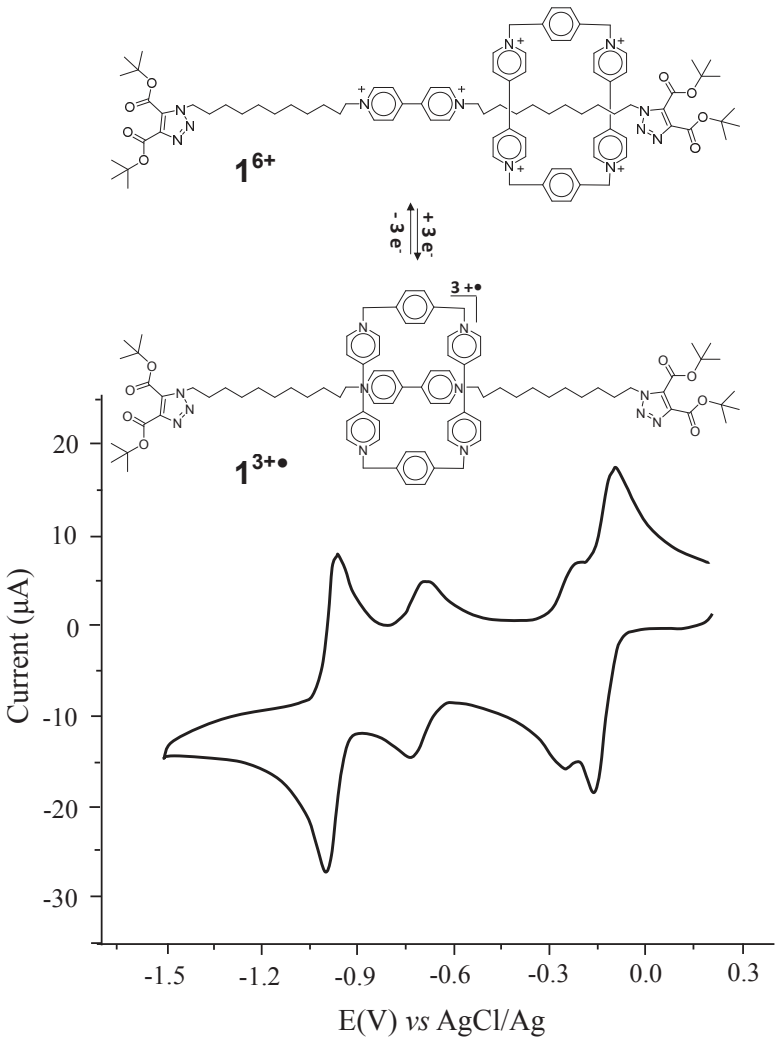

Figure 2.4: Representation of the redox-triggered switch based on the rotaxane $\mathbf{1}^{6+}$ and cyclic voltamogram of $\mathbf{1}^{6+}$. Conc.: 1mM in CH_3CN + 0.1 M $TBAPF_6$, working electrode: 0.071 cm^2 glassy C, scan rate: 200 $mV.s^{-1}$, E *vs* AgCl/Ag, Temp.: 298 K.[11]

The CV curve of $\mathbf{1}^{6+}$ is first characterized by two different electron-transfer processes. The first reduction peak corresponds to a two-electron process, which forms two paired $BIPY^{+\bullet}$ radical cations: one of the dumbbell $BIPY^{+\bullet}$ unit and another from the ring resulting in the bisradical tetracationic inclusion complex $\mathbf{1}^{(2+)2(+\bullet)}$. The reduction of the remaining unpaired $BIPY^{2+}$ in the $CBPQT^{(2+)(+\bullet)}$ ring occurs via subsequent one-electron transfer reduction peak, and generates the trisradical tricationic $\mathbf{1}^{3(\bullet+)}$ form represented. All these reduction processes are independent on the scan rate in the range 50-1000 mV s^{-1}, *i.e.* they are totally reversible because the mechanical bond excludes the possibility of dissociation the trisradical tricationic $\mathbf{1}^{3(\bullet+)}$ form.[11]

Several donor-acceptor rotaxanes containing the $CBPQT^{4+}$ host as ring and the bipyridinium unit in their dumbbell components have been synthesized, in which electron rich dioxynaphthalene (DNP) or tetrathiafulvalene (TTF) groups have been added.[11] Such structures and their redox behavior are illustrated in Figures 2.5 and 2.6. In these systems, the $CBPQT^{4+}$ ring sticks exclusively around the 1,5-dioxynaphthalene (DNP) and tetrathiafulvalene (TTF) electron-rich units in both $\mathbf{2}^{6+}$ and $\mathbf{3}^{6+}$ respectively.

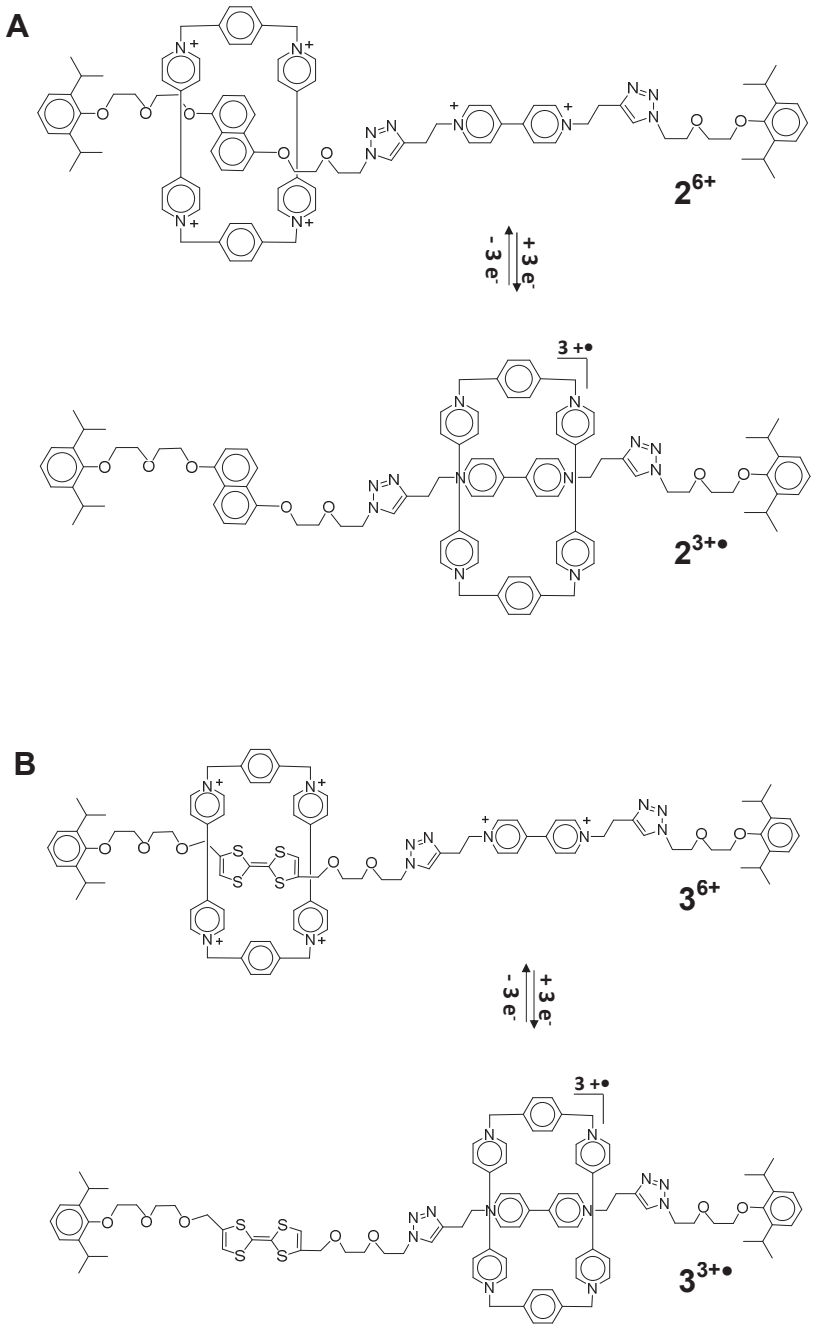

Figure 2.5: Mechanically interlocked bistable [2]rotaxanes: (A) $\mathbf{2}^{6+}$ and (B) $\mathbf{3}^{6+}$ incorporating the $CBPQT^{4+}$ ring and two donor groups 1,5-dioxynaphthalene (DNP) and tetrathiafulvalene (TTF) units respectively along with a $BIPY^{2+}$ unit.[12, 13]

Under zero electrochemical bias, the $CBPQT^{4+}$ ring in $\mathbf{2}^{6+}$ locates on the DNP unit as it is demonstrated by an absorption band at 529 nm in the electronic spectrum. This band is due to the characteristic charge transfer interaction between the electron-donating DNP unit and the $CBPQT^{4+}$ ring. When a potential of -0.7 V is applied, new absorption bands at 536 and 1075 nm arise as a signature of the formation of a pimer among viologen radical cations. In other words, the $CBPQT^{2(+\bullet)}$ cavity surrounds the $BIPY^{+\bullet}$ unit of the thread. Again, after switching back the potential to 0 V, the electronic spectrum progressively returns back to the first spectrum showing that the bistable [2]rotaxane $\mathbf{2}^{6+}$ is reversibly reduced. Therefore, the bistable [2]rotaxane $\mathbf{2}^{6+}$ switches fully within its two DNP and $BIPY^{+\bullet}$ stations and the encircling $CBPQT^{4+}$ ring (Figure 2.5 A).[12, 13]

The switching behavior of $\mathbf{3}^{6+}$ is similar to that mentioned for $\mathbf{2}^{6+}$ (Figure 2.5 B). Initially, the π-electron-deficient $CBPQT^{4+}$ ring spends its time localized on the π-electron-rich TTF unit. Upon the 3-electron reduction of the bistable [2]rotaxane $\mathbf{3}^{6+}$, the resulting bis-reduced ring $CBPQT^{2(+\bullet)}$ encircle the single reduced viologen radical cation ($V^{+\bullet}$) to form a strong triradical cationic inclusion complex within $\mathbf{3}^{3+\bullet}$. Reoxidation of $\mathbf{3}^{3+\bullet}$ reproduces the initial charge transfer complex TTF-$CBPQT^{4+}$ in the bistable [2]rotaxane $\mathbf{3}^{6+}$. Interestingly, in this example, additional redox-induced switching processes are brought by the presence of the redox-active TTF unit. Indeed, the stepwise oxidation of TTF to $TTF^{+\bullet}$ and then TTF^{2+} was shown to destabilizes the mechanically interlocked molecule, consequently rendering its complexation with $CBPQT^{4+}$ invalid.[12] The $CBPQT^{4+}$ ring in $\mathbf{3}^{6+}$ is guessed to carry forward and backward along the dumbbell axis without any preferences. Giving back the system to zero bias (E = 0 V *vs* AgCl/Ag) reduces the TTF^{2+} dication back to its neutral state TTF and hence returning to the initial charge transfer complex TTF-$CBPQT^{4+}$.

Using the previous concept, a tristable [2]rotaxane $\mathbf{4}^{6+}$ has been reported by Stoddart and co-workers (Figure 2.6)[12].

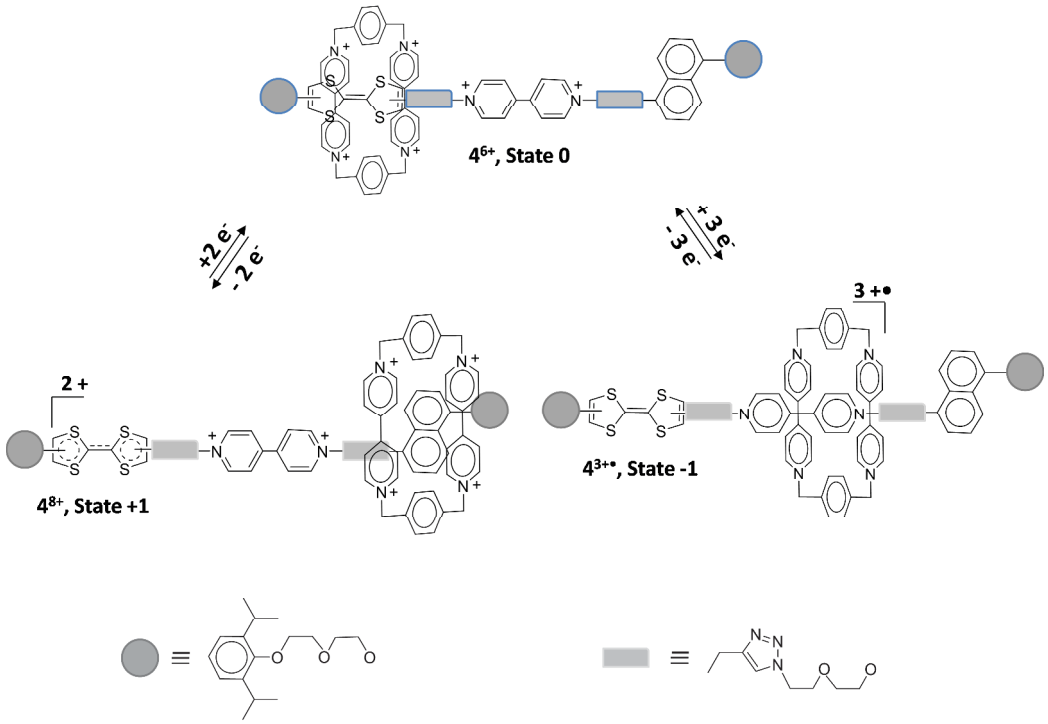

Figure 2.6: Mechanically interlocked tristable [2]rotaxanes $\mathbf{4}^{6+}$.[12]

In this system, the three recognition units TTF, DNP and $BIPY^{2+}$ have the ability to guide differently the $CBPQT^{4+}$ ring depending on electron transfer. This results in three distinct states. In the initial state (state 0), the tetracationic bis-viologen $CBPQT^{4+}$ ring prefers to form a charge transfer complex with the electron rich unit tetrathiafulvalene TTF than with the dioxynaphthalene unit DNP. Therefore, $CBPQT^{4+}$ ring spends the majority of its time localized on the TTF station, while the $CBPQT^{4+}$ and $BIPY^{2+}$ units are repelled by the columbic interaction.[13, 14] Oxidation of the TTF unit to $TTF^{+\bullet}$ and then TTF^{2+} results in a strong repulsion of the $CBPQT^{4+}$ ring, making it to pass over the $BIPY^{2+}$ unit and encircle the DNP unit, as the only other available π-electron donor. A second charge transfer complex is thus formed (state +1).[14] Moreover, reduction of the initial charge transfer complex (state 0) results in the motion of the ring from the TTF unit to the $BIPY^{+\bullet}$ unit with the formation of the strong $CBPQT^{2(+\bullet)}\subset BIPY^{+\bullet}$ complex (state -1). The molecular rotoxane $\mathbf{4}^{6+}$ thus represents a wonderful molecular switch having three different stable states controlled by three different electrical inputs (neutral, positive and negative electrochemical bias *vs* AgCl/Ag). This

system is based on different and complementary molecular recognition moieties capable of donor-acceptor stacking and radical π-dimerization[13].

Figure 2.7 A illustrates the threading and dethreading of pseudorotaxane $\mathbf{5}^{4+}$.[15] In its initial form, the self-complexation occurred between the dioxynaphthalene arm and the cyclic tetracationic bis-viologen. This self-assembling process involves donor-acceptor interactions between π-electron rich arm (1,5- dioxynaphthalene) and the π-electron deficient bipyridinium units, as well as hydrogen bonding of protons of the disubstituted naphthalene residue with π-faces of the p-xylyl units of the tetracationic cyclophane and also between the oxygen atom of terminal methoxy residue and the α-proton of bipyridinium unit.[16]

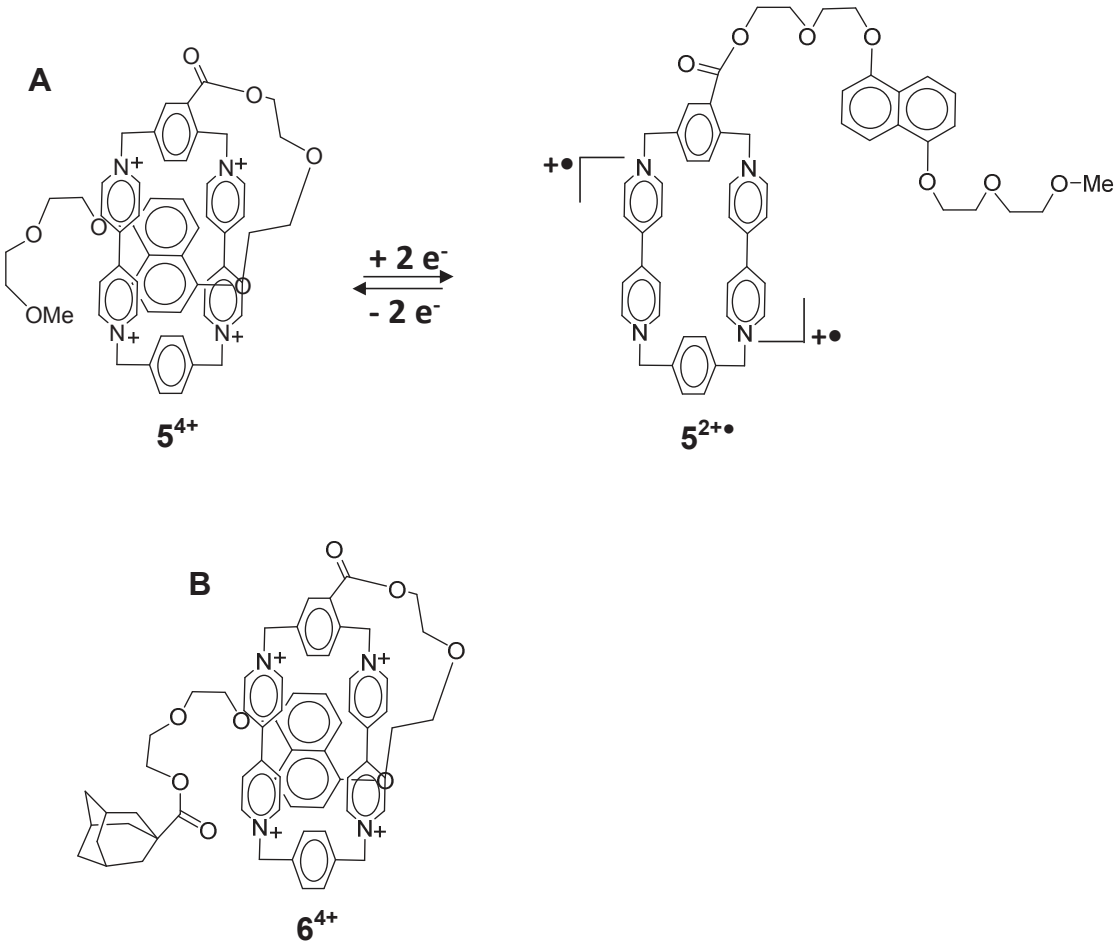

$\mathbf{5}^{4+}$ $\mathbf{5}^{2+\bullet}$ $\mathbf{6}^{4+}$

Figure 2.7: (A) Electrochemically driven dethreading-rethreading of pseudorotaxane $\mathbf{5}^{4+}$ and (B) the model compound: the mechanically interlocked rotaxane $\mathbf{6}^{4+}$.[15]

The complexation of the naphthalene arm with the cyclophane cavity in $\mathbf{5}^{4+}$ results in a charge transfer band at 515 nm with ε = 650 M^{-1} cm^{-1} in water. This band is practically the same as

that of the mechanically interlocked rotaxane $\mathbf{6}^{4+}$ (Figure 2.7 B). In addition, the fluorescence of the dioxynaphthalene unit in both $\mathbf{5}^{4+}$ and $\mathbf{6}^{4+}$ is completely quenched (the low-energy charge transfer levels prevent the fluorescence). These two observations besides the proton NMR studies show that the oxidized form $\mathbf{5}^{4+}$ exists as 100% self-complexed species like in the rotaxane $\mathbf{6}^{4+}$.[15] The reduction of cyclophane in $\mathbf{5}^{4+}$ weakens these stabilizing interactions, accordingly permitting the naphthalene derivative arm to dethread from the cyclophane cavity forming $\mathbf{5}^{2+\bullet}$. The solution of the dethreaded $\mathbf{5}^{2+\bullet}$ shows the well-known absorption bands of the reduced bipyridinium units. This process of threading/dethreading of the naphthalene derivative arm is reversible and can be repeated by oxidation/reduction cycles.[15-17]

2. Objectives of this Chapter

In this chapter, and in the context of a collaboration with the research group of Dr. Jean Weiss in Strasbourg (Laboratoire de chimie des ligands à architecture contrôlée), our aim was to investigate the properties of two new bis-viologen cyclophane derivatives $\mathbf{R5}^{4+}$ and $\mathbf{R7}^{4+}$. In these two cyclic bis-viologen systems, represented in Figure 2.8, the two bipyridinium units are linked by simple alkyl chains having five or seven methylene groups. These two cyclophane are thus expected to be much more flexible than in the previously described $CBPQT^{4+}$ ring. These compounds have been prepared in Strasbourg and our role was to evaluate their electrochemical behavior and in particular to evaluate their ability to form intramolecular π-dimers in organic solvents.

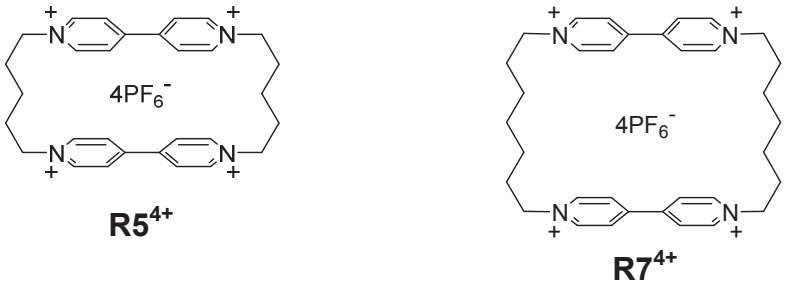

$\mathbf{R5}^{4+}$ $\mathbf{R7}^{4+}$

Figure 2.8: New bis-viologen cyclophane derivatives $\mathbf{R5}^{2+}$ and $\mathbf{R7}^{4+}$.

In addition, our second goal was to investigate the possible formation of electrochemically-activated inclusion complexes. The tested inclusion complexes are based on encapsulation of dimethyl viologen radical $\mathbf{V}^{+\bullet}$ within the bis (radical-cation) cyclophane cavities $\mathbf{R5}^{2(+\bullet)}$ or $\mathbf{R7}^{(+\bullet)}$ and will be presented in third part of this Chapter. Two rational routes have been tested to attain the targeted redox activated trisradical cationic inclusion complexes $\mathbf{Rn}^{2(+\bullet)}\subset\mathbf{V}^{+\bullet}$ (see

Figure 2.9). The first strategy was to realize the direct electrochemical 3-electron reduction of an equimolar solution of dimethyl viologen $\mathbf{V}^{2+}$ and $\mathbf{R5}^{4+}$ or $\mathbf{R7}^{4+}$. The second tested method was to add the dimethyl viologen radical $\mathbf{V}^{+\bullet}$ to a solution of bis (radical-cation) form, *i.e.* $\mathbf{R5}^{2(+\bullet)}$ or $\mathbf{R7}^{(+\bullet)}$.

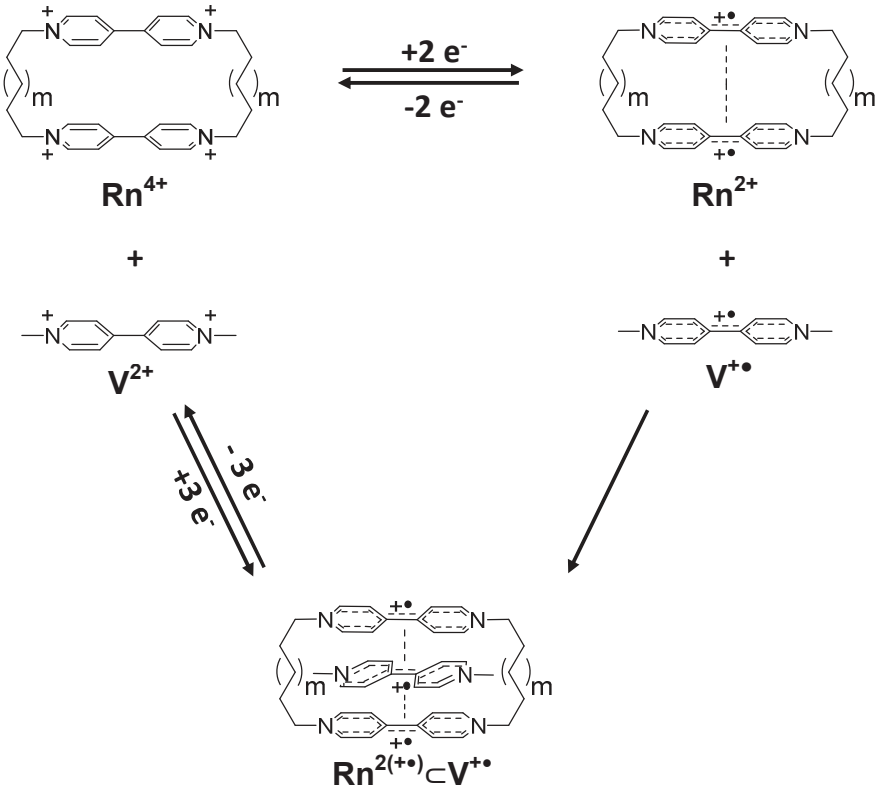

Figure 2.9: Representation of the two possible strategies to generate inclusion complexes $\mathbf{Rn}^{2(+\bullet)}\subset\mathbf{V}^{+\bullet}$ from the bis-viologen cyclophanes $\mathbf{Rn}^{2+}$. n refer to the alkyl chain linking the two viologen units; m = 1 ($\mathbf{R5}^{4+}$), 3 ($\mathbf{R7}^{4+}$).

3. Bis-viologen cyclophanes

3.1 Electrochemical studies

The electrochemical properties of the two bis-viologen cyclophanes $\mathbf{R5}^{4+}$ and $\mathbf{R7}^{4+}$ along with reference compound, dimethyl viologen $\mathbf{V}^{2+}$ have been investigated in DMF+0.1M TBAP using cyclic voltammetry (CV). All the potentials in the text are given against the Ag^{+} (10 mM) /Ag reference electrode. In order to avoid a chemical oxidation of the electrogenerated compounds under air, all electrochemical experiments have been carried out at room temperature under an argon atmosphere in a dry glove box using a conventional three electrode electrochemical cell. A vitreous carbon disc electrode was used as working electrode and a platinum wire as auxiliary electrode. Other experimental details about each record are given in the experimental part or in figure captions.

Figure 2.10 depicts the CVs for 0.5 mM of both bis-viologen cyclophanes **R5**$^{4+}$ (upper curve) and **R7**$^{4+}$ (bottom curve) and 1 mM of the reference, dimethyl viologen **V**$^{2+}$ (middle curve). The potential data are summarized in Table 2.1.

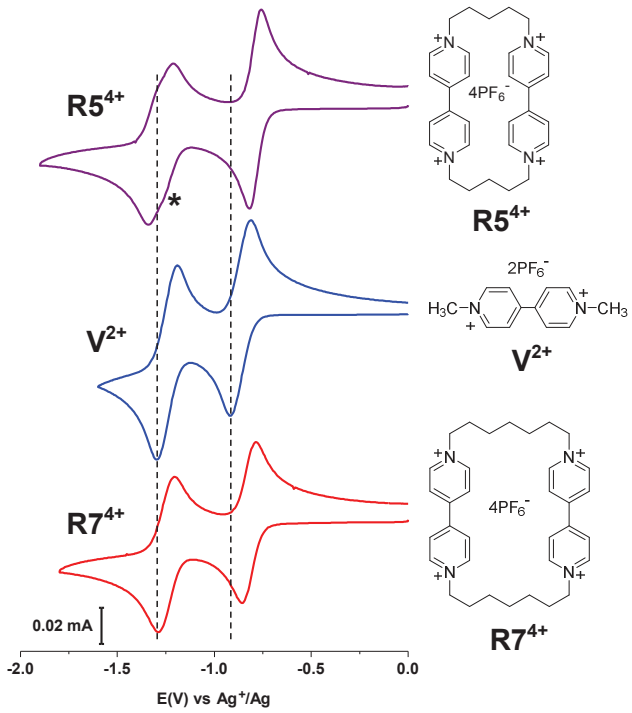

Figure 2.10: CVs for 0.5 mM of both bis-viologen cyclophanes **R5**$^{4+}$ (upper curve), **R7**$^{4+}$ (bottom curve) and 1 mM of **V**$^{2+}$ (middle curve) in 0.1 M TBAP/DMF at 100mV/s. Working electrode: 3mm Vitreous Carbon. Reference electrode: 0.01M $AgNO_3$ + 0.1 M TBAP/DMF/Ag.*: two overlapped and ill-defined systems.

Table 2.1: Experimental voltammetric potentials[a] with number of transferred electrons (in parenthesis) for bis-viologen cyclophanes **R5**$^{4+}$, **R7**$^{4+}$ and for the reference **V**$^{2+}$ at 100 mV/s. Working electrode: 3mm Vitreous Carbon. Reference electrode: 0.01M $AgNO_3$ + 0.1 M TBAP/DMF/Ag.

	$E^1_{1/2}$ (V) $V^{2+}/V^{+\bullet}$	ΔE_p^1 (mV) $V^{2+}/V^{+\bullet}$	$E^2_{1/2}$ (V) $V^{+\bullet}/V^0$	$E^1_{1/2}$-$E^2_{1/2}$(V)
V^{2+}	−0.86(1)	62	−1.24(1)	0.38
R5^{4+}	−0.79(2)	61	−1.30(2)[b]	0.51
R7^{4+}	−0.82(2)	66	−1.24(2)	0.42

[a]: Conc. = 1 mM/viologen unit in 0.1 M TBAP/DMF; $E^1_{1/2} = (E_{pa}^1 + E_{pc}^1)/2$; $\Delta E_p^1 = |E_{pa}^1 - E_{pc}^1|$. [b]: two overlapped and ill-defined systems.

During the potential scan from 0 to -1.9 V, the reference dimethyl viologen, $\mathbf{V^{2+}}$ shows two one-electron reversible CV waves[9] (middle curve in Figure 2.10). These waves for $\mathbf{V^{2+}}$ occurred respectively at $E^1_{1/2}$ = -0.86 V and $E^2_{1/2}$ = -1.24 V leading to the radical-cation species $\mathbf{V^{+\bullet}}$ and then to the neutral quinoid species $\mathbf{V^0}$ respectively. The potential separation between these two reductions ($E^1_{1/2}$-$E^2_{1/2}$, table 2.1) is 0.38 V. As documented before, no inter-molecular association occurs among the radical-cation species $\mathbf{V^{+\bullet}}$ for $\mathbf{V^{2+}}$ at millimolar concentrations in organic polar solvents at room temperature.[9, 18, 19]

Similarly, the CV curves for both of $\mathbf{R5^{4+}}$ and $\mathbf{R7^{4+}}$ are characterized by two observable reduction waves (Figure 2.10). These two consecutive reversible signals account each for 2 electrons per molecule (*i.e.* 1 electron per viologen subunit). The two redox waves occurred at -0.79 V and -1.3 V for $\mathbf{R5^{4+}}$ and -0.82 V and -1.24 V for $\mathbf{R7^{4+}}$ and are attributed to the successive cathodic reductions centered on the viologen subunits leading respectively to the bis (radical-cation) cyclophane species $\mathbf{V_2^{2(+\bullet)}}$ and then to the neutral bis-quinoid cyclophane species $\mathbf{V_2^0}$.[20-24] In addition, it should be pointed out that the second electrochemical response of $\mathbf{R5^{4+}}$ can be best described as the superimposition of two partially overlapped systems (denoted as * in Figures 2.10, upper curve). This effect can be ascribed to interaction between the two redox units that are reduced at different potentials. Another possibility is that the electrogenerated π-dimer ($\mathbf{R5^{2+}}$) could be in equilibrium with its non-associated form ($\mathbf{R5^{2(+\bullet)}}$), leading to the observation of two partially overlapped cathodic systems at lower potential.

Figures 2.11 A and B represents the CVs of $\mathbf{R5}^{4+}$ and $\mathbf{R7}^{4+}$ respectively at voltage scan rates (v) spanning from 0.01 to 1 $V.s^{-1}$. The viologen centered electrochemical responses remain reversible and diffusion controlled in this range of voltage scan rates. The voltage scan rate has a negligible effect on the redox peaks as illustrated from the plots of both of first and second half-wave potentials ($E^1_{1/2}$ and $E^2_{1/2}$) against voltage scan rates (Figures 2.11 C and D). The peak currents vary linearly with the square root of the voltage scan rate (Figures 2.11 E and F), showing diffusion controlled processes.

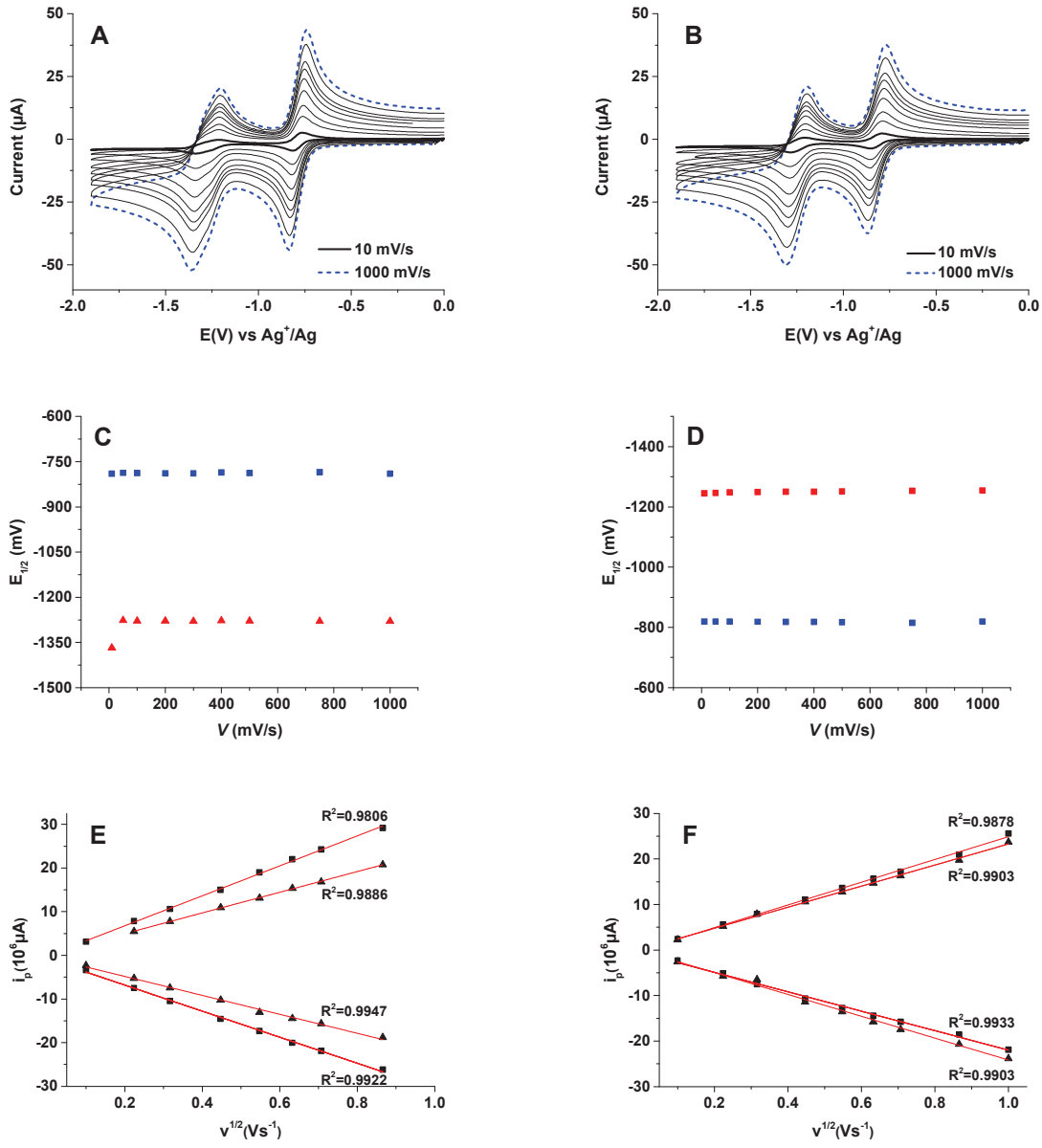

Figure 2.11: Cyclic voltammograms of (A) $\mathbf{R5}^{4+}$ and (B) $\mathbf{R7}^{4+}$ at different voltage scan rates, 0.01-1 V/s. Plots of half-wave potentials ($E^1_{1/2}$ and $E^2_{1/2}$) as functions of voltage scan rate for (C) $\mathbf{R5}^{4+}$ and (D) $\mathbf{R7}^{4+}$. Plots of peak currents *vs* the square-root of voltage scan rate for (E) $\mathbf{R5}^{4+}$ and (F) $\mathbf{R7}^{4+}$. Working electrode: 3mm Vitreous Carbon electrode, reference electrode: 0.01M $AgNO_3$ + 0.1 M TBAP/DMF/Ag. Conc. = 0.5 mM, solvent: 0.1 M TBAP/DMF.

If we examine the CV curves (Figure 2.10) more deeply, we can remark that both bis-viologen cyclophanes $\mathbf{R5^{4+}}$ and $\mathbf{R7^{4+}}$ have higher potential separations between the two reduction peaks ($E^1_{1/2}$-$E^2_{1/2}$ = 0.51 V and 0.42 V respectively) compared with that of the reference dimethyl viologen, $\mathbf{V^{2+}}$ (0.38 V, see table 2.1 and Figure 2.10). This data indicates a larger stability domain for the bis (radical-cation) cyclophane $\mathbf{R5^{2(+\bullet)}}$ or $\mathbf{R7^{2(+\bullet)}}$ formed after the first two-electron reduction than for the simple $\mathbf{V^{+\bullet}}$ radical. Such effect could be the result of π-dimerization processes between viologen radicals (see literature survey, Chapter I). In other words, the stabilization of the bis (radical-cation) cyclophane species ($\mathbf{R5^{2(+\bullet)}}$ or $\mathbf{R7^{2(+\bullet)}}$) could be due to a π-dimerization process that would facilitate the first reduction of the viologen units $\mathbf{V^{2+}}$ to $\mathbf{V^{+\bullet}}$, while making the second reduction harder.[18-22] However, it should be noticed that this effect, although more pronounced in the case of $\mathbf{R5^{2(+\bullet)}}$, remains relatively weak. In addition, for all the systems, ΔE^1_p values (= potential separation between the cathodic and anodic peaks of the first system) are similar and close to 60 mV at a scan rate of 100 $mV.s^{-1}$, which indicates a lack of significant interactions between the two viologen groups.

At this stage, it is thus difficult to determine if an intramolecular π-dimerization is encountered in $\mathbf{R5}^{4+}$ and $\mathbf{R7}^{4+}$. Thus, all the redox and chemical reactions represented in Scheme 2.1 have to be considered (see also Annexes for a complete description of a more general system):

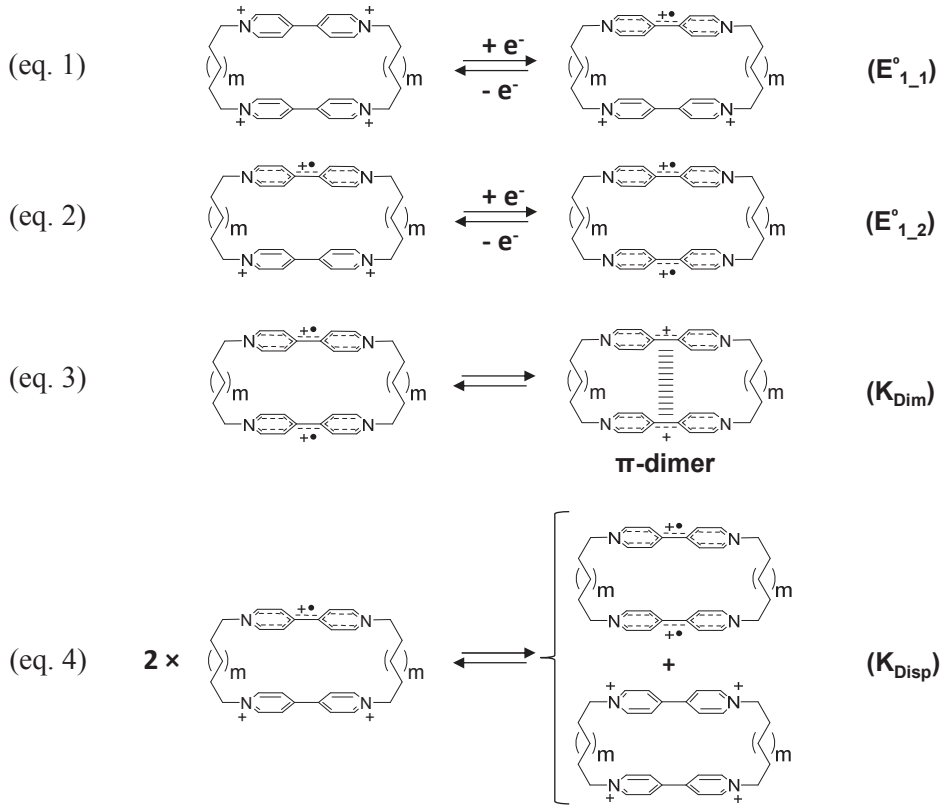

Scheme 2.1: single-electron successive reductions of bis-viologen cyclophane species (equations: 1 and 2) and their potential coupled reactions (dimerization: eq. 3 and disproportionation: eq. 4). m = 1 ($\mathbf{R5}^{4+}$), 3 ($\mathbf{R7}^{4+}$).

The first two-electron reversible reduction wave of both bis-viologen cyclophanes $\mathbf{R5}^{4+}$ and $\mathbf{R7}^{4+}$ observed in the experimental CV (Figure 2.10) can be decomposed in two successive single-electron transfer processes characterized by the standard potentials $E°_{1\_1}$ and $E°_{1\_2}$ (see scheme 2.1). The first one-electron reduction ($E°_{1\_1}$) of the bipyridinium unit is followed by the second one-electron reduction ($E°_{1\_2}$) of the second bipyridinium unit leading to the bis (radical-cation) cyclophane species $\mathbf{V_2}^{2(+\bullet)}$. In the case of non-interacting units, the difference between these two potentials is expected to be $\Delta E°_1 = E°_{1\_2} - E°_{1\_2} = 35.6$ mV.[25, 26] However, this value will be strongly modified if a spontaneous π-dimerization process exists (K_{Dim} in scheme 2.1): the π-dimerization process will influence the second electron transfer ($E°_{1\_2}$) rendering it easier to happen than the reduction of the first bipyridinium unit. As a

consequence, the $\Delta E°_1$ value will be lower than 35.6 mV and might even be negative. In addition, the disproportionation reaction (K_{disp}, Scheme 2.1) of the single reduced bis-viologen cyclophane species $\mathbf{V_2^{3+(\bullet)}}$ into $\mathbf{V_2^{2(+\bullet)}}$ and $\mathbf{V_2^{2+}}$ has to be also considered.[25, 26] This constant can be calculated using $\log_{10}(K_{Disp}) = -\Delta E^{\circ}_1(V)/0.059$[23] and in the case of a favored disproportionation ($K_{disp} > 1$, $\Delta E^{\circ}_1 < 0$), the second electron transfer is easier than the first one. In this case, the resulting CV wave corresponds to a two-electron reversible process. By opposition, a low K_{disp} is obtained if ΔE°_1 is high, and two 1-electron-transfers are obtained (two waves begin to separate if $\Delta E^{\circ}_1 > \sim 100$ mV). Finally, in the case of non-interacting units ($\Delta E^{\circ}_1 = 35.6$ mV), K_{disp} equals 0.24.[18]

In the present case, following the method described by Shain[27] and Taube,[28] the values of the standard potential separations $\Delta E°_1$ were estimated from ΔE_p^1 values measured on CV curves recorded at low scan rate (20 $mV.s^{-1}$). The disproportionation constant (K_{Disp}) were also calculated from the relationship $\log_{10}(K_{Disp}) = -\Delta E^{\circ}_1(V)/0.059$.[23] Data are collected in Table 2.2.

Table 2.2: Experimental voltammetric potentials for the first reduction[a] with number of transferred electrons (in parenthesis) for bis-viologen cyclophanes $\mathbf{R5^{4+}}$ and $\mathbf{R7^{4+}}$.[a]

	$E^1_{1/2}$ (mV)	ΔE^1_p (mV)	$\Delta E°_{1=} E°_{1-1} - E°_{1-2}$ (mV)	K_{Disp}[c]
$\mathbf{R5^{4+}}$	−789	46	12	0.62
$\mathbf{R7^{4+}}$	−820	57	34	0.26

[a]: Conc. = 1 mM/viologen unit in 0.1 M TBAP/DMF; scan rate: 10mV/s. Working electrode: 3mm Vitreous Carbon. Reference electrode: 0.01M $AgNO_3$ + 0.1 M TBAP/DMF/Ag. $\Delta E_p^1 = |E_{pc}^1 - E_{pa}^1|$; $E^1_{1/2} = (E_{pa}^1 + E_{pc}^1)/2$. [b]: $E^1_{pc/2}$: half-peak potential. [c]: calculated using Taube's method[28]; $\log K_{Disp} = -\Delta E°_1/0.059$.

These data show that with $\mathbf{R7^{4+}}$, the two viologen units act quasi-independently and the formation of a dimer is thus unlikely. It seems that the bridge in $\mathbf{R7^{4+}}$ is not adapted for the formation of the π-dimer. It can also be noted that no repulsion is observed between the two cationic viologen units (in this case a high $\Delta E°_1$ value would have been obtained).

In contrast, with $\mathbf{R5^{4+}}$, a low ΔE^1_p value is found (lower than the theoretical 58.5 mV) and this feature could be logically imputable to a dimerization process. However, the corresponding

K_{disp} constant (0.62, see Table 2.2) remains relatively weak and lower than 1, suggesting that such dimerization reaction is far to be quantitative.

These electrochemical investigations indicate that the $\mathbf{R5^{4+}}$ cyclophane may generate dimer, but these data must be completed by additional spectroelectrochemical experiments in order to prove or not the possible formation of intramolecular π-dimers.

3.2 Spectroelectrochemical studies

The spectroscopic imprints of the electrogenerated species provide additional information on the existence of non-covalent association between the bipyridinium radical cations. It needs to be mentioned that studies realized in Strasbourg have shown both bipyridinium radicals in $\mathbf{R7^{2(+\bullet)}}$ have not the capacity to self-assemble into π-dimer in aqueous media.[29] This behavior led us to be sure that the formation of dimerized species $\mathbf{R7^{2+}}$ from $\mathbf{R7^{2(+\bullet)}}$ can't be seen in organic media. Therefore, our spectroelectrochemical analyses were focused on $\mathbf{R5^{4+}}$ only. Spectrochemical studies were carried out under argon atmosphere in a dry glove box on 0.1 M TBAP/DMF solutions of 0.35 mM and 0.025 mM of $\mathbf{R5^{4+}}$ and 0.7 mM of $\mathbf{V^{2+}}$ in a conventional three-electrode cell using either 0.1 cm or 1 cm all-quartz immersion probes. The exhaustive one- or two-electron reductions of $\mathbf{V^{2+}}$ and $\mathbf{R5^{4+}}$ were performed respectively by fixing the potential of high surface area platinum (working electrode) at -1.12 V *vs*. Ag^{+} 10 mM /Ag. This potential is lower than the first cathodic response, resulting in the viologen radical cations $\mathbf{V^{+\bullet}}$ from $\mathbf{V^{2+}}$ and $\mathbf{R5^{2(+\bullet)}}$ from $\mathbf{R5^{4+}}$ (see Figure 2.12 and Table 2.3). The completion of the electrolysis was checked by comparing the voltammetry using rotating disk electrode (VRDE) before and after the electrolysis experiments. Figure 2.12 A and B represent the VRDEs recorded for $\mathbf{V^{2+}}$ and $\mathbf{R5^{4+}}$ (solid lines) along with those of their radical cation species $\mathbf{V^{+\bullet}}$ and bis (radical-cation) cyclophane $\mathbf{R5^{2(+\bullet)}}$ (dash lines) respectively. The dicationic reference $\mathbf{V^{2+}}$ and the tetracationic cyclophane $\mathbf{R5^{4+}}$ exhibit two 1- and 2-electron reduction waves (solid lines) respectively. After complete 1- and 2-electron reductions, both the resulting $\mathbf{V^{+\bullet}}$ and $\mathbf{R5^{2(+\bullet)}}$ species show perfectly 1- and 2-electron waves (dash lines) corresponding to oxidation of $\mathbf{V^{+\bullet}}$ to $\mathbf{V^{2+}}$ and $\mathbf{R5^{2(+\bullet)}}$ to $\mathbf{R5^{4+}}$ and reduction of $\mathbf{V^{+\bullet}}$ to $\mathbf{V^{0}}$ and $\mathbf{R5^{2(+\bullet)}}$ to $\mathbf{R5^{0}}$ respectively.

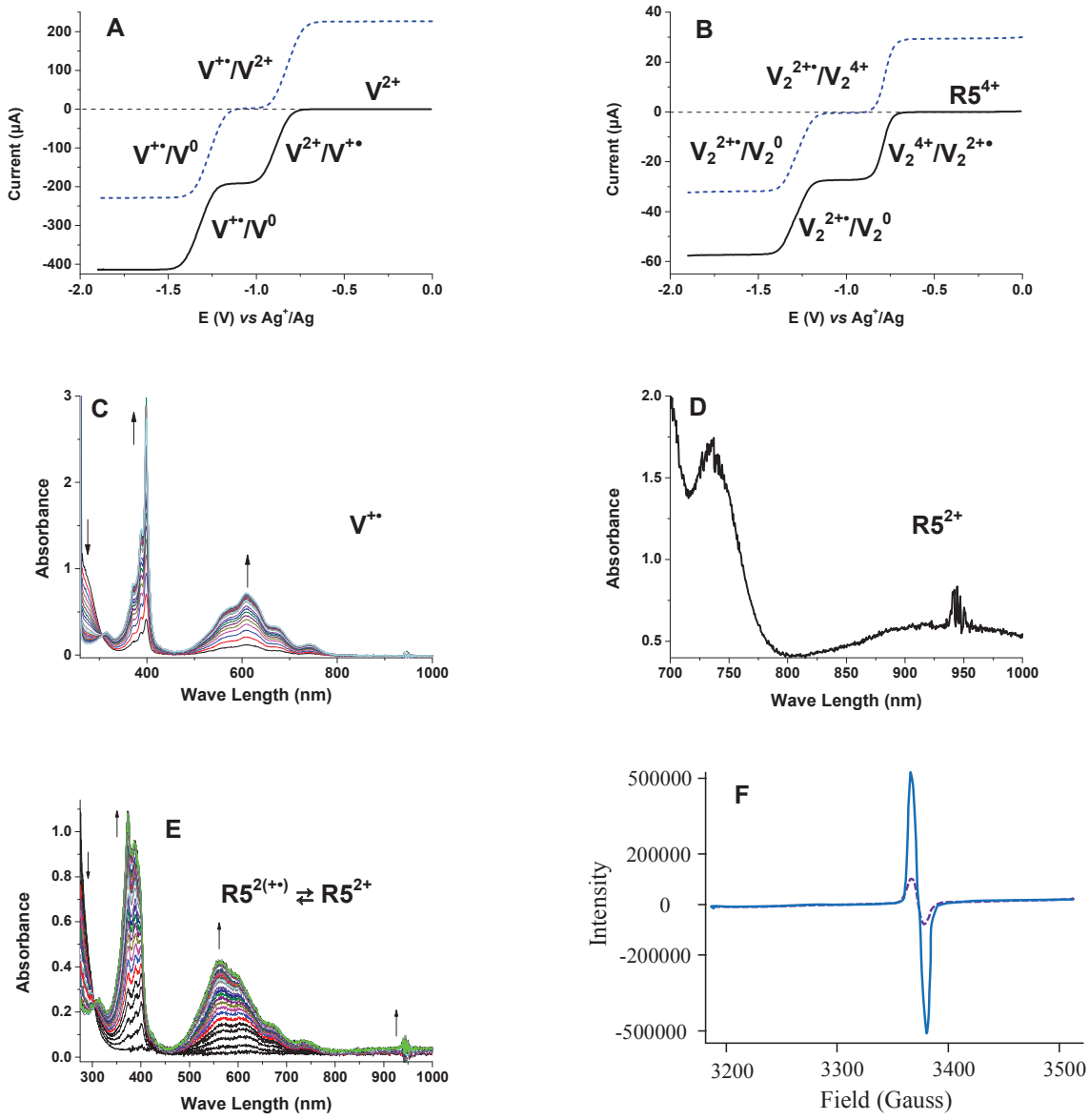

Figure 2.12: VRDE curves recorded for (A) 5 mM of $\mathbf{V}^{2+}$ (solid line) and $\mathbf{V}^{+\bullet}$ (dash line) and (B) 0.5 mM of $\mathbf{R5}^{4+}$ (solid line) and $\mathbf{R5}^{2+\bullet}$ (dash line) at 10mV/s and 3000 tr/min. Working electrode: 3mm Vitreous Carbon. (C) Absorption spectra recorded during the exhaustive 1-electron reduction (E_{app} = -1.12 V) for 0.7 mM solution of $\mathbf{V}^{2+}$. (D) Absorption spectra recorded for 0.35 mM of $\mathbf{R5}^{2+\bullet}$. (E) Absorption spectra recorded during the exhaustive 2-electron reduction (E_{app} = -1.12 V) for 0.025 mM solution of $\mathbf{R5}^{4+}$. Solvent: 0.1 M TBAP/DMF, 298K; working electrode: high surface area platinum, reference electrode: 0.01M $AgNO_3$ + 0.1 M TBAP/DMF/Ag and UV-vis all-quartz immersion probe with l = 1 cm (D and E) or 1 mm (C). (F) ESR spectra of $\mathbf{R5}^{2+\bullet}$ (dash line) and $\mathbf{V}^{+\bullet}$ (solid line), 1 mM per viologen unit.

Table 2.3: Maximum wavelengths and molar absorption coefficients for $\mathbf{V^{2+}}$, $\mathbf{R5^{4+}}$ and their reduced forms in 0.1 M TBAP/DMF at 298 K.

Compound	λ_{max} /nm (ε/$M^{-1}.cm^{-1}$)
$\mathbf{V^{2+}}$	264 (16800)
$\mathbf{R5^{4+}}$	275 (38800), 296 (12700)
$\mathbf{V^{+\bullet}}$	315 (3800), 373 (11900), 389 (20900), 400 (39300), 578 (8000), 608 (10300), 625 (9200), 667 (4800), 739 (1800)
$\mathbf{R5^{2+}}$	314 (10500), 373 (43400), 386 (38300), 564 (17100), 600 (14600), 668 (6000), 735 (3100), 940 (3400)

The bulk one-electron reduction of a solution of the reference compound $\mathbf{V^{2+}}$ (E_{app} = -1.12 V) leads to the disappearance of the initial π–π^* absorption band in the UV region (Figure 2.12 C). In addition, two new sets of absorption bands have been detected, the first absorption bands appeared at 315 nm, 373 nm, 398 nm, 400 nm and the second absorption bands appeared at 578 nm, 608 nm, 625 nm, 667 nm and 739 nm (Figure 2.12 C, Table 2.3). The blue color and the accompanied UV-vis signature of the resulting solution (especially the absence of absorption band in the NIR region (>800 nm)) are unambiguously attributed to the non-associated radical cations $\mathbf{V^{+\bullet}}$.[30], *i.e.* no π-dimer could be detected, as was expected.

The UV-Visible spectrum (Figure 2.12 D) recorded for a 0.35 mM solution of $\mathbf{R5^{2(+\bullet)}}$ is characterized by a broad absorption band centered at 940 nm which is strongly indicative for the formation of the π-dimerized structure $\mathbf{R5^{2+}}$ of the bis (radical-cation) cyclophane species $\mathbf{R5^{2(+\bullet)}}$. At lower concentration, the electrochemical 2-electron reduction (E_{app} = -1.12 V) for 0.025 mM solution of $\mathbf{R5^{4+}}$ (Figure 2.12 E) resulted in a disappearance of the π–π^* absorption band of the initial tetracationic cyclophane $\mathbf{R5^{4+}}$ in the UV region and led also to the emergence of new bands at 315 nm, 373 nm, 386 nm, 564 nm, 600 nm, 668 nm, 735 nm and 940 nm. The observation of both the absorption bands related to π-dimerized species $\mathbf{R5^{2+}}$ (373 nm, 386 nm, 564 nm and 940 nm) and the band at 600 nm concerning to non dimerized structure $\mathbf{R5^{2(+\bullet)}}$ is clearly consistent with the existence of an equilibrium between the dimerized and the non-dimerized $\mathbf{R5^{2+}}$ and $\mathbf{R5^{2(+\bullet)}}$ species respectively.

The formation of the π-dimerization process between viologen radicals can be also demonstrated by electron spin resonance measurements (ESR) where the spin coupling between viologen radicals makes their ESR spectra silent. As expected, the ESR spectrum of

the $\mathbf{V}^{+\bullet}$ (1mM) solution displays the usual high intense response of non-associated bipyridinium cation radicals (Figure 2.12 F). Under the same experimental conditions (1mM per viologen, 0.5 mM in the cyclophane $\mathbf{R5}^{4+\bullet}$), the ESR spectrum of the electrogenerated species $\mathbf{R5}^{2(+\bullet)}$ shows an attenuated signal suggesting again the existence of an equilibrium between the dimerized, diamagnetic, ESR silent structure $\mathbf{R5}^{2+}$ and the paramagnetic non-dimerized structure $\mathbf{R5}^{2(+\bullet)}$. The fact that no dimerized structure is found with $\mathbf{V}^{+\bullet}$ under the same concentration range in viologen unit indicates that the π-dimerization process in $\mathbf{R5}^{2(+\bullet)}$ occurs intramolecularly. The distance between two viologen units in $\mathbf{R5}^{4+}$ appears thus adequate to allow an orbital overlapping between the two somo orbitals of the electrogenerated bis (radical-cation) $\mathbf{R5}^{2+\bullet}$ species.

If the presence of π-dimers in the flexible cyclophanes is observed in organic solvent, their formation is unfortunately far to be quantitative and corroborates our electrochemical experiments. The flexible bridges seem not really adapted for the formation of intramolecular dimers in organic solvents.

Following our study, the electrochemical behavior of $\mathbf{R5}^{4+}$ and $\mathbf{R7}^{4+}$ in water was investigated by the group of Weiss in Strasbourg.[29] Experiments were performed in aqueous media using 0.1 M KCl as supporting electrolyte. With $\mathbf{R7}^{4+}$, adsorption of the doubly reduced form at the working electrode was noted, without any indication of dimerization of $\mathbf{R7}^{2(+\bullet)}$. The non-occurrence of the dimerization in $\mathbf{R7}^{2(+\bullet)}$ is attributed to the fact that with this flexible and long spacer, this compound can adopt a stable geometry in which the two viologen units are too far apart to interact. In contrast, in the same study[29] and under the same experimental conditions, a growth of broad absorption band at 878 nm was observed during the 2-electron reduction of $\mathbf{R5}^{4+}$ which emphasize the formation of the dimerized $\mathbf{R5}^{2(+\bullet)}$ species, i.e. formation of $\mathbf{R5}^{2+}$ species. It seems that the five-carbon chain in $\mathbf{R5}^{2(+\bullet)}$ is short enough to favor a cofacial orientation between the two viologen radical which results in the formation of dimerized $\mathbf{R5}^{2(+\bullet)}$ species, i.e. $\mathbf{R5}^{2+}$ species.[29, 31] These data are thus in accordance with our results obtained in organic media.

4. Study of inclusion complexes

As indicated above, our second objective was to investigate the possible formation of inclusion complexes with the $\mathbf{R5}^{4+}$ and $\mathbf{R7}^{4+}$ cyclophanes. More accurately, our study was dedicated to the reactivity of the flexible cyclophanes towards the dimethyl viologen unit, in their oxidized or reduced forms. Two rational routes have been tested to attain the targeted

redox activated triradical cationic inclusion complexes $\mathbf{Rn^{2(+\bullet)}}\subset\mathbf{V^{+\bullet}}$ (see Scheme 2.2). The first strategy was to realize the direct electrochemical 3-electron reduction of an equimolar solution of dimethyl viologen $\mathbf{V^{2+}}$ and $\mathbf{R5^{4+}}$ or $\mathbf{R7^{4+}}$. The second tested method was to add the dimethyl viologen radical $\mathbf{V^{+\bullet}}$ to a solution of bis (radical-cation) form, *i.e.* $\mathbf{R5^{2(+\bullet)}}$ or $\mathbf{R7^{(+\bullet)}}$.

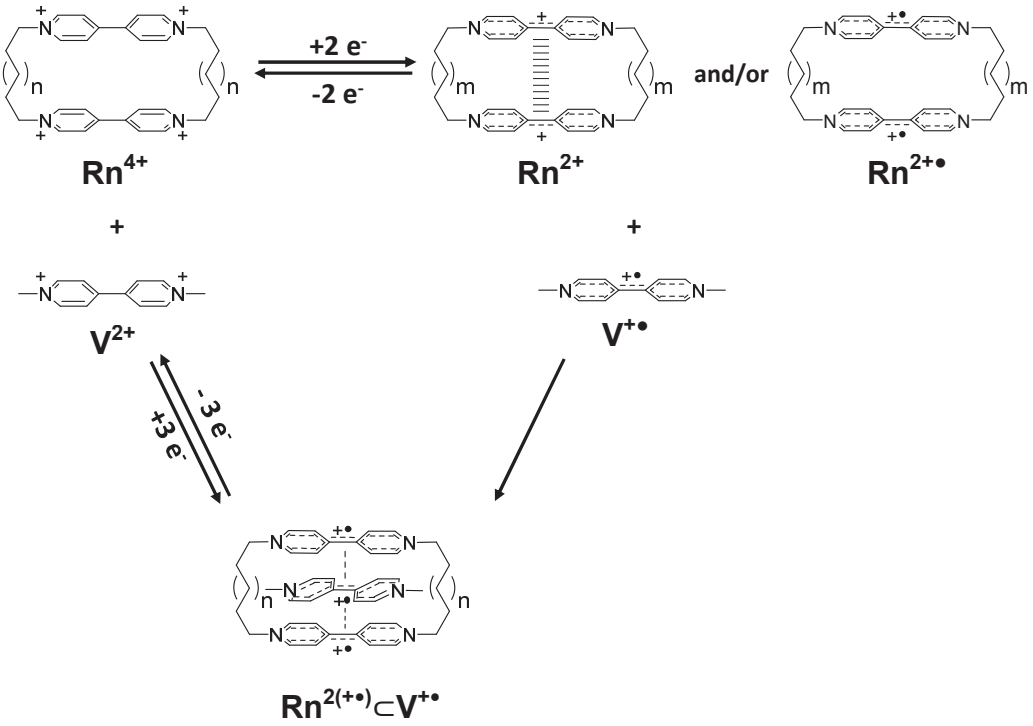

Scheme 2.2: Representation of the two possible strategies to generate inclusion complexes $\mathbf{Rn^{2(+\bullet)}}\subset\mathbf{V^{+\bullet}}$ from the bis-viologen cyclophanes $\mathbf{Rn^{2+}}$. n refers to the alkyl chain linking the two viologen units; m = 1 ($\mathbf{R5^{4+}}$), 3 ($\mathbf{R7^{4+}}$).

4.1 Spectrovoltammetric titrations of $\mathbf{R5^{4+}}$ and $\mathbf{R7^{4+}}$ by $\mathbf{V^{2+}}$

The eventual formation of inclusion complexes between cyclophanes and dimethyl viologen ($\mathbf{V^{2+}}$) in their oxidized or reduced states was checked by following electrochemical and spectroelectrochemical responses of these mixtures in DMF electrolytic solutions. The CVs titration of $\mathbf{R5^{4+}}$ or $\mathbf{R7^{4+}}$ solutions (0.5 mM) with a $\mathbf{V^{2+}}$ solution (5 mM) are shown in Figures 2.13 A and B respectively. The electrochemical data of the voltammetric titrations are summarized in Table 2.4. Basically, the resulting CV curves are the strict superimposition of the individual responses of the isolated compounds. In particular, no significant potential shift could be determined. Furthermore, the broadening of cathodic responses of 1:1 mixtures of $\mathbf{R5^{4+}}$ or $\mathbf{R7^{4+}}$ with $\mathbf{V^{2+}}$ are clearly seen upon varying the voltage scan rates, especially for

R5^{4+} (Figures 2.13 C - E). These broad peaks are attributed to the overlapping of the individual responses of $\mathbf{V}^{2+}$ with **R5**$^{4+}$ or **R7**$^{4+}$ where the characteristic potentials of **R5**$^{4+}$, **R7**$^{4+}$ and $\mathbf{V}^{2+}$ do no match strictly.

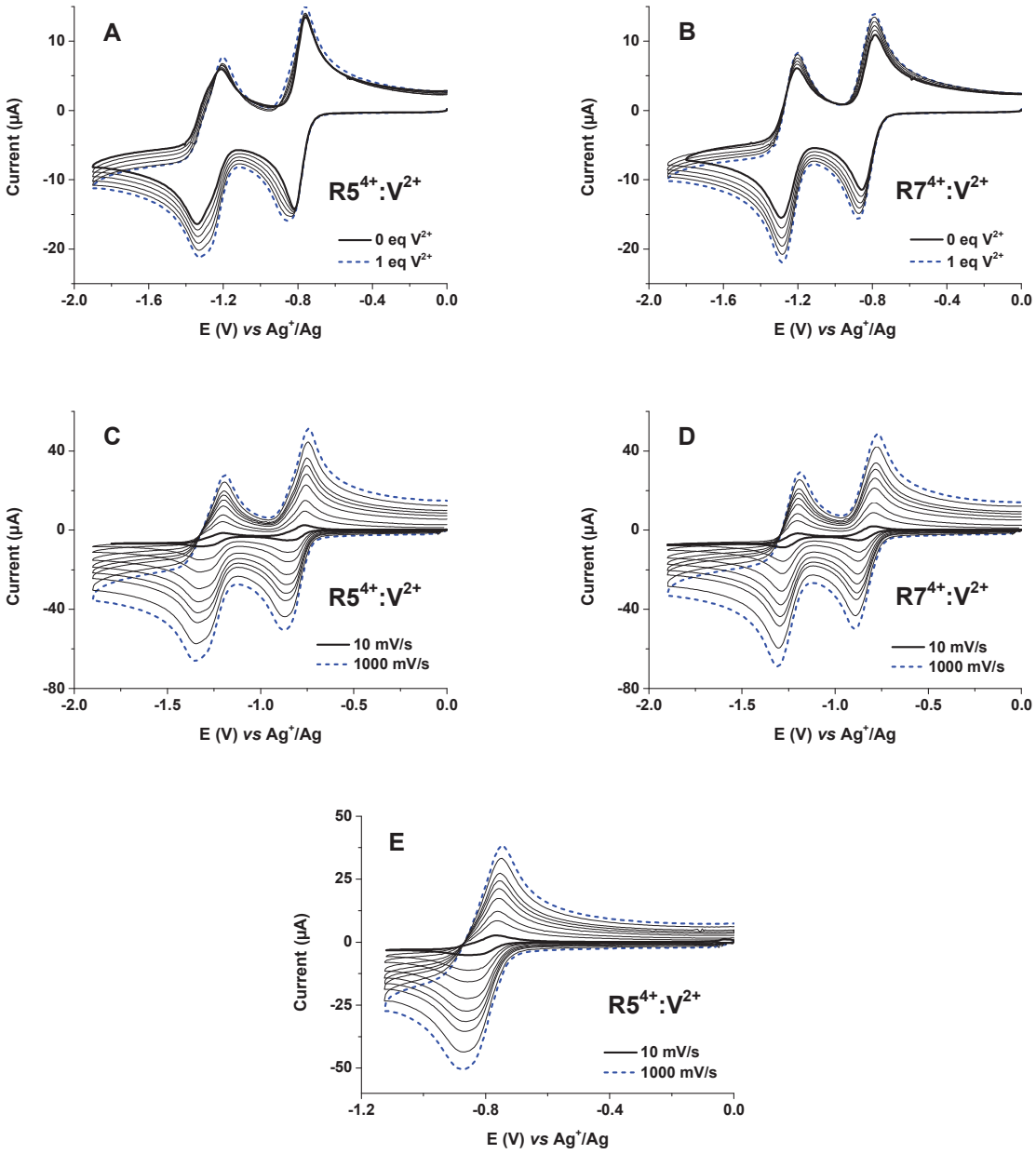

Figure 2.13: (A) and (B) CV titrations for $\mathbf{V}^{2+}$ into **R5**$^{4+}$ and **R7**$^{4+}$ respectively. $[\mathbf{V}^{2+}]_{final}$ = $[\mathbf{R5}^{4+}]_{final}$ = $[\mathbf{R7}^{4+}]_{final}$ = 0.45 mM. Voltage Scan rate: 0.1 V/s. (C and E) and (D) CVs for 1:1 mixture of **R5**$^{4+}$ or **R7**$^{4+}$ and $\mathbf{V}^{2+}$ respectively at different voltage scan rates, 0.01-1 V/s. Working electrode: 3mm Vitreous Carbon electrode, reference electrode: 0.01M $AgNO_3$ + 0.1 M TBAP/DMF/Ag. $[\mathbf{R5}^{4+}]_{initial}$ = $[\mathbf{R7}^{4+}]_{initial}$ = 0.5 mM, $[\mathbf{V}^{2+}]_{initial}$ = 5 mM and solvent: 0.1 M TBAP/DMF.

Table 2.4: Experimental voltammetric potentials[a] with number of transferred electrons (in parenthesis) for $\mathbf{R5^{4+}}$, $\mathbf{R7^{4+}}$, $\mathbf{V^{2+}}$ and 1:1 mixtures of $\mathbf{V^{2+}}$ and $\mathbf{R5^{4+}}$ or $\mathbf{R7^{4+}}$ respectively at 100mV/s. Working electrode: 3mm Vitreous Carbon. Reference electrode: 0.01M $AgNO_3$ + 0.1 M TBAP/DMF/Ag.

	$E^1_{1/2}$ (V) $V^{2+}/V^{+\bullet}$	ΔE_p^1 (mV) $V^{2+}/V^{+\bullet}$	$E^2_{1/2}$ (V) $V^{+\bullet}/V^0$	$E^1_{1/2}$-$E^2_{1/2}$(V)
$\mathbf{V^{2+}}$	−0.86(1)	62	−1.24(1)	0.38
$\mathbf{R5^{4+}}$	−0.79(2)	61	−1.30(2)	0.51
$\mathbf{V^{2+}}$:$\mathbf{R5^{4+}}$	−0.80(3)	72	−1.26(3)	0.46
$\mathbf{R7^{4+}}$	−0.82(2)	66	−1.24(2)	0.42
$\mathbf{V^{2+}}$:$\mathbf{R7^{4+}}$	−0.83(3)	76	−1.24(3)	0.41

[a]: $[\mathbf{R5^{4+}}]_{initial} = [\mathbf{R7^{4+}}]_{initial} = 0.5$ mM, $[\mathbf{V^{2+}}]_{initial} = 5$ mM and $[\mathbf{V^{2+}}]_{final} = [\mathbf{R5^{4+}}]_{final} = [\mathbf{R7^{4+}}]_{final} = 0.45$ mM for 1:1 mixtures in 0.1 M TBAP/DMF; $\Delta E_p^1 = E_{pa}^1 - E_{pc}^1$; $E^1_{1/2} = (E_{pa}^1 + E_{pc}^1)/2$.

The full bulk one-electron reduction per viologen unit was performed for a 0.45 mM 1:1 mixture of $\mathbf{V^{2+}}$ and $\mathbf{R5^{4+}}$ or $\mathbf{R7^{4+}}$ solution leading to a 0.45 mM mixture of $\mathbf{V^{+\bullet}}$ and $\mathbf{R5^{2+\bullet}}$ or $\mathbf{R7^{2+\bullet}}$ respectively. The completion of the electrolysis and stability of the resulting reduced forms were checked by comparing the voltammetry using the rotating disc electrode (VRDE) for 1:1 mixture of $\mathbf{V^{2+}}$ and $\mathbf{R5^{4+}}$ or $\mathbf{R7^{4+}}$ solutions with those of 1:1 mixture of $\mathbf{V^{+\bullet}}$ and $\mathbf{R5^{2+\bullet}}$ or $\mathbf{R7^{2+\bullet}}$ solutions respectively (see Figures 2.14 A and B). Figures 2.14 C and D depict the UV-Visible spectra recorded during 1-electron electrolysis per viologen unit for 1:1 mixture of $\mathbf{V^{2+}}$ and $\mathbf{R5^{4+}}$ or $\mathbf{R7^{4+}}$ respectively. As for the absorption spectrum of $\mathbf{R5^{2(+\bullet)}}$ (Figure 2.12 D), the $\mathbf{V^{+\bullet}}$:$\mathbf{R5^{2(+\bullet)}}$ mixture showed the same broad absorption band at 940 nm (ε = 2500 $M^{-1}.cm^{-1}$) which is attributed to the formation of π-dimers into the solution (see Figure 2.14 C). From this result, it is not possible to conclude if the dimerization occurred intermolecularly between $\mathbf{V^{+\bullet}}$ and $\mathbf{R5^{2(+\bullet)}}$ or intramolecularly between the reduced viologen units in $\mathbf{R5^{2(+\bullet)}}$, *i.e.* the formation of a tris-radical inclusion complex $\mathbf{V^{+\bullet}\subset R5^{2(+\bullet)}}$ remains speculative.

In the case of the $\mathbf{V}^{2+}$:$\mathbf{R7}^{4+}$ system, the absorption spectra recorded during the formation of 1:1 mixture of $\mathbf{V}^{+\bullet}$ and $\mathbf{R7}^{2+\bullet}$ showed the growth of a very weak NIR band at 943 nm (ε = 400 $M^{-1}.cm^{-1}$) which is attributed to the formation of π-dimer (Figure 2.14 D). As mentioned before, whereas the dimerization is favored in aqueous media and since no NIR absorption band was observed for $\mathbf{R7}^{2+\bullet}$ in H_2O + 0.1 M KBr indicating the absence of the dimer $\mathbf{R7}^{2+}$, the occurrence of such a dimerization process in our present study correlated logically to the formation of the tris-radical inclusion complex $\mathbf{R7}^{2(+\bullet)}\subset\mathbf{V}^{+\bullet}$. However, the very low intensity of this diagnostic band seems to indicate that the formation of the inclusion complex is very poorly efficient.

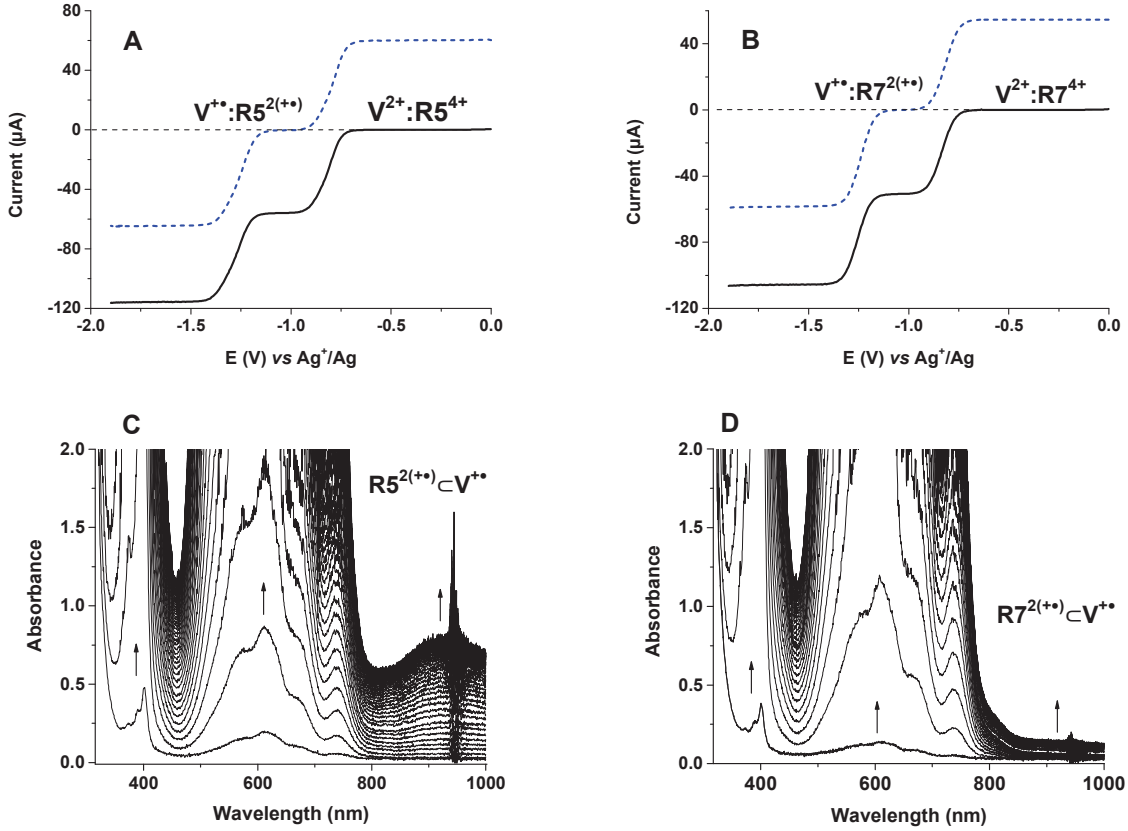

Figure 2.14: VRDE curves recorded at 10mV/s and 3000 tr/min for a 0.45 mM 1:1 mixture of (A) $\mathbf{R5}^{4+}$ and $\mathbf{V}^{2+}$ (B) $\mathbf{R7}^{4+}$ and $\mathbf{V}^{2+}$. Working electrode: 3mm Vitreous Carbon. Absorption spectra recorded during the exhaustive 3-electron reduction (E_{app} = -1.12 V) for a 0.45 mM 1:1 mixture of (C) $\mathbf{R5}^{4+}$ and $\mathbf{V}^{2+}$. (D) $\mathbf{R7}^{4+}$ and $\mathbf{V}^{2+}$. Solvent: 0.1 M TBAP/DMF, 298K; working electrode: high surface area platinum, reference electrode: 0.01M $AgNO_3$ + 0.1 M TBAP/CH_3CN/Ag and UV-vis all-quartz immersion probe with l = 1 cm.

Furthermore, spectrovoltammetric titration of $\mathbf{V}^{2+}$ into $\mathbf{R7}^{4+}$ was also performed in aqueous media using 0.1 M KBr as supporting electrolyte. The adsorption at the vitreous carbon electrode was observed for both the 3-electron redox responses of $\mathbf{V}^{2+}$ and $\mathbf{R7}^{4+}$ mixtures at different voltage scan rates. In spite of observed adsorption phenomenon and to monitor the characteristic NIR absorption band of the π-dimer, the bulk 3-electron reduction for 1:1 mixture of $\mathbf{V}^{2+}$ and $\mathbf{R7}^{4+}$ was proceeded by holding the reduction potential lower than the first 3-electron cathodic response. The adsorption on the Pt plate (working electrode) was also encountered. At the beginning of this electrolysis, a purple color film has been clearly formed at the surface of the Pt electrode which is probably indicative of the formation of the inclusion complex $\mathbf{R7}^{2(+\bullet)}\subset\mathbf{V}^{+\bullet}$. The color of the solution was light blue during all the electrolysis process meaning that no NIR absorption band was detected. This result indicates that π-dimers (intramolecular or inclusion complex) may occur in the solid state (as film on the electrode surface), but not in solution.

4.2 Spectrovoltammetric titration of $\mathbf{R5}^{2(+\bullet)}$ with $\mathbf{V}^{+\bullet}$

The possible formation of inclusion complex $\mathbf{R5}^{2(+\bullet)}\subset\mathbf{V}^{+\bullet}$ in DMF electrolytic solutions was also checked following the second strategy, *i.e.* performing the titration experiments starting directly from isolated electrogenerated solutions of 5 mM or 0.25 mM of $\mathbf{V}^{+\bullet}$ into 0.35 mM or 0.025mM of $\mathbf{R5}^{2(+\bullet)}$ respectively (Figures 2.15 and 2.16 and table 2.5). First, dimethyl viologen radical $\mathbf{V}^{+\bullet}$ (5 mM and 0.25 mM) and bis (radical-cation) cyclophane $\mathbf{R5}^{2(+\bullet)}$ (0.35 mM and 0.025 mM) were generated electrochemically by performing bulk 1- and 2-electron reductions separately at fixed potential (E_{app} = -1.12 V), lower than the first cathodic response. Both the absorption spectra and CV titrations were then performed on these low and high concentrations of the electrochemical generated viologen radicals. Once again, the electrochemical responses of the 1:1 mixture of radical cations $\mathbf{R5}^{2(+\bullet)}$ with $\mathbf{V}^{+\bullet}$ are the superimposition of the individual response without any clear indications of the formation of a tris-radical inclusion complex $\mathbf{R5}^{2(+\bullet)}\subset\mathbf{V}^{+\bullet}$, see Figures 2.15 A, B and E.

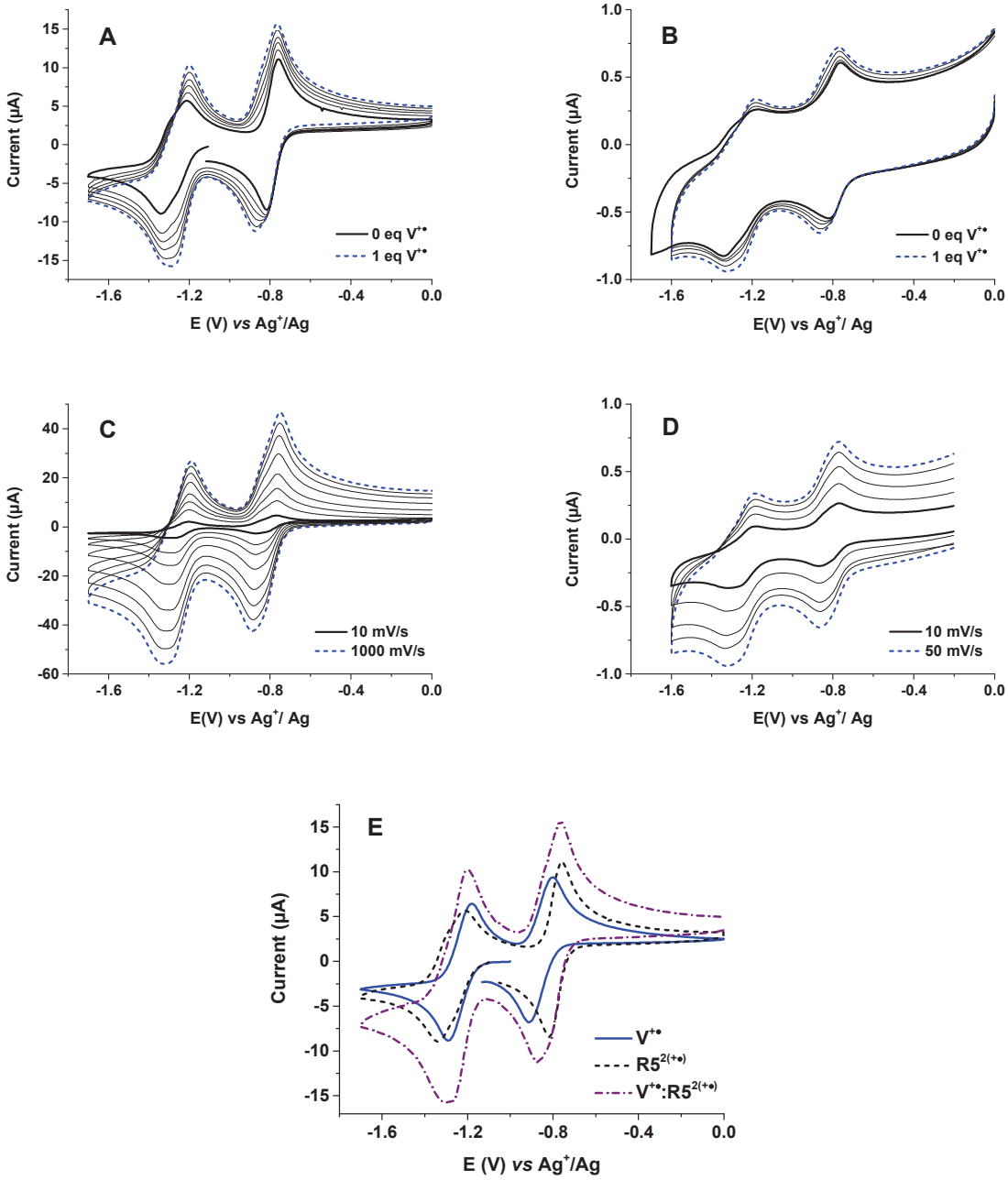

Figure 2.15: (A) and (B) CV titrations for 5 mM and 0.25 mM of $\mathbf{V}^{+\bullet}$ into 0.35 mM and 0.025 mM of $\mathbf{R5}^{2(+\bullet)}$ respectively. $[\mathbf{V}^{+\bullet}]_{final} = [\mathbf{R5}^{2(+\bullet)}]_{final} = 0.33$ mM (A) and 0.023 mM (B). Voltage Scan rate = 100 mV/s (A) and 50 mV/s (B). CVs for (C) 0.33 mM and (D) 0.023 mM mixtures of $\mathbf{V}^{+\bullet}$ and $\mathbf{R5}^{2(+\bullet)}$ respectively at different voltage scan rates. (E) CVs for 5 mM $\mathbf{V}^{+\bullet}$, 0.35 mM $\mathbf{R5}^{2(+\bullet)}$ and 0.33 mM mixture of $\mathbf{V}^{+\bullet}$ and $\mathbf{R5}^{2(+\bullet)}$ at 100 mV/s. Working electrode: 3mm Vitreous Carbon electrode, reference electrode: 0.01M $AgNO_3$ + 0.1 M TBAP/DMF/Ag. Solvent: 0.1 M TBAP/DMF, 298 K.

Table 2.5: Experimental voltammetric potentials[a] with number of transferred electrons (in parenthesis) for $\mathbf{V}^{+\bullet}$, $\mathbf{R5}^{2+\bullet}$ and 1:1 mixtures of $\mathbf{V}^{+\bullet}$ and $\mathbf{R5}^{2+\bullet}$ at 100mV/s. Working electrode: 3mm Vitreous Carbon. Reference electrode: 0.01M $AgNO_3$ + 0.1 M TBAP/DMF/Ag.

	$E^1_{1/2}$ (V) $V^{2+}/V^{+\bullet}$	$\Delta E_p{}^1$ (mV) $V^{2+}/V^{+\bullet}$	$E^2_{1/2}$ (V) $V^{+\bullet}/V^0$	$E^1_{1/2}$-$E^2_{1/2}$(V)
$\mathbf{V}^{+\bullet}$	−0.85(1)	96	−1.23(1)	0. 38
$\mathbf{R5}^{2+\bullet}$	−0.79(2)	83	−1.30(1)	0.51
$\mathbf{V}^{+\bullet}$:$\mathbf{R5}^{2+\bullet}$	−0.81(3)	89	−1.24(3)	0.43

[a]: $[\mathbf{R5}^{2+\bullet}]$ = 0.35 mM and $[\mathbf{V}^{+\bullet}]$ = 5 mM and $[\mathbf{V}^{+\bullet}]_{final}$ = $[\mathbf{R5}^{2+\bullet}]_{final}$ = 0.33 mM in 0.1 M TBAP/DMF; $\Delta E_p{}^1 = E_{pa}{}^1 - E_{pc}{}^1$; $E^1_{1/2} = (E_{pa}{}^1 + E_{pc}{}^1)/2$.

The CVs at different voltage scan rates of 1:1 mixtures of $\mathbf{R5}^{2(+\bullet)}$ with $\mathbf{V}^{+\bullet}$ were illustrated in Figures 2.15 C and D. The time scales of CV experiments have no influences on both the first and second 3-electron responses, *i.e.*: the possible self-assembling formation of inclusion complex $\mathbf{R5}^{2(+\bullet)}\subset\mathbf{V}^{+\bullet}$ is not dependent on CV time scale. The UV-Visible spectra titrations of $\mathbf{V}^{+\bullet}$ into $\mathbf{R5}^{2(+\bullet)}$ at two different high and low concentrations of radicals were carried out and presented in Figures 2.16 A and B respectively. These titration showed the same characteristic NIR signature attributed to dimerization like those noted for $\mathbf{R5}^{2(+\bullet)}$ and reduced 1:1 mixtures of $\mathbf{R5}^{4+}$ and $\mathbf{V}^{2+}$, see Figures 2.12 D, E and Figures 2.14 C, D respectively.

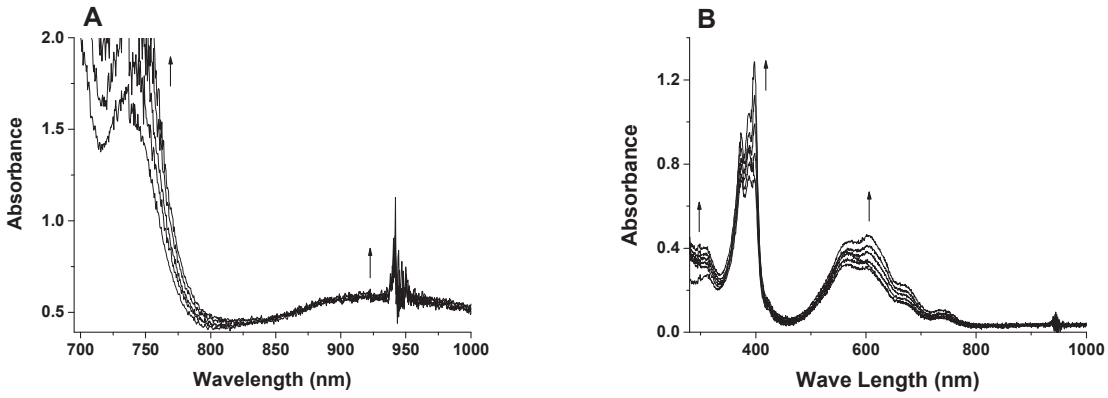

Figure 2.16: (A) and (B) Absorption spectra titrations for 5 mM and 0.25 mM of $\mathbf{V}^{+\bullet}$ into 0.35 mM and 0.025 mM of $\mathbf{R5}^{2(+\bullet)}$ respectively. $[\mathbf{V}^{+\bullet}]_{final}$ = $[\mathbf{R5}^{2(+\bullet)}]_{final}$ = 0.33 mM (A) and 0.023 mM (B). Solvent: 0.1 M TBAP/DMF, UV-vis all-quartz immersion probe with l = 1 cm, 298 K.

Although the presence of π-dimers are detected, these electrochemical and spectroelectrochemical data did not provide reliable evidences for the encapsulation of the radical $\mathbf{V}^{+\bullet}$ by the radical cavity $\mathbf{R5}^{2(+\bullet)}$ in organic DMF media. It is probably worthy to investigate spectroelectrochemical study of the bis-viologen cyclophane $\mathbf{R5}^{4+}$ and $\mathbf{R7}^{4+}$ in the presence of $\mathbf{V}^{2+}$ in aqueous media taking in account that electrochemical behavior could vary depending on the counter anions. This possibility, being however hazardous, was not investigated in this work.

5. Some insights on bis-viologen cyclophane structures

In parallel with our work, the group of Jean Weiss has obtained X-ray diffraction structures of the tetracationic cyclophanes ($\mathbf{R5}^{4+}$ and $\mathbf{R7}^{4+}$) along with their bis (radical-cation) states ($\mathbf{R5}^{2(+\bullet)}$ and $\mathbf{R7}^{2(+\bullet)}$). They have also shown that the inclusion complex $[\mathbf{R7.V_2}]^{3(+\bullet)(2+)}$ can be isolated as solid state.[31] Figures 2.17, 2.18 and 2.19 depict the x-ray structures of ($\mathbf{R5}^{4+}$ and $\mathbf{R7}^{4+}$), ($\mathbf{R7}^{2(+\bullet)}$ and $\mathbf{R7}^{2(+\bullet)}$) and $[\mathbf{R7.V_2}]^{3(+\bullet)(2+)}$ respectively.

Regardless of the distance between their two viologen units, both tetracationic bis-viologen cyclophanes $\mathbf{R5}^{4+}$ and $\mathbf{R7}^{4+}$ exhibit comparable structures. The alkyl spacers adopt unconstrained gauche conformations. The cavities sizes of $\mathbf{R5}^{4+}$ and $\mathbf{R7}^{4+}$ could be defined by the C4-C4 atomic distances and their widths. The C4-C4 atomic distances are 5.87 Å and 7.97 Å in $\mathbf{R5}^{4+}$ and $\mathbf{R7}^{4+}$ respectively. The cavities widths are similar, 9.67 Å and 9.86 Å respectively, see Figure 2.17.

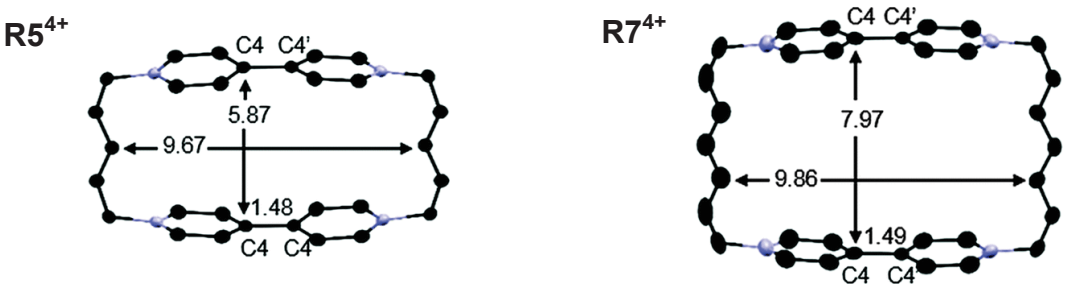

Figure 2.17: X-ray structures of the tetracationic bis-viologen cyclophanes $\mathbf{R5}^{4+}$ and $\mathbf{R7}^{4+}$ adapted from ref. (31). The counter anions PF_6^-, hydrogen atoms and solvents are omitted for clarity.

The chemical reduction of the bis-viologen cyclophanes $\mathbf{R5}^{4+}$ and $\mathbf{R7}^{4+}$ by zinc powder resulted in dark blue crystals of bis (radical-cation) cyclophanes $\mathbf{R5}^{2(+\bullet)}$ and $\mathbf{R7}^{2(+\bullet)}$, their X-ray structures are illustrated in Figure 2.18. It was noted that both $\mathbf{R5}^{2(+\bullet)}$ and $\mathbf{R7}^{2(+\bullet)}$ are arranged in a continuous alignment.

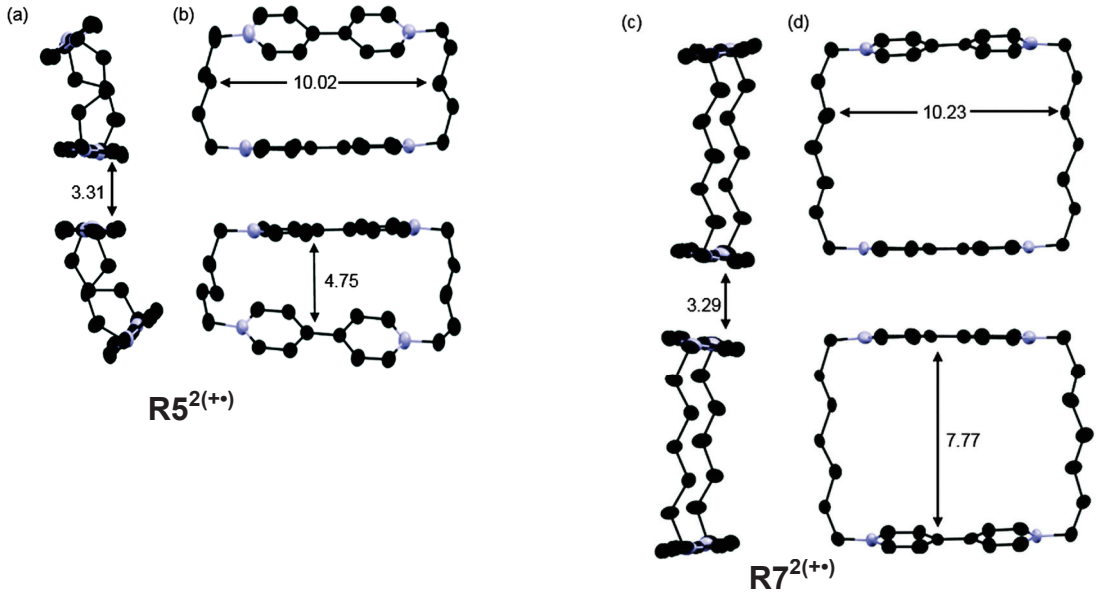

Figure 2.18: X-ray structures of the bis (radical-cation) cyclophane derivatives $\mathbf{R5}^{2(+\bullet)}$ (a and b) and $\mathbf{R7}^{2(+\bullet)}$ (c and d) adapted from ref. (31). The counter anions PF_6^-, hydrogen atoms and solvents are omitted for clarity.

In these structures, cyclophane moieties are arranged in a continuous alignment. The intermolecular distances between two viologen units located on distinct molecules are 4.86 Å and 4.13 Å in $\mathbf{R5}^{4+}$ and $\mathbf{R7}^{4+}$ respectively and these distances were measured at 3.31 Å and 3.29 Å for the bis (radical-cation) cyclophanes $\mathbf{R5}^{2(+\bullet)}$ and $\mathbf{R7}^{2(+\bullet)}$ respectively. This close proximity between the two viologen radicals in the solid state provides strong evidence for intermolecular dimerization in both $\mathbf{R5}^{2(+\bullet)}$ and $\mathbf{R7}^{2(+\bullet)}$ species in the solid state.

In the $\mathbf{R7}^{2(+\bullet)}$ structure, the geometry keep the gauche conformation of the heptyl spacer and provides a large intramolecular distance of 7.77 Å (Figure 2.18 D), which clearly prevents any intramolecular dimerization between the two radical viologen units. Ongoing from $\mathbf{R5}^{4+}$ to $\mathbf{R5}^{2(+\bullet)}$ species, a great distortion of the alkyl chains is observed and the intramolecular distance, defined by C4-C4 atomic distance, becomes closer to be at 4.75 Å. However, if weak

Van Der Waals interactions between the two radical units are certainly involved, this distance remains too long for intramolecular π-dimerization.

The formation of inclusion complexes in the solid state was also tested. In accordance with our results, the cavity of the $\mathbf{R5}^{4+}$ cyclophane was clearly too small for any inclusion. In contrast, the chemical reduction of both 1:1 or 1:2 mixtures of $\mathbf{R7}^{4+}$ and $\mathbf{V}^{2+}$ resulted in similar dark blue crystals containing mixed valence inclusion complex $[\mathbf{R7.V_2}]^{3(+\bullet)(2+)}$. This novel complex, represented in Figure 2.19, consists of stacks made of one guest $\mathbf{V}^{+\bullet}$ species inside $\mathbf{R7}^{2(+\bullet)}$ and another $\mathbf{V}^{+\bullet}$ located outside the host. The $\mathbf{R7}^{2(+\bullet)}$ cavity in the inclusion complex showed significant adjustments by decreasing the cavity size from 7.77 × 10.22 Å to 6.48 × 11.19 Å for $\mathbf{R7}^{2(+\bullet)}$ and $[\mathbf{R7.V_2}]^{3(+\bullet)(2+)}$ species respectively. In addition, unlike Stoddart blue-boxes having rigid spacers, the electron density in $[\mathbf{R7.V_2}]^{3(+\bullet)(2+)}$ species is distributed over large distances without pairing effects. The isolation of this inclusion complex comes again to support strongly our conclusion from present spectro-voltammetric titration of $\mathbf{R7}^{4+}$ with $\mathbf{V}^{2+}$ molecule.

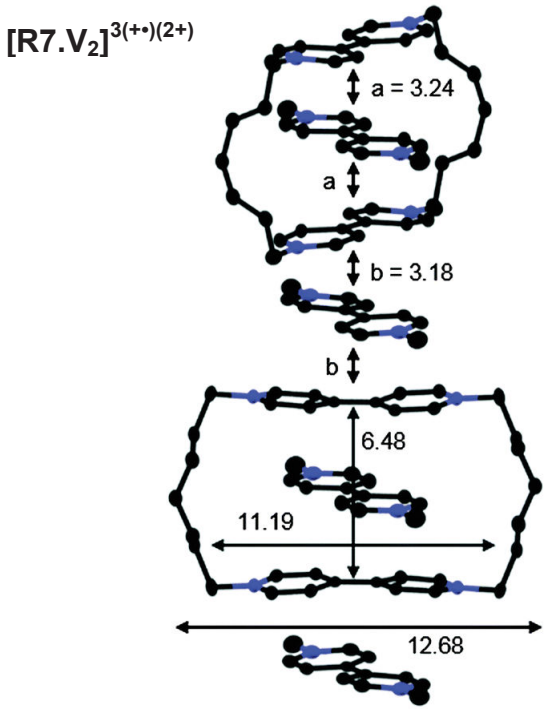

Figure 2.19: X-ray structure of the mixed valence inclusion complex $[\mathbf{R7.V_2}]^{3(+\bullet)(2+)}$ adapted from ref. (31). The counter anions PF_6^-, hydrogen atoms and solvents are omitted for clarity.

6. Conclusions and perspective

In this Chapter, we have investigated the redox properties in organic solvent of new flexible cyclophanes incorporating two viologen units linked by pentyl ($\mathbf{R5}^{4+}$) or heptyl ($\mathbf{R7}^{4+}$) chain. Upon the 2-electron reduction of $\mathbf{R5}^{4+}$, a multicentered orbital bonding occurs between the two viologen radicals within $\mathbf{R5}^{2(+\bullet)}$ species resulting in the partial formation of an intramolecular and diamagnetic π-dimer ($\mathbf{R5}^{2+}$) formed between the two radical viologen groups. The electrochemical triggered formation of this dimer is well-reversible at room temperature and was demonstrated by electrochemical study, UV-vis spectroscopy and ESR spectra. In the case of the bigger bis-viologen cyclophane $\mathbf{R7}^{4+}$, no evidence of intra- or inter-molecular dimerization was observed upon reduction. Unlike the cyclophane $\mathbf{R5}^{4+}$, the non-formation of the π-dimer $\mathbf{R7}^{2+}$ could be attributed to the larger length of heptyl linker and its higher conformational flexibility compared with pentyl spacer in $\mathbf{R5}^{4+}$. These two reasons could forbid the proximity of the two viologen radicals in $\mathbf{R7}^{2(+\bullet)}$ and hence prevent efficient orbital overlapping which is necessary to form the π-dimer $\mathbf{R7}^{2+}$.

Concerning the second part, our present study did not provide clear evidence on the formation of the inclusion complex between $\mathbf{V}^{+\bullet}$ and $\mathbf{R5}^{2(+\bullet)}$. In fact, in the absence and presence of $\mathbf{V}^{+\bullet}$ species, the π-dimerization process has been demonstrated which suggests that the formation of $\mathbf{R5}^{2(+\bullet)}\subset\mathbf{V}^{+\bullet}$ species is still speculative. However, thses results clearly show that these systems are not really adapted for the formation of π-dimer or inclusion complexes with viologen radicals, and we thus studied a new project on coordination polymers.

References

1. P. M. S. Monk. The Viologens: Physicochemical Properties, Synthesis and Applications of the Salts of 4, 4'-Bipyridine. Chichester: John Wiley & Sons Ltd. **1998**.
2. B. Odell, M. V. Reddington, A. M. Z. Slawin, N. Spencer, J. F. Stoddart and D. J. Williams, *Angew. Chem. Inf. Ed. Engl.*, **1988**, 27, 1547.
3. P. Neta, M.-C. Richoux and A. Harriman, *J. Chem. Soc., Faraday Trans. 2*, **1985**,81, 1427.
4. M. Mohammad, *Electrochim. Acta*, **1988**, 33, 417.
5. X. Tang , T. W. Schneider, J. W. Walker and D. A. Buttry, *Langmuir*, **1996**, 12, 5921.
6. S.-I. Imabayashi, N. Kitamura and S. Tazuke, *J. Electroanal. Chem.*, **1988**, 239, 397 and 403.
7. M. Future and S. Nazakura, *Chem. Lett.*, **1980**, 821.
8. S. Hünig, W. Geuder and A. Suchy, *Angew. Chem. Int. Ed. Eng.*, **1983**, 22, 489.
9. W. Geuder, S. Hünig and A. Suchy, *Tetrahedron*, **1986**, 42, 1665.
10. J. M. Spruell, A. Coskun, D. C. Friedman, R. S. Forgan, A. A. Sarjeant, A. Trabolsi, A. C. Fahrenbach, G. Barin, W. F. Paxton, S. K. Dey, M. A. Olson, D. Ben_tez, E. Tkatchouk, M. T. Colvin, R. Carmielli, S. T. Caldwell, G. M. Rosair, S. G. Hewage, F. Duclairoir, J.-L. Seymour1, A. M. Z. Slawin, W. A. Goddard III, M. R. Wasielewski, G. Cooke and J. F. Stoddart, *Nat. Chem.*, **2010**, 2, 870.
11. A. C. Fahrenbach, J. C. Barnes, D. A. Lanfranchi, H. Li, A. Coskun, J. J. Gassensmith, Z. Liu, D. Benítez, A. Trabolsi, W. A. Goddard, M. Elhabiri and J. F. Stoddart, *J. Am. Chem. Soc.*, **2012**, 134, 3061.
12. A. Trabolsi, N. Khashab, A. C. Fahrenbach, D. C. Friedman, M. T. Colvin, K. K. Coti, D. Benítez, E. Tkatchouk, J.-C. Olsen, M. E. Belowich, R. Carmielli, H. A. Khatib, W. A. Goddard, M. R. Wasielewski and J. F. Stoddart, *Nat. Chem.*, **2010**, 2, 42.
13. J. M. Spruell, *Pure Appl. Chem.*, **2010**, 82, 2281.
14. A. H. Flood, S. Nygaard, B. W. Laursen, J. O. Jeppesen and J. F. Stoddart, *Org. Lett.*, **2006**, 8, 2205.
15. P. R. Ashton, R. Ballardini, V. Balzani, S. E. Boyd, A. Credi, M. T. Gandolfi, M. G.-López, S. Iqbal, D. Philp, J. A. Preece, L. Prodi, H. G. Ricketts, J. F. Stoddart, M. S. Tolley, M. Venturi, M. Venturi, A. J. P. White and D. J. Williams, *Chem. Eur. J.*, **1997**, 3, 152.

16. P. R. Ashton, C. L. Brown, E. J. T. Chrystal, T. T. Goodnow, A. E. Kaifer, K. P. Parry, D. Philp, A. M. Z. Slawin, N. Spencer, J. F. Stoddart and D. J. Williams, *J. Chem. Soc., Chem. Commun.*, **1991**, 634.
17. P. L. Anelli, P. R. Ashton, R. Ballardini, V. Balzani, M. Delgado, M. T. Gandolfi, T. T. Goodnow, A. E. Kaifer and D. Philp, *J. Am. Chem. Soc.*, **1992**, 114, 193.
18. A. Deronzier, B. GaIland and M. Vieira, *Nouv. J. Chim.*, **1982**, 6, 97.
19. C. L. Bird and A. T. Kuhn, *Chem. Soc. Rev.*, **1981**, 10, 49.
20. A. Iordache, M. Oltean, A. Milet, F. Thomas, B. Baptiste, E. Saint-Aman and C. Bucher, *J. Am. Chem.Soc.*, **2012**, 134, 2653.
21. A. Iordache, M. Retegan, F. Thomas, G. Royal, E. Saint-Aman and C. Bucher, *Chem. Eur. J.*, **2012**, 18, 7648.
22. A. Iordache, R. Kannappan, E. Métay, M.-C. Duclos, S. Pellet-Rostaing, M. Lemaire, A. Milet, E. Saint-Aman and C. Bucher, *Org. Biomol. Chem.*, **2013**, 11, 4383.
23. C. Kahlfuss, E. Metay, M.-C. Duclos, M. Lemaire, M. Oltean, A. Milet, E. Saint-Aman and C. Bucher, *C. R. Chimie*, **2014**, 17(6), 505.
24. C. Kahlfuss, S. Denis-Quanquin, N. Calin, E. Dumont, M. Garavelli, G. Royal, S. Cobo, E. Saint-Aman and C. Bucher, *J. Am. Chem. Soc.*, **2016**, 138, 15234.
25. P. Neta, M.-C. Richoux and A. Harriman, *J. Chem. Soc., Faraday Trans. 2*, **1985**,81, 1427.
26. M. Mohammad, *Electrochim. Acta*, **1988**, 33, 417.
27. R. L. Myers and I. Shain, *Anal. Chem.*, **1969**, 41, 980.
28. D. E. Richardson and H. Taube, *Inorg. Chem.* **1981**, 20, 1278.
29. M. Berville, S. Choua, C. Gourlaouen, C. Boudon, L. Ruhlmann, C. Bailly, S. Cobo, E. Saint-Aman, J. Wytko and J. Weiss, *ChemPhysChem.*, **2017**, 18, 796.
30. G-J. Zhang, X. Gan, Q-Q. Xu, Y. Chen, X-J. Zhao, B. Qin, X-J. Lv, S-W. Lai, W-F. Fu and C-M. Che, *Dalton Trans.*, **2012**, 41, 8421.
31. M. Berville, L. Karmazin, J. Wytko and J. Weiss, *Chem. Commun.*, **2015**, 51, 15772.
32. N. Leblanc, N. Mercier, O. Toma, A. H. Kassiba, L. Zorina, P. Auban-Senzier and C. Pasquier, *Chem. Commun.*, **2013**, 49, 10272.
33. T. M. Bookman and J. K. Kochi, *J. Org. Chem.*, **1990**, 55, 4127.
34. W. W. Porter and T. P. Vaid, *J. Org. Chem.*, **2005**, 70, 5028.

CHAPTER III

Redox responsive coordination polymers based on the viologen units

Preamble

In this chapter, our objective was to prepare and investigate new coordination polymers having responsive properties. These systems, based on the properties of the viologen units, exhibit redox controlled switching properties.

1. Coordination polymers

Coordination polymers are built-up by a supramolecular approach (self-assembly) through the interaction of metal ions and a multidentate ligand which incorporates two or more discrete metal-binding domains linked by an appropriate spacer group (Figure 3.1). The resulting metal-ligand compound extends into one, two or three dimensions metal-ligand bonding.[1-5] The one-dimensional coordination polymer soluble in solution can be described as follows (Figure 3.1 A): an organic ligand having two binding sites separated by a spacer is placed in the presence of a stoichiometric equivalent of metal ion (M). In solution, structures organize themselves spontaneously to minimize the overall energy of the system by forming coordination complexes. The coordination polymer will grow in solution under the effect of spontaneous self-assembly of its components, until its maximum length is reached, or that one of the two components is lacking. This is a first feature of the coordination polymers, namely that the maximum length will be modulated by the stoichiometry.

The synthesis of the basic bridging ligands of the terpyridines **1** (Figure 3.1 B) and the concept of the construction of coordination polymers based on terpyridine ligands were introduced by Constable and coworkers.[6-14]

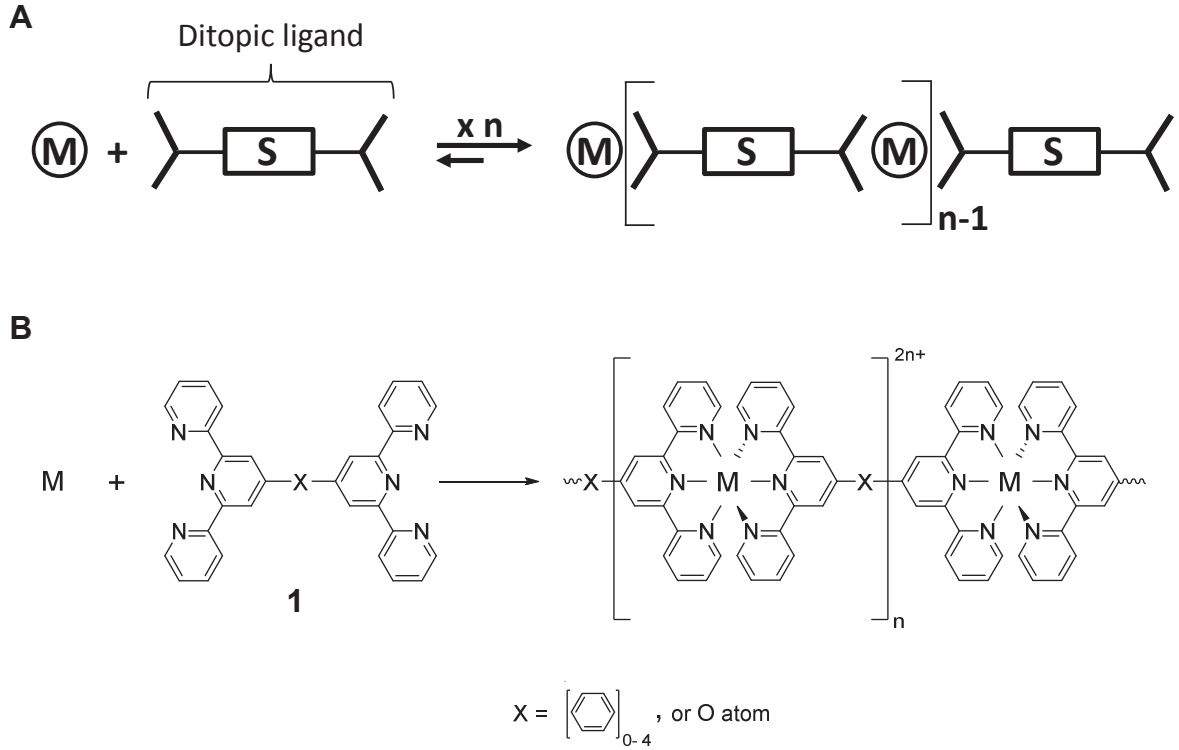

Figure 3.1: (A) Schematic representation for a one-dimensional coordination polymer. M denotes to metal ion and S denotes to the organic spacer connected by two terminal binding sites (bold shapes > and <). (B) Example of 1D coordination polymers based on terpyridine unit.[6-14]

In the case of soluble coordination polymers, the metal-ligand interaction forces (the coordination bonds) must be sufficiently strong to hold the polymer chain in solution. Such coordination polymers may possess the classical polymer properties such as improved viscosity in comparison with their monomeric building blocks and/or a glassy solid state.[4]
The presence of transition metal complexes in the structure offers many properties such as strong absorption, suitable excited state lifetimes luminescence, tunable redox states or spin cross-over.[4, 5, 15]

In addition, the possible reversibility of the coordination bonds in the self-assembled coordination polymer introduces a dynamic nature. The chain length of the coordination polymer and hence the degree of polymerization (DP) depend mainly on two factors: the binding constant (K) of the metal-ligand association and the concentration of reactive species ([Metal] and [Ligand]). The binding constant is also sensitive to external variables such as

temperature or solvent. In the case of reversible polymers, the relationship between the degree of polymerization (DP) and the binding constant (K) follows the following expression: [4, 16, 17]

$$DP \approx (K\,[M])^{1/2}$$

According to this relationship, long polymers can be obtained at high concentrations of monomer species [M] and by utilizing a system with high binding constants K. Since the binding constant K is a thermodynamic variable, this law is only valid at equilibrium through a fully reversible complexation process. If dynamic polymers are aimed, a good choice is to elaborate coordination polymers with high binding constants (thermodynamically stable) and pronounced reversibility (kinetically labile). The production of such polymers in solution thus requires either the use of non-coordinating solvents or the use of strong chelating polydentate ligands so that their strong association constants limit the competition with the solvent molecules.[18]

In particularly, bipyridine, and terpyridine-based derivatives are excellent candidates for the building-up of coordination polymers.[5] The terpyridine ligands are often used in the preparation of many well defined supramolecular architectures.[5] Indeed, this unit can coordinate many transition metal ions generally with high binding constants and forms stereochemically well-defined (pseudo-) octahedral complexes with most transition metal ions. Therefore, these complexes can be used for the construction of linear coordination polymers through the substitution in the 4-position of the central pyridine ring. Due to the high binding constants of the terpyridine complexes, it is possible to study the formation of their self-assembly coordination polymers in aqueous solutions which increases their possible uses on large scales.[19] In contrast to the octahedral 3:1 ligand metal complexes of phenanthroline or 2,2'-bipyridine ligands, the 4'-substituted bis-terpyridine octahedral complexes does not result in enantiomers. On the other hand, the reversible formation and cleavage of the coordination bond controlled by external stimuli such as redox processes or competing ligands addition are permitted in terpyridine complexes. In addition, the metal-ligand bond can be tuned by changing the employed metal ion.[5] For example, zinc(II) complexes are kinetically labile. The systems containing metal cations of the second and third series, d^3 or d^6, such as platinum(II), or palladium(II) are also generally kinetically labile.[20] As mentioned above, these dynamic equilibrium systems can respond to external stimuli to switch between monomer and polymer states or between different self-assembled systems like macrocycles and polymers.[4] In this manner, the terpyridine unit can act as a self-

complementary as well as a complementary recognition unit, only dependent on the type of complexation procedure utilized.[19] Next paragraph ruthenium(II) complexes are very stable and rather kinetically inert. For example, the rod-like ruthenium(II) coordination polymer **3** (Figure 3.2), was prepared in which the rigid ligand **2** was functionalized with two n-hexyl groups to enhance solubility. This diamagnetic polymer **3** has been prepared via the metal complexation polymerization of the ditopic ligand 4,4″- bis(2,2′:6′,2″-terpyridine)-2′,5′-dihexyl-p-terphenyl **2** with an activated ruthenium(III) species $RuCl_3.3H_2O$ in 1-butanol/dimethylacetamide, DMA (Figure 3.2). Using endcapping experiments combined with ^1H and ^{13}C-NMR spectroscopies, the degree of polymerization of the high-molecular-weight polymers **3** was estimated to be ≥ 30 which corresponds to a molecular weight of more than 36000 g mol^{-1}. The considerable length of the rods **3** is further supported by viscosimetry experiments with intrinsic viscosities of [η] ≈ 300 ml. g^{-1} (determined in 0.02 M NH_4PF_6/DMA) which is in the same order of magnitude as the intrinsic viscosities observed for poly (p-phenylene)s. Furthermore, the UV-vis absorption spectra recorded in DMA solution do not show any evidence of intramolecular electronic interactions of the metal centers along the polymer chains: the coordination polymer thus behaves like sequences of electronically independent ruthenium(II) complexes.[21-24]

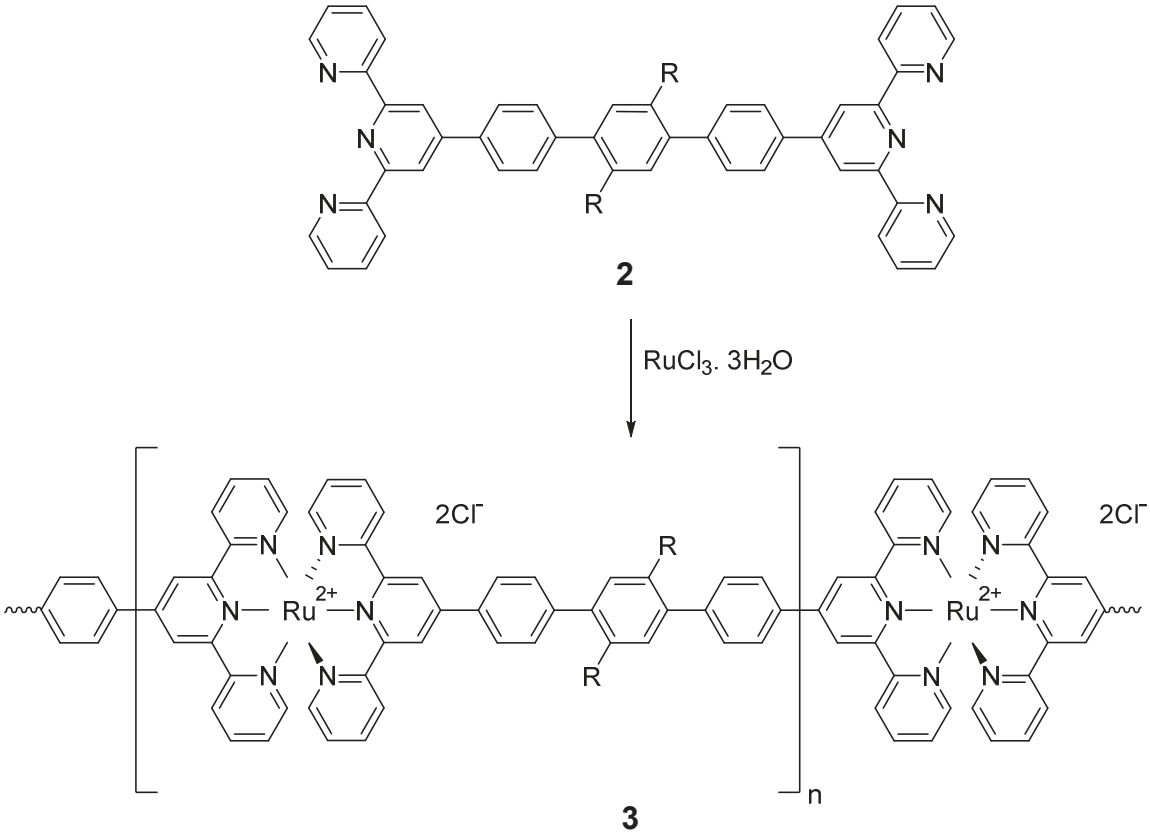

Figure 3.2: Rigid rod-like coordination poıymer based on terpyridineruthenium(II) complexes, R = hexyl group.[21-24]

It was demonstrated that low molecular weight coordination polymers are obtained when coordinating solvents like acetonitrile or pyridine are used.[23] Rehahn and coworkers [23] supposed that the coordination polymer decomposes through uprooting of the polymer ligands by alternative coordination with coordinating solvent molecules. Therefore, the ligand exchange could be precluded in solution by using only non-coordinating solvents in the synthetic routes of polymers and subsequently the polymer forms could be characterized. Unfortunately, most coordination polymers are polyelectrolytes that are sparingly soluble in organic solvents and instead they prefer highly polar solvents. Therefore, in order to increase the solubility of the targeted ligand in organic solvents, alkyl side chains can be introduced in the structures. Consequently, coordination polymers could be formed actually in a non-polar solvent such as 1,1,2,2-tetrachloroethane (TCE).

A typical dynamic coordination polymer is the system **5** which was introduced by Kurth's group (Figure 3.4).[16, 25] Herein, the reaction of the rigid ditopic ligand 1,4-bis(2,2',6',2''-terpyrid-4'-yl)benzene (**4**) with first row transition metal ion in a 1:1 ratio in solution results in the spontaneously assembled the linear rigid-rod polymer **5** in which the positive charge lies along the molecular axis (Figure 3.4). The linear arrangement of the repeating units is attributed to the octahedral coordination geometry of the metal ion. Moreover, sufficient inflexibility must be adopted by the ditopic ligand to avoid ring formation; otherwise the entropy will prevent high molecular weight chains to occur and instead lower molecular weight polymers will be favored. On the other hand, the employed transition metals should form 2:1 complexes with the coordinating sides of the monomer ligand; otherwise, branched or cross-linked products will form.[23]

The coordination polymer **5** is the first water soluble which was reported more than five years after the first work of Constable and Thompson on coordination polymers based on terpyridine ligands. This coordination polymer **5** and subsequent similar systems are easy to handle and appropriate to be used on a large scale in industrial applications where organic solvents must be avoided.[19, 26]

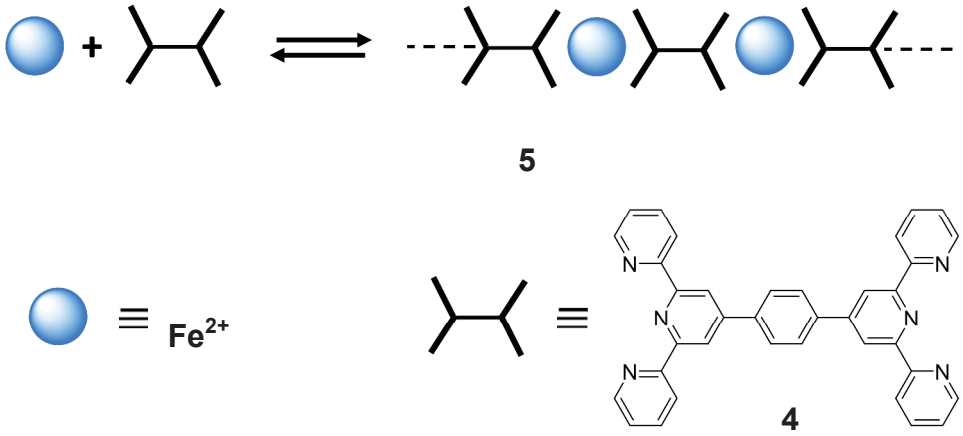

Figure 3.3: Self-assembly of ditopic ligand **4** and $Fe(OAc)_2$ in a 1:1 ratio results in the linear rigid rod-like coordination polymer **5**.[16, 19, 25, 26]

Figure 3.4 illustrates the α,ω-*bis*(terpyridine) functionalized poly(ethylene oxide)$_{180}$ prepolymer **6** and α,ω-*bis*(terpyridine) functionalized poly(oxytetramethylene)s prepolymers **7** and **8**. The addition of transition metal ion which coordinates in octahedral geometry to the bis-terpyridine functionalized prepolymer **6**, **7**, or **8** results in the spontaneous self-assembly formation of coordination polymers. The coordination polymerization process has been monitored by NMR spectroscopy, UV-Vis spectroscopy and titration microcalorimetry.[24, 27-30]

The capability of **6** for the spontaneous formation of extended coordination polymers towards a wide range of metal salts was also investigated extensively and monitored by measurements of the relative viscosity (see Figure 3.5). The stepwise addition of each of metal salts solutions (Cd(II), Cu(II), Co(II), Ni(II), and Fe(II)) to a **6** solution in methanol led to an increase in relative viscosity gradually to reach its maximum value at a ratio of 1:1. Then, the viscosity values decrease for higher ratios of metal: ligand. This behavior of the viscosity values is attributed to the formation of the coordination polymers where their maximum molecular weight and consequently the degree of polymerization are the highest at equivalent amounts of metal ion and ditopic ligand.[30]

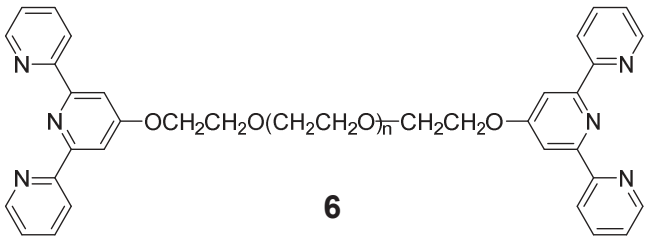

6

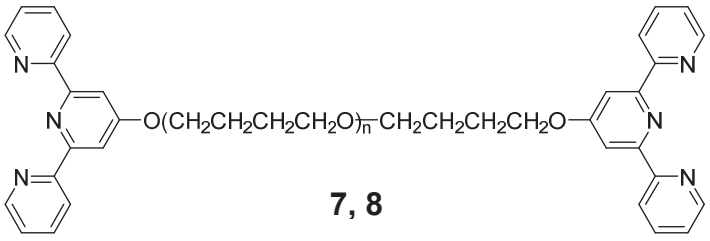

7, 8

Figure 3.4: Different bis-terpyridine functionalized telechelic ligands **6** (n = 178), **7** (n = 7), and **8** (n = 38).[24, 27-30]

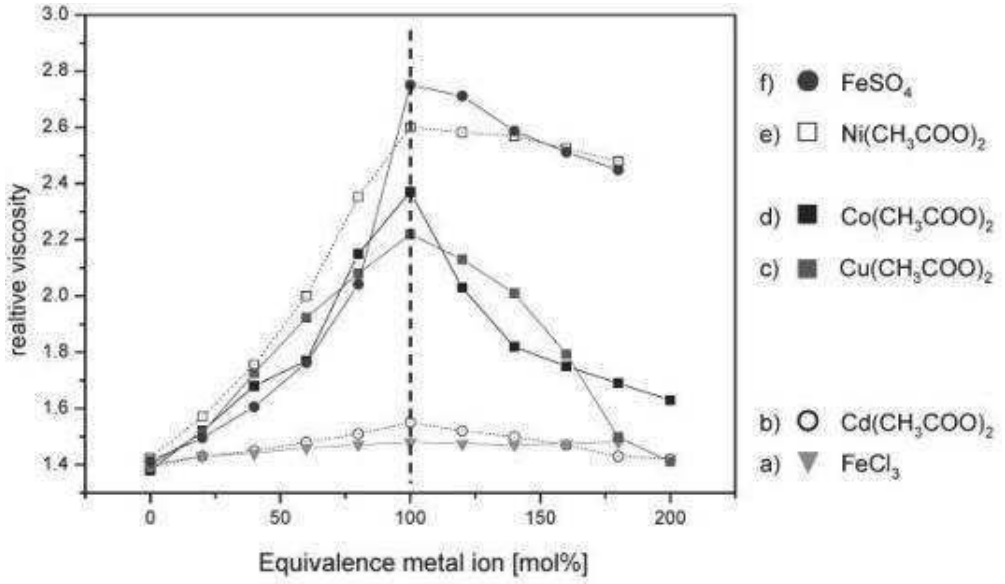

Figure 3.5: Viscosimetry titration of 20 mg/mL of **6** by Fe(III), Cd(II), Cu(II), Co(II), Ni(II) and Fe(II) ions in methanol at 293 K. (Reprinted with permission from (30), © 2017 American Chemical Society).

The small amounts of coordination monomers or oligomers formed for higher equivalents of metal ions lead to a significant decrease in the degree of polymerization and consequently to a decrease of the viscosity values. The maximum change in viscosity values is pronounced before the ratio of 1:1 metal ion/ligand and this is a proof of the quantitative complexation, i.e., the gradual and quantitative formation of coordination polymers. However, the decrease in viscosity values after the ratio of 1:1 metal ion/ligand is less pronounced in the case of Fe(II). The iron(II) ion forms the higher molecular-weight poly (ethylene oxide) coordination polymers based on metal-induced self-assembly of **6**. The molecular weight of this polymer was estimated on the basis of concentration-dependent viscosity measurements to be of 80000 g. mol^{-1} which represents one of the highest reported molecular weights for iron coordination polymers.[29, 30]

2. Responsive coordination polymers

A bistable system is required to make a molecular switch working, which means a molecular system that can be converted reversibly and noticeably from one stable state to another in response to external stimuli. Furthermore, the system should be controllable and readable on the molecular level to give a helpful system. For example, spin cross-over phenomena are very common in this regard because of this bistability in solution and also in the solid state.[31] The first-row transition metals having the d^4–d^7 electron configuration may display normally

spin crossover phenomena.[26] These metals have two possible ground state configurations possessing different multiplicities. These two ground states are the low-spin state (LS) in which the energy separation Δ between the t_{2g} and e_g sets of the d-orbitals is higher than the spin-pairing energy and the other is the high-spin state (HS). At the point when the spin-pairing energy is in the same domain as Δ, these two ground states can be switched after exposure to an external stimulus such as temperature, pressure, or light. Therefore, low spin compounds can undergo a thermal spin crossover from low spin to high spin, resulting in a number of possible applications for example as contrast agents for biomedical imaging, temperature threshold indicators or as optical elements in spin display devices.[32]

The concept of spin cross-over induced by an amphiphilic phase transition in coordination polymers was introduced by Kurth and co-workers in 2005 (Figure 3.6).[15, 34] They investigated a Fe(II)-terpyridine coordination polymer whose acetate counter ions were replaced by suitably charged amphiphiles (Figure 3.6 A). The self-assembly of the coordination polymer **5** and the negatively charged surfactants, dihexadecyl phosphate **9** results in the corresponding polyelectrolyte-amphiphile coordination polymer **10**. The coordination polymer **10** (which readily dissolves in organic solvents) was spread at the air-water interface and the resulting Langmuir monolayer was transferred on solid substrate by means of the Langmuir–Blodgett (LB) technique which results in a highly ordered multilayer.[26]

Upon heating, the amphiphile anions experienced a phase transition, resulting in a strong mechanical strain which in turn is sufficient to distort the coordination geometry around the central metal ions. Consequently, the crystal field splitting of the d-orbital subsets decreased bringing about a spin transition from a diamagnetic low-spin state to a paramagnetic high-spin state (Figure 3.6 B). The diamagnetic-paramagnetic transition was reversible.[15]

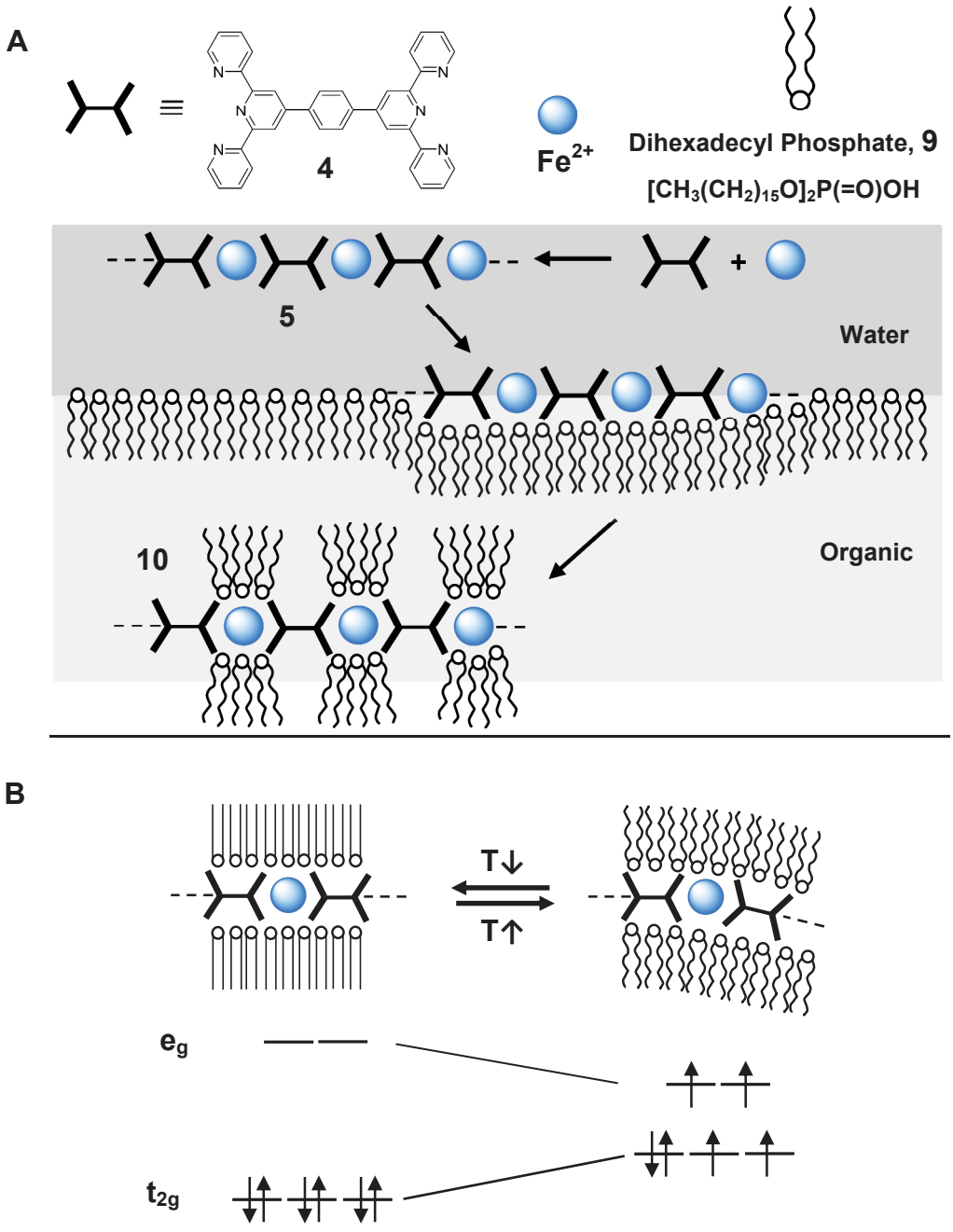

Figure 3.6: (A) Self-assembly of ditopic ligand **4** and $Fe(OAc)_2$ results in coordination polymer **5**. The self-assembly of the coordination polymer **5** and the negatively charged surfactants, dehexadecyl phosphate **6** results in the corresponding polyelectrolyte-amphiphile coordination polymer **10**. (B) Upon heating, the melting of the alkyl chains in **10** results in reversible transition from a diamagnetic low-spin to a paramagnetic high-spin state within d-orbitals of coordinated iron ion.[26] (Modified from (26), with permission from (15), © 2017 American Chemical Society).

Furthermore, the control of the steric bulk or strain of the ligand system is another way to control the spin state of coordinated metal ions. The 2,2′:6′,2″ terpyridine induces generally the electrons of d-orbitals to be with low spin configurations.[33] But the substitution of the terpyridine ligand at the 6- and 6″-position with bulky groups can distort the octahedral coordination environment and then changing the field splitting which in turns influence the spin state.[15] But in this case, the steric demands of these bulky substituents will hinder the formation of high molecular weight chains of the coordination polymers.[16]

Rowan and Beck [35, 36] have introduced multi-stimuli, multi-responsive gels based on coordination polymers. The self-assembling of both transition metal and lanthanide ions with the ligand **11** (Figure 3.7; 1,6-bis(1'-methylbenzimidazolyl)-4-hydroxypyridine) produces coordination polymeric gels which can exhibit thermo-, chemo- and mechanical responses, as well as light-emitting properties. The ditopic ligand **11** can coordinate to transition metal ions in octahedral geometry with a 2:1 ratio while it binds in a ratio of 3:1 to lanthanide ions. Addition of 3 mol% of the lanthanide (Eu(III) or La(III)) (with respect to the ligand) to the ditopic ligand **11** forms a supramolecular tri-functional unit, which acts as a crosslinking moiety. Then addition of 97 mol% of Zn(II) or Co(II) ions spontaneously results in polymeric gel-formation (Figure 3.7). Consequently, four different gels were prepared and characterized (Co–La, Zn–La, Co–Eu and Zn–Eu). The nature of the gel responses to external stimulus depends on the metal ion, counter-ion and on the amount of swelling solvent. All these resulting gels response to heating showing reversible transition to the solution accompanied with optical changes resulting from thermal break of lanthanide-ligand interaction. The same reversible gel-solution transition happens upon addition of formic acid which in turn bounds to the lanthanide ions after displacing ligand **11**. Such process is reversed upon drying the material in vacuum to remove the formic acid. The Zn(II)-La(II) gels exhibit reversible thixotropic or shear-thinning under stress responses, meaning that shaking these gels results in solutions which thicken again to the gel phase upon standing.[19, 35, 36]

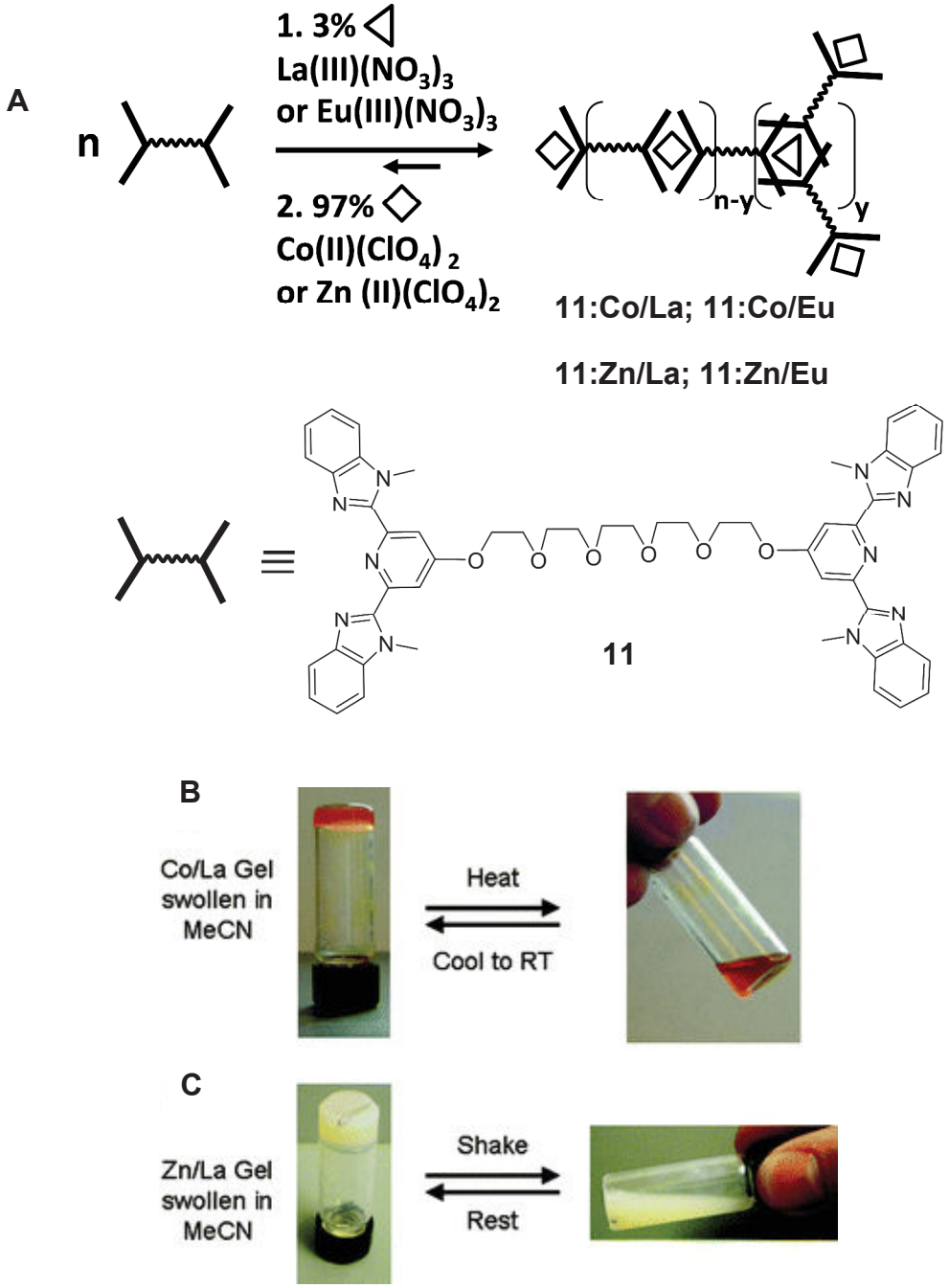

Figure 3.7: (A) Formation of supramolecular gels from the assembling of ditopic ligand 1,6-bis(1'-methylbenzimidazolyl)-4-hydroxypyridine **11** and appropriate ratios of transition metal ions and lanthanide ions. (B) Thermoresponsive nature of **11:Co/La** and (C) Mechanoresponsive properties of the thixotropic **11:Zn/La** system. Both materials (B) and (C) are swollen in acetonitrile (80% by wt.).[35, 36] (B and C are reprinted with permission from (19), © 2017 Royal Society of Chemistry).

Rowan and coworkers [37] also investigated new self-healable Zn(II) metallo-polymers based on a macromonomer comprising a rubbery poly(ethylene-co-butylene) core with two terminal 2,6-bis(1'-methylbenzimidazolyl)pyridine ligands (Figure 3.8). After deliberate damage of these polymer films, they can efficiently repair themselves upon applying ultraviolet light to the damaged region. Upon exposure to ultraviolet light, the metal-ligand at the damaged region is excited electronically, and a considerable portion of absorbed light is converted into heat. Concomitantly, temporary dissociation of the metal-ligand motifs occurred at light-applied region followed by reversible depolymerization and decrease in viscosity, thereby causing fast damage repairing. This light-healing behavior relies on an excess of free ligands and on the nature of metal/ligand bonding within the structures of these polymers. Therefore, the polymers with the higher metal contents showed less light-induced healing compared with polymers of 0.7 metal-ligand ratio. Additionally, because of the weaker and more dynamic bonding of 3:1 La^{3+} complexes relative to 2:1 Zn^{2+} complexes, the healing efficiencies of La^{3+} polymers are more efficient.

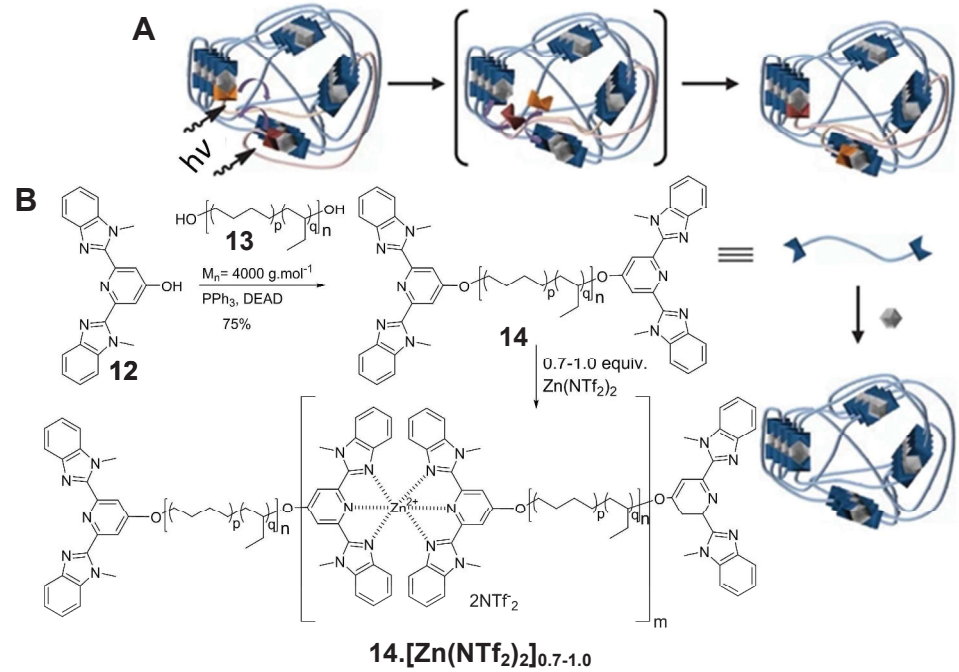

Figure 3.8: (A) Proposed mechanism for ultraviolet-healing of metallo-supramolecular polymers **14.$[Zn(NTf_2)_2]_{0.7\text{-}1.0}$**. (B) Synthesis of macromonomer **14** and its self-assembling with $Zn(NTf_2)_2$ affording the metalosupramolecular polymers **14.$[Zn(NTf_2)_2]_{0.7\text{-}1.0}$**. DEAD: diethyl azodicarboxylate.[37]

In our team, Royal and coworkers [38-42] investigated and studied extensively novel 1D coordination polymers and redox-responsive gels based on the use of a multitopic ligand: (1,8-di (p-2,2': 6', 2''- terpyridin-4-yl) tolyl)-1,4,8,11-tetraazacyclotetradecane, CHTT) comprising the cyclam (1,4,8,11-tetraazacyclotetradecane) as spacer with two terminal chelating terpyridine units. Depending on the different affinity constants of the two chelating centers (cyclam spacer and terpyridine units) with the metal ions, CHTT was self-assembled through selective preparation with copper(II), cobalt(II), and nickel(II) forming homo- or heteronuclear 1D coordination polymers. These new metallopolymer materials showed interesting properties: (i) chemosensitivity: where the ability to gelate have been shown to depend on the type of metal, stoichiometry of metal/cyclam, solvent, and counterion; (ii) mechanical sensitivity**:** where the system is able to commute from weak to high viscous states upon fast application/suppression of a shearing stress; and (iii) electrosensitivity: the Co_2^{II}CHTT system can be electrochemically and reversibly switched between the red gel Co_2^{II}CHTT and green liquid Co_2^{III}CHTT states (Figure 3.9).

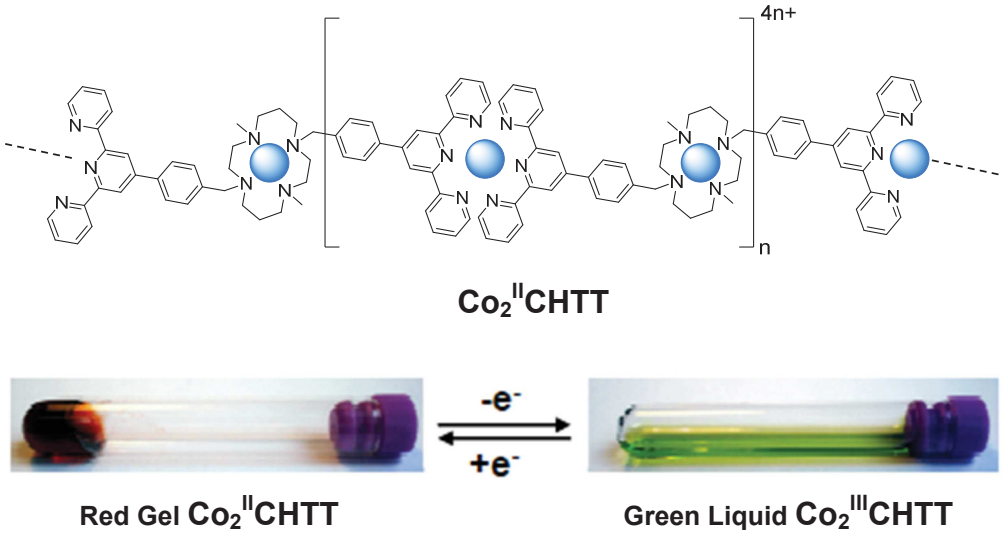

Figure 3.9: Representation of the reversible electrochemical switching in DMF between red gel **Co_2^{II}CHTT** and green liquid **Co_2^{III}CHTT** states.[38-42]

3. Objectives

In this chapter, our aim was to develop switchable coordination polymers based on the π-dimerization of viologen units (following the concept represented in scheme 3.1). This dimerization will be employed to control an organization within metal-ligand bonded

assemblies. First we will design the π-dimerizable organic monomer C_3^{4+} functionalized with two metal bonding units. This monomer is based on the propylene spacered bis-viologens featuring two terminal terpyridine units.

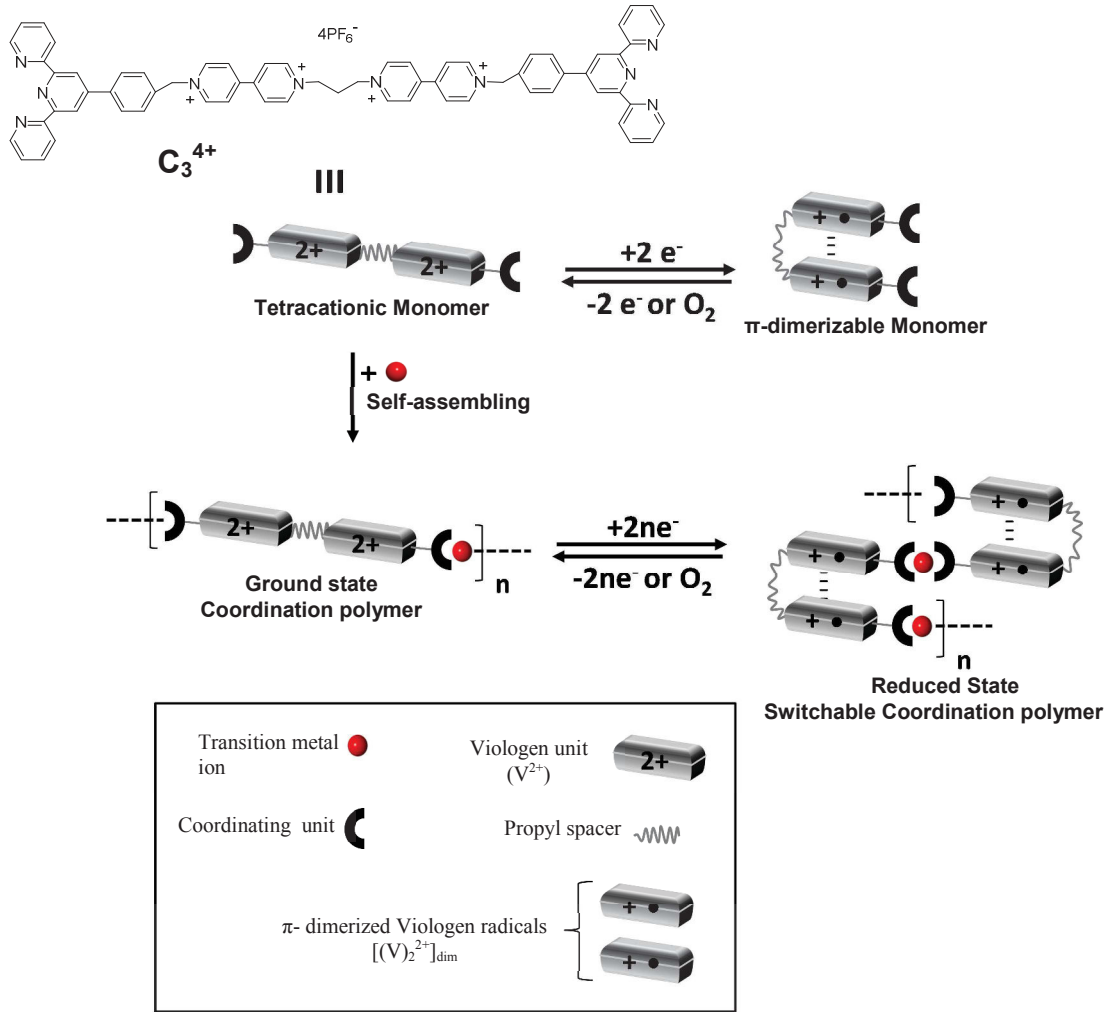

Scheme 3.1: Switchable coordination polymers based on π-dimerization of viologen units.

Reversible movements between the tetracation monomer and π-dimerized monomer form will be induced by redox stimulus. Two rational routes will be followed to attain the targeted switchable coordination polymers operated by electron transfers centered on π-dimerizable viologen fragments. In the presence of transition metal ions, the tetracation monomer C_3^{4+} will form self-assembled metal-ligand coordination bonds between repeated terpyridine units leading to extended 1D coordination polymers. Then after electron transfer to the viologen units, dimerized series of coordination polymers, or/and zig-zag dimerized coordination polymers may form. The nature of the electrogenerated switchable coordination polymers will depend on the repeated coordination complexes (involving the metal ion and the two

chelating units although the terpyridine transition metal complexes are of well-known properties), the bulkiness of the coordination polymers and finally the dimerization between viologen radicals whether intra- or intermolecular process. The essential comprehension of the nature (and the variables which drive it) of the targeted switchable coordination polymers will be necessary to modify the properties of these polymers according to the required needs.

Additionally, we will design the reference non-dimerizable monomer $\mathbf{C_2}^{4+}$ (scheme 3.2) functionalized with two metal bonding units. This reference monomer will be based on the ethylene spacered bis-viologens featuring two terminal terpyridine units. Since the impossibility of achieving the folding between two viologen radicals spacered by ethylene chain, then no intramolecular dimerization should take place for the reduced form of the reference monomer (see scheme 3.2).

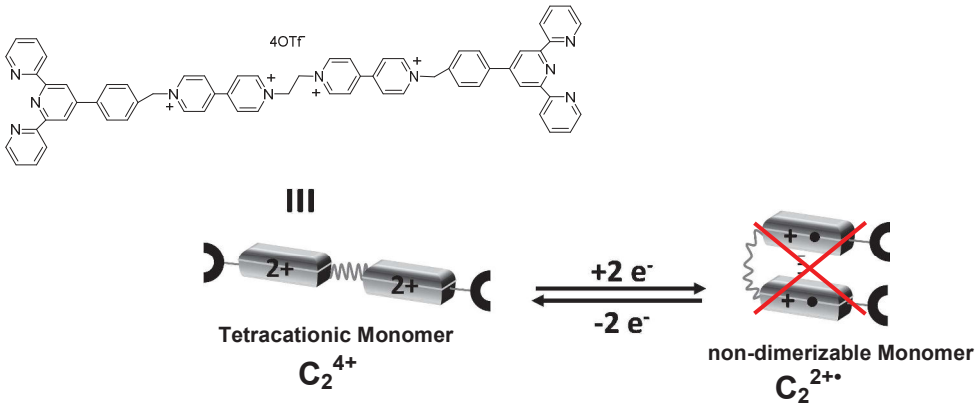

Scheme 3.2: The non-dimerized reference monomer radical.

4. Synthesis and characterization of the ligands

4.1 Syntheses

The synthetic routes leading to the targeted bis-functionalized terpyridine bis-viologen derivatives $\mathbf{C_2}^{4+}$ and $\mathbf{C_3}^{4+}$ are summerized in Figure 3.10. Derivatives $\mathbf{C_2}^{4+}$ and $\mathbf{C_3}^{4+}$ were obtained in stepwise manners. The first step involves a nucleophilic substitution (S_N2) of 1, 2-dibromopropane or 1, 3-dibromoethane with two equivalents of 4,4´-bipyridine to afford the ethyl- or propyl-tethered bis-viologens $\mathbf{V2}^{2+}$ and $\mathbf{V1}^{2+}$ in yields of 18% and 40% respectively.[43] Secondly, the bromination reaction of 4´-(4-methylphenyl)-2,2´,6´,2´´-terpyridine **15** with N-bromosuccinimide lead to a mixture of the desired mono-bromo benzyl terpyridine derivative **16** and its analogous dibromide derivative.[43-45] The mono-bromo benzyl terpyridine derivative **16** was involved in double quaternization reactions for the ethyl- or propyl-tethered bis-viologens $\mathbf{V2}^{2+}$ and $\mathbf{V1}^{2+}$ resulting in quantitatively the triflate form of $\mathbf{C_2}^{4+}$ (by a slightly different procedure) or the bromide form of $\mathbf{C_3}^{4+}$. The bromide form of $\mathbf{C_3}^{4+}$ was subject to an ion exchange reaction to afford in a quantitative yield (96%) the novel targeted bis-functionalized terpyridine bis-viologen derivative $\mathbf{C_3}^{4+}$ as PF_6^- salt.[46-50] The bis-functionalized terpyridine ethyl linked bis-viologen derivative $\mathbf{C_2}^{4+}$ was previously reported by the group of Prof S. J. Loeb (but was prepared with a low yield of 31% as triflate salt for synthetic reasons) for further study of metal-organic [2] rotaxane.[49, 50]

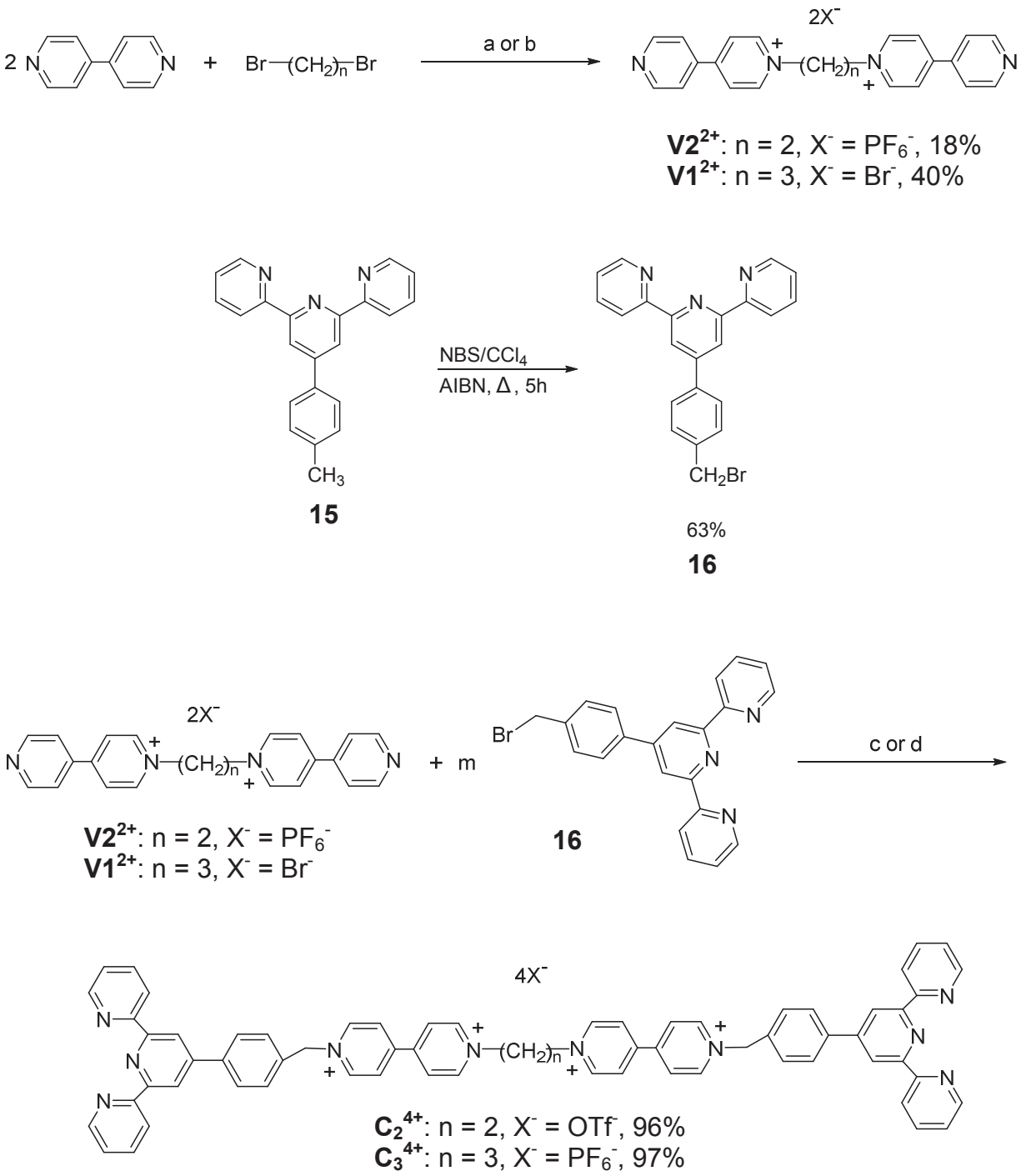

Figure 3.10: Synthesis of the bis-functionalized terpyridine bis-viologen derivatives $\mathbf{C_2}^{4+}$ and $\mathbf{C_3}^{4+}$. a) ACN, 80°C, 24h, Ar, KPF_6; b) ACN, 70°C, 24h; c) $MeNO_2$: DMF(6:0.5), 75°C, 72h, NaOTf(aq)/ $MeNO_2$, m = 3 equiv.; d) DMF, 85°C, 1 week, KPF_6, m = 2.1 equiv.

4.2 NMR Characterization

Both of the bis-functionalized terpyridine viologens $\mathbf{C_3}^{4+}$ and $\mathbf{C_2}^{4+}$ were characterized by ^{1}H- and ^{13}C-NMR spectroscopy in deuterated DMSO. ^{1}H-NMR and their attributions are represented in Figures 3.11 and 3.12. Supplementary data are given in appendix.

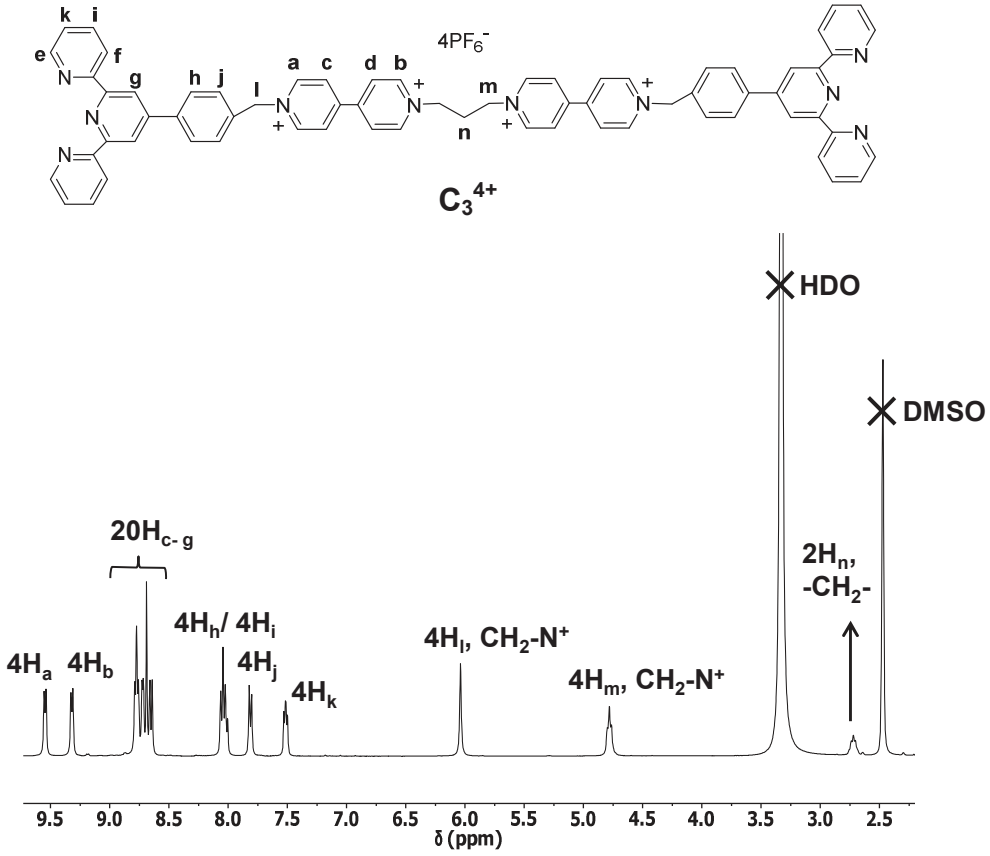

Figure 3.11: ^{1}H-NMR spectrum (400 MHz) of the derivative $\mathbf{C_3}^{4+}$ in DMSO-d6 at 298K.

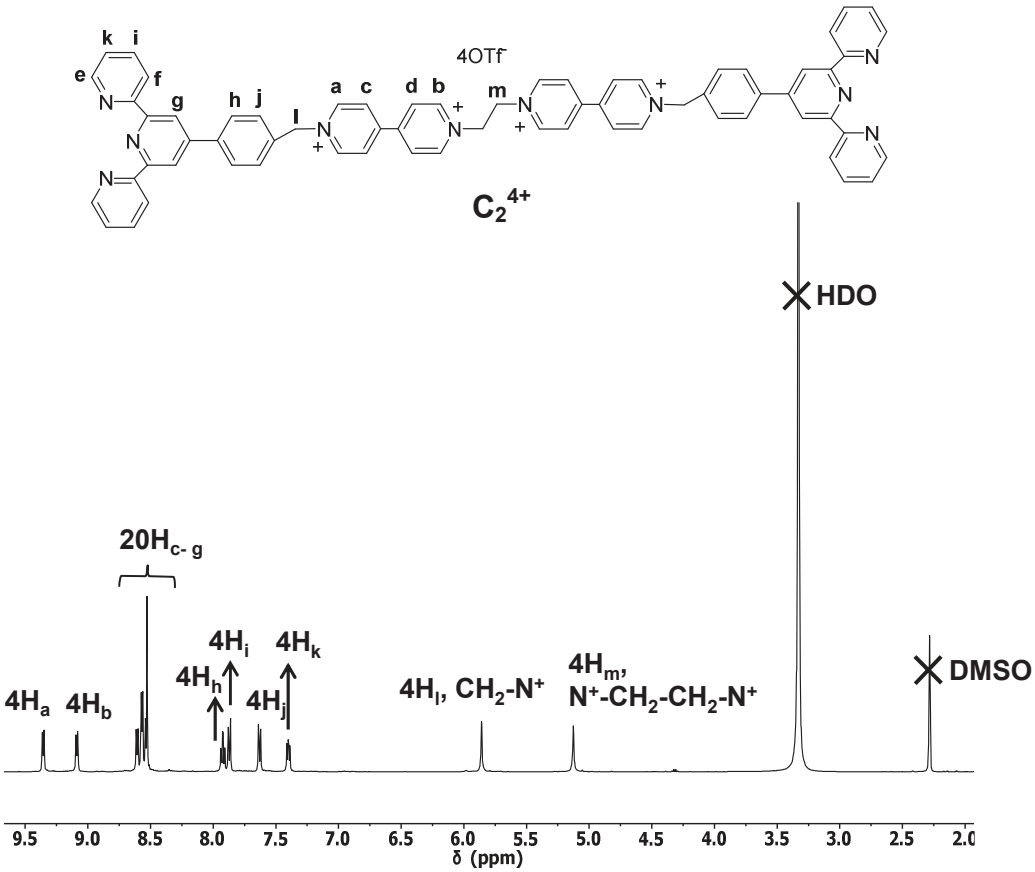

Figure 3.12: ^{1}H-NMR spectrum (500 MHz) of the derivative $\mathbf{C_2}^{4+}$ in DMSO-d6 at 298K.

The exact attributions of the ^{1}H-NMR spectra for both of $\mathbf{C_2}^{4+}$ and $\mathbf{C_3}^{4+}$ showed above have been performed with the assistance of GCOSY NMR spectra which are represented along with DEPTQ and 1D ^{13}C-NMR spectra (see annexe). ^{1}H-NMR signals of $\mathbf{C_2}^{4+}$ and $\mathbf{C_3}^{4+}$ can be divided into three main regions which are: 1) the aromatic region involving signals of bipyridinium and phenyl terpyridine moieties, 2) the signals of the benzylic CH_2 groups ($PhCH_2$-N^+) and 3) the propyl and ethyl spacers signals (CH_2-N^+). The formation of the di-quaternized propyl- and ethyl-tethered bis-viologen $\mathbf{C_2}^{4+}$ and $\mathbf{C_3}^{4+}$ were supported by the observation of these signals. The first is the singlet peak attributed to the four protons of the benzylic CH_2 group ($PhCH_2$-N^+) which are resonating at 6.04 ppm and 5.86 ppm in the targeted derivatives $\mathbf{C_3}^{4+}$ and $\mathbf{C_2}^{4+}$ ($4H_l$) respectively. The signal integration is confirming the double quaternization of the free propyl- or ethyl-tethered bis-viologen $\mathbf{V1}^{2+}$ or $\mathbf{V2}^{2+}$ by two molecules of **16**. The second evidence to be considered is the triplet signal of both CH_2-N^+ groups ($4H_m$) of the propyl spacer at 4.78 ppm which is upfield shifted upon quaternization compared with that of the free propyl-tethered bis-viologen $\mathbf{V1}^{2+}$. Similarly, the singlet signal of both CH_2-N^+ groups ($4H_m$) of the ethyl spacer at 5.13 ppm is also upfield shifted upon quaternization compared with that of the free ethyl-tethered bis-viologen $\mathbf{V2}^{2+}$. Thirdly, due to

the electron-withdrawing property of the two benzyl terpyridine groups in $\mathbf{C_3}^{4+}$ or $\mathbf{C_2}^{4+}$, the doublet signal due to H_a protons is downfield shifted compared with those of H_b in $\mathbf{C_3}^{4+}$ or $\mathbf{C_2}^{4+}$ respectively. The remaining aromatic signals of the viologen moieties in $\mathbf{C_3}^{4+}$ resonate at downfield chemical shifts compared with those of the free propyl-tethered bis-viologen $\mathbf{V1}^{2+}$.[44]

4.3 Characterization by mass spectrometry

The HRMS-ESI and MALDI-TOF Mass spectrometries were also used to confirm the structures for both of the bis-functionalized terpyridine viologens $\mathbf{C_3}^{4+}$ and $\mathbf{C_2}^{4+}$. The HRMS-ESI mass analysis of $\mathbf{C_3}^{4+}$ revealed the fragment ion $[M\text{-}PF_6]^+$ which corresponds to the loss of one PF_6^- counterion from the parent molecule $\mathbf{C_3}^{4+}$. Four fragment ions corresponding to the successive loss of four PF_6^- counterions from the parent molecule $\mathbf{C_3}^{4+}$ were observed by the MALDI-TOF Mass spectrometry. These mono charged fragments correspond to $[M\text{-}PF_6]^+$, $[M\text{-}2PF_6]^+$, $[M\text{-}3PF_6]^+$ and $[M\text{-}4PF_6]^+$ respectively.

The HRMS-ESI mass spectrum of $\mathbf{C_2}^{4+}$ showed the double charged fragment $[M\text{-}2OTf^-]^{2+}$ after losing two OTf^- counterions from the parent molecule $\mathbf{C_2}^{4+}$. Two mono charged fragments: $[M\text{-}OTf^-]^+$ and $[M\text{-}3OTf^-]^+$ were detected by the MALDI-TOF Mass spectrometry.

4.4 Electrochemical studies

The electrochemical properties of the bis-functionalized terpyridine bis-viologens have been investigated in DMF (0.1 M TBAP) using cyclic voltammetry (CV) and linear voltammetry with the rotating disk electrode (VRDE). All the potentials in the text are given against the Ag^+ (10 mM) /Ag reference electrode. The electrochemical experiments have been carried out at room temperature under an argon atmosphere in a dry glove box using a conventional three electrode electrochemical cell, vitreous carbon disc electrode as working electrode and a platinum wire as auxiliary electrode. Other experimental details about each record are given in the experimental part or in figure captions.

The electrochemical properties of $\mathbf{C_3}^{4+}$ and $\mathbf{C_2}^{4+}$ were also compared with those of the di-methylated propyl-tethered bis-viologen ($\mathbf{C_{3ref}}^{4+}$), and the di-ethylated ethyl-tethered bis-viologen ($\mathbf{C_{2ref}}^{4+}$) respectively. Figure 3.13 illustrates the CVs of the bis-functionalized terpyridine viologens $\mathbf{C_3}^{4+}$ and $\mathbf{C_2}^{4+}$ along with their corresponding reference compounds $\mathbf{C_{3ref}}^{4+}$, and $\mathbf{C_{2ref}}^{4+}$ respectively. Figures 3.14 and 3.15 depict the CVs (solid lines) and voltammetry VRDE (dotted line) curves for 0.5 mM of both of $\mathbf{C_3}^{4+}$ and $\mathbf{C_2}^{4+}$ respectively. The corresponding measured data are summarized in Table 3.1.

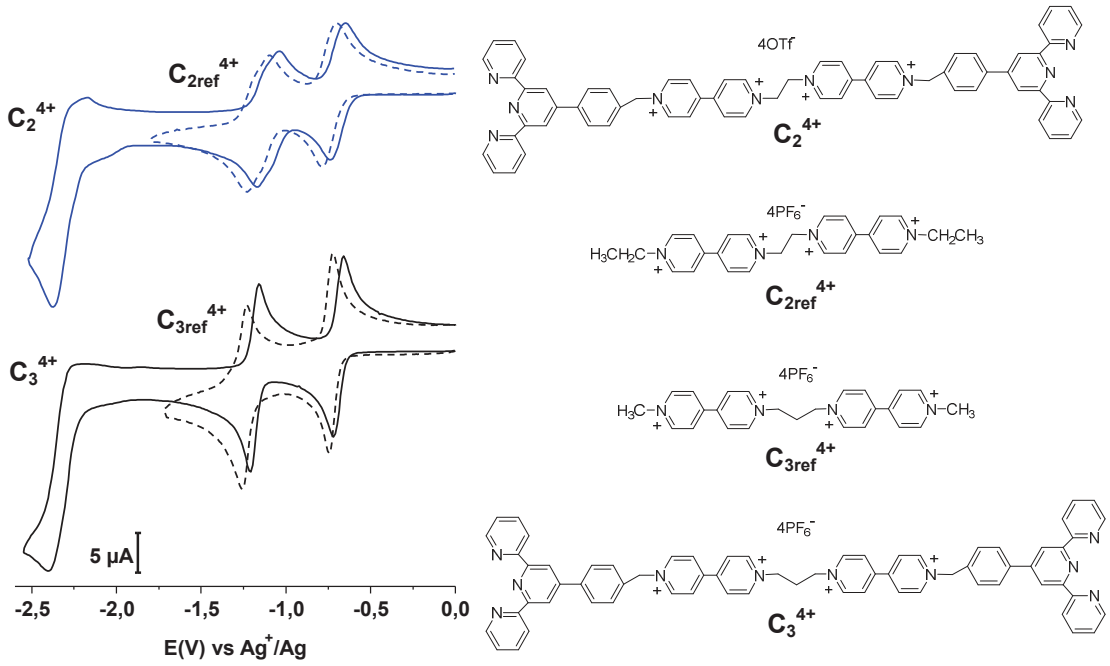

Figure 3.13: CVs of $\mathbf{C_3}^{4+}$ (solid line, bottom), $\mathbf{C_{3ref}}^{4+}$ (dash line, bottom), $\mathbf{C_2}^{4+}$ (solid line, upper), and $\mathbf{C_{2ref}}^{4+}$ (dash line, upper) in 0.1 M TBAP/DMF at 100mV/s. Working electrode: 3mm Vitreous Carbon. Reference electrode: 0.01M $AgNO_3$ + 0.1 M TBAP/CH_3CN/Ag. Conc. = 0.5 mM.

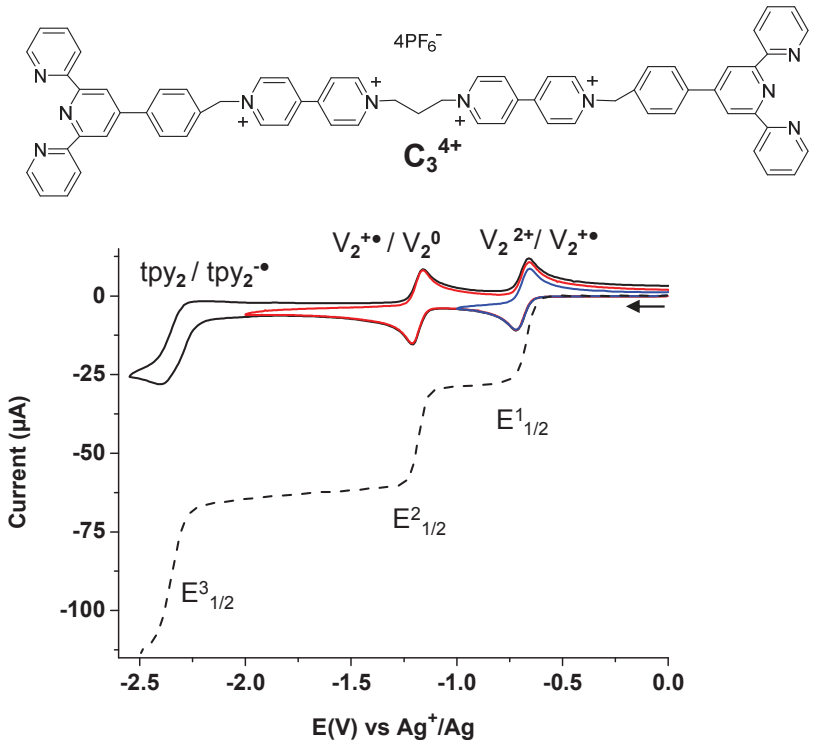

Figure 3.14: CV (solid line) and voltammetry curve VRDE (dotted line) for 0.5 mM of $\mathbf{C_3}^{4+}$ in 0.1 M TBAP/DMF at 100mV/s for CV or 10mV/s and 3000 rpm for VRDE. Working electrode: 3mm Vitreous Carbon. Reference electrode: 0.01M $AgNO_3$ + 0.1 M TBAP/CH_3CN/Ag.

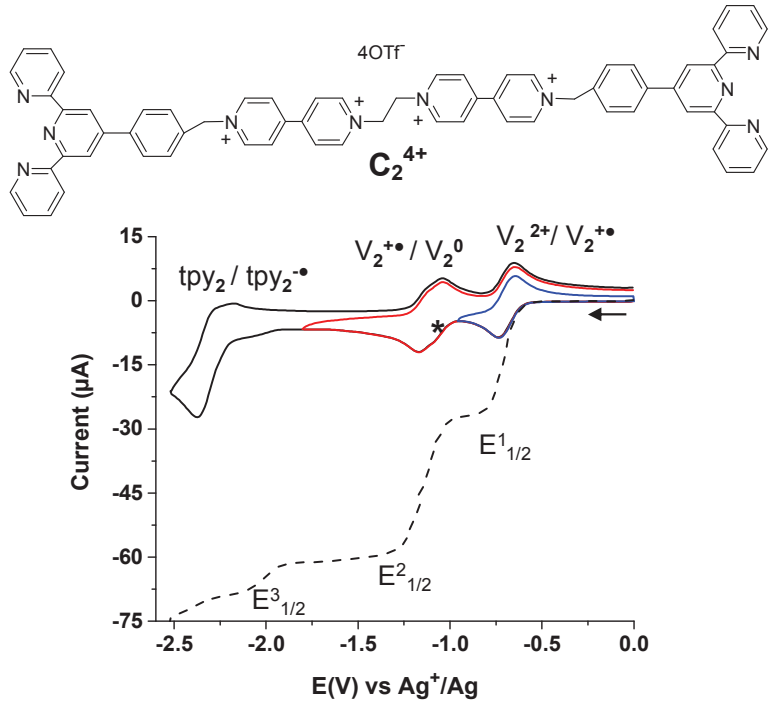

Figure 3.15: CV (solid line) and voltammetry curve VRDE (dotted line) for 0.5 mM of $\mathbf{C_2}^{4+}$ in 0.1 M TBAP/DMF at 100mV/s for CV or 10mV/s and 3000 rpm for VRDE. Working electrode: 3mm Vitreous Carbon. Reference electrode: 0.01M $AgNO_3$ + 0.1 M TBAP/CH_3CN/Ag.*: two overlapped systems.

Table 3.1: experimental voltammetric potentials[a] with number of transferred electrons (in parenthesis) for $\mathbf{C_3}^{4+}$, $\mathbf{C_{3ref}}^{4+}$, $\mathbf{C_2}^{4+}$, and $\mathbf{C_{2ref}}^{4+}$ at 100 mV/s. Working electrode: 3mm Vitreous Carbon. Reference electrode: 0.01M $AgNO_3$ + 0.1 M TBAP/CH_3CN/Ag.

	$E^1_{1/2}$ (V) $V^{2+}/V^{+\bullet}$	$\Delta E_p{}^1$ (mV) $V^{2+}/V^{+\bullet}$	$E^2_{1/2}$ (V) $V^{+\bullet}/V^0$	$E^1_{1/2}$-$E^2_{1/2}$(V)	$E^3_{1/2}$(V)
$\mathbf{C_{2ref}}^{4+}$	−0.74(2)	80	−1.16(2)	0.42	–
$\mathbf{C_2}^{4+}$	−0.69 (2)	80	−1.10 (2)	0.41	–2.44
$\mathbf{C_{3ref}}^{4+}$	–0.73(2)	25	−1.24(2)	0.51	–
$\mathbf{C_3}^{4+}$	−0.68(2)	60	−1.18(2)	0.50	–2.36[b]

[a]: 0.5 mM for each of $\mathbf{C_3}^{4+}$, $\mathbf{C_{3ref}}^{4+}$, $\mathbf{C_2}^{4+}$ and $\mathbf{C_{2ref}}^{4+}$ in 0.1 M TBAP/DMF; $\Delta E_p{}^1 = E_{pa}{}^1 - E_{pc}{}^1$; $E^1_{1/2} = (E_{pa}{}^1 + E_{pc}{}^1)/2$; [b]: irreversible system: peak potential.

The CV curves of the propyl-tethered bis-viologen $\mathbf{C_{3ref}}^{4+}$ and of the ethyl-tethered bis-viologen $\mathbf{C_{2ref}}^{4+}$ exhibit two 2-electron reversible CV waves (dash lines in Figure 3.13). These waves occurred at $E^1_{1/2}$ = -0.73 V, -0.74 V and $E^2_{1/2}$ = -1.24 V, -1.16 V for $\mathbf{C_{3ref}}^{4+}$ and $\mathbf{C_{2ref}}^{4+}$ respectively and lead to the formation of the bis (radical-cation) species $\mathbf{V_2}^{2(+\bullet)}$ and then to the neutral bis-quinoid species $\mathbf{V_2}^{0}$. The potential separation between these two reductions ($E^1_{1/2}$-$E^2_{1/2}$, table 3.1) is 0.51 V and 0.42 respectively. As documented before, upon its two electrons reduction, the di-methylated propyl-tethered bis-viologen $\mathbf{C_{3ref}}^{4+}$ exhibits the intramolecular association between the bis (radical-cation) form $\mathbf{V_2}^{2(+\bullet)}$. In contrast, because of the too short ethyl spacer, no association occurs within the bis (radical-cation) species $\mathbf{V_2}^{2(+\bullet)}$ for $\mathbf{C_{2ref}}^{4+}$ at millimolar concentrations in organic polar solvents at room temperature.[51-53]

Concerning the $\mathbf{C_3}^{4+}$ and $\mathbf{C_2}^{4+}$ systems, three reduction waves are observed between 0 and about -2.5 V. The first two consecutive reversible waves are similar to those observed with their corresponding references, *i.e.* $\mathbf{C_{3ref}}^{4+}$ and $\mathbf{C_{2ref}}^{4+}$ respectively. These signals account each for 2 electrons per molecule (*i.e.* 1 electron per viologen subunit) and occurred at $E^1_{1/2}$ = -0.68 V and -0.69 V and $E^2_{1/2}$ = -1.18 V and -1.10 V for $\mathbf{C_3}^{4+}$ and $\mathbf{C_2}^{4+}$ respectively. They correspond respectively to the formation of the bis (radical-cation) species $\mathbf{V_2}^{2(+\bullet)}$ and then to the neutral bis-quinoid species $\mathbf{V_2}^{0}$. However, it should be noted that because of withdrawing effects of the terpyridine moieties, the first reduction signal of $\mathbf{C_3}^{4+}$ is positively shifted by

~50 mV compared with that of the reference compound $\mathbf{C_{3ref}}^{4+}$. The same potential shift of ~50 mV is also observed between the first reduction waves of $\mathbf{C_2}^{4+}$ and $\mathbf{C_{2ref}}^{4+}$. We can also remark that, in the case of $\mathbf{C_2}^{4+}$, the second redox wave at $E^1_{1/2}$ = -1.10 V (denoted as * in Figures 15) appears as two overlapped and ill-defined systems which are accounting each for 1 electron.(54)

Finally, the last redox wave observed for $\mathbf{C_3}^{4+}$ and $\mathbf{C_2}^{4+}$at more negative potential ($E^3_{1/2}$ = -2.35 V and -2.44 V respectively) is assigned to the poorly reversible reduction of both two terpyridine moieties resulting in $\mathbf{tpy_2}^{-\bullet}$ species.(55)

Importantly, a larger stability domain of the bis-radical state $\mathbf{V_2}^{2(+\bullet)}$ and a lower ΔE_p^1 is found in the case of $\mathbf{C_3}^{4+}$ compared to $\mathbf{C_2}^{4+}$, suggesting that only the $\mathbf{C_3}^{4+}$ system could yield the intramolecular dimerization upon reduction. In order to confirm and investigate these processes more deeply, the single-electron successive reductions of the viologen units in $\mathbf{C_2}^{4+}$ and $\mathbf{C_3}^{4+}$ along with their possible coupled reactions must be considered. These reactions are represented in Scheme 3.1 (see also Annexes for further description).(51, 56)

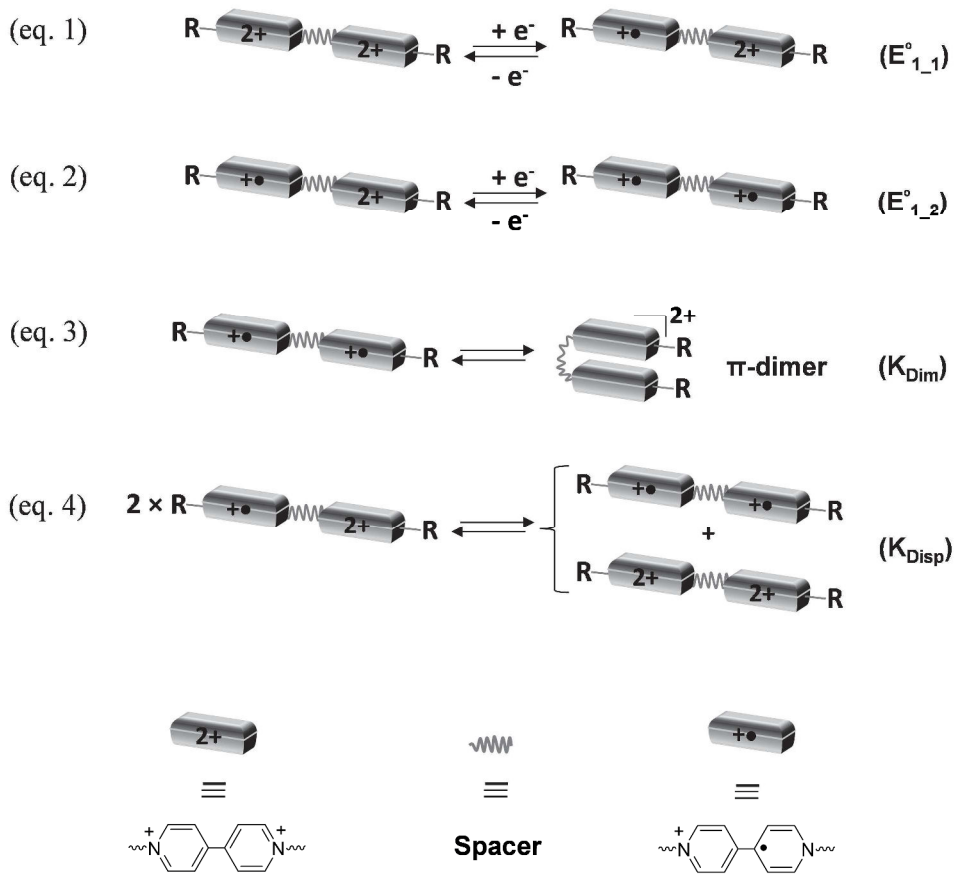

Scheme 3.1: single-electron successive reductions of bis-viologens species (equations: 1 and 2) and their potential coupled reactions (dimerization: eq. 3 and disproportionation: eq. 4).

The first two-electron reversible reduction wave of the bis-viologen derivatives observed in the experimental CV curves (Figures 3.13 and 3.14) consists of two successive single-electron transfer processes characterized by the standard potentials $E°_{1\_1}$ and $E°_{1\_2}$. The first one-electron reduction ($E°_{1\_1}$) of the bipyridinium unit is followed by the second one-electron reduction ($E°_{1\_2}$) of the second bipyridinium unit leading to the formation of the bis (radical-cation) $\mathbf{V_2^{2(+\bullet)}}$ species which can be then spontaneously involved in the thermodynamically favorable π-dimerization process (K_{Dim}). As discussed before, the presence of a π-dimerization process influences the second electron transfer ($E°_{1\_2}$), rendering it easier to happen than the reduction of the first bipyridinium unit. In addition, after the first electron transfer ($E°_{1\_1}$), the formed single reduced bis-viologen species $\mathbf{V_2^{3+(\bullet)}}$ in which the bipyridinium centers are electrochemically non-equivalent, will be subject to a disproportionation equilibria resulting in the formation of the bis (radical-cation) $\mathbf{V_2^{2(+\bullet)}}$ which can be then readily stabilized as a π-dimer (K_{Dim}).[57, 58]

In this work, the standard potential separations $\Delta E°_1$ for $\mathbf{C_3^{4+}}$ and $\mathbf{C_2^{4+}}$ were estimated from the experimental ΔE_p^1 values measured by cyclic voltammetry at low scan rate and using the method described by Shain and Taube.[59, 60] The corresponding disproportionation constants (K_{Disp}) were calculated from the relationship $\log_{10}(K_{Disp}) = -\Delta E°_1(V)/0.059$.[53] The results are collected in Table 3.2.

Table 3.2: Experimental voltammetric potentials for the first reduction with number of transferred electrons (in parenthesis) and calculated K_{disp} values for bis-viologen derivatives.[a]

	$E^1_{1/2}$ (mV)	ΔE^1_p (mV)	$\Delta E° = E°_{1\text{-}1} - E°_{1\text{-}2}$ (mV)	K_{Disp}[b]
$\mathbf{C_2^{4+}}$	-702	68	45	0.17
$\mathbf{C_3^{4+}}$	-687	37	-20	2.18

[a]: Conc. = 1 mM/viologen unit in 0.1 M TBAP/DMF; scan rate: 10mV/s. Working electrode: 3mm Vitreous Carbon. Reference electrode: 0.01M $AgNO_3$ + 0.1 M TBAP/DMF/Ag. $\Delta E_p^1 = |E_{pc}^1 - E_{pa}^1|$; $E^1_{1/2} = (E_{pa}^1 + E_{pc}^1)/2$; [b]: calculated using Taube's method[59, 60]; $\log K_{Disp} = -\Delta E°/0.059$.[53]

The large $\Delta E°_1$ value and the low K_{Disp} constant (<1) found for $\mathbf{C_2^{4+}}$ corroborate the absence of dimerization process. In contrast, the possibility of intramolecular π-dimerization process within $\mathbf{C_3^{2(+\bullet)}}$ is highly consistent with the high potential separation value $E^1_{1/2}$-$E^2_{1/2}$ (table 3.1) along with the low standard potential separation $\Delta E°_1$ (table 3.2). The dimerization process in $\mathbf{C_3^{4+}}$ thus rendered the second electron transfer ($E°_{1\_2}$) to be carried out more easily (positively shifted) than the first electron transfer ($E°_{1\_2}$). Logically, the disproportionation process is favored for $\mathbf{C_3^{4+}}$ (K_{Disp} >1).

These electrochemical data show that, the π-dimerization process can be observed only using three methylene groups between the two viologen units and that the presence of the bulky terpyridine groups in $\mathbf{C_3^{4+}}$ does not prevent its dimerization. However, it seems that the π-dimerization process in $\mathbf{C_3^{4+}}$ is a less efficient than that in the reference compound $\mathbf{C_{3ref}^{4+}}$. Indeed, the possibility of a lower π-dimerization process in $\mathbf{C_3^{4+}}$ is predicted from the lower potential separation $E^1_{1/2}$-$E^2_{1/2}$ and the higher ΔE^1_p values for $\mathbf{C_3^{4+}}$ (see Table 3.1). This effect may be logically attributed to the steric effects of the terpyridine moieties in $\mathbf{C_3^{4+}}$. Importantly, since no dimerization is expected with the $\mathbf{C_2^{4+}}$ ligand under the employed experimental conditions, it can be concluded that the formation of the π-dimer from $\mathbf{C_3^{4+}}$ is exclusively an intramolecular process. However, more experiments and in particular spectroelectrochemical investigations must be done to confirm these results.

4.5 Spectroelectrochemical studies

The spectroscopic imprints of the electrogenerated species provide additional information on the existence of non-covalent association between the bipyridinium radical cations. Spectrochemical studies were carried out under argon atmosphere in a dry glove box on 0.1 M TBAP/DMF solutions of 0.5 mM for both of $\mathbf{C_3^{4+}}$, $\mathbf{C_2^{4+}}$ and 0.7 mM of $\mathbf{V^{2+}}$ in a conventional three-electrode cell using 0.1 cm all-quartz immersion probe. The exhaustive two-electron reduction of $\mathbf{C_3^{4+}}$ and $\mathbf{C_2^{4+}}$ or one-electron reduction of $\mathbf{V^{2+}}$ were performed by fixing the potential of high surface area platinum as working electrode at -1, -0.995 and -1.12 V respectively *vs*. Ag^+ 10 mM /Ag, i.e. lower than the first cathodic response, resulting in the viologen radical cations $\mathbf{V_2^{2(+\bullet)}}$ from both of $\mathbf{C_3^{4+}}$, $\mathbf{C_2^{4+}}$, and $\mathbf{V^{+\bullet}}$ from $\mathbf{V^{2+}}$ respectively (see Figure 3.16 and table 3.3). The completion of the electrolysis is checked by comparing the voltammetry using the rotating disk electrode before and after the electrolysis.

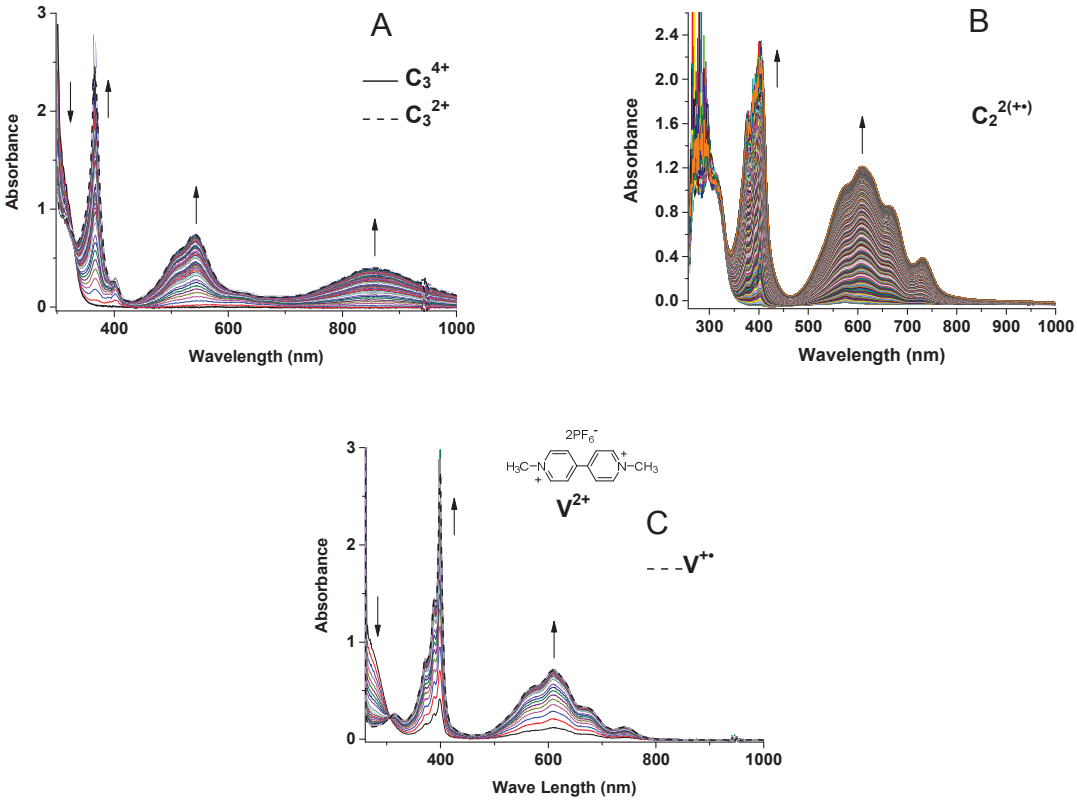

Figure 3.16: Absorption spectra recorded (A) during the exhaustive 2-electron reduction for 0.5 mM solution of $\mathbf{C_3}^{4+}$ (E_{app} = -1 V), (B) for 0.5 mM solution of $\mathbf{C_2}^{4+}$ (E_{app} = -0.955 V), and (C) during the exhaustive 1-electron reduction (E_{app} = -1.12 V) for 0.7 mM solution of $\mathbf{V}^{2+}$. Solvent: 0.1 M TBAP/DMF, 298K; working electrode: high surface area platinum, reference electrode: 0.01M $AgNO_3$ + 0.1 M TBAP/CH_3CN/Ag; UV-vis all-quartz immersion probe with l = 0.1 cm.

Table 3.3: Maximum wavelengths and molar absorption coefficients for $\mathbf{C_3}^{4+}$, $\mathbf{C_2}^{4+}$ and $\mathbf{V}^{2+}$ and their reduced compounds in 0.1 M TBAP/DMF, 298K.

Compound	λ_{max} /nm (ε/$M^{-1}.cm^{-1}$)
$\mathbf{C_3}^{4+}$	274 (25000), 298 (28000)
$\mathbf{C_3}^{2+}$	366 (49100), 401 (5200), 516 (11900), 543 (15000), 858 (8100)
$\mathbf{C_2}^{4}$	273 (22900), 300 (28200)
$\mathbf{C_2}^{2(+\bullet)}$	283 (31600), 308 (22000), 377 (32300), 401 (44000), 608 (24300), 658 (17200), 731 (7800)
$\mathbf{V}^{2+}$	264 (16800)
$\mathbf{V}^{+\bullet}$	315 (3800), 373 (11900), 389 (20900), 400 (39300), 578 (8000), 608 (10300), 667 (4800), 739 (1800)

The bulk one-electron reduction of a solution of the reference compound $\mathbf{V}^{2+}$ (E_{app} = -1.12 V) leads to the gradual decrease in the intensity of the initial π–π* absorption band which appears in the UV absorption spectra recorded during the reduction (see Figure 3.16 C). In addition, two new sets of absorption bands have been detected: the first group of absorption bands appeared at 315 nm, 373 nm, 389 nm, 400 nm and the second absorption bands appeared at 578 nm, 608 nm, 667 nm and 739 nm. The blue color and the accompanied UV-vis signature of the resulting solution (especially the absence of absorption band in the NIR region (>800 nm)) are unambiguously attributed to the non-associated radical cations $\mathbf{V}^{+\bullet}$.[48] The existence of an isosbestic point at ~305 nm reveals undoubtfully a well-defined equilibrium between the species $\mathbf{V}^{2+}$ and $\mathbf{V}^{+\bullet}$.

The exhaustive 2-electron reduction of the reference ligand $\mathbf{C_2}^{4+}$ (E_{app} = -0.955 V) leads to a formation of the bis (radical-cation) $\mathbf{C_2}^{2(+\bullet)}$ characterized with similar spectrum to that of the radical cation $\mathbf{V}^{+\bullet}$ (see Figure 3.16 B). Both the absorption bands for $\mathbf{C_2}^{2(+\bullet)}$ owned higher molar absorption coefficients compared with those of $\mathbf{V}^{+\bullet}$. Anyway, the absorption spectrum of $\mathbf{C_2}^{2(+\bullet)}$ is consistent with documented spectra of non-associated viologen radical cations, especially the absence of the NIR absorption band of the dimerized viologen radicals.

The electrochemical 2-electron reduction (E_{app} = -1 V) of $\mathbf{C_3}^{4+}$ resulted in a decrease in the intensity of the π–π* absorption band of the initial tetracationic compound and led also to the growth of new bands at 366 nm, 401 nm, 516 nm, 543 nm which can be assigned to $\mathbf{C_3}^{2+}$ as a dimer (see Figure 3.16 A). These absorption bands are blue shifted compared with those of the non-dimerized viologen radicals $\mathbf{C_2}^{2(+\bullet)}$ and $\mathbf{V}^{+\bullet}$ which indicates that the $\mathbf{C_3}^{2+}$ species are intra- or inter-molecularly dimerized. Importantly, the diagnostic signature for the formation of π-dimers is observed clearly with a large band at 858 nm. The reversibility of the bulk reduction processes was confirmed by the complete recovery of the UV-Vis absorption spectra for the initial compounds $\mathbf{C_3}^{4+}$, $\mathbf{C_2}^{4+}$ and $\mathbf{V}^{2+}$ after exposure of the purple solution of $\mathbf{C_3}^{2+}$ and the blue solutions of $\mathbf{C_2}^{2(+\bullet)}$ and $\mathbf{V}^{+\bullet}$ respectively to air (oxidation by O_2).

The spectroelectrochemical arguments are reliably consistent with our previous electrochemical studies and emphasize that whereas the reference species $\mathbf{C_2}^{2(+\bullet)}$ do not exhibit an inter-dimerization within the millimolar concentration, then the dimerization process shown by the $\mathbf{C_3}^{2+}$ species is obviously of intramolecular type.

4.6 Characterization by ESR spectroscopy

As indicated previously, the formation of the π-dimerization process between viologen radicals can be demonstrated by electron spin resonance measurements (ESR) where the spin coupling between viologen radicals makes their ESR spectra silent. The ESR spectra were recorded at 298 K for the solutions of the electrochemically generated viologen radicals of $\mathbf{V}^{+\bullet}$, $\mathbf{C_2}^{2(+\bullet)}$ and $\mathbf{C_3}^{2(+\bullet)}$. The concentrations of these viologen radicals were set at 1 mM for $\mathbf{V}^{+\bullet}$ and 0.5 mM for both of $\mathbf{C_2}^{2(+\bullet)}$ and $\mathbf{C_3}^{2(+\bullet)}$. These concentrations are above the usual limit of sensitivity of the EPR spectroscopy (10^{-5} M), but not too high to avoid the possible dimerization that may occur at higher concentrations of viologen radicals. Figure 3.17 illustrates the ESR spectra at room temperature for the radical cation $\mathbf{V}^{+\bullet}$ and the bis (radical-cation) species $\mathbf{C_2}^{2(+\bullet)}$ and $\mathbf{C_3}^{2(+\bullet)}$.

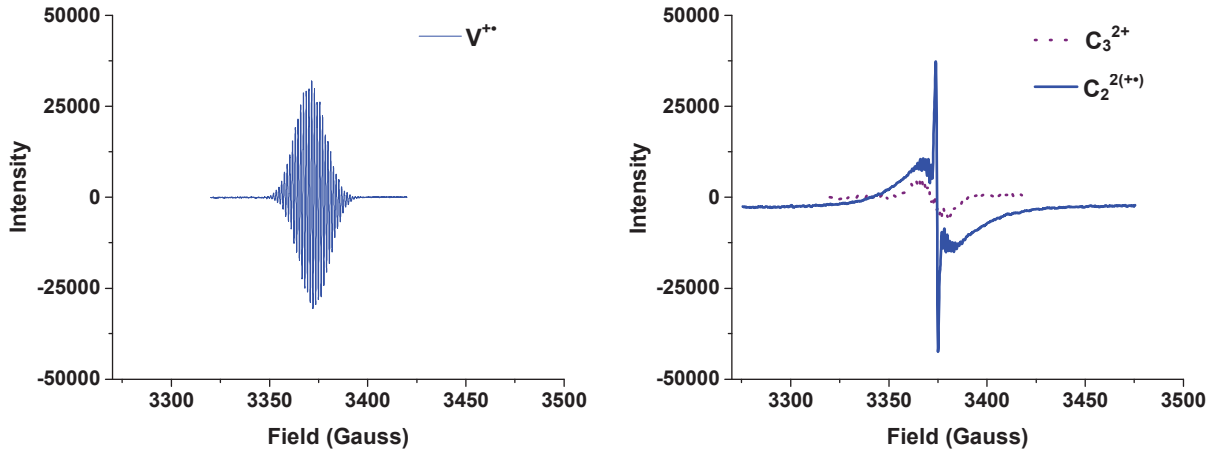

Figure 3.17: ESR spectra for (A) 1 mM of $\mathbf{V}^{+\bullet}$ (solid line), (B) 0.5 mM of each of $\mathbf{C_3}^{2}$ (dotted line) and $\mathbf{C_2}^{2(+\bullet)}$ (solid line) in 0.1 M TBAP/DMF at 298 K.

As expected, the species $\mathbf{V}^{+\bullet}$ and $\mathbf{C_2}^{2(+\bullet)}$ afforded a high intense signals attributed to the non-associated bipyridinium cation radicals (Figure 3.17 A and B, solid lines respectively), whereas the two-electron reduced species $\mathbf{C_3}^{2(+\bullet)}$ was found to be almost with silent ESR as the π-dimerization between two bipyridinium cation radicals in the dimer $\mathbf{C_3}^{2(+\bullet)}$ or/and the coupling occurring between two species of $\mathbf{C_3}^{2(+\bullet)}$ (Figure 3.17 B, dotted line).[48, 61] These results are really in good agreements with both of the electrochemical and spectroelectrochemical studies.

5. Preparation and characterization of the metallopolymers

In the previous paragraphs (4.1- 4.6), we showed the synthesis and characterization of the ligands ($\mathbf{C_2}^{4+}$ and $\mathbf{C_3}^{4+}$) along with the redox-controlled dimerization process for the ligand $\mathbf{C_3}^{4+}$. In the next paragraphs, we will show the self-assembled formation and characterization of the $\mathbf{C_2}^{4+}$ and $\mathbf{C_3}^{4+}$ (oxidized) metallopolymers. Then, we will investigate the targeted switchable properties of the metallopolymers. The switching movement between the oxidized and the dimerized reduced metallopolymers will be studied by spectroscopic, voltammetric and viscometric means along with using the reference $\mathbf{C_2}^{4+}$ metallopolymers. In the following, the coordination polymers will be named $\mathbf{MC_2}^{4+}$ or $\mathbf{MC_3}^{4+}$ with M = Zn^{2+}, Fe^{2+}, Ni^{2+} or Co^{2+}.

5.1 UV-Visible spectroscopy characterization

Figure 3.18 shows the UV-Visible absorption titration of the bis-functionalized terpyridine bis-viologen $\mathbf{C_3}^{4+}$ with the tetrafluoroborate salts of zinc(II) (A), nickel(II) (C), cobalt(II) (E), and iron(II) (G) in DMF. The titration with these metal ions led to appearance of new absorption bands in the region below 400 nm. These new absorption bands correspond to ligand centered (LC, π–π* and n–π*) absorptions that appear upon formation of the complex and are likely to be due to the conformational changes in the terpyridine moiety from the trans conformation to the planar cis conformation upon complexation in the solution. Consequently, new bands appeared at 329 nm and 343 nm, 329 nm, 335 nm and 370 nm during the titration of $\mathbf{C_3}^{4+}$ with Zn^{2+} ; Ni^{2+}; Co^{2+}; Fe^{2+} respectively (see Figure 3.18 A, C, E and G and table 3.4).[62] Both $\mathbf{C_3}^{4+}$ and $\mathbf{C_2}^{4+}$ show very similar titration behavior. Figure 19 represents the results obtained with $\mathbf{C_2}^{4+}$.

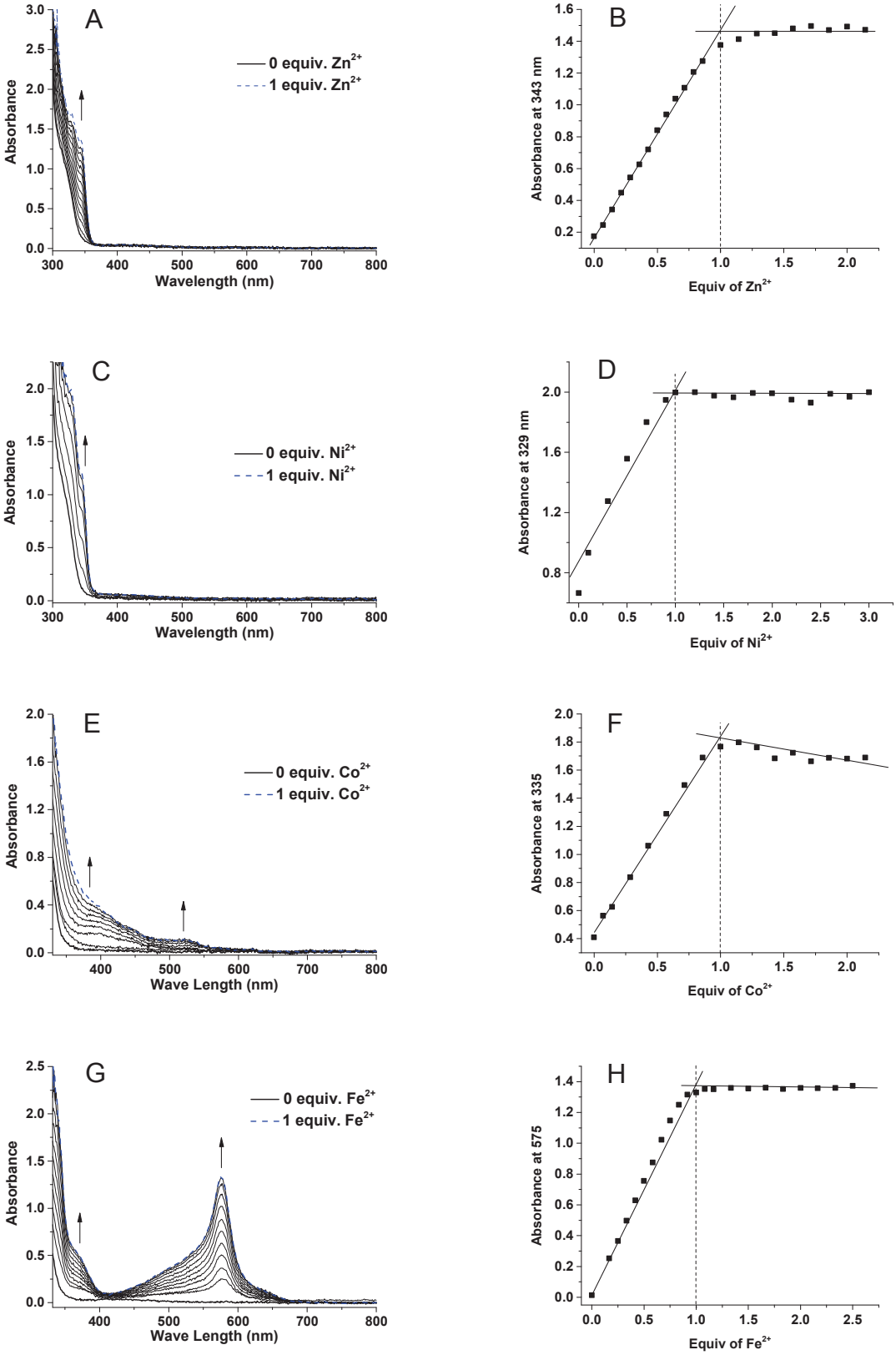

Figure 3.18: UV-Visible absorption titration of $\mathbf{C_3}^{4+}$ (0.5 mM in DMF) by tetrafluoroborate hexahydrate salts (85 mM in DMF) of Zn^{2+} (A), Ni^{2+} (C), Co^{2+} (E) and Fe^{2+} (G), 298K, UV-Vis all-quartz immersion probe with l = 0.1 cm. Titration curves at significant wavelengths for (B) Zn^{2+}; (D) Ni^{2+}; (F) Co^{2+} and (H) Fe^{2+} ions.

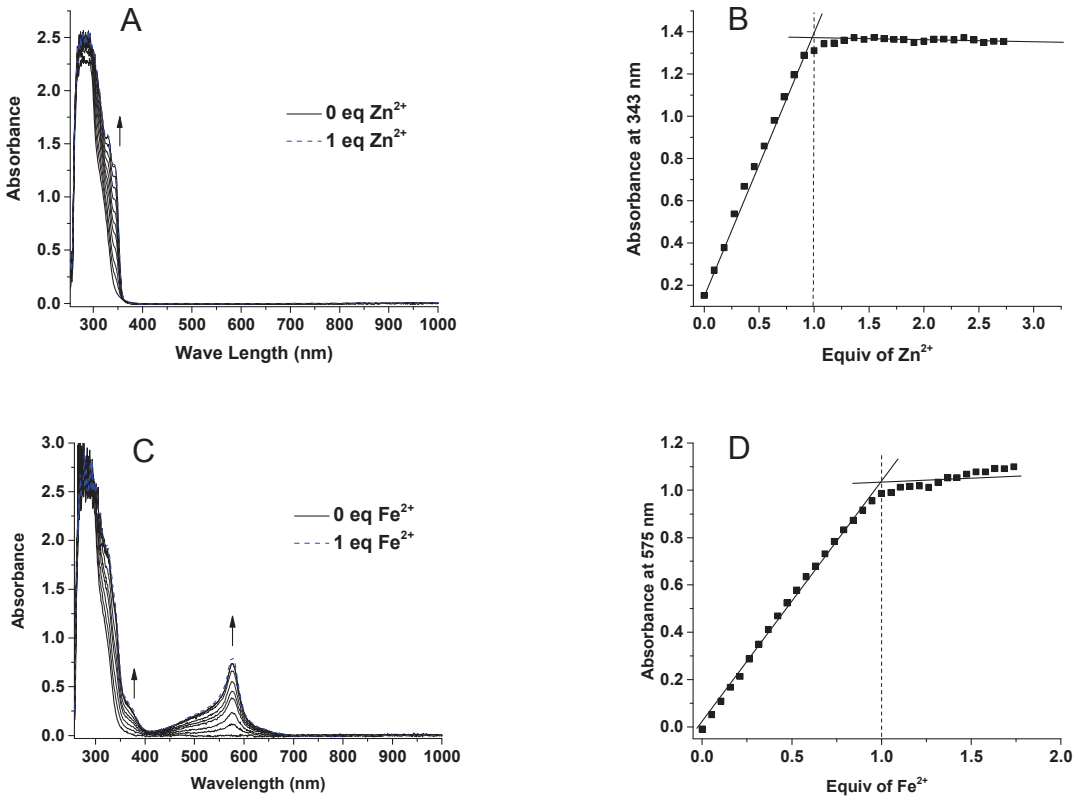

Figure 3.19: UV-Visible absorption titration of $\mathbf{C_2}^{4+}$ (0.5 mM in DMF) by the metal tetrafluoroborate hexahydrate salts (85 mM in DMF) of Zn^{2+} (A) and Fe^{2+} (C), 298K, UV-Vis all-quartz immersion probe with l = 0.1 cm. Titration curves at significant wavelengths for (B) Zn^{2+} and (D) Fe^{2+} ions.

Table 3.4: Maximum wavelengths and molar absorption coefficients for the metallopolymers of $\mathbf{19}^{4+}$ and $\mathbf{20}^{4+}$ in DMF at 298K.

Metallopolymer	λ_{max} /nm (ε/$M^{-1}.cm^{-1}$)
$\mathbf{ZnC_3}^{4+}$	329 (33300), 343 (27500)
$\mathbf{ZnC_2}^{4+}$	329 (31800), 343 (26200)
$\mathbf{NiC_3}^{4+}$	329 (40000)
$\mathbf{CoC_3}^{4+}$	335 (35300)
$\mathbf{FeC_3}^{4+}$	370 (10100), 575 (26600)
$\mathbf{FeC_2}^{4+}$	325 (38700), 370 (6100), 575 (16000)

In case of Fe^{2+} complexes, in addition to the changes observed above, a characteristic intense band appeared at 575 nm ($\mathbf{C_3}^{4+}$: Figures 3.18 G; $\mathbf{C_2}^{4+}$: Figures 3.19 C). This feature is attributed to a metal to ligand charge transfer (MLCT) band which is responsible for the deep violet color of iron complexes.(62) Similarly, the titration of $\mathbf{C_3}^{4+}$ with cobalt(II) (Figure 3.18 E) showed weak absorption band in the visible region at 522 nm.

The absorptions at characteristic wavelengths are plotted against the added equivalents of metal salts for $\mathbf{C_3}^{4+}$ and $\mathbf{C_2}^{4+}$ (Figures 3.18 and 3.19). All these titration curves showed that the spectral changes were below the ratio of 1:1 metal: ligand and almost no change in absorbance after this ratio which corroborates the formation of $[(M\ (\mathbf{C_3}))^{6+}]_n$ and $[(M\ (\mathbf{C_2}))^{6+}]_n$ coordination polymers, as represented in scheme 3.2:

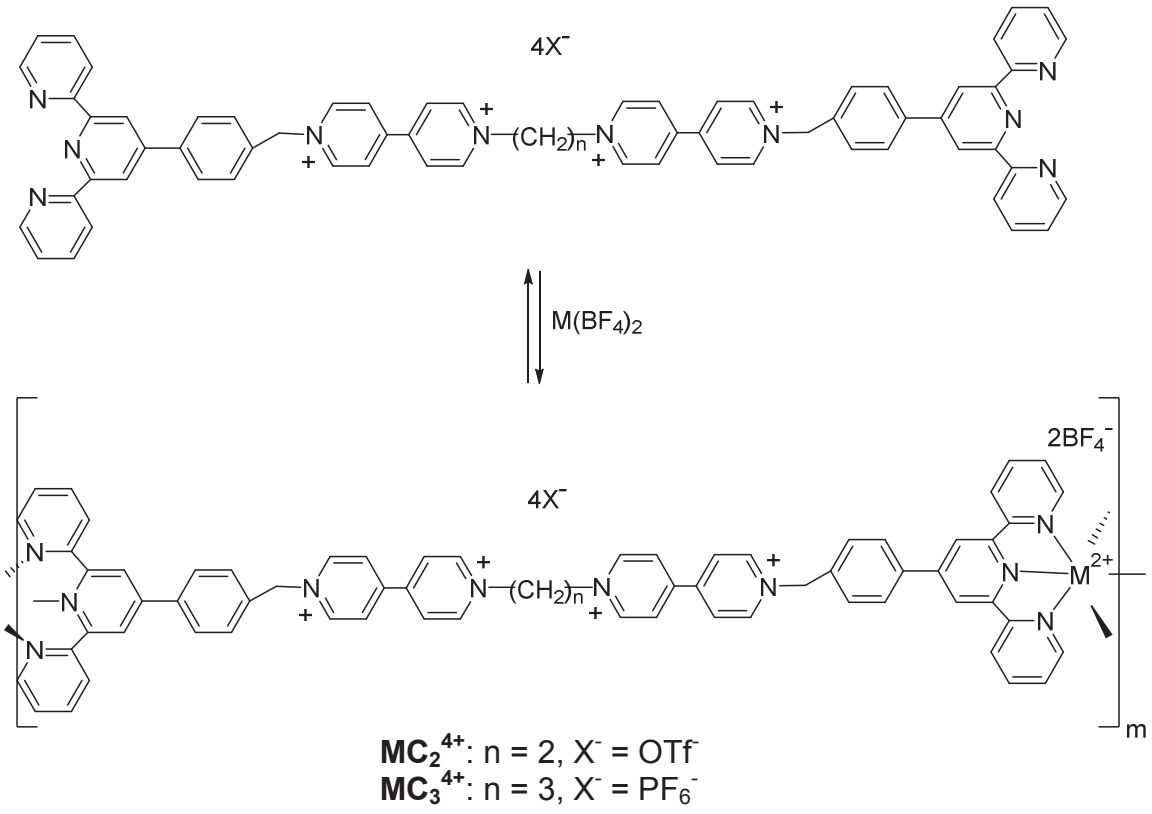

Scheme 3.2: Self-assembly of the ditopic bis-viologen ligands $\mathbf{C_2}^{4+}$ or $\mathbf{C_3}^{4+}$ with $M(BF_4)_2$ in a 1:1 ratio results in the 1D (oxidized) metallopolymers $\mathbf{MC_2}^{4+}$ or $\mathbf{MC_3}^{4+}$ with M = Zn^{2+}, Fe^{2+}, Ni^{2+} or Co^{2+}.

5.2 ^{1}H-NMR titration of C_3 and C_2 with zinc(II) and iron(II) salts

^{1}H-NMR titrations of $\mathbf{C_3}^{4+}$ and $\mathbf{C_2}^{4+}$ have been performed with iron (II) and zinc (II) tetrafluoroborate in DMF-d_7. These metal salts are expected to generate diamagnetic coordination polymers and are suitable for standard NMR spectroscopy.(63) Figures 3.20 and 3.21 show the ^{1}H-NMR spectra at different metal: ligand ratios.

In both titration cases, significant and dramatic differences occurred, but the most relevant change was related to the singlet peak attributed to the four protons of the benzylic CH_2 group ($PhCH_2$-N^+). This singlet is located at 6.52 ppm (denoted as * in Figures 3.20 and 3.21) in the free compounds $\mathbf{C_3}^{4+}$ or $\mathbf{C_2}^{4+}$ and its intensity decreases upon gradual additions of the Fe^{2+} ion accompanied with the appearance of new peaks at 6.62 ppm or 6.63 pm respectively up to 1 equiv. of metal added, in accordance with the formation of the expected $\mathbf{FeC_3}^{4+}$ or $\mathbf{FeC_2}^{4+}$ polymers. In addition, the formed Fe^{2+} coordination polymers stay stable in the presence of an excess of Fe^{2+} ion without decomposition. This is in agreement with the high stability of iron terpyridine complexes. In the case of Zn^{2+} ion, the intensities of the new peaks at 6.59 ppm or at 6.61 ppm for the coordination polymers of $\mathbf{C_3}^{2+}$ or $\mathbf{C_2}^{2+}$ decrease progressively with the gradual addition of Zn^{2+} ion after the one equivalent, which indicates the fragmentation of the Zn^{2+} coordination polymers. These results are in accordance with other bis(terpyridine) Zn^{2+} and Fe^{2+} based polymers.(63)

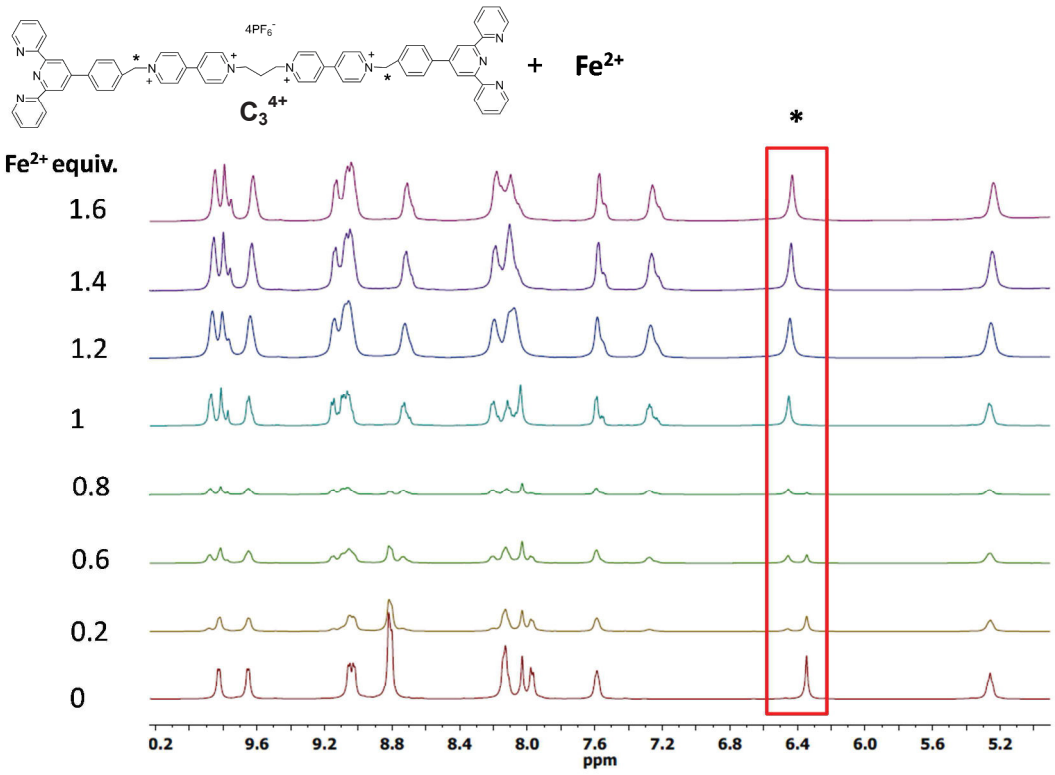

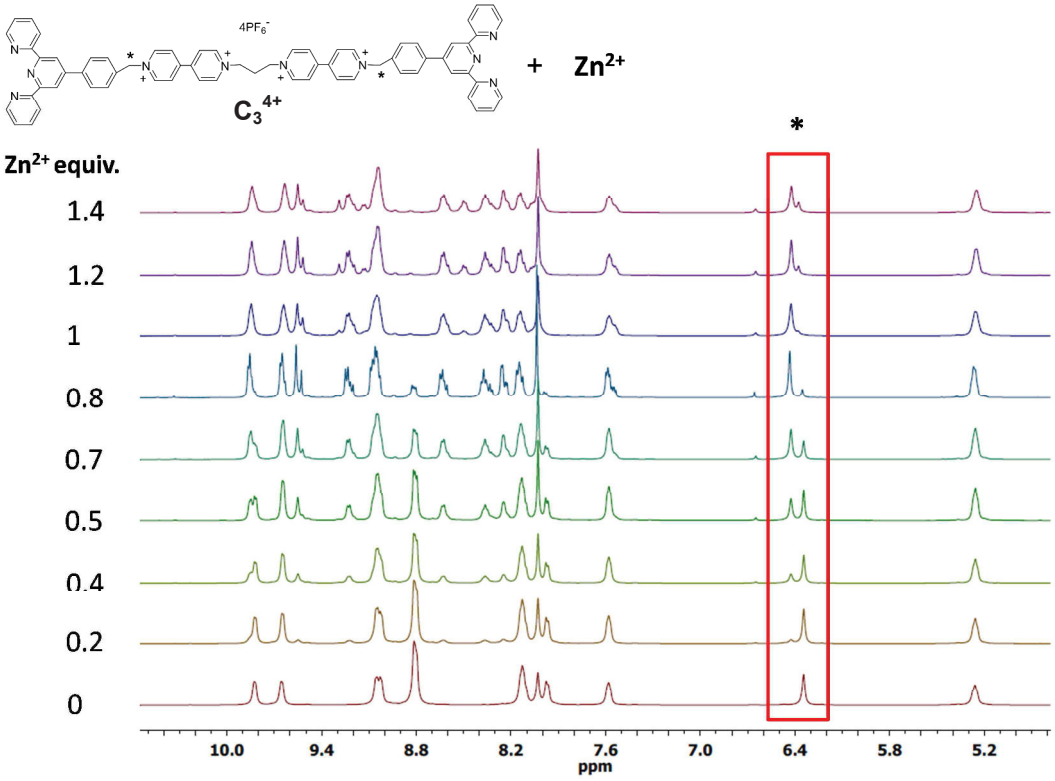

Figure 3.20: ^{1}H-NMR titrations of $\mathbf{C_3}^{4+}$ (10 mM in DMF-d7) by Fe^{2+} (0.2 M in DMF-d7, top) and Zn^{2+} (0.12 M in DMF-d7, bottom) ions.

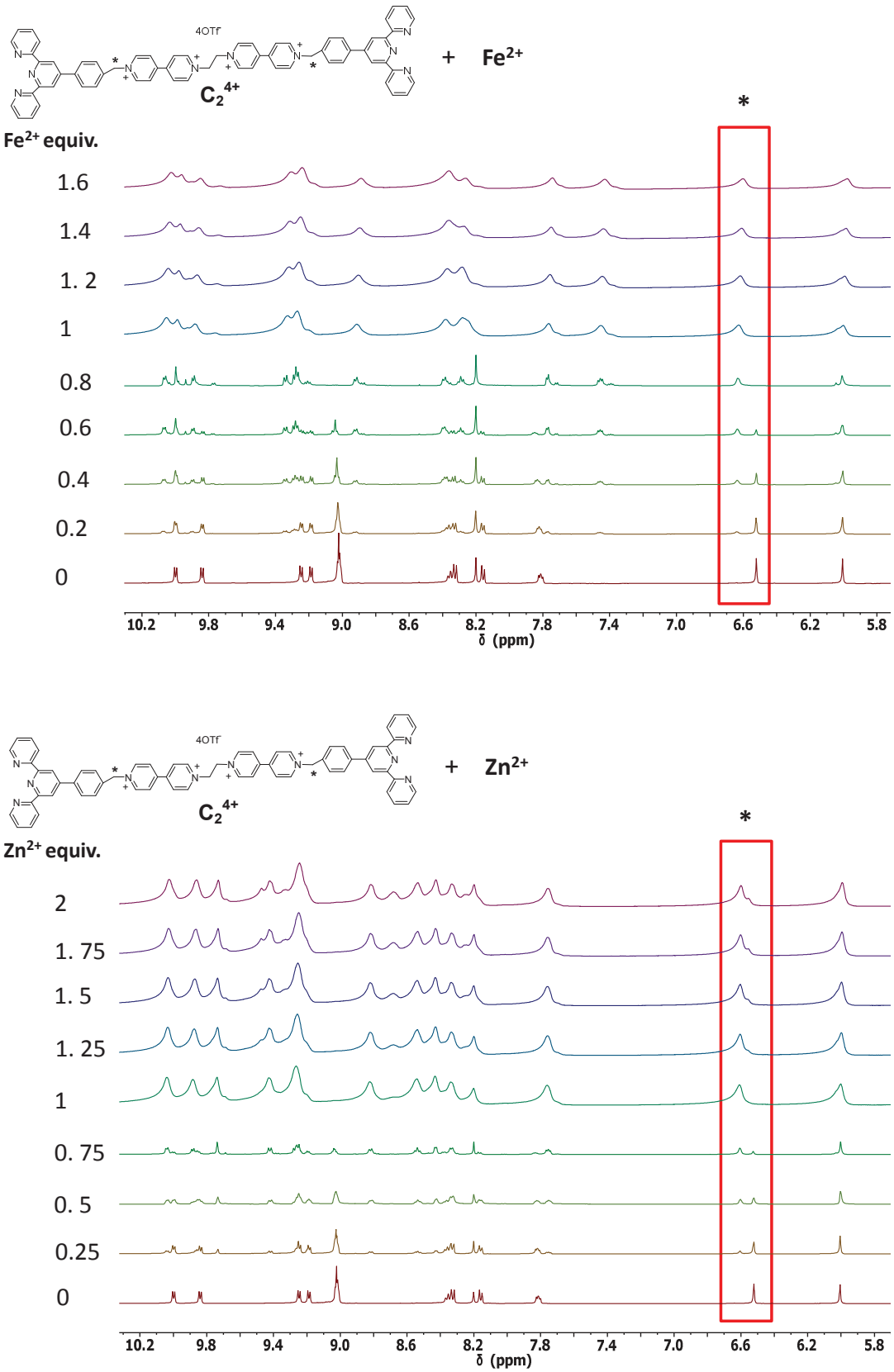

Figure 3.21: ^{1}H-NMR titrations of $\mathbf{C_2}^{4+}$ (10 mM in DMF-d7) by Fe^{2+} (Top) and Zn^{2+} (Bottom) ions (0.2 M in DMF-d7).

5.3 Study of the coordination polymers formation by spectroelectrochemistry

Figures 3.22 (A and B) and 3.23 (A and B) show the CVs titration of electrolytic solutions of the bis-functionalized terpyridine bis-viologen derivatives $\mathbf{C_3}^{4+}$ and $\mathbf{C_2}^{4+}$ by the metal tetrafluoroborate salts of zinc(II) and iron(II) respectively. As expected, significant current changes are obtained and are consistent with the gradual formation of the corresponding coordination polymers. In addition to current changes, new reduction peaks appeared upon complexation with the Zn^{2+} ion. These reduction peaks occurred at -1550 mV, -1700 mV and at -1560 mV, -1720 mV for the zinc coordination polymers $\mathbf{ZnC_3}^{4+}$ and $\mathbf{ZnC_2}^{4+}$ respectively. The iron coordination polymers $\mathbf{FeC_3}^{4+}$ and $\mathbf{FeC_2}^{4+}$ showed new reduction peaks at -1550 mV, -1660 mV and at -1570 mV, 1680 mV respectively. Also not clearly attributed, similar systems, were also observed for other bis-terpyridine Zn^{2+} and Fe^{2+} based polymers.[63] Furthermore, both $\mathbf{FeC_3}^{4+}$ and $\mathbf{FeC_2}^{4+}$ showed oxidation peaks at $E_{1/2}$ = 700 mV and 710 mV respectively. These signals are assigned to the 1-electron oxidation of coordinated Fe^{2+} metal ions (see Table 3.5). Again, the redox differences between $\mathbf{C_3}^{4+}$ and $\mathbf{C_2}^{4+}$ mentioned in paragraph 4.4, the $E^1_{1/2}$-$E^2_{1/2}$ values for both of $\mathbf{ZnC_2}^{4+}$ and $\mathbf{FeC_2}^{4+}$ are still far away from those of $\mathbf{ZnC_3}^{4+}$ and $\mathbf{FeC_3}^{4+}$, indicating the absence of the dimerization among viologen radicals within the coordination polymers of $\mathbf{C_2}^{4+}$ (see Table 3.5).

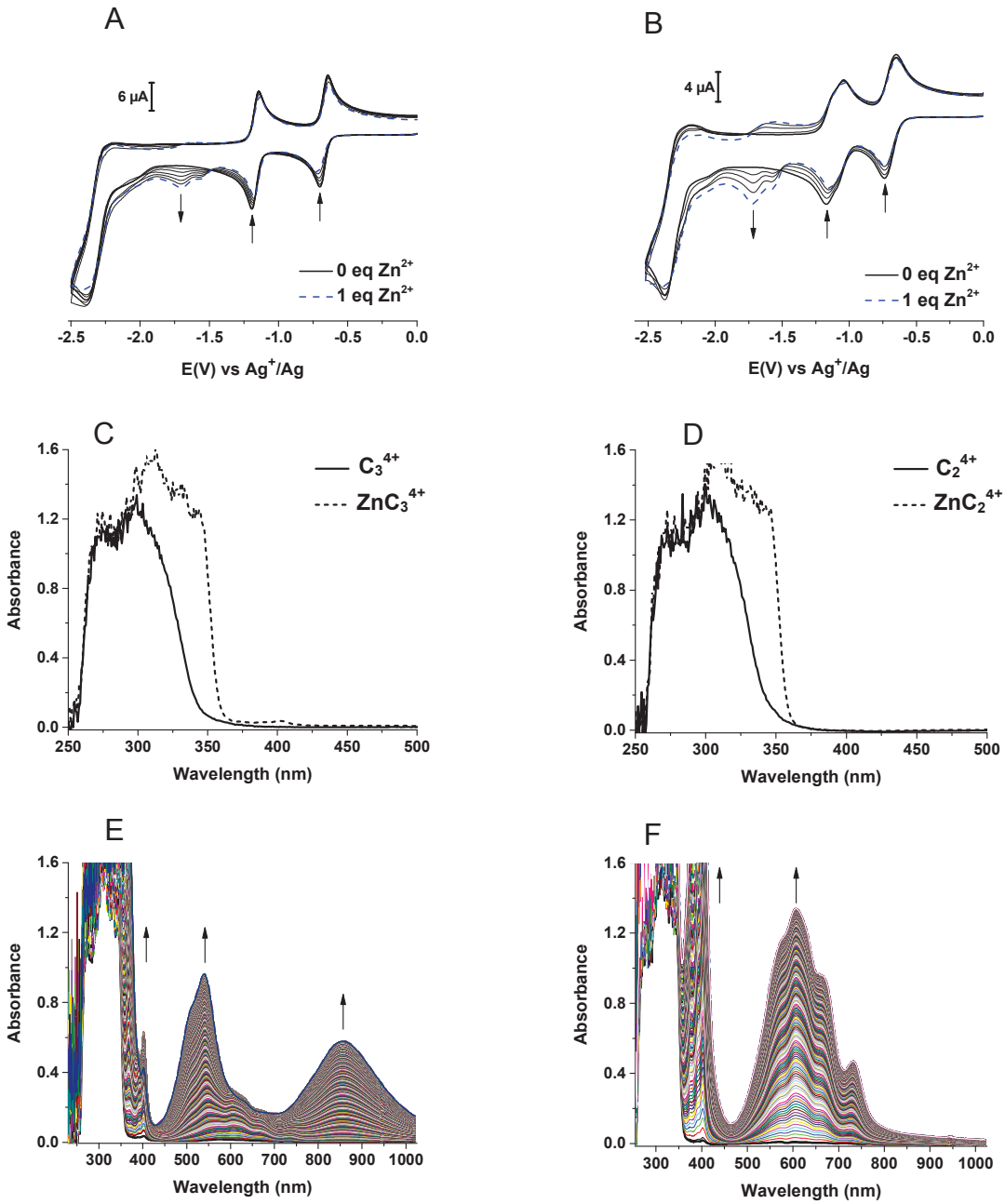

Figure 3.22: CVs titration of $\mathbf{C_3}^{4+}$ (A) and $\mathbf{C_2}^{4+}$ (B) by a 0.085 M of $[Zn(BF_4)_2.6H_2O]$, voltage Scan rate: 100 mV/s. Absorption spectra of $\mathbf{C_3}^{4+}$ and $\mathbf{ZnC_3}^{4+}$ (C) and $\mathbf{C_2}^{4+}$ and $\mathbf{ZnC_2}^{4+}$ (D). Absorption spectra recorded during the exhaustive 2-electron reductions of (E) $\mathbf{ZnC_3}^{4+}$ (E_{app} = -1 V) and (F) $\mathbf{ZnC_2}^{4+}$ (E_{app} = -0.94 V). Conc. = 0.5 mM, solvent: 0.1 M TBAP/DMF, UV-vis all-quartz immersion probe with l = 0.1 cm, 298K. Working electrodes: 3mm Vitreous Carbon electrode (CVs) and high surface area platinium (bulk reductions), reference electrode: 0.01M $AgNO_3$ + 0.1 M TBAP/CH_3CN/Ag.

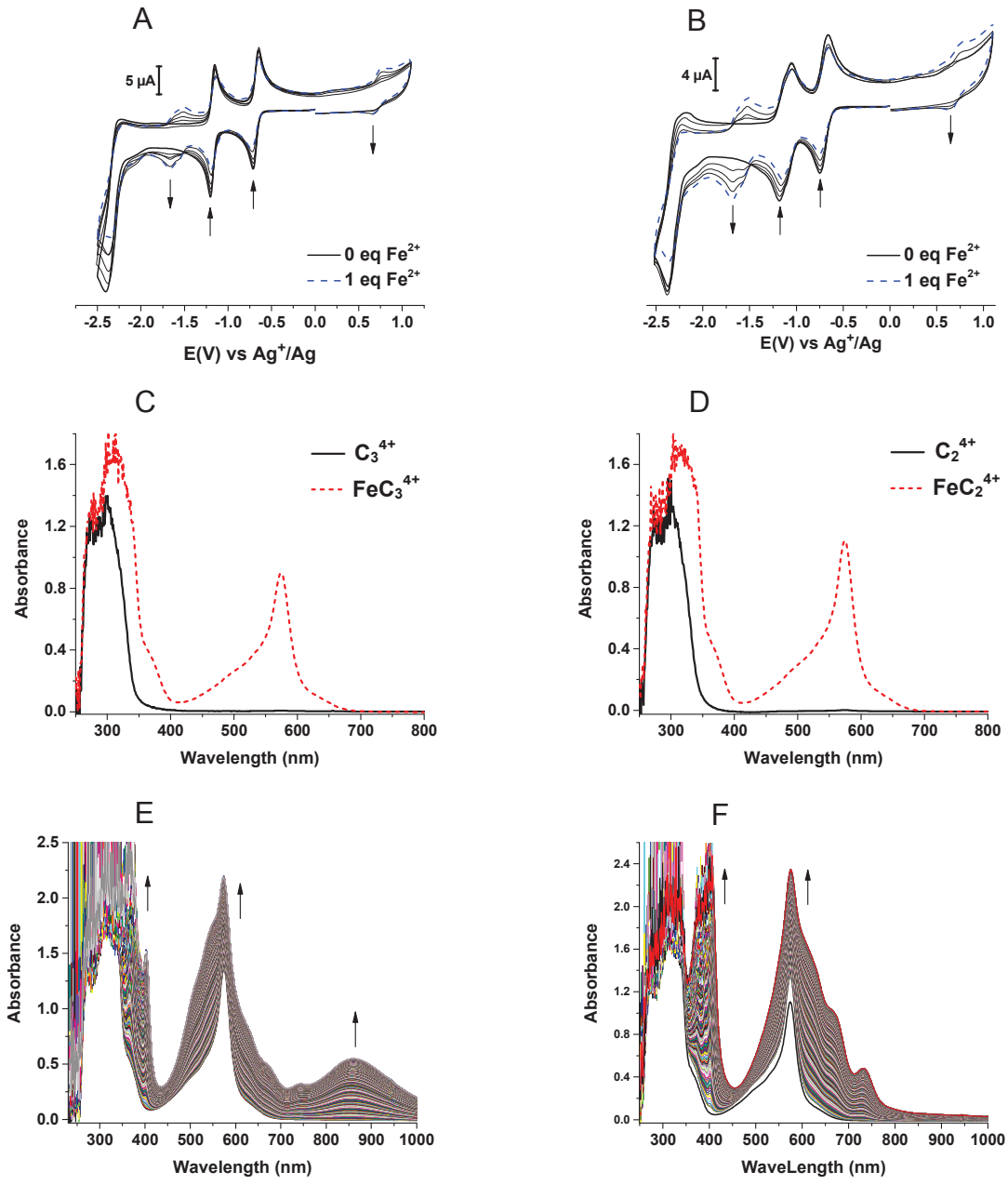

Figure 3.23: CVs titration of $\mathbf{C_3}^{4+}$ (A) and $\mathbf{C_2}^{4+}$ (B) by a 0.085 M of $[Fe(BF_4)_2.6H_2O]$, voltage Scan rate: 100 mV/s. Absorption spectra of $\mathbf{C_3}^{4+}$ and $\mathbf{FeC_3}^{4+}$ (C) and $\mathbf{C_2}^{4+}$ and $\mathbf{FeC_2}^{4+}$ (D). Absorption spectra recorded during the exhaustive 2-electron reductions of (E) $\mathbf{FeC_3}^{4+}$ (E_{app} = -1 V) and (F) $\mathbf{FeC_2}^{4+}$ (E_{app} = -0.94 V). Conc. = 0.5 mM, solvent: 0.1 M TBAP/DMF, UV-vis all-quartz immersion probe with l = 0.1 cm, 298K. Working electrodes: 3mm Vitreous Carbon electrode (CVs) and high surface area platinium (bulk reductions), reference electrode: 0.01M $AgNO_3$ + 0.1 M TBAP/CH_3CN/Ag.

Table 3.5: Experimental voltammetric potentials $E_{1/2}$ with peak separations (ΔE_P, mV), in parenthesis) for the metallopolymers of $\mathbf{C_3}^{4+}$ and $\mathbf{C_2}^{4+}$ at 100mV/s. Working electrode: 3mm Vitreous Carbon. Reference electrode: 0.01M $AgNO_3$ + 0.1 M TBAP/CH_3CN/Ag.

	$E^1_{1/2}$ (V) $V^{2+}/V^{+\bullet}$	$E^2_{1/2}$ (V) $V^{+\bullet}/V^0$	$E^1_{1/2}$-$E^2_{1/2}$(V)	$E^2_{1/2}$ (V) Fe^{3+}/Fe^{2+}
$\mathbf{ZnC_3}^{4+}$	- 0.68(90)	- 1.16(35)	0.48	—
$\mathbf{ZnC_2}^{4+}$	- 0.69(70)	- 1.05(30) - 1.10(10)	0.41	—
$\mathbf{FeC_3}^{4+}$	- 0.68(70)	- 1.16(45)	0.48	0.70(110)
$\mathbf{FeC_2}^{4+}$	- 0.69(85)	- 1.06(25) - 1.10(25)	0.41	0.71(90)

Table 3.6: Maximum wavelengths and molar absorption coefficients for $\mathbf{C_3}^{4+}$, $\mathbf{C_2}^{4+}$ and their oxidized and reduced metallopolymers in 0.1 M TBAP/DMF at 298 K.

Compound	λ_{max} /nm ($\varepsilon/M^{-1}.cm^{-1}$)
$\mathbf{C_3}^{4+}$	274 (25000), 298 (28000)
$\mathbf{C_2}^{4+}$	273 (22900), 300 (28200)
$\mathbf{C_3}^{2+}$	366 (49100), 401 (5200), 516 (11900), 543 (15000), 858 (8100)
$\mathbf{C_2}^{2(+\bullet)}$	283 (31600), 308 (22000), 377 (32300), 401 (44000), 608 (24300), 658 (17200), 731 (7800)
$\mathbf{ZnC_3}^{4+}$	275 (25000), 313 (32100), 340 (25200)
$\mathbf{ZnC_2}^{4+}$	272 (25000), 317 (33400), 332 (27900)
$\mathbf{ZnC_3}^{2+}$	281 (46000), 305 (47700), 345 (51500), 364 (50500), 402 (10800), 540 (24500), 856 (14700)
$\mathbf{ZnC_2}^{2(+\bullet)}$	284 (47000), 305 (42900), 406 (45200), 607 (26800), 656 (19500), 732 (9400)
$\mathbf{FeC_3}^{4+}$	314 (38500), 361 (11800), 574 (27300)
$\mathbf{FeC_2}^{4+}$	282 (29000), 303 (37000), 574 (22100)
$\mathbf{FeC_3}^{2+}$	287 (45200), 311 (57500), 365 (50200), 402 (30000), 553 (36000), 574 (44000), 744 (6400), 856 (11000)
$\mathbf{FeC_2}^{2(+\bullet)}$	328 (51100), 406 (49200), 575 (47000), 732 (10000)

The absorption spectra of $\mathbf{C_3}^{4+}$ and $\mathbf{C_2}^{4+}$ with their Zn^{2+} and Fe^{2+} metallopolymers are presented in Figures 3.22 and 3.23. Both Zn^{2+} and Fe^{2+} metallopolymers showed new bands attributed to a ligand centered (LC, π–π*, and n–π*) absorption located in the UV absorption region. These bands occurred at longer wavelengths compared with those of the ligands $\mathbf{C_3}^{4+}$ and $\mathbf{C_2}^{4+}$. Additionally, $\mathbf{FeC_3}^{4+}$ and $\mathbf{FeC_2}^{4+}$ showed the ligand charge transfer (MLCT) absorption band at 574 nm (see Table 3.6).

These Figures show also the evolutions of absorption spectra recorded during the 2-electrons bulk reduction for Zn^{2+} and Fe^{2+} metallopolymers respectively in 0.1 M TBAP/DMF. The diagnostic signatures for the formation of π-dimers within the coordination polymers $\mathbf{ZnC_3}^{2+}$ (Figure 3.22 E) and $\mathbf{FeC_3}^{2+}$ (Figure 3.23 E) are clearly observed in the NIR region of the spectrum with a large band at 856 nm which is similar to that of the free reduced $\mathbf{C_3}^{2+}$ (Figure 3.16 A). The occurrence of the same NIR absorption band for $\mathbf{C_3}^{2+}$, $\mathbf{ZnC_3}^{2+}$ and $\mathbf{FeC_3}^{2+}$ demonstrates the same type of the intra-molecular π-dimerization process existing between viologen radicals within each of $\mathbf{C_3}^{2+}$, $\mathbf{ZnC_3}^{2+}$ and $\mathbf{FeC_3}^{2+}$. In addition, absorption bands at 540 and 364 nm were also observed for $\mathbf{ZnC_3}^{2+}$ which are commonly owing to the dimerized viologen bis (radical-cation). These two bands are blue shifted compared with those of non-dimerized $\mathbf{ZnC_2}^{2(+\bullet)}$ (618 and 402 nm). Upon the exhaustive 2-electrons reductions of $\mathbf{FeC_3}^{4+}$ and $\mathbf{FeC_2}^{4+}$, the MLCT absorption band (574 nm) is emerged with the absorption bands below 600 nm and at $\lambda \geq 600$ nm respectively which are due to associated and non-associated viologen radical cations within $\mathbf{FeC_3}^{2+}$ and $\mathbf{FeC_2}^{2(+\bullet)}$ respectively (see Figures 3.23 E and 3.23 F).

All these results support our clear assumption that the zinc and iron coordination polymers $\mathbf{ZnC_3}^{2+}$ and $\mathbf{FeC_3}^{2+}$ are formed at one molar equivalent of Zn^{2+} and Fe^{2+} metal ions added respectively and that these coordination polymers afford the redox controlled intra-molecular π-dimerization processes between the viologen radicals. In contrast, the absorption spectra of $\mathbf{ZnC_2}^{2(+\bullet)}$ (Figure 3.22 F) and $\mathbf{FeC_2}^{2(+\bullet)}$ (Figure 3.23 F) growing during the 2-electrons bulk reductions of $\mathbf{ZnC_2}^{4+}$ and $\mathbf{FeC_2}^{4+}$ respectively are consistent with that of $\mathbf{C_2}^{2(+\bullet)}$ and show that no dimerization occurs.

The reversibility of the process was then investigated. Figures 3.24 A and B show the evolutions of absorption spectra recorded during the exhaustive 2-electron reoxidations (E_{app} = 0 V) of the purple solutions of $\mathbf{ZnC_3}^{2+}$ and $\mathbf{FeC_3}^{2+}$ respectively.

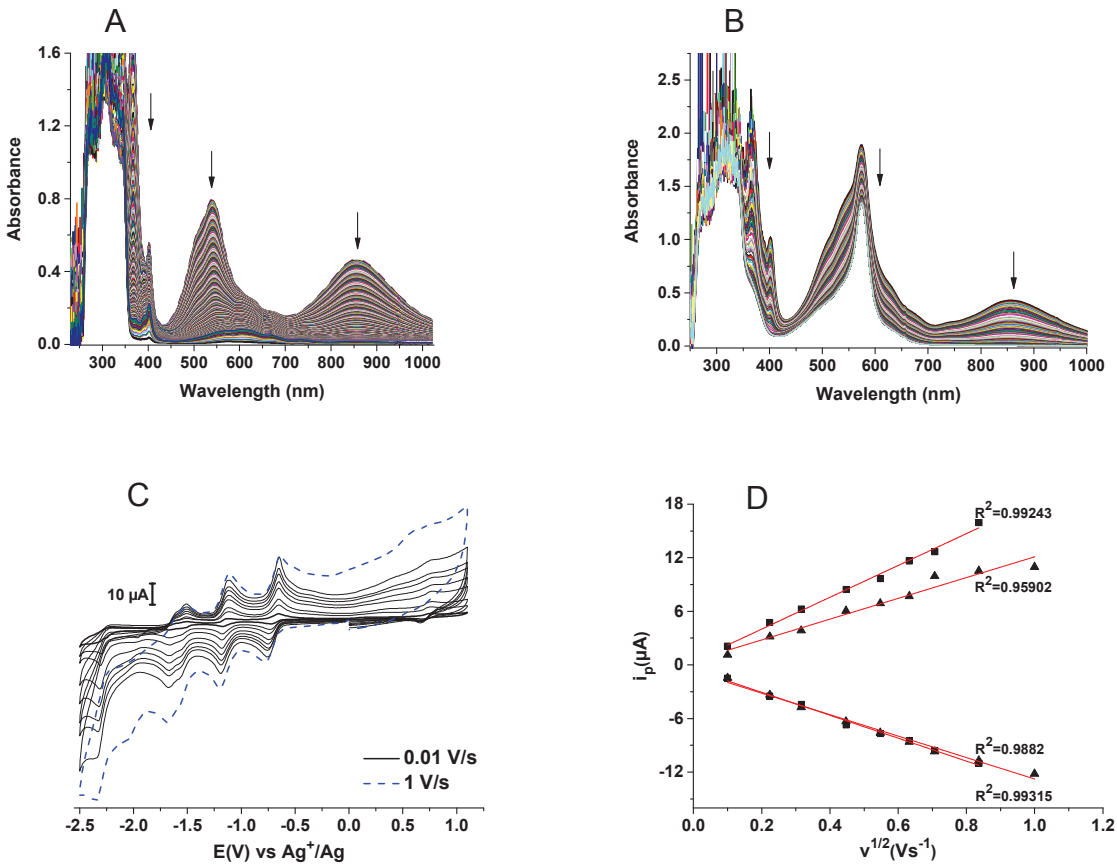

Figure 3.24: Absorption spectra recorded during the exhaustive 2-electron oxidations (E_{app} = 0 V) of (A) $\mathbf{ZnC_3}^{2+}$ and (B) $\mathbf{FeC_3}^{2+}$. Conc. = 0.5 mM, solvent: 0.1 M TBAP/DMF, UV-vis all-quartz immersion probe with l = 0.1 cm, 298K. (C) Cyclic voltammograms of $\mathbf{FeC_3}^{4+}$ at different voltage scan rate, 0.01-1 V/s. (D) Plots of peak currents *vs* the square-root of voltage scan rate.Working electrodes: 3mm Vitreous Carbon electrode (CVs) and high surface area platinium (bulk reductions), reference electrode: 0.01M $AgNO_3$ + 0.1 M TBAP/CH_3CN/Ag.

These experiences confirm the reversibility of the bulk reduction processes leading to $\mathbf{ZnC_3}^{2+}$ and $\mathbf{FeC_3}^{2+}$ with the complete recovery of the UV-Vis absorption spectra for the initial oxidized metallopolymers $\mathbf{ZnC_3}^{4+}$ and $\mathbf{FeC_3}^{4+}$ respectively. In addition, Figure 3.24 C represents the CVs of a $\mathbf{FeC_3}^{4+}$ coordination polymer solution at voltage scan rates (v) spanning from 0.01 to 1 $V.s^{-1}$. The viologen centered electrochemical responses remain reversible and diffusion controlled in this range of voltage scan rates. Indeed, the peak currents vary linearly with the square root of the voltage scan rate (Figure 3.24 D).

5.4 Photo-assisted reductions followed by absorption spectroscopy

In addition to electrochemical reductions, the formation of viologen radicals was also achieved under photochemical stimulus. The visible light irradiation for viologen units in the presence of tris (bipyridine) ruthenium(II) complex as photosensitizer and triethanolamine as sacrificial electron donor results in viologen radicals. The photo-assisted reduction of viologen species proceeds according to the following equations (5-9) :[64, 65]

$$Ru(II) + h\nu \longrightarrow {}^{*}Ru(II) \quad (5)$$

$${}^{*}Ru(II) \longrightarrow Ru(II) + h\nu' + \Delta \quad (6)$$

$${}^{*}Ru(II) + V^{2+} \longrightarrow Ru(III) + V^{+\bullet} \quad (7)$$

$$Ru(III) + V^{+\bullet} \longrightarrow Ru(II) + V^{2+} \quad (8)$$

$$Ru(III) + TEOA \longrightarrow Ru(II) + TEOA_{ox} \quad (9)$$

Where TEOA: triethanolamine, Ru(II): the complex $Ru(bpy)_3.2Cl^{-}.6H_2O$ and *Ru(II): visible light excited species. The mechanism of photo-assisted reduction of viologen are presented in Figure 3.25. The viologen unit (V^{2+}) can be reduced by receiving an electron from the visible light excited *Ru(II) species, leaving Ru(III) species (equation 7). The latter in turn has another possibility of reaction (8), which is a back electron transfer reaction. However, the reaction (8) could be restricted by the higher concentration of TEOA (94 mM) compared with that of the ruthenium ion (55 µM), and also to a certain extent by an entrance of the resulting viologen radical $V^{+\bullet}$ in a dimerization reaction. One photon eventually results in the reduction of one viologen unit, i.e.: two photons are required to reduce $\mathbf{C_3}^{4+}$ or $\mathbf{C_2}^{4+}$.

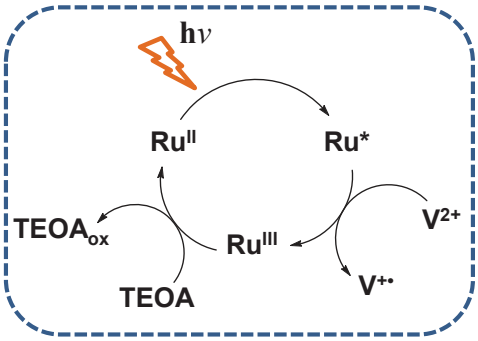

Figure 3.25: Mechanism of the photo-assisted reduction of viologen dications.[64, 65]

The visible light irradiation (λ > 436 nm) was carried out for an oxygen-free solution of 1 mM viologen cation, 55 μM of $Ru(bpy)_3.2Cl^-.6H_2O$ and 94 mM triethanolamine in DMF using a quartz apparatus and a 500 W Xe lamp at 281 K.[64, 65] These visible light irradiations led to photo-assisted reductions of viologen cations, that is, the formation of viologen radical cations which were monitored by UV-visible absorption spectroscopy at different time intervals of irradiations. The time profiles of the photo-assisted reductions for $\mathbf{V}^{2+}$, $\mathbf{C_3}^{4+}$, $\mathbf{C_2}^{4+}$ and their metallopolymers are presented in Figures 3.26, 3.27 and 3.28. As mentioned before, the photo-assisted generated $\mathbf{V}^{+\bullet}$ radical does not give a dimerized structure as showed clearly from the absence of NIR absorption in Figure 3.26.

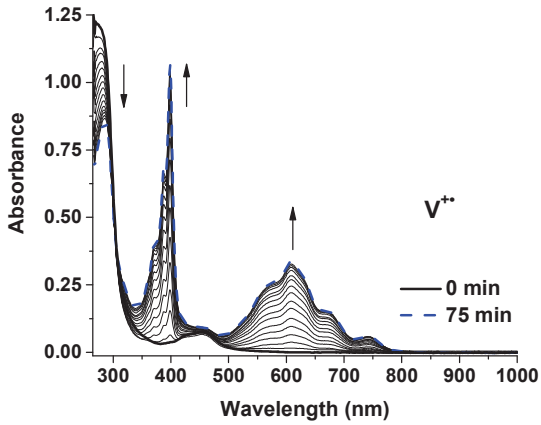

Figure 3.26: Absorption spectra recorded during the irradiation of 0.1 mM $\mathbf{V}^{2+}$ solution containing 5.5×10^{-6} M of $Ru(bpy)_3.2Cl^-.6H_2O$ and 9.4×10^{-3} M of triethanolamine/DMF in a UV-vis quartz cell with l = 1 cm under un argon atmosphere. Photo-assisted reduction reaction was performed using a 500 W Xe lamp equipped with a UV cut-off filter (λ > 436 nm) at 281 K.

The visible light irradiation of $\mathbf{C_2}^{4+}$ generates new absorption bands at 366 nm, 402 nm, 433 nm and broad bands extended from 615 nm to 661 nm and 706 nm (see Figure 3.27 B). The resulted viologen radical cations $\mathbf{C_2}^{2(+\bullet)}$ does not dimerize due to the conformational difficulty attributed to ethylene spacer.[66] Figure 3.27 A shows the absorption spectra of $\mathbf{C_3}^{4+}$ under visible light irradiation. The resulted bis (radical-cation) species $\mathbf{C_3}^{2(+\bullet)}$ showed the absorption bands, increased gradually with time of irradiation, at 367 nm, 402 nm and 543 nm. The absorption band noted for $\mathbf{C_3}^{2(+\bullet)}$ species at 543 nm is blue shifted compared with those of $\mathbf{V}^{+\bullet}$ and $\mathbf{C_2}^{2(+\bullet)}$ species. This appreciable blue absorption shift clearly shows that $\mathbf{C_3}^{2(+\bullet)}$ species can dimerize.[66] Furthermore, $\mathbf{C_3}^{2(+\bullet)}$ species displays the characteristic NIR absorption band due to the dimerized viologen radicals at 858 nm.

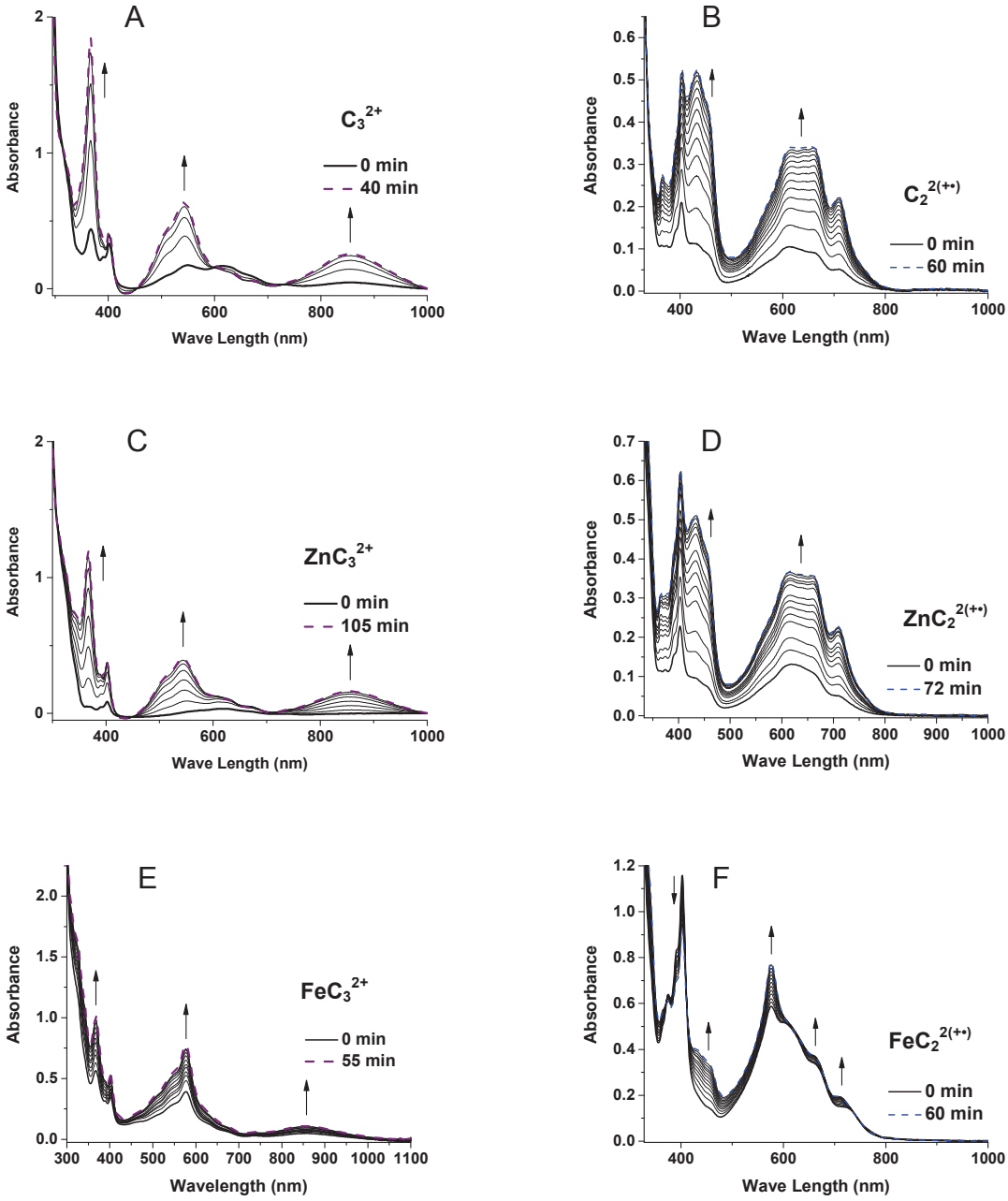

Figure 3.27: Absorption spectra recorded during the irradiation of 0.05 mM for each of $\mathbf{C_3}^{4+}$(A), $\mathbf{C_2}^{4+}$ (B), $\mathbf{ZnC_3}^{4+}$ (C) , $\mathbf{ZnC_2}^{4+}$ (D), $\mathbf{FeC_3}^{4+}$ (E) and $\mathbf{FeC_2}^{4+}$ (F) solutions containing 5.5×10^{-6} M of $Ru(bpy)_3.2Cl^-.6H_2O$ and 9.4×10^{-3} M of triethanolamine/DMF in a UV-vis quartz cell with l = 1 cm under un argon atmosphere. Photo-assisted reduction reaction was performed using a 500 W Xe lamp equipped with a UV cut-off filter ($\lambda > 436$ nm) at 281 K.

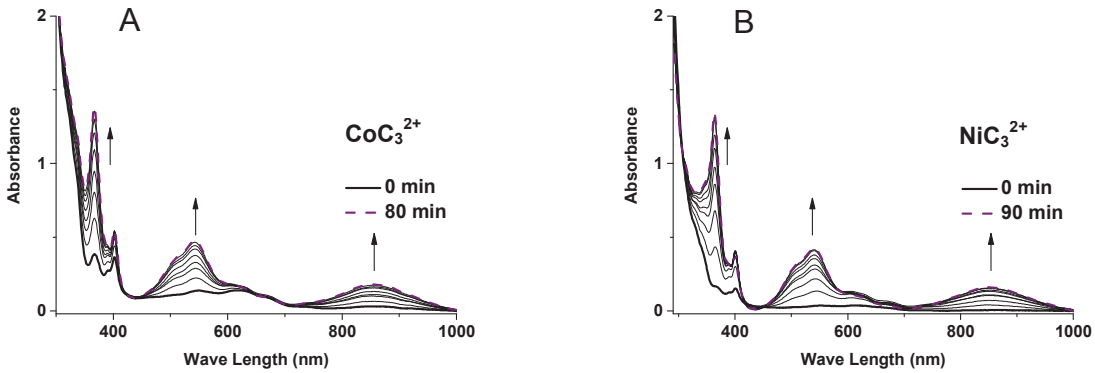

Figure 3.28: Absorption spectra recorded during the irradiation of 0.05 mM for both of $\mathbf{CoC_3^{4+}}$ (A) and $\mathbf{NiC_3^{4+}}$ (B) solutions containing 5.5×10^{-6} M of $Ru(bpy)_3.2Cl^-.6H_2O$ and 9.4×10^{-3} M of triethanolamine/DMF in a UV-vis quartz cell with l = 1 cm under un argon atmosphere. Photo-assisted reduction reaction was performed using a 500 W Xe lamp equipped with a UV cut-off filter ($\lambda > 436$ nm) at 281 K.

Similar to the electrochemically reduced species, the photo-assisted reduced $\mathbf{ZnC_2^{4+}}$ (Figure 3.27 D) and $\mathbf{FeC_2^{4+}}$ (Figure 3.27 F) do not display any indications for the inter-molecular dimerization among viologen radicals within the structures of the reduced coordination polymers.

The reduced coordination polymers $\mathbf{ZnC_3^{2+}}$, $\mathbf{FeC_3^{2+}}$, $\mathbf{CoC_3^{2+}}$ and $\mathbf{NiC_3^{2+}}$ showed similar absorption patterns compared to the reduced ligand $\mathbf{C_3^{2+}}$, *i.e.* the dimerized viologen radicals within the structures of the coordination polymers. Because of the impossibility of achieving the folding between two viologen radicals spacered by ethylene chain, only the intermolecular association could take place in the bis (radical-cation) species $\mathbf{C_2^{2(+\bullet)}}$ and its coordination polymers $\mathbf{ZnC_2^{2(+\bullet)}}$ and $\mathbf{FeC_2^{2(+\bullet)}}$, but such intermolecular dimerization is not observed. In contrast, the species $\mathbf{C_3^{2+}}$, $\mathbf{ZnC_3^{2+}}$, $\mathbf{FeC_3^{2+}}$, $\mathbf{CoC_3^{2+}}$ and $\mathbf{NiC_3^{2+}}$ showed remarkable association among the viologen radicals in the millimolar concentrations. These mentioned facts imply that these dimerization processes with $\mathbf{MC_3^{4+}}$ polymers are undoubtedly of intramolecular type.

5.5 Study of the coordination polymers by ESR spectroscopy

ESR experiments were carried out with the same solutions developed before for the coordination polymers $\mathbf{ZnC_3}^{2+}$, $\mathbf{ZnC_2}^{2(+\bullet)}$, $\mathbf{FeC_3}^{2+}$ and $\mathbf{FeC_2}^{2(+\bullet)}$ during the spectroelectrochemical and viscosity measurements. Figures 3.29 and 3.30 show the ESR spectra for the electrochemical and photochemical generated radicals.

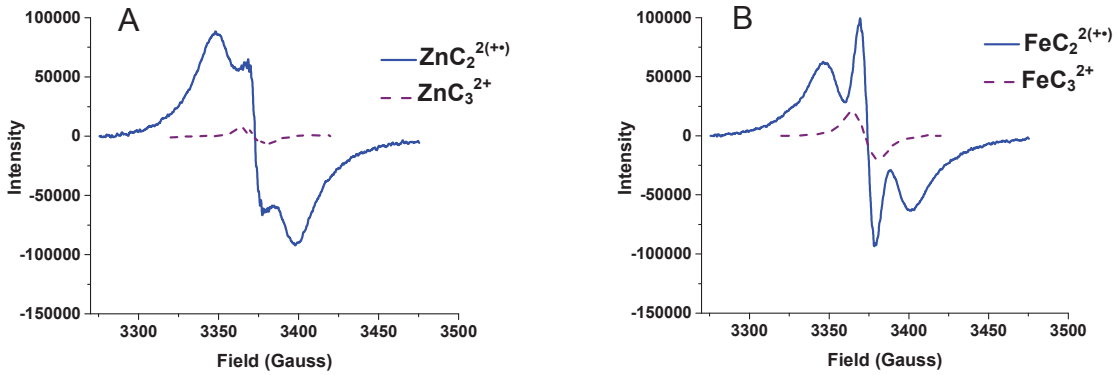

Figure 3.29: ESR spectra for electrochemical generated 0.5 mM each of (A) $\mathbf{ZnC_3}^{2+}$ and $\mathbf{ZnC_2}^{2(+\bullet)}$ and (B) $\mathbf{FeC_3}^{2+}$ and $\mathbf{FeC_2}^{2(+\bullet)}$. Solvent: 0.1 M TBAP/DMF, 298 K.

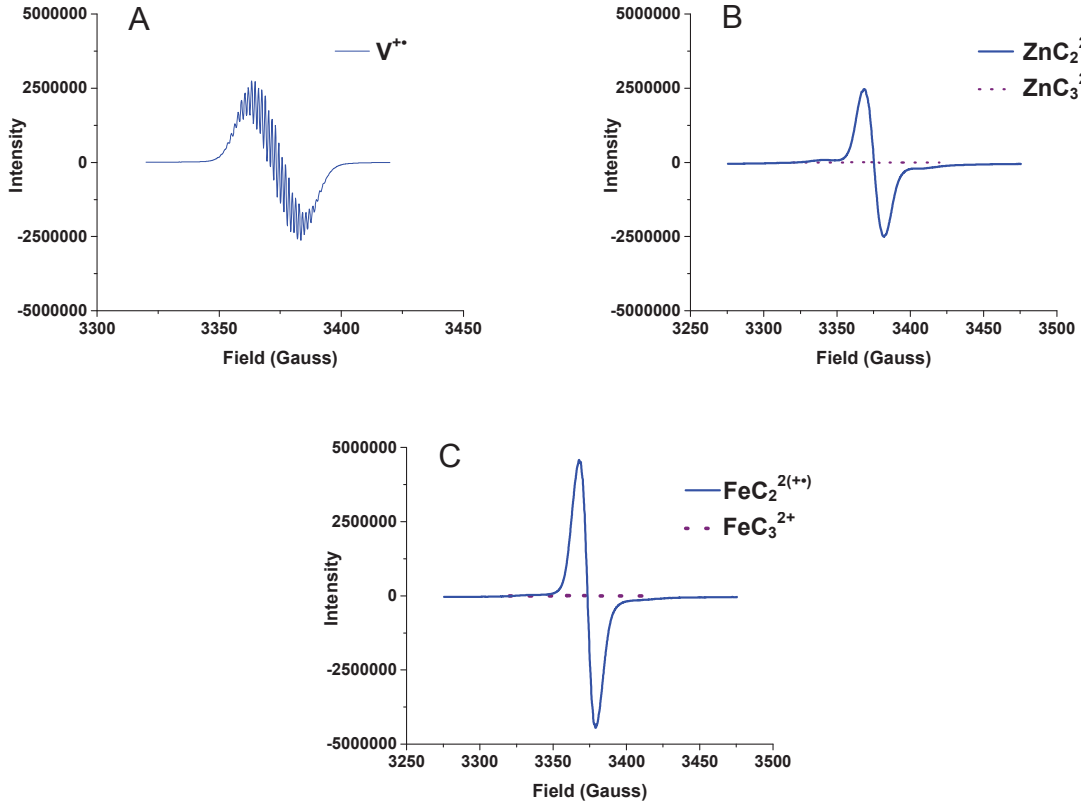

Figure 3.30: ESR spectra for (A) 26 mM $\mathbf{V}^{+\bullet}$ and 13 mM for each of (B) $\mathbf{ZnC_2}^{2(+\bullet)}$ and $\mathbf{ZnC_3}^{2+}$ and (C) $\mathbf{FeC_2}^{2(+\bullet)}$ and $\mathbf{FeC_3}^{2+}$.The reduced species are photochemically generated in their solutions containing 1.43 mM of $Ru(bpy)_3.2Cl^{-}.6H_2O$ and 2.444 M of triethanolamine/DMF, 298 K.

The reduced coordination polymers $\mathbf{ZnC_3^{2+}}$ and $\mathbf{FeC_3^{2+}}$ exhibited nicely almost silent ESR signals compared with those of $\mathbf{V^{+\bullet}}$, $\mathbf{ZnC_2^{2(+\bullet)}}$ and $\mathbf{FeC_2^{2(+\bullet)}}$ species. Indeed, the ESR results agree well with the spectroelectrochemical studies and they support the sufficient and reversible switching between the initial free ligand $\mathbf{C_3^{4+}}$ along with its coordination polymers and the corresponding bis (radical-cation) species. The reduced coordination polymer either electrochemically or photo-chemically generated showed almost silent ESR signals. This reflects the efficiency of the visible light-assisted reduction compared with the exhaustive electrolysis in the formation of the viologen radicals under our experimental conditions.

5.6 Study of the coordination polymers by viscometry

Viscosimetry measurements were done on the different ligands and polymers under their reduced and oxidized forms. Viscosimetry measurements have been done under supervision of Dr. Denis Roux in Grenoble (Laboratoire Rhéologie et Procédés). The viscosity for the solutions of ligands and metallopolymers was measured based on the Rolling Ball Principle.[67] For each experiment, the sample is filled into a glass capillary (Ø = 1.59 mm) where a spherical stainless steel ball coated with gold (1.5 mm diameter) is suitable for Newtonians liquids having viscosity range of 0.2-65 mPa.s. The capillary filled with the sample is then introduced into the temperature controlled capillary block which can be inclined at suitable angles. Varying the inclination angle allows to investigate different shear rates in order to check the Newtonian behavior of the sample. The viscosity was then determined by measuring automatically the rolling ball times between specific positions along the glass tube. Samples' viscosities are calculated from the obtained interval time repeated at least 10 times. Viscosities presented here are the mean of each condition with an uncertainty of 0.5%.

To demonstrate the dependency of the degree of metal ion induced self-assembly polymerization, viscosimetric measurements of solutions at different ligand to metal ratios have been carried out. Figure 3.31 presents the viscosity titration of 13mM of $\mathbf{C_3^{4+}}$ and $\mathbf{C_2^{4+}}$ solutions by the metal tetrafluoroborate hexahydrate salts of zinc(II) (A and B), and iron(II) (C and D) respectively in DMF at 298 K.

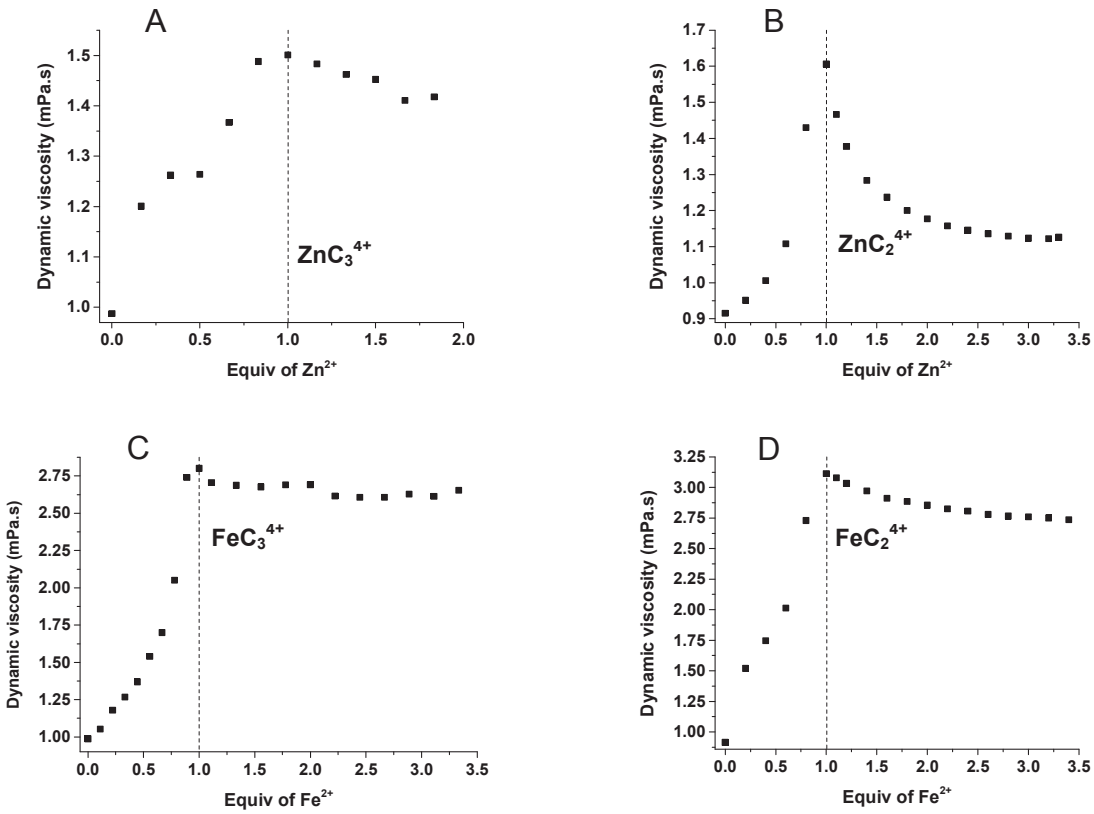

Figure 3.31: Viscosity titrations of 13mM for each of $\mathbf{C_3}^{4+}$ (A and C) and $\mathbf{C_2}^{4+}$ (B and D) by $[Zn(BF_4)_2.6H_2O]$ and $[Fe(BF_4)_2.6H_2O]$ respectively in DMF at 298 K.

It could be seen from Figure 3.31 that the stepwise additions of zinc (II) or iron (II) resulted in increase in the dynamic viscosities of the $\mathbf{C_3}^{4+}$ and $\mathbf{C_2}^{4+}$ solutions up to maximum values at metal ion-to-ligand ratio of 1:1, indicating that the species formed are the longest to this stoichiometry. Beyond the equivalence, the addition of the metal salt is accompanied by a decrease in viscosity, and this change in the viscosity can be only attributed to the formation of zinc or iron coordination polymers. The decrease in viscosity for higher ratio indicates the onset of the shortening of the polymer chains. The viscosity trend upon addition an excess amount of metal ion varies significantly depending on the used metal ion. For iron (II) polymers (Figure 3.31 C and D), the decreasing in viscosities at more than one equivalent are much less pronounced than with zinc (II) which is related to the thermodynamic stability of iron biscomplexes.

The dynamic viscosity of $\mathbf{C_3}^{4+}$ (0.987 ± 0.056 mPa.s) is a little higher than that of $\mathbf{C_2}^{4+}$ (0.915 ± 0.009 mPa.s) which can be attributed to the presence of the ethylene spacer between the two viologen units in $\mathbf{C_2}^{4+}$ compared with the propylene linker in $\mathbf{C_3}^{4+}$. This difference in linker

chain can lower the diffusion of $\mathbf{C_3}^{4+}$. Therefore, taking in account the standard error values, the dynamic viscosity of $\mathbf{ZnC_3}^{4+}$ (1.501 ± 0.156 mPa.s) is also a little higher than that of $\mathbf{ZnC_2}^{4+}$ (1.606 ± 0.01 mPa.s). However, the viscosity of $\mathbf{FeC_3}^{4+}$ (2.801 ± 0.152 mPa.s) was a little lower than that of $\mathbf{FeC_2}^{4+}$ (3.113 ± 0.01 mPa.s). The viscosities of iron (II) coordination polymers $\mathbf{FeC_3}^{4+}$ and $\mathbf{FeC_2}^{4+}$ are normally higher than those of zinc (II) coordination polymers $\mathbf{ZnC_3}^{4+}$ and $\mathbf{ZnC_2}^{4+}$ due to the expected longer iron (II) coordination polymers.

Figure 3.32 shows the dynamic viscosity fashions upon the formation of the oxidized and reduced coordination polymers for each of $\mathbf{C_3}^{4+}$ and $\mathbf{C_2}^{4+}$.

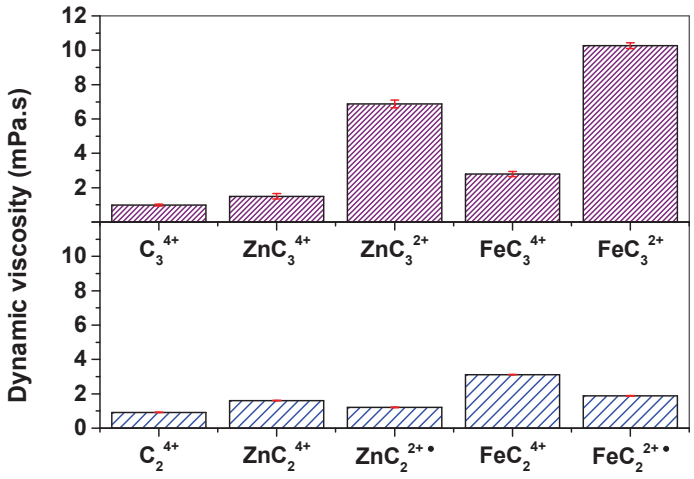

Figure 3.32: Viscosity trends of 13 mM for each of $\mathbf{C_3}^{4+}$, $\mathbf{C_2}^{4+}$ and their oxidized and photo-assisted reduced coordination polymers in DMF at 298 K.

The reduced coordination polymers showed amazing viscosity trends which gave strong evidences and fingerprint accordance with the above electrochemical and the spectroelectrochemical results. The photo-assisted 2-electron reduction/each unit of $\mathbf{ZnC_3}^{4+}$ and $\mathbf{FeC_3}^{4+}$ led ordinarily to $\mathbf{ZnC_3}^{2+}$ and $\mathbf{FeC_3}^{2+}$ and spontaneously to the emergence of the π-dimerization among the viologen radicals within the reduced coordination polymer $\mathbf{ZnC_3}^{2+}$ and $\mathbf{FeC_3}^{2+}$. Wonderfully, this dimerization processes increased evidently the viscosities of the resulting reduced coordination polymers to 6.872 ± 0.225 mPa.s and 10.270 ± 0.172 mPa.s for $\mathbf{ZnC_3}^{2+}$ and $\mathbf{FeC_3}^{2+}$ respectively.

In strong contrast, the dynamic viscosities of the reduced coordination polymers $\mathbf{ZnC_2}^{2+\bullet}$ and $\mathbf{FeC_2}^{2+\bullet}$ dropped to (1.209 ± 0.018 mPa.s) and (1.885 ± 0.021 mPa.s) for $\mathbf{ZnC_2}^{2+\bullet}$ and $\mathbf{FeC_2}^{2+\bullet}$ respectively. Such diminutions in viscosity after the reductions of these coordination

polymers exclude definitely the inter-molecular dimerization among the viologen radicals in both of $\mathbf{ZnC_2^{2(+\bullet)}}$ and $\mathbf{FeC_2^{2(+\bullet)}}$ species. Consequently, the π-dimerization detected within both of $\mathbf{ZnC_3^{2+}}$ and $\mathbf{FeC_3^{2+}}$ species will be distinctly of intra-molecular type.

As shown before, the open conformations are the most stable state for $\mathbf{C_2^{4+}}$ and $\mathbf{C_3^{4+}}$ along with their oxidized metallopolymers. These open conformations are mainly imposed by the electrostatic repulsive forces occurring between tetracationic viologens.(68) In other words, any interactions are extremely excluded within the structures of the tetracationic molecules $\mathbf{C_2^{4+}}$ and $\mathbf{C_3^{4+}}$ and their oxidized metallopolymers. In addition, the reduced metallopolymers do not reveal the inter-molecular dimerization, i.e.: no interactions among reduced metallopolymer series are detected. As long as we deal with metallopolymers in which their series not interact, then the viscosity obeys to the classical model of Einstein for infinitely dilute, non-interacting species. This model showed that single particles increase the viscosity of the medium as a linear function of the hydrodynamic volume fraction Ø, according to the following equation:(67)

$$\eta = \eta_s (1 + 2.5\ Ø)$$

Where η = solution viscosity, η_s = solvent viscosity and Ø = hydrodynamic volume fraction. Accordingly, the emergence of the π-dimerization among the viologen radicals within the reduced coordination polymer could increase the hydrodynamic volume occupied by the reduced polymer and hence logically increase the solution viscosity of reduced polymer $\mathbf{ZnC_3^{2+}}$ or $\mathbf{FeC_3^{2+}}$.

6. Conclusions and perspective

We have developed new organic and polytopic monomer $\mathbf{C3^{4+}}$ combining two viologen fragments spacered by flexible propylene linker in which these viologen units are functionalized by terpyridine moieties. The activation of the tetracationic ground state (state 0) by electron transfer allows the two viologen radicals to promote an effective orbital overlap of two adjacent SOMO orbitals (state 1). This efficient switching movement has been demonstrated at room temperature by various techniques: electrochemical study, UV-vis spectroscopy and ESR spectra.

The self-assembly 1D coordination polymers were attained utilizing the tetracationic molecule $\mathbf{C_3^{4+}}$ through the coordination of divalent transition metals with the terminal

terpyridine units. The formation of these cationic polymers was followed by UV-vis spectroscopy and ^{1}H-NMR spectrometry along with the viscosity measurements. Then the reduction of the viologen units within the coordination polymer led to folded polymeric structures by adopting a π-intramolecular (zig-zag conformation) association among viologen radicals within the polymeric conformation (see Figure 3.33). Therefore, this motion upon reduction modifies the mechanical properties of the polymer such as the enhancement of the viscosity.

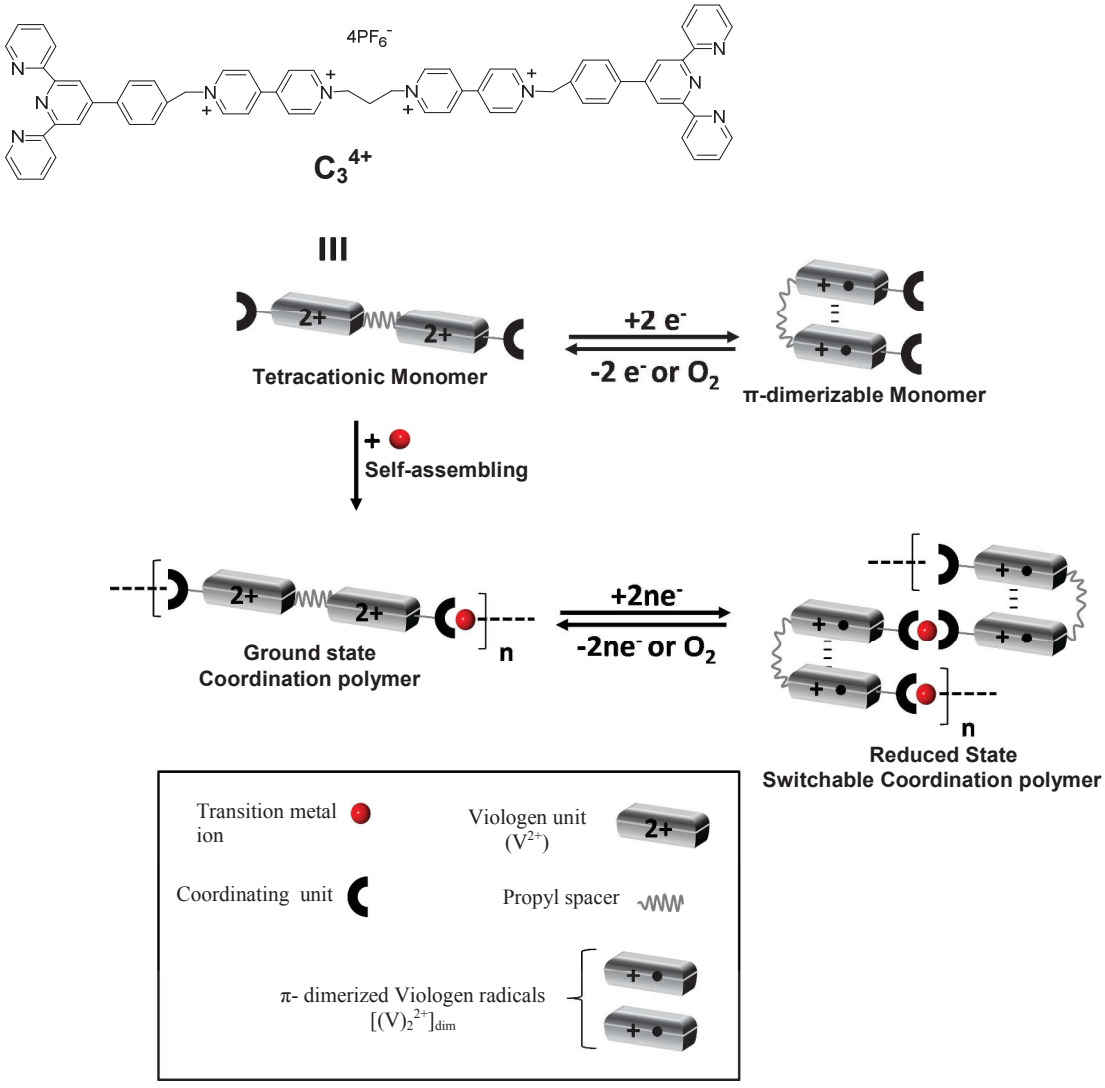

Figure 3.33: The novel developed switchable coordination polymers of the bis-functionalized terpyridine bis-viologen derivative $\mathbf{C_3}^{4+}$.

This work opens several perspectives. An extension of this work should include the anchoring of $\mathbf{C_3}^{4+}$ metallopolymer systems on electrodes. The transfer of this reversible movement on a surface could provide useful electronic devices taking advantage of color-, paramagnetism-, or mechanical switching. Consequently, switchable metallopolymers on surfaces thanks to the intra-molecular dimerization among viologen radicals within the structures of $\mathbf{C_3}^{2+}$ metallopolymers.

References

1. E. C. Constable, A. M. W. Cargill Thompson and D. A. Tocher, *Macromol. Symp.*, **1994**, 77, 219.
2. E. C. Constable, *Macromol. Symp.*, **1995**, 98, 503.
3. C. Janiak, *J. Chem. Soc., Dalton Trans.*, **2003**, 2781.
4. R. Dobrawa and F. Wurthner, *J. Polym. Sci. A: Polym. Chem.*, **2005**, 43, 4981.
5. H. Hofmeier and U. S. Schubert, *Chem. Commun.*, **2005**, 2423.
6. E.C. Constable, A.M.W. C. Thompson and D.A. Tocher. *"Into the third dimension of coordination chemistry: towards starburst arrays"*, pp 219 in Supramolecular Chemistry, Eds: V. Balzani and L. De Cola, Kluwer Academic Press, Dordrecht. **1992**.
7. E.C. Constable, A.M.W. C. Thompson and D.A. Tocher, *New J. Chem.*, **1992**, 16,855.
8. F. Barigelletti, L. Flamigni, V. Balzani, J.-P. Collin, J.-P. Sauvage, A. Sour, E.C. Constable and A.M.W. C. Thompson, *Coord. Chem. Rev.*, **1994**, 132, 209.
9. F. Barigelletti, L. Flamigni, **V.** Balzani, J.-P. Collin, J.-P. Sauvage, A. Sour, E.C. Constable and A.M.W. C. Thompson, *J. Chem. Soc., Chem. Commun.*, **1993**, 942.
10. E.C. Constable, A.M.W. C. Thompson and D.A. Tocher, *Supramol. Chem.*, **1993**, 3, 9.
11. E. C. Constable, A. M.W. C. Thompsona and D. A. Tocherb, *Macromol. Symp.*, **1994**, 77, 219.
12. E. C. Constable and A. M.W. C. Thompsona, *J. Chem. Soc. Dalton Trans.*, **1992**, 3467.
13. E. C. Constable, *Macromol. Symp.*, **1995**, 98,503.
14. E. C. Constable, *Chem. Commun.*, **1997**, 1073.
15. Y. Bodenthin , U. Pietsch , H. Möhwald and D. G. Kurth, *J. Am. Chem. Soc.*, **2005**, 127, 3110.
16. V. A. Friese and D. G. Kurth, *Coord. Chem. Rev.*, **2008**, 252, 199.
17. A. Ciferri, *Macromol. Rapid. Commun.* **2002**, *23*, 51.
18. U. Velten, B. Lahn and M. Rehahn, *Macromol. Chem. Phys.*, **1997**, 198, 2789.
19. D. G. Kurth and M. Higuchi, *Soft Matter*, **2006**, 2, 915.
20. S. J. Lippard, *Nature*, **2002**, 416, 587.
21. S. Kelch and M. Rehahn, *Macromolecules* **1999**, 32, 5818.
22. S. Kelch and M. Rehahn, *Chem. Commun.*, **1999**, 1123.
23. R. Knapp, S. Kelch, O. Schmelz and M. Rehahn, *Macromol. Symp.*, **2003**, 204, 267.

24. U. S. Schubert and C. Eschbaumer, *Angew. Chem. Int. Ed.*, **2002**, 41, 2892.
25. M. Schütte, D. G. Kurth, M. R. Linford, H. Cölfen and H. Möhwald, *Angew. Chem. Int. Ed.*, **1998**, 37, 2891.
26. V. A. Friese and D. G. Kurth, *Curr. Opin. Colloid Interface Sci*, **2009**, 14, 81.
27. U. S. Schubert, O. Hien and C. Eschbaumer, *Macromol. Rapid Commun.*, **2000**, 21, 1156.
28. U. S. Schubert and C. Eschbaumer, *Polymer Preprints*, **2000**, 41, 542.
29. U. S. Schubert, H. Hofmeier and G. R. Newkome. Modern Terpyridine Chemistry. wiley-vch Verlag GmbH & Co. KGaA, Weinheim. **2006**.
30. S. Schmatloch , A. M. J. van den Berg , A. S. Alexeev , H. Hofmeier and U. S. Schubert, *Macromolecules*, **2003**, 36, 9943.
31. J.A. Real. Bistability in Iron(II) Spin-Crossover Systems: A Supramolecular Function, pp 53 in Transition Metals in Supramolecular Chemistry: Perspectives in Supramolecular Chemistry volume 5, Eds: J.-P. Sauvage, John Wiley & Sons Ltd., **1999**.
32. O. Kahn and E. Codjovi, *Philos Trans Royal Soc A: Math, Phys Eng Sciences*, **1996**, 184, 354.
33. E. C. Constable, G. Baum, E. Bill, R. Dyson, R. v. Eldik, D. Fenske, S. Kaderli, D. Morris, A. Neubrand, M. Neuburger, D. R. Smith, K. Wieghardt, M. Zehnder and A. D. Zuberbuhler, *Chem. Eur. J.*, **1999**, 5, 498.
34. D. G. Kurth, P. Lehmann and M. Schutte, *Proc Natl Acad Sci*, **2000**, 97, 5704.
35. S. J. Rowan and J. B. Beck, *Faraday Discuss.*, **2005**, 128, 43.
36. J. B. Beck and S. J. Rowan, *J. Am. Chem. Soc.*, **2003**, 125, 13922.
37. M. Burnworth, L. Tang, J. R. Kumpfer, A. J. Duncan, F. L. Beyer, G. L. Fiore, S. J. Rowan and C. Weder, *Nature.*, **2011**, 472, 7343, 334.
38. A. Gasnier, G. Royal and P. Terech, *Langmuir*, **2009**, 25(15), 8751.
39. M. Yan, S. K. P. Velu, M. Maréchal, G. Royal, J. Galvez and P. Terech, *Soft Matter*, **2013**, 9, 4428.
40. M. Yan, S. K. P. Velu, G. Royal and P. Terech, *J. Coll. Inter. Sci.*, **2013**, 399, 6.
41. P. Terech, M. Yan, M. Maréchal, G. Royal, J. Galveza and S. K. P. Velua, *Phys.Chem. Chem. Phys.*, **2013**, 15, 7338
42. L. Qu, J. Fan, Y. Ren, K. Xiong, M. Yan, X. Tuo, P. Terech and G. Royal, *Mater. Chem. Phys.*, **2015**, 153, 54.

43. Y. S. Park, K. Lee, C. Lee and K. B. Yoon, *Langmuir*, **2000**, 16, 4470.
44. R. B. Romashkina, A. G. Majouga, E. K. Beloglazkina, D. A. Pichugina, M. S. Askerka, A. A. Moiseeva, R. D. Rakhimov and N. V. Zyk, *Russ.Chem.Bull., Int.Ed.*, **2012**, 61, 2265.
45. J. Wang and G. S. Hanan, *Synlett* **2005**, 1251.
46. T. Mutai, J-D. Cheon, S. Arita and K. Araki, *J. Chem. Soc., Perkin Trans. 2*, **2001**, 1045.
47. G-J. Zhang, X. Gan, Q-Q. Xu, Y. Chen, X-J. Zhao, B. Qin, X-J. Lv, S-W. Lai, W-F. Fu and C-M. Che, *Dalton Trans.*, **2012**, 41, 8421.
48. D. J. Mercer and S. J. Loeb, *Dalton Trans.*, 2011, **40**, 6385.
49. D. J. Mercer, J. Yacoub, K. Zhu, S. K. Loeb and S. J. Loeb, *Org. Biomol. Chem.*, **2012**, 10, 6094.
50. C. L. Bird and A. T. Kuhn, *Chem. Soc. Rev.*, **1981**, 10, 49.
51. W. Geuder, S. Hunig and A. Suchy, *Tetrahedron*, **1986**, 42, 1665.
52. A. Deronzier, B. GaIland and M. Vieira, *Nouv. J. Chim.*, **1982**, 6, 97.
53. B. Gorodetsky and N. R. Branda, *Tetrahedron letters*, **2005**, 46, 6761.
54. J.-P. Collin, S. Guillerez and J.-P. Sauvage, *J. Chem. Soc., Chem. Commun.*, **1989**, 776.
55. S.-I. Imabayashi, N. Kitamura and S. Tazuke, *J. Electroanal. Chem.*, **1988**, 243, 143.
56. P. Neta, M.-C. Richoux and A. Harriman, *J. Chem. Soc., Faraday Trans. 2*, **1985**,81, 1427.
57. M. Mohammad, *Electrochim. Acta*, **1988**, 33, 417.
58. R. L. Myers and I. Shain, *Anal. Chem.*, **1969**, 41, 980.
59. D. E. Richardson and H. Taube, *Inorg. Chem.* **1981**, 20, 1278.
60. M. R. Geraskina, A. T. Buck and A. H. Winter, *J. Org. Chem.*, **2014**, 79, 7723.
61. E. Belhadj, A. El-Ghayoury, E. Ripaud, L. Zorina, M. Allain, P. Batail, M. Mazari and M. Sallé, *New J. Chem.***, 2013**,37, 1427.
62. R. Dobrawa and F. Würthner, *Chem. Commun.*, **2002**, 1878.
63. M. Jacquet, F. Lafolet, S. Cobo, F. Loiseau, A. Bakkar, M. Boggio-Pasqua, E. Saint-Aman and G. Royal, *Inorg. Chem.*, **2017**, 56, 4357.
64. M. Suzuki, C. C. Waraksa, H. Nakayama, K. Hanabusa, M. Kimura, and H. Shirai, *Chem. Commun.*, **2001**, 2012.
65. M. Furue and S.-I. Nozakura, *Bull. Chem. Soc. Jpn.*, **1982**, 55, 513.
66. L. Zhaoxi, L. Wen and L. Manfu, *Chinese J. Polym. Sci.*, **1987**, 5, 3, 254.
67. C. W. Macosko. Rheology principles, measurements and applications. WILEY-VCH, Inc. **1994**.

68. C. Kahlfuss, S. Denis-Quanquin, N. Calin, E. Dumont, M. Garavelli, G. Royal, S. Cobo, E. Saint-Aman and C. Bucher, *J. Am. Chem. Soc.*, **2016**, 138, 15234.

General Conclusion

In this thesis we aimed to develop four new molecular switches taking advantage the non-covalent π-dimerization among viologen radicals. First, the redox properties of two new flexible cyclophanes have been investigated. These cyclophanes incorporate two viologen units which are linked by pentyl ($\mathbf{R5}^{4+}$) or heptyl ($\mathbf{R7}^{4+}$) chains. Upon 1-electron reduction per viologen unit, $\mathbf{R5}^{4+}$ results in the partial formation of diamagnetic intramolecular π-dimer $\mathbf{R5}^{2+}$. We have notably shown that the redox-triggered switching movements between the initial tetracationic $\mathbf{R5}^{4+}$ molecule and the intramolecular π-dimer $\mathbf{R5}^{2+}$ is well-reversible at room temperature. In contrast, $\mathbf{R7}^{4+}$ was not able to form such a dimer. The large length of the heptyl spacer and its conformation forbid the proximity of the two viologen radicals in $\mathbf{R7}^{2(+\bullet)}$ and thus prevent the formation of the π-dimer $\mathbf{R7}^{2+}$.

We then tested the possibility to use $\mathbf{R5}^{4+}$ or heptyl $\mathbf{R7}^{4+}$ for the preparation of inclusion complexes in the presence of a viologen unit under its radical cation state. In particular, the large cavity of the bis (radical-cation) species $\mathbf{R7}^{2(+\bullet)}$ as well as its conformational flexibility brought by the heptyl spacer was though to gain access to an encapsulation of a viologen radical and to the formation of the inclusion complex $\mathbf{R7}^{2(+\bullet)}\subset\mathbf{V}^{+\bullet}$. Unfortunately, using $\mathbf{R5}^{4+}$ or $\mathbf{R7}^{4+}$, our different investigations showed that the formation of these inclusion complexes was clearly not favorable in solution.

For this reason, our project was then dedicated to the study of responsive metallopolymers that incorporate the viologen unit. The concept of redox-responsive coordination polymers based on π-dimerization among viologen radicals has, to the best of our knowledge, never been addressed. Firstly, we developed a new organic and polytopic monomer $\mathbf{C3}^{4+}$ combining two viologen fragments spacered by a flexible propylene linker and terpyridine moieties as coordinating units. Both electrical- and visible light-assisted 2-electron reductions of the ligands have been successfully employed to trigger the reversible movement from the tetracationic $\mathbf{C3}^{4+}$ monomer to the diamagnatic π-intradimerized monomer $\mathbf{C3}^{2+}$. Then, we prepared self-assembled coordination polymers using the tetracationic $\mathbf{C3}^{4+}$ monomer through coordination of some divalent transition metals with the terminal terpyridine units. We have followed and demonstrated the formation of these polycationic coordination polymers by absorption spectroscopy, ^{1}H-NMR spectrometry as well as viscosity measurements. The reduction of the viologen units within cationic polymers, achieved electrochemically or

indirectly under visible light irradiation, led to the folding of the reduced polymeric structures (zig-zag conformation), in which the viologen radical are intramolecular associated. In addition, we have shown that the mechanical properties of the reduced polymer have been modified significantly by a large enhancement of the viscosity.

As perspectives to this work, we now believe that it could be interesting to test the formation of redox-triggered assemblies of both cyclophanes and their inclusion complexes in aqueous media especially after varying carefully counter anions besides the supporting electrolytes to avoid adsorption. Other inclusions complexes (for example with electron rich TTF units) could be also tested.

Regarding the redox-responsive coordination polymers, and after clarifying the switching properties of these assemblies in solution, a further study would be to use these materials as solid thin film. For example, the grafting or coating of the cationic metallopolymers on solid surfaces could be realized and the redox induced reversible movement between the initial and extended cationic polymer chains and the reduced and folded form could result in an interesting variation of the film thikness. Such systems could be useful in electronic devices based on color-, magnetic-, or mechanical-switching.

CHAPTER IV

Experimental Part

1. Solvents and reagents

Reagents and solvents were commercially sourced and used as received. 1,3-dibromo propane, methyl iodide, dichloromethane, nitric acid, butyl bromide, hexyl bromide, and dodecyl bromide, 4′-(4-Tolyl)-2,2′,6′,2′′-terpyridine, 2,4-dinitrochlorobenzene, 4-acetamidobenzaldehyde, ammonia, sodium hydroxide, chloroform, diethyl ether, carbone tetra chloride, azobisisobutyronitrile, and acetone were obtained from Sigma-Aldich; dimethylformamide, 4, 4′-bipyridin, methanol, and 2-acetylpyridine were from Fisher; acetonitrile, potassium hydroxide, and n-pentane were from Carlo Erba; N-bromosuccinimide was from Alfa Aesar; octadecyl bromide was from Janssen Chimica; hydrochloric acid, tetra-n-butylammonium perchlorate was from Fluka and ethanol were from VWR. Water was purified by reverse osmometry using an Elgastat purification system (5 MΩ.cm).

2. Nuclear Magnetic resonance

NMR spectra were recorded at 298 K on a Bruker Avance-500 MHz or 400 MHz spectrometer in CD_3CN, D_2O, CD_2Cl_2 or DMSO-d7. Chemical shifts/ppm are referenced to residual solvent peaks. Coupling constants values (J) are given in hertz.

3. Mass spectrometry analyses

Mass spectrometry analyses (ESI positive and MALDI-TOF modes) and HRMs were carried out at the DCM mass spectrometry facility with an Esquirre 3000 Plus (Bruker Daltonics) and ESI/QTOF-Waters Xevo G2-S QTof respectively.

4. Electron Spin Resonance Spectroscopy

ESR X-band spectra were recorded on an EMX Bruker spectrometer equipped with the ER–4192 ST Bruker cavity or ER–4131 VT cavity for 193 K measurements.

5. UV-Visible absorption spectroscopy

UV-visible absorption spectra were recorded on a Varian Cary 50 Scan UV-visible spectrophotometer using conventional quartz cells or all-quartz immersion probes (Hellma Inc.) having an optical path length of 0.1 cm or 1 cm.

6. Elemental analyses

Elemental analyses (C, H and N) were carried out on a Perkin–Elmer 240 at the DCM microanalysis facility.

7. Electrochemistry

Cyclic voltammetry (CV) and voltammetry with rotating disc electrode (VRDE) were recorded using a CHI660 potentiostat or using a Bio-logic SP300 potentiostat (under inert atmosher, in a dry glove box for non-aqueous media or under an argon stream for aqueous solutions). A standard one-compartment, three-electrode electrochemical cell was used. Tetra-*n*-butylammonium perchlorate salt was used as supporting electrolyte in non-aqueous media (0.1 M in CH_3CN, DMF, CH_2Cl_2) whereas KBr was used in aqueous media (0.1 M in H_2O). The working electrode was a vitreous carbon disk (diameter 3 mm, freshly polished) for CV. Voltage scan rates of 5 - 1000 $mV{\cdot}s^{-1}$ were used in CV experiments. The voltamperometry with a rotating disk electrode (VRDE) was carried out with radiometer (CTV101 radiometer analytical) equipment at a rotation rate of 500-4500 rpm using a glassy carbon RDE tip (diameter 3 mm) at a sweep rate of 10 $mV.s^{-1}$. Working electrodes were polished with 1 μm diamond paste (Mecaprex Presi) before each recording. A platinum wire has been used as auxiliary electrode. The reference electrodes was 0.01M $AgNO_3$ + 0.1 M TBAP/CH_3CN/Ag in organic media and AgCl (Sat. KCl/H_2O)/Ag in aqueous media. The reference electrode: 0.01M $AgNO_3$ + 0.1 M TBAP/CH_3CN/Ag was calibrated with respect to the formal potential of the Ferrocenium/Ferrocene (Fc^+/Fc) couple in CH_3CN or DMF, which was estimated at + 0.07 V under our experimental conditions. The reference electrode: AgCl (Sat. KCl/H_2O)/Ag was calibrated with respect to the formal potential of Zobell's solution in water, which was estimated at 229 mV. An automatic ohmic drop compensation procedure was systematically performed when using cyclic voltammetry.

UV-visible spectroelectrochemical experiments were carried out with a CHI660 potentiostat or using a Bio-logic SP300 potentiostat coupled to a Varian Cary 50 Scan UV-visible spectrophotometer using conventional quartz cells or all-quartz Helmma immersion probes (optical path length of 0.1 cm or 1 cm) equipped with optic fibers (041.002).

Electrolyses were conducted using a platinum plate (~1 cm^2) working electrode and a platinum coil as a counter-electrode isolated from the electrolytic solution through an ionic bridge.

8. Irradiation experiments

All the visible irradiation experiments were performed under argon atmosphere. The Visible irradiation experiments have been carried out with a 500 W Xenon-Helium lamp equipped with a cut-off filter ($\lambda > 436$ nm). The samples were prepared inside a dry glove box in a

classical UV-Visible quartz cell, in a Lovis manual filling set (Ø = 1.59 mm) for viscosit, or in a one-closed end glass pipette for ESR experiments. Both the sample-filled Lovis manual filling set or the sample-filled glass pipette are in turn put inside well-sealed glass tubes. The samples are placed at a distance of 15 cm from the visible lamp. The sample-filled quartz cell was kept at 8°C using a cryostat equipped with a cell holder. The sample-charged Lovis manual filling set or the sample-filled glass pipette were kept in an ice/water bath (0°C). The formation of the viologen radicals inside the quartz cells is followed by recording the UV-Visible spectra at a certain time interval during the visible irradiation. The total available irradiation time for samples-charged in both of the Lovis manual filling set and the glass pipette was 6 hours.

9. Viscosity experiments

The viscosity measurements were carried out using a Lovis 2000 M/ME microviscometer supplied by Anton Paar Gmbh. A capillary glass tube (Ø = 1.59 mm) equipped with a spherical stainless steel ball coated with gold (Ø = 1.5 mm) well suitable for Newtonians liquids having viscosity range of 0.2-65 mPa.s. Before measurements, the Lovis microviscometer was calibrated with degased bi-distilled water in the recommended temperature range of 20-40°C. The temperature was automatically controlled to be 25 ± 0.02°C. The solutions of the bis-viologen ditopic ligands were at concentrations of 13 mM. The concentrations of $[Zn(BF_4)_2.6H_2O]$ and $[Fe(BF_4)_2.6H_2O]$ solutions in DMF were 0.12 M and 0.2 M respectively. The viscosity titration experiments were carried out under air atmosphere. After each addition of the metal salt solution to the ligand solution, the resulting mixture solution (I mL) was stirred for 5 minutes, and a 0.4 ml is transferred into the Lovis manual filling set. The solutions of reduced coordination polymers were prepared in a dry glove box, transferred into the same capillary glass tube and then irradiated outside the glove box. The Lovis 2000 M/ME microviscometer measures the rolling times of a ball in liquid samples between two marks and calculate the samples viscosities from this obtained ball rolling times detected by inductive sensor. By varying the inclination of the capillary tube, the rolling ball will travel under controlled gravity acceleration allowing to explore different shear rate in order to catch an eventual non Newtonian behavior. The sample's viscosity is directly proportional to the rolling time (the greater the viscosity the longer the rolling time). In our case, the solutions were ideally found to be always Newtonian under the range of 30°-70° angles. Knowing this fact, viscosity experiments were carried out at the steep angle of 70°

to get the minimum flow time with a gold ball probe. Each viscosity value is at least an average of ten measurements (ten flow times).

10. Syntheses

10.1 Synthesis of 1, 1'-dimethyl-4, 4'-bipyridinium (V^{2+})

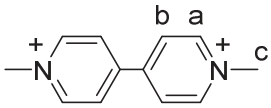

V^{2+} was synthesized following a modified reported procedure[1, 2]. Methyl iodide (10 ml, 160.6 mmol, 25.1 eq) was added with stirring into a solution of 4, 4´-bipyridine (1.000 g, 6.4 mmol, 1 eq) in 10 mL of dry acetonitrile and then the solution was stirred at 50°C for 24 hours. The produced precipitate was collected by filtration, washed with hot acetonitrile, and then dried under vacuum to afford $V^{2+}.2I^-$ as red precipitate, yield (2.629 g, 93%). A saturated aqueous KPF_6 solution was subsequently added in excess into the solution of $V^{2+}.2I^-$ dissolved in a minimum volume of water until precipitation of a $V^{2+}.2PF_6^-$ which was separated, washed with distilled water and dried under vacuum.

To prepare $V^{2+}.2NO_3^-$, the following ion exchange procedure was performed: 15-20 g of amberlite IRA93 (free base, mesh: 20-50) was stirred with 150 ml of 5% HNO_3 for 6 hours, washed with distilled water till the pH of washing water reached to 6-7, and the resulting amberlite loaded with nitrate ions was packed to column (25×3 cm). 0.100 g of $V^{2+}.2I^-$ dissolved in excess volume of distilled water was charged and the elution speed was adjusted to be slow (less than 0.7 $ml.min^{-1}$). The aqueous eluate was evaporated under vacuum to afford $V^{2+}.2NO_3^-$.

($V^{2+}.2I^-$): ^{1}H-NMR (400 MHz, D_2O), δ_H/ppm : 9.11 (d, J = 6.0 Hz, 4H, H_a), 8.59 (d, J = 6.5 Hz, 4H, H_b), 4.57 (s, 6H, H_c).

($V^{2+}.2PF_6^-$): ^{1}H-NMR (500 MHz, DMSO-d6), δ_H/ppm : 9.29 – 9.24 (m, 4H, H_a), 8.74 (d, J = 6.7 Hz, 4H, H_b), 4.43 (s, 6H, H_c).

10.2 Synthesis of 1, 1´-(1, 2-ethanediyl)-bis (4, 4´-bipyridinium) ($V2^{2+}$)[3]

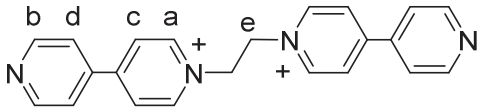

A solution of 1, 2-dibromoethane (0.73 ml, 8.5 mmol, 1 eq) dissolved in 10 mL of dry acetonitrile was added with stirring in a drop wise manner into a solution (40 mL) of 4, 4´-bipyridine (4.000 g, 25.6 mmol, 3 eq) while the temperature of the reaction mixture was maintained at 80°C for 24h under argon. The produced yellow precipitate was collected by filtration, washed with diethyl ether, recrystallized from water, washed with dichloromethane, acetone and then dried under vacuum to afford $\mathbf{V2}^{2+}.2Br^-$ as a light-brown precipitate. $\mathbf{V2}^{2+}.2PF_6^-$ (yield: 0.946 g, 18%) was prepared following the same procedure described for $\mathbf{V}^{2+}.2PF_6^-$. The bromide salt $\mathbf{V2}^{2+}.2Br^-$ was anion exchanged to the triflate salt $\mathbf{V2}^{2+}.2OTf^-$ by dissolving the solid (0.200 gm, 0.4 mmol, 1 eq) in 7 mL of distilled water, warming the solution to 40°C with ultrasonication, and adding a solution of NaOTf (0.344 g, 2.0 mmol, 5 eq) in 2 mL of distilled water. The temperature of the reaction mixture was maintained at 40°C with ultrasonication for 1h, stirred overnight at room temperature. The resulting triflate salt $\mathbf{V2}^{2+}.2OTf^-$ as reddish white precipitate was filtered off and dried under vacuum.

$\mathbf{V2}^{2+}.2Br^-$: ^{1}H-NMR (500 MHz, DMSO-d_6), δ_H/ppm : 9.25 – 9.22 (m, 4H, H_a), 8.92 – 8.89 (m, 4H, H_b), 8.76 – 8.73 (m, 4H, H_c), 8.09 – 8.06 (m, 4H, H_d), 5.33 (s, 4H, H_e).

$\mathbf{VC_2V}^{2+}.2PF_6^-$: ^{1}H-NMR (500 MHz, DMSO-d_6), δ_H/ppm : 9.11 (d, J = 6.2 Hz, 4H, H_a), 8.89 (d, J = 5.5 Hz, 4H, H_b), 8.70 (d, J = 6.4 Hz, 4H, H_c), 8.03 (d, J = 5.4 Hz, 4H, H_d), 5.24 (s, 4H, H_e).

$\mathbf{V2}^{2+}.2OTf^-$: ^{1}H-NMR (500 MHz, DMSO-d_6), δ_H/ppm : 9.12 (d, J = 6.9 Hz, 4H, H_a), 9.93 – 9.90 (m, 4H, H_b), 8.72 (d, J = 7.0 Hz, 4H, H_c), 8.08 – 8.02 (m, 4H, H_d), 5.26 (s, 4H, H_e).

10.3 Synthesis of 1, 1'-(1, 2-ethanediyl)-bis (ethyl)-4, 4'-bipyridinium) (C_{2ref}^{4+})[3]

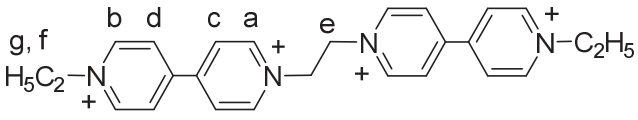

$\mathbf{V2_{ref}}^{4+}$ was synthesized following a modified procedure[3]. Ethyl iodide (0.63 ml, 7.87 mmol, 50 eq) was added with stirring into a solution of $\mathbf{V}^{2+}.2PF_6^-$ (0.100 g, 0.16 mmol, 1 eq) in dry dimethylformamide and then the solution was stirred at 80°C for 67 hours. The produced precipitate was collected by filtration, washed with acetonitrile, and then dried under vacuum to afford $\mathbf{V2_{ref}}^{4+}.2PF_6^-.2I^-$ as a red precipitate, yield (0.304 g, 98%). $\mathbf{V2_{ref}}^{4+}.4PF_6^-$ was prepared following the same procedures described for $\mathbf{V}.2PF_6^-$.

$V2_{ref}^{4+}$.$2PF_6^-$.$2I^-$: ^{1}H-NMR (500 MHz, DMSO-d6), δ_H/ppm : 9.43 (d, *J* = 6.8 Hz, 4H, H_a), 9.38 (d, *J* = 6.7 Hz, 4H, H_b), 8.90 (d, *J* = 6.8 Hz, 4H, H_c), 8.80 (d, *J* = 6.7 Hz, 4H, H_d), 5.38 (s, 4H, H_e), 4.75 (q, *J* = 7.3 Hz, 4H, H_f), 1.62 (t, *J* = 7.3 Hz, 6H, H_g).

10.4 Synthesis of 1, 1'-(1, 3-propanediyl)-bis (4, 4'-bipyridinium) ($V1^{2+}$)[4]

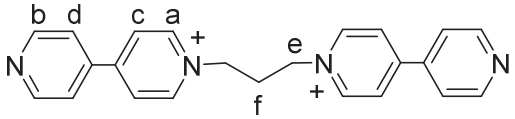

A solution of 1, 3-dibromopropane (0.65 ml, 6.4 mmol, 1 eq) dissolved in 10 mL of dry acetonitrile was added with stirring in a drop wise manner into a solution (20 mL) of 4, 4´-bipyridine (2.000 g, 12.8 mmol, 2 eq) while the temperature of the reaction mixture was maintained at 70°C for 24h. The produced yellow precipitate was collected by filtration, washed with acetonitrile, recrystallized from water, and then dried under vacuum to afford $V1^{2+}$.$2Br^-$ as a yellowish white precipitate, yield (1.317 g, 40%). Both $V1^{2+}$.$2PF_6^-$ and $V1^{2+}$.$2NO_3^-$ were prepared following the same procedures described for V^{2+}.$2PF_6^-$ and V^{2+}.$2NO_3^-$ respectively.

$V1^{2+}$.$2Br^-$: ^{1}H-NMR (400 MHz, DMSO-d_6), δ_H/ppm : 9.27 (d, *J* = 6.3 Hz, 4H, H_a), 8.93 – 8.87 (m, 4H, H_b), 8.74 – 8.68 (m, 4H, H_c), 8.10 – 8.03 (m, 4H, H_d), 4.80 (t, *J* = 7.1 Hz, 4H, H_e), 2.75 (p, *J* = 7.3 Hz, 2H, H_f).

10.5 Synthesis of 1, 1'-(1, 3-propanediyl)-bis (methyl)-4, 4'-bipyridinium) (C_{3ref}^{4+})[5, 6]

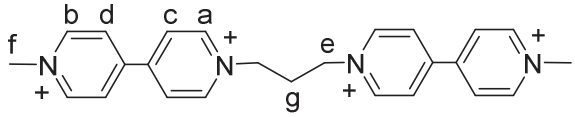

Methyl iodide (0.6 ml, 9.64 mmol, 25 eq) was added with stirring into a solution of 1, 1´-(1, 3-propanediyl)-bis (4, 4´-bipyridinium) dibromide ($V1_{ref}^{4+}$.$2Br^-$) (0.200 g, 0.4 mmol, 1 eq) in dry dimethylformamide and then the solution was stirred at 90°C for 24 hours. The produced precipitate was collected by filtration, washed with acetonitrile, and then dried under vacuum to afford $V1_{ref}^{4+}$.$2Br^-$.$2I^-$ as a red precipitate, yield (0.304 g, 98%). Both $V1_{ref}^{4+}$.$4PF_6^-$ and $V1_{ref}^{4+}$.$4NO_3^-$ were prepared following the same procedures described for V^{2+}.$2PF_6^-$ and V^{2+}.$2NO_3^-$ respectively.

$V1_{ref}^{4+}$.$2Br^-$.$2I^-$: ^{1}H-NMR (400 MHz, DMSO-d6), δ_H/ppm : 9.44 (d, *J* = 6.5 Hz, 4H, H_a), 9.32 (d, *J* = 6.5 Hz, 4H, H_b), 8.88 (d, *J* = 6.4 Hz, 4H, H_c), 8.80 (d, *J* = 6.6 Hz, 4H, H_d), 4.88 (t, *J* = 7.3 Hz, 4H, H_e), 4.47 (s, 6H, H_f), 2.80 (p, *J* = 7.4 Hz, 2H, H_g). ^{13}CNMR (100 MHz, DMSO-d6), δ/ppm : 149.27, 148.42, 147.20, 146.56, 127.11, 126.55, 58.03, 48.61, 40.44, 34.88, 23.01.

$V1_{ref}^{4+}$.4PF_6^- : ESI-MS (*m/z*) = 819.2 [M-PF_6^-]$^+$. HRMS-ESI (*m/z*): calcd: 819.124 [M- PF_6^-]$^+$, found: 819.12. MALDI-TOF Mass (*m/z*) = 674.168 [M-2PF_6^-]$^+$, 529.180 [M-3PF_6^-]$^+$, 384.202 [M-4PF_6^-]$^+$.
$V1_{ref}^{4+}$.4NO_3^- : ESI-MS (*m/z*) = 570.3 [M-NO_3^-]$^+$. HRMS-ESI (*m/z*): calcd: 570.1948 [M-NO_3^-]$^+$, found: 570.19. MALDI-TOF Mass (*m/z*) = 384.237 [M-4NO_3^-]$^+$.

10.6 Synthesis of 4′-(4-bromobenzyl)-2,2′,6′,2′′-terpyridine (Brtpy)[7]

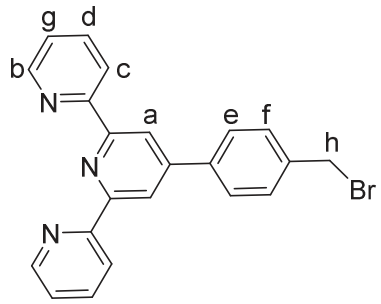

A suspension of 4′-(4-methylphenyl)-2,2′,6′,2′′-terpyridine (2.000 g, 6.2 mmol, 1 eq), N-bromosuccinimide (1.320 g, 7.4 mmol, 1.2 eq), and Azobisisobutyronitrile (0.082 g, 0.5 mmol, 0.08 eq) in CCl_4 (25 mL) was refluxed for 5 hours with stirring under dark conditions. The hot suspension was filtered and the solvent was evaporated under reduced pressure. The resulting solid residue was recrystallized from an ethanol-acetone mixture (2:1), and then dried under vacuum to afford **Brtpy** as a white solid, yield (1.560 g, 63%).

^{1}H-NMR (400 MHz, $CDCl_3$), δ_H/ppm : 8.77 – 8.65 (m, 6H, H_a, H_b and H_c), 7.88 (dt, *J* = 12.1 Hz, 6.7 Hz, 4H, H_d and H_e), 7.51 (dt, *J* = 13.8, 7.3 Hz, 2H, H_f), 7.36 (q, *J* = 9.5, 8.1 Hz, 2H, H_g), 4.56 (d, *J* = 5.6, 2H, H_h).
ESI-MS (*m/z*) = 402.1 [M]$^+$. HRMS-ESI (*m/z*): calcd: 402.0606 [M]$^+$, found: 402.06.

10.7 Synthesis[8-10] of C_3^{4+}

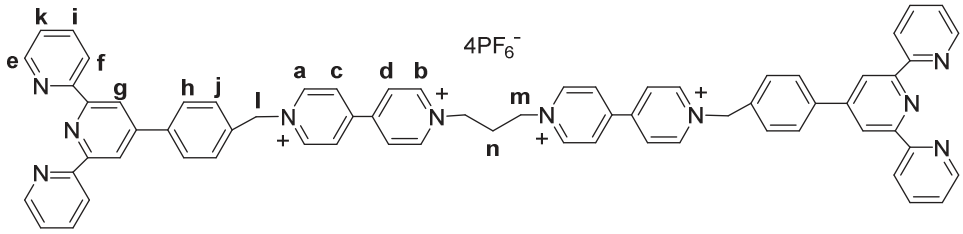

Method A: A mixture of 1, 1′-(1, 3-propanediyl)-bis (4, 4′-bipyridinium) dibromide, **$V1^{2+}$**.2Br^- (0.572 g, 1.112 mmol, 1 eq) and 4′-(4-bromobenzyl)-2,2′,6′,2′′-terpyridine, **Brtpy** (0.940 g, 2.336 mmol, 2.1 eq) in dry dimethylformamide (20 mL) was stirred at 85°C for 7 days. The resulting yellow precipitate was collected by filtration, washed with hot dimethylformamide, hot acetonitrile, hot chloroform, and then dried under vacuum to afford

$\mathbf{C_3}^{4+}$.4Br$^-$, yield (1.414 g, 96%). $\mathbf{C_3}^{4+}$.4PF_6^- was prepared following the same procedure of anion exchange described for $\mathbf{V}^{2+}$.2PF_6^-.

Method B: 1, 1′-(1, 3-propanediyl)-bis (4, 4′-bipyridinium) dibromide, $\mathbf{V1}^{2+}$.2Br$^-$ (0.100 g, 0.2 mmol, 1 eq) was dissolved in acetonitrile: dimethylformamide mixture (14:1) (15 mL) and 4′-(4-bromobenzyl)-2,2′,6′,2′′-terpyridine, **Brtpy** (0.162 g, 0.4 mmol, 2.08 eq) was added and the mixture allowed to heat at 85°C for 82 hours. The resulting yellow precipitate was separated, washed with acetonitrile, chloroform, and then dried under vacuum to afford the mono-terpyridine derivative $\mathbf{tpyV1}^{2+}$.3Br$^-$, yield (0.163 g, 92%).

A mixture of $\mathbf{tpyV1}^{2+}$.3Br$^-$ (0.540 g, 0.6 mmol, 1 eq) and 4′-(4-bromobenzyl)-2,2′,6′,2′′-terpyridine, **Brtpy** (0.246 g, 0.6 mmol, 2.1 eq) in dry dimethylformamide (20 mL) was stirred at 90°C for 72 hours. The resulting yellow precipitate was collected by filtration, washed with acetonitrile, chloroform, and then dried under vacuum to afford $\mathbf{C_3}^{4+}$.4Br$^-$, yield (0.536 g, 69%).

$\mathbf{C_3}^{4+}$.4PF_6^-: ^{1}H-NMR (400 MHz, DMSO-D_6), δ_H(ppm) : 9.55 (d, J = 6.3 Hz, 4H, H_a), 9.32 (d, J = 6.5 Hz, 4H, H_b), 8.81-8.62 (m, 20H, H_c, H_d, H_e, H_f, and H_g), 8.09-7.98 (m, 8H, H_h, and H_i), 7.81 (d, J = 7.8 Hz, 4H, H_j), 7.51 (dd, J = 7.4, 4.7 Hz, 4H, H_k), 6.04 (s, 4H, H_l), 4.78 (t, J = 7.5 Hz, 4H, H_m), 2.74-2.70 (m, 2H, H_n). ^{13}CNMR (126 MHz, DMSO-d6), δ/ppm : 155.92, 154.87, 149.47, 149.35, 149.26, 148.88, 146.16, 146.08, 138.85, 137.90, 135.22, 130.21, 128.11, 127.30, 126.92, 124.92, 121.30, 18.64. DEPTQ ^{13}CNMR (126 MHz, DMSO-d6), δ/ppm : 155.92(u), 154.87(u), 149.47, 149.35(u), 149.26(u), 148.88(u), 146.17, 146.08, 138.85(u), 137.90, 135.22(u), 130.21, 128.11, 127.30, 126.92, 124.92, 121.30, 118.30, 63.36(u), 57.91(u), 31.72(u). ESI-MS (*m/z*) = 1433.4 [M-PF_6^-]$^+$. HRMS-ESI (*m/z*): calcd: 1433.3458 [M-PF_6^-]$^+$, found: 1433.35. MALDI-TOF Mass (*m/z*) = 1433.16 [M-PF_6^-]$^+$, 1288.224 [M-2PF_6^-]$^+$,1143.281 [M-3PF_6^-]$^+$, 998.285 [M-4PF_6^-]$^+$. In DEPTQ ^{13}CNMR values, the indicated with (u) = up signals, and non indicated others mean down signals.

10.8 Synthesis[8-10] of C_2^{4+}

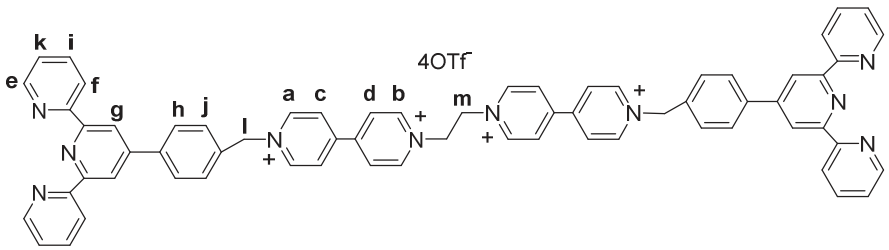

C_2^{4+} was synthesized following a modified procedure[8]. A mixture of 1, 1′-(1, 2-ethanediyl)-bis (4, 4′-bipyridinium) bis(phosphorus hexafloride), $V2^{2+}.2PF_6^-$ (0.107 g, 0.170 mmol, 1 eq) and 4′-(4-bromobenzyl)-2,2′,6′,2′′-terpyridine, **Brtpy** (0.205 g, 0.510 mmol, 3.0 eq) in nitromethane: dry dimethylformamide mixture (6:0.5) (6.5 mL) was stirred at 75°C for 3 days. The resulting yellow precipitate was collected by filtration, washed with acetonitrile, chloroform, and then dried under vacuum. The solid was mixed with 10 mL of distilled water, and an aqueous solution of NaOTf (1.517 g in 10 mL distilled water) was added with ultrasonication at 75°C for 30 min. To the resulting turbid mixture, 20 ml of nitomethane was added and the resulting two clear layers were stirred overnight at room temperature. The organic nitromethane layer was separated and dried naturally. The solid residue was stirred with 80 ml of chloroform for 4 hours. The solid was collected by filtration, and then dried under vacuum to afford $C_2^{4+}.4OTf^-$, yield (0.260 g, 96%).

$C_2^{4+}.4OTf^-$: ^{1}H-NMR (500 MHz, DMSO-D_6), δ_H(ppm) : 9.36 (d, J = 6.9 Hz, 4H, H_a), 9.09 (d, J = 6.9 Hz, 4H, H_b), 8.61 (d, J = 6.9 Hz, 4H, H_c), 8.57 (d, J = 6.5 Hz, 4H, H_d, and H_e), 8.53 (d, J = 5.9 Hz, 4H, H_f, and H_g), 7.92 (td, J = 7.8, 1.7 Hz, 4H, H_h), 7.87 (d, J = 8.3 Hz, 4H, H_i), 7.63 (d, J = 8.3 Hz, 4H, H_j), 7.41-7.38 (m, 4H, H_k), 5.86 (s, 4H, H_l), 5.13 (s, 4H, H_m). ^{13}CNMR (126 MHz, DMSO-d6), δ/ppm : 155.03, 153.92, 149.69, 149.10, 149.03, 148.73, 146.58, 146.11, 138.81, 138.49, 135.32, 130.16, 128.09, 127.24, 127.05, 125.19, 121.99, 121.74, 119.43, 118.76, 63.30, 59.59. DEPTQ90 ^{13}CNMR (126 MHz, DMSO-d6), δ/ppm : 148.48, 146.33, 145.85, 138.55, 129.90, 127.84, 126.99, 126.79, 124.93, 121.49, 118.50, 63.05, 59.33, 39.86, 39.69, 39.52, 39.35, 39.18. ESI-MS (*m/z*) = 1431.4 $[M\text{-}OTf^-]^+$. HRMS-ESI (*m/z*): calcd: 641.1708 $[M\text{-}2OTf^-]^{2+}$, found: 641.1700. MALDI-TOF Mass (*m/z*) = 1133.427 $[M\text{-}OTf^-]^+$, and 984.503 $[M\text{-}3OTf^-]^+$. Elemental analysis (%): calculated for $C_{70}H_{52}F_{12}N_{10}O_{12}S_4$ (1581.6): C, 53.155; H, 3.320; N, 8.858. Found: C, 52.64; H, 3.58; N, 9.12.

References

1. S. Andersson, D. Zou, R. Zhang, S. Sun, and L. Sun, *Org. Biomol. Chem.*, **2009**, **7**, 3605.
2. M. F. Pepitone, G. G. Jernigan, J. S. Melinger, and O.-K. Kim, Org. Lett., **2007**, 9, 801.
3. M. I. Attalla, N. S. McAlpine and L. A. Summers, *Z. Naturforsch.*, **1984**, 39b, 7 4.
4. Y. S. Park, K. Lee, C. Lee, and K. B. Yoon, Langmuir, 2000, 16, 4470.
5. S-I. Imabayashi, N. Kitamura and S. Tazuke, J. Electroanal. Chem., **1988**, 234, 143.
6. M. Future, and S.-I. Nozakura, Chem. Lett., **1980**, 821.
7. R. B. Romashkina, A. G. Majouga, E. K. Beloglazkina, D. A. Pichugina, M. S. Askerka, A. A. Moiseeva, R. D. Rakhimov, and N. V. Zyk, Russ.Chem.Bull., Int.Ed., **2012**, 61, 2265.
8. G-J. Zhang, X. Gan, Q-Q. Xu, Y. Chen, X-J. Zhao, B. Qin, X-J. Lv, S-W. Lai, W-F. Fu, and C-M. Che, Dalton Trans., **2012**, 41, 8421.
9. D. J. Mercer and S. J. Loeb, *Dalton Trans.*, 2011, **40**, 6385.
10. D. J. Mercer, J. Yacoub, K. Zhu, S. K. Loeb and S. J. Loeb, *Org. Biomol. Chem.*, **2012**, 10, 6094.

Annexe 1

Electrochemistry of molecules with multiple redox centers

The electrochemical behavior of molecules having multiple redox centers has already been thoroughly investigated.[1, 2] The electron transfers to or from molecules containing n identical, non-interacting, electroactive centers give rise to a single experimental voltammetric wave with a similar shape to that observed in a single electroactive center but with a current magnitude dependent on the number of redox centers (n). Such a process will be reversible obeying to the reversibility criterion: the anodic and cathodic peak potentials (and also the half-peak potentials) should be separated by by $\Delta E_p = | E_{pc} - E_{pa} | = 59$ mV at slow scan rates and 25°C.[3-5] Obeying Nernst equation and independent on the oxidation state of any of the other redox centres in the molecule, each centre is characterized by standard potential $E°_1$, $E°_2$,….. $E°_n$, then it is possible to calculate the formal potential spearation corresponding to each pair of n successive oxidation states of the multi-centres molecules. In the absence of interaction, for example in molecules having two redox centers such as bis-viologens, the theoretical standard potential separation expected between both first viologen formal reduction potentials ($E°_{1\_1}$ and $E°_{1\_2}$) should equal $\Delta E°_1 = E°_{1\_2} - E°_{1\_1} = 35.6$ mV, although both reduction processes will be observed as single experimental CV with $\Delta E_p = 59$ mV at slow scan rates and 25°C.

The general and complete redox and chemical behavior of bis-viologen species is presented in Scheme 1. As shown in Scheme 1, two cathodic electron transfer processes ($E°_{1\_1}$ and $E°_{1\_2}$) per linked bis-viologen molecule, one 2-electron reduction wave is observed experimentally, result in bis-radical cations (eq. 2). The latter is then involved in a chemical step, an intramolecular dimerization characterized by K_{Dim} (eq. 3), producing the π-dimer. In addition, a disproportionation equilibria may occur between two molecules of mono-reduced bis-viologen species (eq. 4), characterized by $K_{Disp} = - \Delta E°_1$ (V)/0.059.[6, 7]

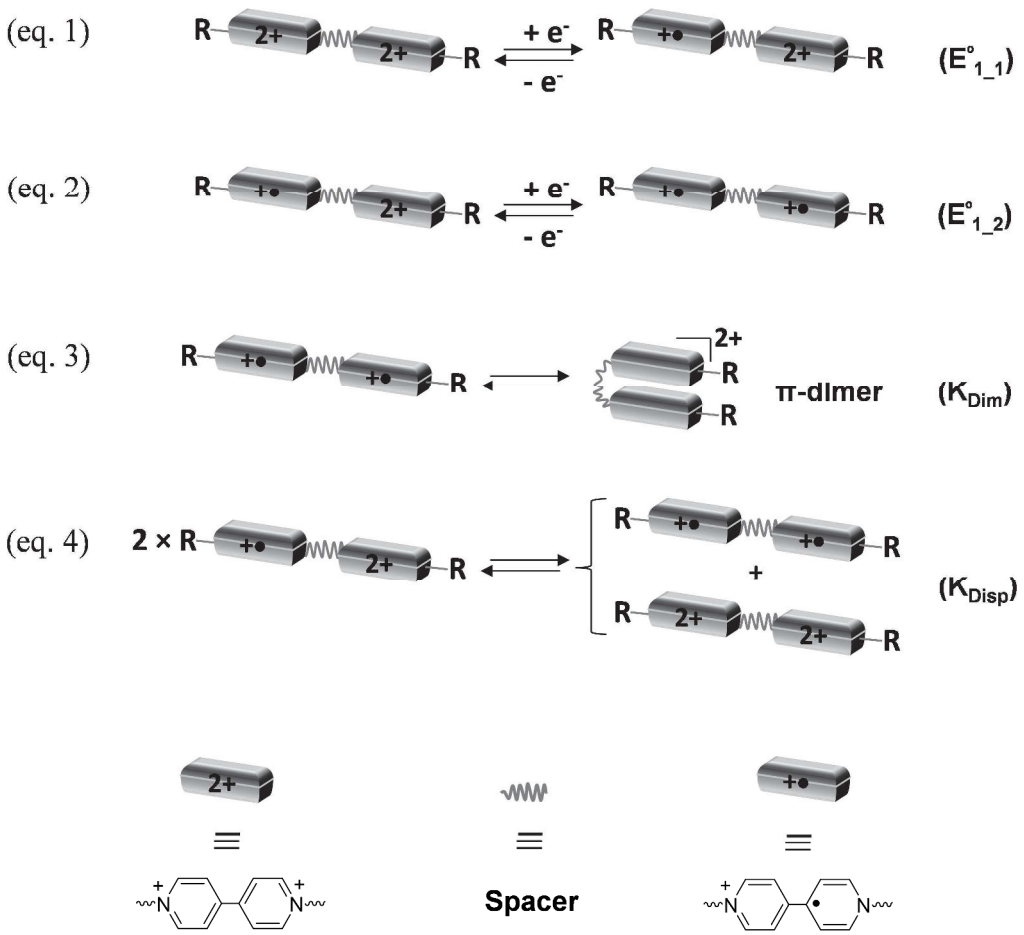

Scheme 1: single-electron successive reductions of bis-viologens species (equations: 1 and 2) and their potential coupled reactions (dimerization: eq. 3 and disproportionation: eq. 4).

Measuring the standard potential separation ΔE° between each redox center allows to quantify the extent of the electrochemical communication between multiple redox centers. Therefore, two separate cases should be considered. In the first case, the addition of the first electron ($E°_{1\_1}$) may render the second electron addition ($E°_{1\_2}$) easier so that the doubly reduced form is preferred. For this situation, ΔE° will be < 35.6 mV and might even be negative and this is what is respected in π-dimerized viologens. In the second case, the addition of the second electron could be made less favorable by the first electron addition and the mono-reduced species will be favored. For this situation, ΔE° will be >35.6mV. [(4)]

References

1. A. J. Bard, *Pure and Applied Chemistry* **1971**, 25, 379.
2. F. Ammar, J. M. Saveant, *J. Electroanal. Chem.* **1973**, 47, 115.
3. J. B. Flanagan, S. Margel, A. J. Bard, and F. C. Anson, *J. Am. Chem. Soc.* **1978**, 100, 4248.
4. P. Neta, M.-C. Richoux, and A. Harriman, *J. Chem. Soc., Faraday Trans. 2*, **1985**,81, 1427.
5. M. Mohammad, *Electrochim. Acta*, **1988**, 33, 417.
6. A. Deronzier, B. Galland and M. Vieira, *Nouv. J. Chim.*, **1982**, 6, 97.
7. D. E. Richardson, H. Taube, *Inorg. Chem.* **1981**, 20, 1278.

Annexe 2: Supplementary Spectra

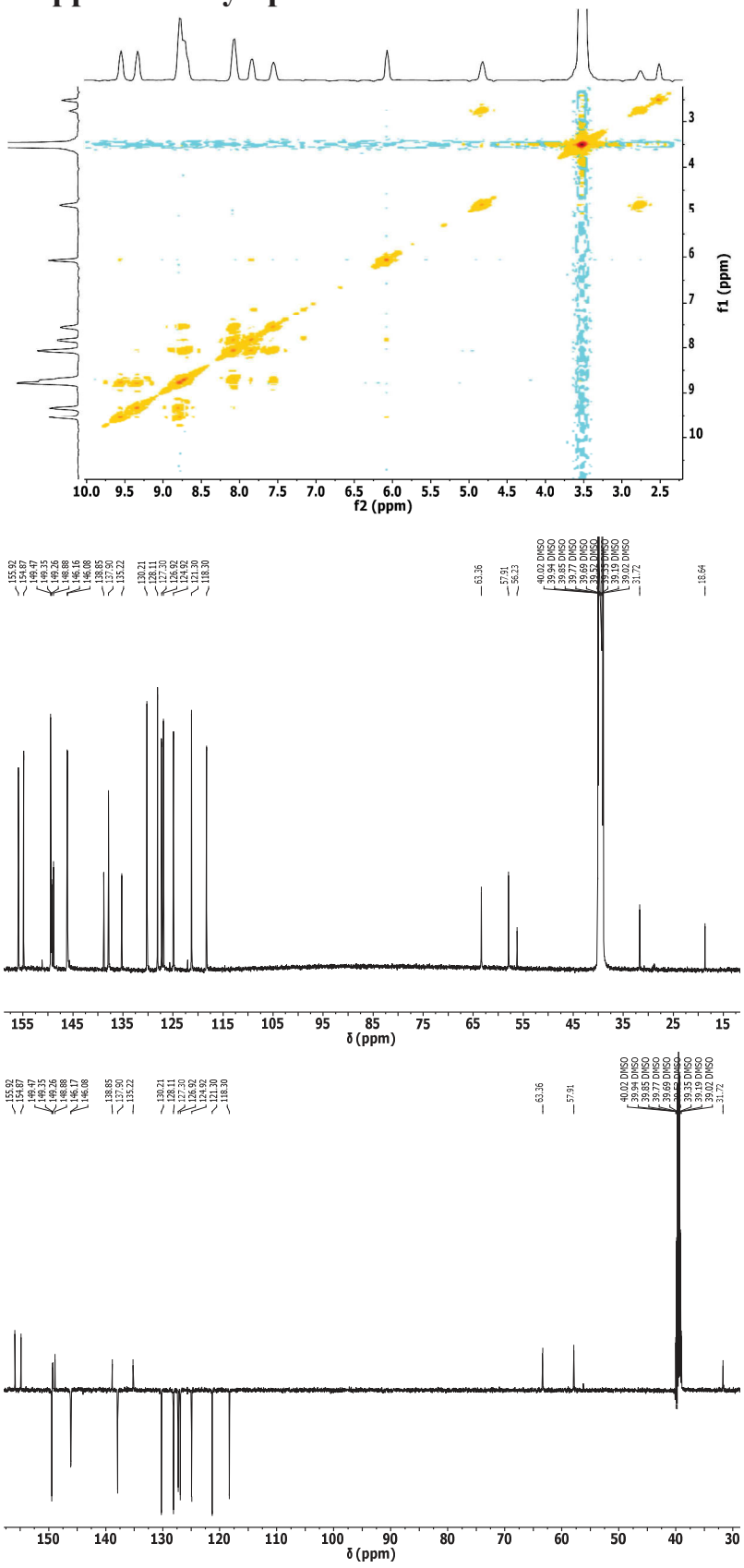

Figure 1: GCOSY (500MHz), DEPTQ and 1D ^{13}C-NMR (126MHz) spectra of $\mathbf{C_3}^{4+}$ in DMSO-d6 at 298K.

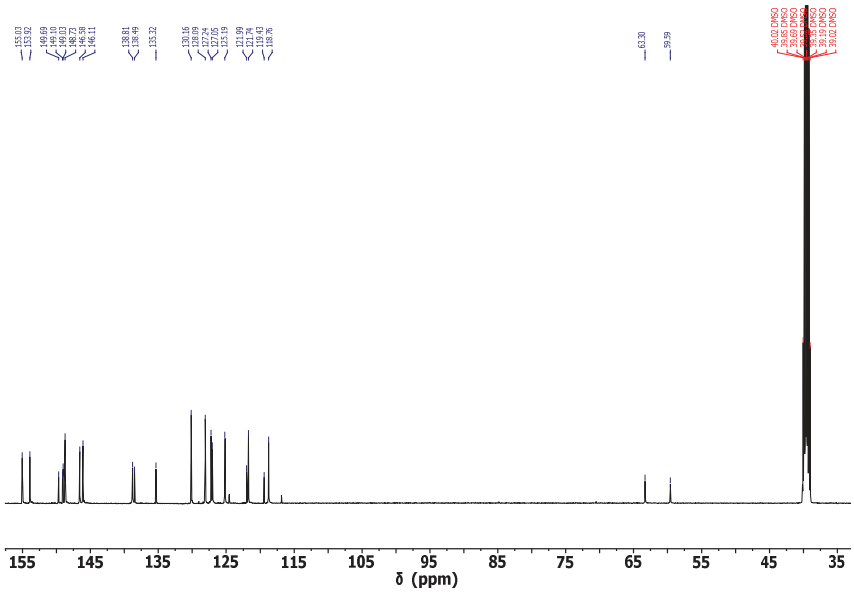

Figure 2: ^{13}C-NMR (126MHz) spectrum of $\mathbf{C_2}^{4+}$ in DMSO-d6 at 298K.

Annexe 3: Synthesis of alkyl viologen

Some alkyl viologen, mono- and di-alkylated bis-viologen molecules have been prepared but not fully investigated. Their syntheses are described below.

1. **Synthesis of 1-methyl-4, 4'-bipyridinium (C_1bpy^+)**[1]

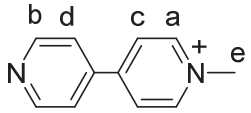

Methyl iodide (5 ml, 80.3 mmol, 12.5 eq) was added with stirring into a solution of 4, 4´-bipyridine (1.000 g, 6.4 mmol, 1 eq) in 10 mL of dry dichloromethane and then the solution was stirred at room temperature for 24 hours. The produced precipitate was collected by filtration, washed with dichloromethane, diethyl ether, recrystallized from methanol, and then dried under vacuum to afford $\mathbf{C_1bpy^+}.I^-$ as yellowish orange precipitate, yield (1.393 g, 73%).
^{1}H-NMR (400 MHz, CD_3CN), δ_H/ppm: 8.86 – 8.80 (m, 2H, H_a), 8.76 (d, J = 6.6 Hz, 2H, H_b), 8.31 (d, J = 6.5 Hz, 2H, H_c), 7.82 – 7.76 (m, 2H, H_d), 4.34 (s, 3H, H_e). ^{1}H-NMR (400 MHz, DMSO-d6)), δ_H/ppm : 9.14 (d, J = 6.4 Hz, 2H, H_a), 8.93 – 8.84 (m, 2H, H_b), 8.62 (d, J = 6.3 Hz, 2H, H_c), 8.07 – 8.01 (m, 2H, H_d), 4.40 (s, 3H, H_e).

2. **Synthesis of 1-butyl-4, 4'-bipyridinium (C_4bpy^+)**

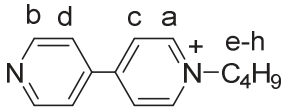

$\mathbf{C_4bpy^+}$ was synthesized as its Br^- salt following a modified procedure[2]. Butyl bromide (3.5 ml, 32.3 mmol, 5 eq) was added with stirring into a solution of 4, 4´-bipyridine (1.000 g, 6.4 mmol, 1 eq) in dry dichloromethane and then the solution was refluxed for 72 hours. The produced precipitate was collected by filtration, washed with dichloromethane, and then dried under vacuum to afford $\mathbf{C_4bpy^+}.Br^-$ as a yellow precipitate, yield (0.570 g, 30%).
^{1}H-NMR (400 MHz, DMSO-d6), δ_H/ppm : 9.29 (d, J = 6.5 Hz, 2H, H_a), 8.94 – 8.83 (m, 2H, H_b), 8.66 (d, J = 6.4 Hz, 2H, H_c), 8.12 – 8.03 (m, 2H, H_d), 4.68 (t, J = 7.5 Hz, 2H, H_e), 2.02 – 1.90 (m, 2H, H_f), 1.35 (h, J = 7.4 Hz, 2H, H_g), 0.95 (t, J = 7.4 Hz, 3H, H_h).

3. Synthesis of 1, 1'-dibutyl-4, 4'-bipyridinium (bC_4V^{2+})

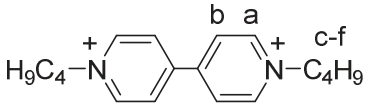

bC_4V^{2+} was synthesized as its Br^- salt following a modified procedure[2]. Butyl bromide (1.73 ml, 16 mmol, 5 eq) was added with stirring into a solution of 4, 4′-bipyridine (0.500 g, 3.2 mmol, 1 eq) in dry acetonitrile and then the solution was refluxed for 24 hours. The produced precipitate was collected by filtration, washed with acetonitrile, and then dried under vacuum to afford $bC_4V^{2+}.2Br^-$ as a yellow precipitate, yield (0.514 g, 37%). Both $bC_4V^{2+}.2PF_6^-$ and $bC_4V^{2+}.2NO_3^-$ were prepared following the same procedures described for $V^{2+}.2PF_6^-$ and $V^{2+}.2NO_3^-$ respectively.

($bC_4V^{2+}.2Br^-$): ^{1}H-NMR (400 MHz, DMSO-d6), δ_H/ppm : 9.49 – 9.43 (m, 4H, H_a), 8.88 – 8.81 (m, 4H, H_b), 4.75 (t, J = 7.4 Hz, 4H, H_c), 2.06 – 1.93 (m, 4H, H_d), 1.44 – 1.29 (m, 4H, H_e), 0.96 (t, J = 7.4 Hz, 6H, H_f). ^{13}C-NMR (100 MHz, DMSO-d6), δ/ppm : 149.09, 146.22, 127.12, 61.11, 33.14, 19.24, 13.79.

($bC_4V^{2+}.2PF_6^-$): ^{1}H-NMR (400 MHz, DMSO-d6), δ_H/ppm : 9.41 – 9.35 (m, 4H, H_a), 8.78 (d, J = 6.6 Hz, 4H, H_b), 4.71 (t, J = 7.4 Hz, 4H, H_c), 2.05 – 1.93 (m, 4H, H_d), 1.44 – 1.29 (m, 4H, H_e), 0.97 (t, J = 7.4 Hz, 6H, H_f).

4. Synthesis of both 1-dodecyl-4,4'-bipyridinium ($C_{12}bpy^+$) and 1,1'-didodecyl-4,4'-bipyridinium ($bC_{12}V^{2+}$)

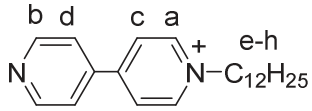

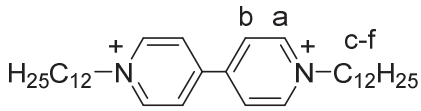

Both $C_{12}bpy^+$ and $bC_{12}V^{2+}$ were synthesized as their Br^- salts following modified procedures[2]. Dodecyl bromide (1.53 ml, 6.5 mmol, ≈1 eq) was added with stirring into a solution of 4, 4′-bipyridine (1.000 g, 6.4 mmol, 1 eq) in acetonitrile and then the solution was refluxed for 24 hours. The produced precipitate was collected by filtration, and dried under vacuum to afford $bC_{12}V^{2+}.2Br^-$ as a light golden precipitate, yield (0.488 g, 10%). After cooling the reaction filtrate to room temperature, the second precipitate was collected by filtration, washed with acetonitrile, and then dried under vacuum to afford $C_{12}bpy^+.Br^-$ as a bright yellow precipitate, yield (0.337 g, 13%). $bC_{12}V^{2+}.2NO_3^-$ was prepared following the same procedure described for $V^{2+}.2NO_3^-$ except using a mixture of (1:1) H_2O/CH_3CN as solvent. $bC_{12}V^{2+}.2NO_3^-$ was then employed to prepare $bC_{12}V^{2+}.2PF_6^-$ as mentioned before.

$C_{12}bpy^+.Br^-$: ^{1}H-NMR (400 MHz, DMSO-d6), δ_H/ppm : 9.25 (d, J = 6.2 Hz, 2H, H_a), 8.91 – 8.84 (m, 2H, H_b), 8.64 (d, J = 6.3 Hz, 2H, H_c), 8.16 – 7.92 (m, 2H, H_d), 4.64 (t, J = 7.5 Hz,

2H, H_e), 1.96 (p, J = 7.0 Hz, 2H, H_f), 1.27 (d, J = 26.1 Hz, 18H, H_g), 0.85 (t, J = 6.7 Hz, 3H, H_h).

$bC_{12}V^{2+}$.2Br$^-$: ^{1}H-NMR (400 MHz, DMSO-d6), δ_H/ppm : 9.41 (d, J = 6.4 Hz, 4H, H_a), 8.81 (d, J = 6.5 Hz, 4H, H_b), 4.70 (t, J = 7.4 Hz, 4H, H_c), 1.98 (p, J = 6.9 Hz, 4H, H_d), 1.28 (d, J = 27.3 Hz, 36H, H_e), 0.86 (t, J = 6.5 Hz, 6H, H_f).

5. Synthesis of 1-octadecyl-4, 4'-bipyridinium ($C_{18}bpy^+$)

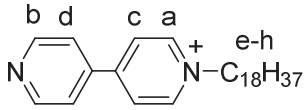

$C_{18}bpy^+$ was synthesized as its Br$^-$ salt following a modified procedure(2). A solution of octadecyl bromide (2.135 g, 6.4 mmol, ≈1 eq) in minimum volume of dry dichloromethane was added with stirring into a solution of 4, 4′-bipyridine (1.000 g, 6.4 mmol, 1 eq) in dry acetonitrile and then the solution was refluxed for 24 hours. The produced precipitate was collected by filtration, washed with acetonitrile, and then dried under vacuum to afford **$C_{18}bpy^+$**.Br$^-$ as a light yellow precipitate, yield (1.392 g, 45%).

^{1}H-NMR (400 MHz, DMSO-d6), δ_H/ppm : 9.26 (d, J = 6.4 Hz, 2H, H_a), 8.87 (d, J = 5.3 Hz, 2H, H_b), 8.65 (d, J = 6.2 Hz, 2H, H_c), 8.05 (d, J = 5.3 Hz, 2H, H_d), 4.64 (t, J = 7.4 Hz, 2H, H_e), 1.96 (p, J = 6.9 Hz, 2H, H_f), 1.23 (s, 30H, H_g), 0.85 (t, J = 6.4 Hz, 3H, H_h).

^{1}H-NMR (400 MHz, CD_2Cl_2), δ_H/ppm : 9.45 (d, J = 6.4 Hz, 2H, H_a), 8.87 – 8.75 (m, 2H, H_b), 8.24 (d, J = 6.0 Hz, 2H, H_c), 7.68 – 7.59 (m, 2H, H_d), 4.90 (t, J = 7.5 Hz, 2H, H_e), 1.49 (s, 2H, H_f), 1.18 (s, 30H, H_g), 0.80 (t, J = 6.7 Hz, 3H, H_h).

6. Synthesis of 1,1'-dioctadecyl-4,4'-bipyridinium ($bC_{18}V^{2+}$)

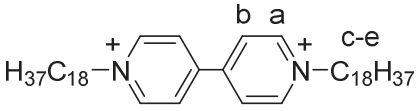

$bC_{18}V^{2+}$ was synthesized as its Br$^-$ salt following a modified procedure(2). A solution of octadecyl bromide (4.500 g, 13.5 mmol, 2.1 eq) in minimum volume of dry dichloromethane was added with stirring into a solution of 4, 4′-bipyridine (1.000 g, 6.4 mmol, 1 eq) in dry dimethylformamide and then the solution was stirred at 90°C for 192 hours. The produced precipitate was collected by filtration, washed with dichloromethane, dimethylformamide, acetonitrile, and then dried under vacuum to afford **$bC_{18}V^{2+}$**.2Br$^-$ as a yellow precipitate, yield (1.013 g, 20%). Both **$bC_{18}V^{2+}$**.2PF_6^- and **$bC_{18}V^{2+}$**.2NO_3^- were prepared following the same procedures described for **V^{2+}**.2PF_6^- and **V^{2+}**.2NO_3^- except using ethanol and acetonitrile as solvents respectively.

bC$_{18}$V^{2+}.2Br$^-$: ^{1}H-NMR (500 MHz, DMSO-d6), δ_H/ppm : 9.50 (d, *J* = 6.4 Hz, 4H, H_a), 8.89 (d, *J* = 6.2 Hz, 4H, H_b), 4.80 (t, *J* = 7.5 Hz, 4H, H_c), 1.36 (d, *J* = 8.6 Hz, 64H, H_d), 0.97 (t, *J* = 6.7 Hz, 6H, H_e).
bC$_{18}$V^{2+}.2NO$_3^-$: ESI-MS (*m/z*) = 724.7 [M-NO_3^-]$^+$. HRMS-ESI (*m/z*): calcd: 724.6356 [M-NO_3^-]$^+$, found: 724.635. MALDI-TOF Mass (*m/z*) = 662.668 [M-2NO_3^-]$^+$.

7. **Synthesis of 1, 1'-(1, 3-propanediyl)-mono (hexyl)-4, 4'-bipyridinium) (C$_6$V1^{3+})**[3, 4]

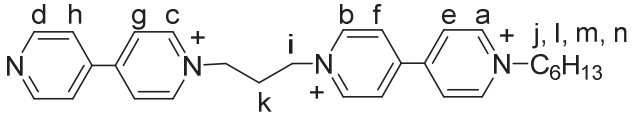

Hexyl Bromide (1 ml, 7.1 mmol, 27 eq) was added with stirring into a solution of 1, 1´-(1, 3-propanediyl)-bis (4, 4´-bipyridinium) dibromide (**C$_6$V1^{3+}**.2Br$^-$) (0.136 g, 0.3 mmol, 1 eq) in dry acetonitrile and then the solution was refluxed for 72 hours. The produced precipitate was collected by filtration, washed with acetonitrile, dichloromethane, and then dried under vacuum to afford **C$_6$V1^{3+}**.3Br$^-$ as a yellow precipitate, yield (0.143 g, 91%). **C$_6$V1^{3+}**.3PF_6^- was prepared following the same procedure described for **V^{2+}**.2PF_6^-.
C$_6$V1^{3+}.3Br$^-$: ^{1}H-NMR (400 MHz, DMSO-d6), δ_H/ppm : 9.45 (dd, *J* = 17.2, 6.5 Hz, 4H, H_a, and H_b), 9.34 (d, *J* = 6.6 Hz, 2H, H_c), 8.94 – 8.80 (m, 6H, H_d, H_e, and H_f), 8.73 (d, *J* = 6.4 Hz, 2H, H_g), 8.11 – 8.05 (m, 2H, H_h), 4.87 (q, *J* = 7.4 Hz, 4H, H_i), 4.72 (t, *J* = 7.4 Hz, 2H, H_j), 2.79 (p, *J* = 7.3 Hz, 2H, H_k), 2.00 (p, *J* = 7.3 Hz, 2H, H_l), 1.32 (p, *J* = 4.2 Hz, 6H, H_m), 0.92 – 0.84 (m, 3H, H_n).

8. **Synthesis of 1, 1'-(1, 3-propanediyl)- methyl, hexyl-4, 4'-bipyridinium) (C$_6$C$_1$V1^{4+})**[3, 4]

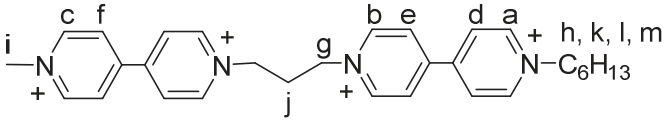

Methyl iodide (0.5 ml, 8 mmol, 43 eq) was added with stirring into a solution of 1, 1'-(1, 3-propanediyl)-mono (hexyl)-4, 4'-bipyridinium) trisbromide (**C$_6$C$_1$V1^{4+}**.3Br$^-$) (0.111 g, 0.2 mmol, 1 eq) in dry acetonitrile and then the solution was refluxed for 72 hours. The produced precipitate was collected by filtration, washed with acetonitrile, and then dried under vacuum to afford **C$_6$C$_1$V1^{4+}**.3Br$^-$.I$^-$ as a red precipitate, yield (0.120 g, 87%). **C$_6$C$_1$V1^{4+}**.4PF_6^- was prepared following the same procedure described for **V^{2+}**.2PF_6^-. **C$_6$C$_1$V1^{4+}**.4PF_6^- disssolved in (1:1) H_2O/CH_3CN mixture was then employed to prepare **C$_6$C$_1$V1^{4+}**.4NO_3^- in the same procedure mentioned before to prepare **V^{2+}**.2NO_3^-.

$C_6C_1V1^{4+}$.3Br$^-$.I$^-$: ^{1}H-NMR (400 MHz, DMSO-d6), δ_H/ppm : 9.44 (dd, *J* = 10.8, 6.4 Hz, 6H, H_a,and H_b), 9.32 (d, *J* = 6.4 Hz, 2H, H_c), 8.92 – 8.77 (m, 8H, H_d, H_e, and H_f), 4.89 (t, *J* = 7.2 Hz, 4H, H_g), 4.71 (t, *J* = 7.4 Hz, 2H, H_h), 4.47 (s, 3H, H_i), 2.81 (p, *J* = 7.3 Hz, 2H, H_j), 1.99 (q, *J* = 7.3 Hz, 2H, H_k), 1.32 (t, *J* = 6.2 Hz, 6H, H_l), 0.93 – 0.84 (m, 3H, H_m).
$C_6C_1V1^{4+}$.4PF_6^- : ESI-MS (*m/z*) = 889.3 [M-PF_6^-]$^+$. HRMS-ESI (*m/z*): calcd: 889.2022 [M-PF_6^-]$^+$, found: 889.20. MALDI-TOF Mass (*m/z*) = 599.373 [M-3PF_6^-]$^+$, 454.391 [M-4PF_6^-]$^+$.
$C_6C_1V1^{4+}$.4NO_3^- : ESI-MS (*m/z*) = 640.4 [M-NO_3^-]$^+$. HRMS-ESI (*m/z*): calcd: 640.2731 [M-NO_3^-]$^+$, found: 640.27. MALDI-TOF Mass (*m/z*) = 454.347 [M-4NO_3^-]$^+$.

9. **Synthesis of 1, 1'-(1, 3-propanediyl))-bis (hexyl)-4, 4'-bipyridinium) (bC_6V1^{4+})**[3, 4]

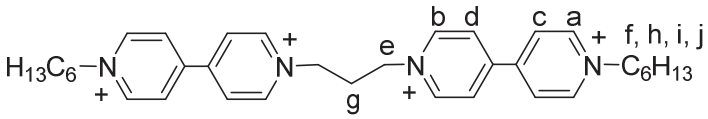

Method 1: Hexyl bromide (1 ml, 7.1 mmol, 133 eq) was added with stirring into a solution of 1, 1'-(1, 3-propanediyl)-mono (hexyl)-4, 4'-bipyridinium) trisbromide (**C_6V1^{3+}**.3Br$^-$) (0.032 g, 0.05 mmol, 1 eq) in dry dimethylformamide and then the solution was stirred at 90°C for 72 hours. The produced precipitate was collected by filtration, washed with acetonitrile, and then dried under vacuum to afford **bC_6V1^{4+}**.4Br$^-$ as a yellow precipitate, yield (0.032 g, 71%).

Method 2: Hexyl bromide (0.7 ml, 5 mmol, 9 eq) was added with stirring into a solution of 1, 1′-(1, 3-propanediyl)-bis (4, 4′-bipyridinium) dibromide (**$V1^{2+}$**.2Br$^-$) (0.300 g, 0.6 mmol, 1 eq) in dry dimethylformamide and then the solution was stirred at 90°C for 48 hours. The produced precipitate was collected by filtration, washed with acetonitrile, and then dried under vacuum to afford **bC_6V1^{4+}**.4Br$^-$ as a yellow precipitate, yield (0.302 g, 61%). **bC_6V1^{4+}**.4PF_6^- was prepared following the same procedure described for **V^{2+}**.2PF_6^-. **bC_6V1^{4+}**.4PF_6^- disssolved in (1:1) H_2O/CH_3CN mixture was then employed to prepare **bC_6V1^{4+}**.4NO_3^- in the same procedure mentioned before to prepare **V^{2+}**.2NO_3^-.

bC_6V1^{4+}.4Br$^-$: ^{1}H-NMR (400 MHz, DMSO-d6), δ_H/ppm : 9.55 (d, *J* = 6.4 Hz, 4H, H_a), 9.45 (d, *J* = 6.4 Hz, 4H, H_b), 8.88 (dd, *J* = 22.0, 6.5 Hz, 8H, H_c,and H_d), 4.95 (t, *J* = 7.3 Hz, 4H, H_e), 4.72 (t, *J* = 7.4 Hz, 4H, H_f), 2.84 (p, *J* = 7.4 Hz, 2H, H_g), 2.00 (p, *J* = 7.2 Hz, 4H, H_h), 1.38 – 1.22 (m, 12H, H_i), 0.92 – 0.84 (m, 6H, H_j). ^{13}C-NMR (100 MHz, DMSO-d6), δ/ppm : 149.29, 148.9, 146.58, 146.32, 127.16, 127.08, 61.38, 57.95, 32.18, 31.19, 31.04, 25.56, 22.33, 14.30.
bC_6V1^{4+}.4PF_6^-: ^{1}H-NMR (400 MHz, DMSO-d6), δ_H/ppm : 9.37 (dd, *J* = 13.1, 6.5 Hz, 8H, H_a,and H_b), 8.80 (dd, *J* = 24.3, 6.4 Hz, 8H, H_c,and H_d), 4.83 (t, *J* = 7.3 Hz, 4H, H_e), 4.70 (t, *J* = 7.5 Hz, 4H, H_f), 2.77 (p, *J* = 7.2 Hz, 2H, H_g), 1.98 (q, *J* = 7.2 Hz, 4H, H_h), 1.32 (p, *J* = 4.4 Hz, 12H, H_i), 0.92 – 0.84 (m, 6H, H_j). ESI-MS (*m/z*) = 959.4 [M-PF_6^-]$^+$. HRMS-ESI (*m/z*):

calcd: 959.2805 [M- PF_6^-]$^+$, found: 959.28. MALDI-TOF Mass (*m/z*) = 814.326 [M-2PF_6^-]$^+$, 669.369 [M-3PF_6^-]$^+$, 524.395 [M-4PF_6^-]$^+$.

bC_6V1^{4+}.4NO_3^- **:** ESI-MS (*m/z*) = 710.4 [M-NO_3^-]$^+$. HRMS-ESI (*m/z*): calcd: 710.3514 [M-NO_3^-]$^+$, found: 710.35. MALDI-TOF Mass (*m/z*) = 524.403 [M-4PF_6^-]$^+$.

10. Synthesis of 1, 1'-(1, 3-propanediyl)-mono (dodecyl)-4, 4'-bipyridinium) trisbromide (C$_{12}$V1^{3+})[3, 4]

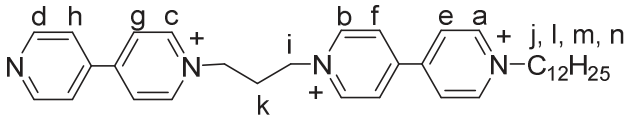

Dodecyl bromide (1.5 ml, 6.3 mmol, 16.1 eq) was added with stirring into a solution of 1, 1´-(1, 3-propanediyl)-bis (4, 4´-bipyridinium) dibromide (**V1**$^{2+}$.2Br^-) (0.200 g, 0.4 mmol, 1 eq) in dry acetonitrile and then the solution was refluxed for 72 hours. The produced precipitate was collected by filtration, washed with acetonitrile, dichloromethane, and then dried under vacuum to afford **C$_{12}$V1**$^{3+}$.3Br^- as a yellow precipitate, yield (0.197 g, 74%). **C$_{12}$V1**$^{3+}$.3NO_3^- was prepared following the same procedure described for **V**$^{2+}$.2NO_3^- except using CH_3CN as solvent. **C$_{12}$V1**$^{3+}$.3NO_3^- was then employed to prepare **C$_{12}$V1**$^{3+}$.3PF_6^- as mentioned before.

C$_{12}$V1^{3+}.3Br^-**:** ^{1}H-NMR (400 MHz, DMSO-d6), δ_H/ppm : 9.50 (d, *J* = 6.3 Hz, 2H, H_a), 9.44 (d, *J* = 6.3 Hz, 2H, H_b), 9.37 (d, *J* = 6.4 Hz, 2H, H_c), 8.90 (dd, *J* = 5.8, 3.3 Hz, 4H, H_d, and , H_e), 8.84 (d, *J* = 6.4 Hz, 2H, H_f), 8.74 (d, *J* = 6.3 Hz, 2H, H_g), 8.09 (d, *J* = 5.2 Hz, 2H, H_h), 4.89 (q, *J* = 7.5 Hz, 4H, H_i), 4.71 (t, *J* = 7.4 Hz, 2H, H_j), 2.80 (p, *J* = 6.9 Hz, 2H, H_k), 2.08 – 1.88 (m, 2H, H_l), 1.29 (d, *J* = 29.9 Hz, 18H, H_m), 0.86 (t, *J* = 6.7 Hz, 3H, H_n). ^{13}C-NMR (100 MHz, DMSO-d6), δ/ppm : 153.08, 151.52, 149.28, 148.85, 146.57, 146.31, 146.10, 141.27, 127.11, 127.05, 125.94, 122.37, 61.41, 58.06, 57.58, 31.74, 31.25, 29.45, 29.39, 29.28, 29.16, 28.89, 25.94, 22.54, 14.41.

11. Synthesis of 1, 1'-(1, 3-propanediyl)- methyl, dodecyl-4, 4'-bipyridinium) iodide trisbromide (C$_{12}$C$_1$V1^{4+})[3, 4]

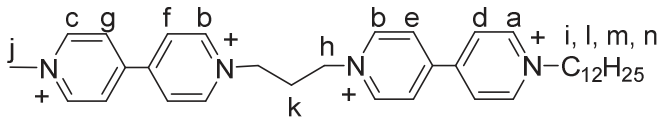

A solution of methyl iodide (0.5 ml, 8 mmol, 28 eq) and acetonitrile was added with stirring into a 1, 1'-(1, 3-propanediyl)-mono (dodecyl)-4, 4'-bipyridinium) trisbromide (**C$_{12}$V1**$^{3+}$.3Br^-) (0.196 g, 0.3 mmol, 1 eq) partially dissolved in minimum volume of dry dichloromethane and then the mixture was refluxed for 72 hours. The produced precipitate was collected by filtration, washed with acetonitrile, and then dried under vacuum to afford **C$_{12}$C$_1$V1**$^{4+}$.3Br^-.I^- as a red precipitate, yield (0.221 g, 93%). **C$_{12}$C$_1$V1**$^{4+}$.4NO_3^- was prepared following the same

procedure described for $\mathbf{V^{2+}}.2NO_3^-$ except using CH_3CN as solvent. $\mathbf{C_{12}C_1V1^{4+}}.4NO_3^-$ was then employed to prepare $\mathbf{C_{12}C_1V1^{4+}}.4PF_6^-$ as mentioned before.

$\mathbf{C_{12}C_1V1^{4+}}.3Br^-.I^-$: ^{1}H-NMR (400 MHz, DMSO-d6), δ_H/ppm : 9.43 (dd, J = 10.3, 6.4 Hz, 6H, H_a,and H_b), 9.32 (d, J = 6.3 Hz, 2H, H_c), 8.88 (dd, J = 6.7, 3.0 Hz, 4H, H_d,and H_e), 8.81 (t, J = 7.0 Hz, 4H, H_f,and H_g), 4.92 – 4.84 (m, 4H, H_h), 4.71 (t, J = 7.4 Hz, 2H, H_i), 4.47 (s, 3H, H_j), 2.81 (p, J = 7.2 Hz, 2H, H_k), 2.00 (q, J = 7.4 Hz, 2H, H_l), 1.40 – 1.19 (m, 18H, H_m), 0.86 (t, J = 6.5 Hz, 3H, H_n). ^{13}C-NMR (100 MHz, DMSO-d6), δ/ppm : 206.92, 149.31, 149.26, 148.81, 148.42, 147.19, 146.55, 146.30, 127.18, 127.12, 127.08, 126.56, 61.44, 58.03, 55.55, 55.28, 55.01, 54.73, 54.45, 48.61, 32.0, 31.75, 31.24, 31.16, 29.46, 29.40, 29.28, 29.16, 28.89, 25.94, 22.54, 14.41.

$\mathbf{C_{12}C_1V1^{4+}}.4PF_6^-$: ESI-MS (*m/z*) = 973.4 $[M\text{-}PF_6^-]^+$. HRMS-ESI (*m/z*): calcd: 973.2961 $[M\text{-}PF_6^-]^+$, found: 973.3. MALDI-TOF Mass (*m/z*) = 828.418 $[M\text{-}2PF_6^-]^+$, 683.434 $[M\text{-}3PF_6^-]^+$, 538.483 $[M\text{-}4PF_6^-]^+$.

$\mathbf{C_{12}C_1V1^{4+}}.4NO_3^-$: ESI-MS (*m/z*) = 724.5 $[M\text{-}NO_3^-]^+$. HRMS-ESI (*m/z*): calcd: 724.3670 $[M\text{-}NO_3^-]^+$, found: 724.37. MALDI-TOF Mass (*m/z*) = 538.416 $[M\text{-}4NO_3^-]^+$.

12. Synthesis of 1, 1'-(1, 3-propanediyl)-bis (dodecyl)-4, 4'-bipyridinium) tetrakisbromide ($\mathbf{bC_{12}V1^{4+}}$)[3, 4]

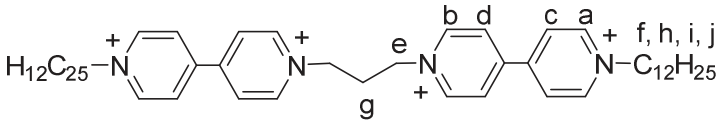

Dodecyl bromide (2 ml, 8.3 mmol, 15 eq) was added with stirring into a solution of 1, 1´-(1, 3-propanediyl)-bis (4, 4´-bipyridinium) dibromide ($\mathbf{V1^{2+}}.2Br^-$) (0.287 g, 0.6 mmol, 1 eq) in dry dimethylformamide and then the solution was stirred at 90°C for 48 hours. The produced precipitate was collected by filtration, washed with acetonitrile, and then dried under vacuum to afford $\mathbf{bC_{12}V1^{4+}}.4Br^-$ as a yellow precipitate, yield (0.285 g, 51%). $\mathbf{bC_{12}V1^{4+}}.4NO_3^-$ was prepared following the same procedure described for $\mathbf{V^{2+}}.2NO_3^-$ except using CH_3CN as solvent. $\mathbf{bC_{12}V1^{4+}}.4NO_3^-$ disssolved in (1:1) H_2O/CH_3OH mixture was then employed to prepare $\mathbf{bC_{12}V1^{4+}}.4PF_6^-$ as mentioned before.

$\mathbf{bC_{12}V1^{4+}}.4Br^-$: ^{1}H-NMR (400 MHz, DMSO-d6), δ_H/ppm : 9.55 (d, J = 6.4 Hz, 4H, H_a), 9.44 (d, J = 6.6 Hz, 4H, H_b), 8.94 – 8.82 (m, 8H, H_c, and H_d), 4.95 (t, J = 7.2 Hz, 4H, H_e), 4.72 (t, J = 7.4 Hz, 4H, H_f), 2.84 (p, J = 7.2 Hz, 2H, H_g), 1.99 (p, J = 7.1 Hz, 4H, H_h), 1.37 – 1.23 (m, 36H, H_i, and H_j), 0.90 – 0.82 (m, 6H, H_k).

$\mathbf{bC_{12}V1^{4+}}.4PF_6^-$: ^{1}H-NMR (400 MHz, DMSO-d6), δ_H/ppm : 9.37 (dd, J = 11.4, 6.5 Hz, 8H, H_a, and H_b), 8.85 – 8.81 (m, 4H, H_c), 8.79 – 8.75 (m, 4H, H_d), 4.82 (t, J = 7.3 Hz, 4H, H_e), 4.69 (t, J = 7.5 Hz, 4H, H_f), 2.77 (p, J = 7.3 Hz, 2H, H_g), 2.01 – 1.96 (m, 4H, H_h), 1.34 – 1.24 (m, 36H, H_i), 0.87 – 0.83 (m, 6H, H_j). ESI-MS (*m/z*) = 1127.6 $[M\text{-}PF_6^-]^+$. HRMS-ESI (*m/z*): calcd: 1127.4683 $[M\text{-}PF_6^-]^+$, found: 1127.47. MALDI-TOF Mass (*m/z*) = 1127.454 $[M\text{-}PF_6^-]^+$, 982.496 $[M\text{-}2PF_6^-]^+$, 837.567 $[M\text{-}3PF_6^-]^+$, 692.642 $[M\text{-}4PF_6^-]^+$.

bC_{12}V1^{4+}.4NO_3^-: MALDI-TOF Mass (*m/z*) = 692.598 [M-4NO_3^-]$^+$.

13. **Synthesis of 1, 1'-(1, 3-propanediyl)-mono (octadecyl)-4, 4'-bipyridinium) trisbromide (C_{18}V1^{3+})**[3, 4]

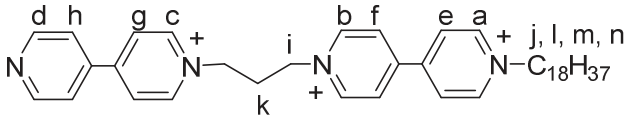

Octadecyl bromide (1.200 g, 3.6 mmol, 3 eq) was added with stirring into a solution of 1, 1´-(1, 3-propanediyl)-bis (4, 4´-bipyridinium) dibromide (**V1**$^{2+}$.2Br^-) (0.600 g, 1.2 mmol, 1 eq) in dry dimethylformamide and then the solution was stirred at 90°C for 168 hours. The produced precipitate was collected by filtration, washed with acetonitrile, and then dried under vacuum to afford **C_{18}V1**$^{3+}$.3Br^- as a yellow precipitate, yield (0.640 g, 65%). Both **C_{18}V1**$^{3+}$.3PF_6^- and **C_{18}V1**$^{3+}$.3NO_3^- were prepared following the same procedures described for **V**$^{2+}$.2PF_6^- and **V**$^{2+}$.2NO_3^- respectively.

C_{18}V1^{3+}.3Br^-**:** ^{1}H-NMR (500 MHz, DMSO-d6), δ_H/ppm : 9.49 (dd, *J* = 6.9, 3.0 Hz, 2H, H_a), 9.44 (d, *J* = 6.3 Hz, 2H, H_b), 9.35 (dd, *J* = 6.9, 2.7 Hz, 2H, H_c), 8.93 – 8.82 (m, 6H, H_d, H_e and H_f), 8.81 – 8.72 (m, 2H, H_g), 8.11 – 8.06 (m, 2H, H_h), 4.88 (q, *J* = 7.6, 7.0 Hz, 4H, H_i), 4.71 (t, *J* = 7.4 Hz, 2H, H_j), 2.80 (p, *J* = 7.3 Hz, 2H, H_k), 1.99 (t, *J* = 7.2 Hz, 2H, H_l), 1.36 – 1.22 (m, 30H, H_m), 0.86 (t, *J* = 6.8 Hz, 3H, H_n).

VC_3VC_{18} $^{3+}$**.**3NO_3^- **:** ESI-MS (*m/z*) = 731.5 [M-NO_3^-]$^+$. HRMS-ESI (*m/z*): calcd: 731.4496 [M-NO_3^-]$^+$, found: 731.45.

14. **Synthesis of 1, 1'-(1, 3-propanediyl)- methyl, octadecyl-4, 4'-bipyridinium) iodide trisbromide ($C_{18}C_1$V1^{4+})**[3, 4]

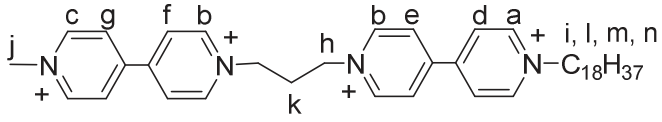

Methyl iodide (0.22 ml, 3.5 mmol, 10 eq) was added with stirring into a solution of 1, 1'-(1, 3-propanediyl)-mono (octadecyl)-4, 4'-bipyridinium) trisbromide (**C_{18}V1**$^{3+}$.3Br^-) (0.300 g, 0.35 mmol, 1 eq) in dry dimethylformamide and then the solution was refluxed for 48 hours. The produced precipitate was collected by filtration, washed with acetonitrile, and then dried under vacuum to afford **$C_{18}C_1$V1**$^{4+}$.3Br^-**.**I^- as a red precipitate, yield (0.110 g, 31%). **$C_{18}C_1$V1**$^{4+}$.4NO_3^- was prepared following the same procedure described for **V**$^{2+}$.2NO_3^- except using (1:1) H_2O/CH_3CN mixture as solvent. **$C_{18}C_1$V1**$^{4+}$.4NO_3^- disssolved in CH_3OH was then employed to prepare **$C_{18}C_1$V1**$^{4+}$.4PF_6^- as mentioned before.

$C_{18}C_1V1^{4+}$.3Br^-.I^-: ^{1}H-NMR (500 MHz, DMSO-d6), δ_H/ppm : 9.44 (dd, *J* = 13.4, 6.4 Hz, 6H, H_a and H_b), 9.33 (d, *J* = 6.4 Hz, 2H, H_c), 8.89 (dd, *J* = 6.6, 3.8 Hz, 4H, H_d and H_e), 8.82 (dd, *J* = 9.8, 6.4 Hz, 4H, H_f and H_g), 4.88 (dq, *J* = 8.2, 3.7 Hz, 4H, H_h), 4.71 (t, *J* = 7.4 Hz, 2H, H_i), 4.47 (s, 3H, H_j), 2.81 (p, *J* = 6.5, 5.7 Hz, 2H, H_k), 1.99 (q, *J* = 7.1 Hz, 2H, H_l), 1.34 – 1.26 (m, 30H, H_m), 0.86 (t, *J* = 6.7 Hz, 3H, H_n). MALDI-TOF Mass (*m/z*) = 622.524 $[M\text{-}4PF_6^-]^+$.
$C_{18}C_1V1^{4+}$.4NO_3^-: MALDI-TOF Mass (*m/z*) = 622.499 $[M\text{-}4NO_3^-]^+$.

References

1. S. Andersson, D. Zou, R. Zhang, S. Sun, and L. Sun, *Org. Biomol. Chem.*, **2009**, **7**, 3605.
2. M. F. Pepitone, G. G. Jernigan, J. S. Melinger, and O.-K. Kim, Org. Lett., **2007**, 9, 801.
3. S-I. Imabayashi, N. Kitamura and S. Tazuke, J. Electroanal. Chem., **1988**, 234, 143.
4. M. Future, and S.-I. Nozakura, Chem. Lett., **1980**, 821.

Résumé:

Ce travail cocerne la préparation et la caractérisation des nouveaux commutateurs moléculaires déclenchés par redox basés sur la π-dimérisation covalente parmi les radicaux viologène en solution. Les propriétés redox ont été étudiées pour deux nouveaux cyclophanes flexibles incorporant deux unités de viologène liées par des chaînes pentyle ou heptyle. Un lieur pentyle portant un cyclophane montre une capacité à former un π-dimère en solution sur une unité de réduction d'électron / viologène. Au contraire, un bisphénol cyclique (cation cationique) avec un lieur heptyle, de plus grande longueur accompagnée d'une flexibilité conformationnelle plus élevée, ne se dimérise pas mais a la capacité d'accommoder le radical diméthyl viologène formant un complexe d'inclusion. La formation du complexe d'inclusion entre le radical diméthyl viologène et le linker pentyle porteur de cyclophane bis (radical-cation) est encore spéculative. Nous rapportons un nouveau changement moléculaire basé sur l'utilisation de la molécule bis-viologène espacée de propylène fonctionnalisée avec deux groupes terpyridine terminaux. Nous montrons que cette molécule tetracationic mute de manière réversible au π-dimère diamagnétique sous des stimuli de réduction. Le monomère tétracationique peut s'auto-assembler avec certains métaux de transition divalents pour former des polymères de coordination cationiques. La réduction assistée par la lumière électrique ou visible des unités de viologène dans les polymères cationiques conduit à des assemblages polymères pliés résultant de la π-dimérisation parmi les radicaux viologène. En effet, les propriétés mécaniques de ces assemblages polymères dimérisés résultants ont été modifiées de manière significative par l'augmentation de la viscosité.

Mots clés: électrochimie, viologène, π-dimères, interrupteur moléculaire, polymère de coordination commutable.

Abstract:

This work deals with the design of novel redox triggered molecular switches based on a non-covalent π-dimerization among viologen radicals in solution. In a first part, the redox properties of two new cyclophanes incorporating two viologen units linked by flexible pentyl or heptyl chains have been investigated, as well as their ability to form inclusion complexes. Unfortunately, only the cyclophane bearing a pentyl linker showed a weak ability to form π-dimer in solution upon 1-electron reduction/viologen unit, whereas the cyclophane made with a long heptyl linker was unable to dimerize intramolecularly. In a second part, we present new responsive metallopolymers that incorporate both viologen units and bis-terpyridine metal complexes in their main chains. It was shown that the electrical- or visible light-assisted reduction of the viologen units within the metallopolymers led to an efficient folding of the polymeric chains, as the result of an intramolecular π-dimerization process. These polycationic suprapolymers have thus the ability to mutate reversibly from an elongated to a folded morphology upon application of redox stimuli and this behavior results in particular in large changes in viscosity.

Keywords: electrochemistry, viologen radicals, π-dimers, molecular switches, responsive coordination polymers.